



## CATALYTIC HYDROGENATION/HYDROGENOLYSIS OF BIOMASS- DERIVED PLATFORM CHEMICALS

**Abdulaziz Aldureid Kadi Amin**

**ADVERTIMENT.** L'accés als continguts d'aquesta tesi doctoral i la seva utilització ha de respectar els drets de la persona autora. Pot ser utilitzada per a consulta o estudi personal, així com en activitats o materials d'investigació i docència en els termes establerts a l'art. 32 del Text Refós de la Llei de Propietat Intel·lectual (RDL 1/1996). Per altres utilitzacions es requereix l'autorització prèvia i expressa de la persona autora. En qualsevol cas, en la utilització dels seus continguts caldrà indicar de forma clara el nom i cognoms de la persona autora i el títol de la tesi doctoral. No s'autoritza la seva reproducció o altres formes d'explotació efectuades amb finalitats de lucre ni la seva comunicació pública des d'un lloc aliè al servei TDX. Tampoc s'autoritza la presentació del seu contingut en una finestra o marc aliè a TDX (framing). Aquesta reserva de drets afecta tant als continguts de la tesi com als seus resums i índexs.

**ADVERTENCIA.** El acceso a los contenidos de esta tesis doctoral y su utilización debe respetar los derechos de la persona autora. Puede ser utilizada para consulta o estudio personal, así como en actividades o materiales de investigación y docencia en los términos establecidos en el art. 32 del Texto Refundido de la Ley de Propiedad Intelectual (RDL 1/1996). Para otros usos se requiere la autorización previa y expresa de la persona autora. En cualquier caso, en la utilización de sus contenidos se deberá indicar de forma clara el nombre y apellidos de la persona autora y el título de la tesis doctoral. No se autoriza su reproducción u otras formas de explotación efectuadas con fines lucrativos ni su comunicación pública desde un sitio ajeno al servicio TDR. Tampoco se autoriza la presentación de su contenido en una ventana o marco ajeno a TDR (framing). Esta reserva de derechos afecta tanto al contenido de la tesis como a sus resúmenes e índices.

**WARNING.** Access to the contents of this doctoral thesis and its use must respect the rights of the author. It can be used for reference or private study, as well as research and learning activities or materials in the terms established by the 32nd article of the Spanish Consolidated Copyright Act (RDL 1/1996). Express and previous authorization of the author is required for any other uses. In any case, when using its content, full name of the author and title of the thesis must be clearly indicated. Reproduction or other forms of for profit use or public communication from outside TDX service is not allowed. Presentation of its content in a window or frame external to TDX (framing) is not authorized either. These rights affect both the content of the thesis and its abstracts and indexes.



# Catalytic Hydrogenation/Hydrogenolysis of Biomass-Derived Platform Chemicals

ABDULAZIZ ALDUREID KADI AMIN

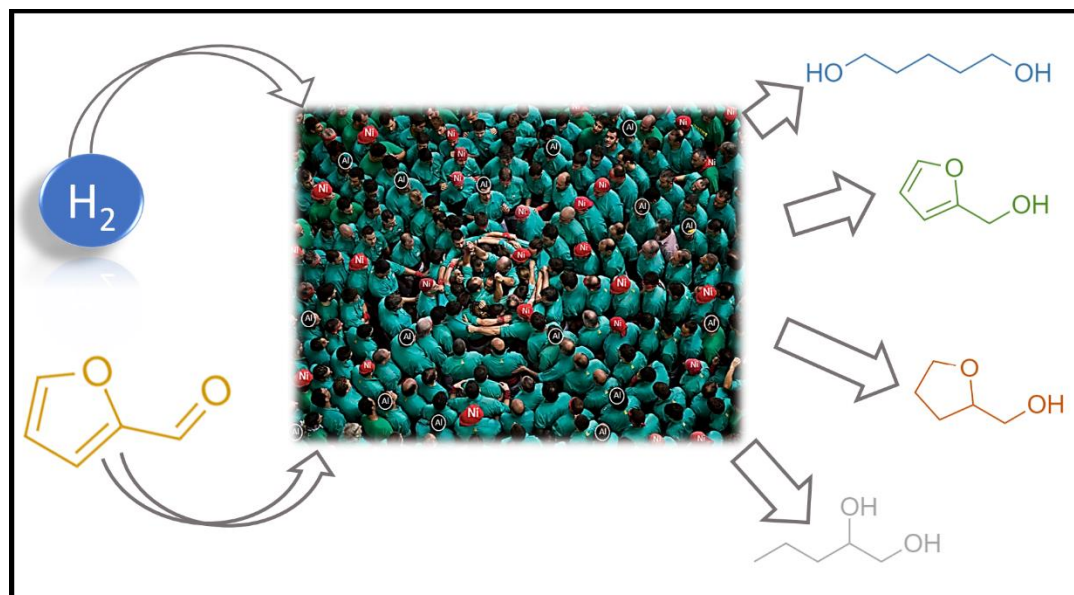


PHOTO BY **David Oliete Casanova**

DOCTORAL THESIS

2022





Abdulaziz Aldureid Kadi Amin

Catalytic Hydrogenation/Hydrogenolysis  
of Biomass-Derived Platform  
Chemicals

**DOCTORAL THESIS**

Supervised By Dr. Daniel Montané Calaf

Dr. Francesc Medina Cabello

**Departament d'Enginyeria Química**



**UNIVERSITAT  
ROVIRA i VIRGILI**

Tarragona  
2022





Universitat Rovira I Virgili  
Departament d'Ingenyeria Química  
Av. Països Catalans, 26 Campus Sescelades 43007, Tarragona  
Tel. 977 55 8675 Fax. 977 55 9621

Dr. Daniel Montané Calaf, Professor of Universitat Rovira i Virgili (Escola  
Tècnica Superior d'Enginyeria Química, Departament d'Enginyeria Química)

STATES:

that the present study, entitled "Catalytic Hydrogenation/Hydrogenolysis of Biomass-Derived Platform Chemicals", presented by Mr. Abdulaziz Aldureid Kadi Amin for the award of the degree of Doctor, has been carried out under my supervision at the Department of Chemical Engineering of this University.

Tarragona, 19<sup>th</sup> October 2022

Doctoral thesis director

A handwritten signature in black ink, appearing to read "D. Calaf", located below the text "Doctoral thesis director".

Dr. Daniel Montané Calaf



Universitat Rovira I Virgili  
Departament d'Ingenyeria Química  
Av. Països Catalans, 26 Campus Sescelades 43007, Tarragona  
Tel. 977 55 8675 Fax. 977 55 9621

Dr. Francesc Medina Cabello, Professor of Universitat Rovira i Virgili (Escola Tècnica Superior d'Enginyeria Química, Departament d'Enginyeria Química) and Group Leader of the research group CatHeter,

STATES:

that the present study, entitled "Catalytic Hydrogenation/Hydrogenolysis of Biomass-Derived Platform Chemicals", presented by Mr. Abdulaziz Aldureid Kadi Amin for the award of the degree of Doctor, has been carried out under my supervision at the Department of Chemical Engineering of this University.

Tarragona, 19<sup>th</sup> October 2022

Doctoral thesis Codirector

A handwritten signature in blue ink, appearing to read 'F. Medina', written over a horizontal line. The signature is stylized and includes a large loop at the beginning.

Dr. Francesc Medina Cabello

# Acknowledgement

I would like to express my deepest appreciation to my Supervisors, Dr. Daniel Montané Calaf and Dr. Francesco Medina Cabello, for all teaching me so many new things throughout this thesis and for all their support, dedication and keen interest for the successful completion of this work.

I thank all the members of the Chemical Engineering Department, especially to my colleagues Alberto and Richard, in addition to Susana Dominguez and Antonio Dafinov for their support in the laboratory.

I would also like to thank Dr. Luis Cabedo and Dr. José Gamez, from the University of Jaume I, for being such brilliant people, for having put me at the beginning of this path and for the science they taught me.

I am grateful to my parents, Mohamad Aldureid and Eman Kadi Amin, my role models, for their nonstop motivation. My sister Muzna, my brother Munzer and my life partner Sara, for standing by and accompanying me to the end of this journey.

I dedicate this work to my late grandfather, to his endless passion, support and encouragement. Today your grandson is a doctor who carries your last name (Kadi Amin).

I also dedicate this work to my homeland, so far away, in the hope that someday it will be closer, and we can rebuild it again.

This work is also dedicated to the victims and detainees of the Faculty of Sciences of Damascus University, they are so close, yet so far away. Lastly, thank God for granting me many opportunities and surrounding me with amazing people.

# Agradecimiento

Agradezco a mis directores, Dr. Daniel Montané Calaf y Dr. Francesco Medina Cabello, por enseñarme tantas cosas nuevas a lo largo de esta tesis y por todo el apoyo, dedicación e interés dispensados en la realización de este trabajo.

A todos los miembros del Departamento de Ingeniería Química, especialmente a mis compañeros Alberto y Richard, también a Susana Dominguez y a Antonio Dafinov por sus apoyo en el laboratorio.

Agradezco a los doctores Luis Cabedo y José Gamez, de la universidad Jaume I, por ser personas brillantes, por haberme puesto en el inicio del camino y por la ciencia que me enseñaron.

A mis padres, Mohamad Aldureid y Eman Kadi Amin, por ser un ejemplo a seguir. A mi hermana Muzna, mi hermano Munzer y a mi compañera de vida Sara, por acompañarme hasta el fin de este camino.

Dedico este trabajo a mi abuelo fallecido, quien me dio todo su apoyo y ánimo. Hoy tu nieto es doctor y lleva tu apellido (Kadi Amin).

Dedico también este trabajo a mi tierra, tan lejana, con la esperanza de que algún día se acerque más y la podamos reconstruir otra vez.

Dedico este trabajo a las víctimas y detenidos de la facultad de las ciencias de la universidad de Damasco, aquellas personas cercanas y lejanas.

Y como no, no podría dejar de agradecer a Dios por haberme proporcionado muchas oportunidades y haberme rodeado de personas increíbles.

## شكر وتقدير

لا يسعني في هذه المناسبة السعيدة جدًا على قلبي إلا أن أقدم آيات العرفان والجميل والشكر الجزيل إلى الذين دعوني ومنحوني ثقتهم وأشرفوا عليّ: الدكتور دانيال مونتانيه الذي تعلمت منه الكثير والدكتور فرانسيسك ميدينا وكافة أعضاء قسم الهندسة الكيميائية، و أخص بالذكر زملائي البرتو و رتشارد، وفي المخبر لسوسانسا و انطونيو.

إلى الدكتور لويس كابيدو و الدكتور خوسيه تامبيث اللذان وضعاني على أول الطريق و علماني الكثير في مجال البحث العلمي.

إلى والداي محمد الدريد و إيمان قاضي أمين لأنهما مثلي الأعلى في هذه الحياة ولأنهما كانا دائماً حافزي على المتابعة والاستمرار، إلى أختي مزنة و أخي منذر وأيضاً إلى شريكتي بالحياة سارة التي عانت معي حتى وصلت إلى آخر هذا الطريق الطويل.

أهدي هذا العمل لروح جدي ، الذي ما توقفت عن إعطائي الدعم و الشغف. اليوم أصبح حفيدك دكتوراً يحمل اسمك (قاضي أمين) بين طيات اسمه.

أهدي هذا العمل لبلدي البعيدة، و كلّي أمل بأن يقترب يوماً ما، و بأن نستطيع بناؤها.

أخيراً، أهديه لشهداء ومعتقلي كُلية العلوم في جامعة دمشق، هؤلاء الأشخاص البعيدون القريبون، الجنود المجهولون لهذه الكُلية.

و كما لا أستطيع أن أنسى شكر الله، لمنحني العديد من الفرص و إحاطتي بأشخاص رائعين.

# Table Of Contents

TABLE OF CONTENTS .....	XI
CHAPTER 1: GENERAL INTRODUCTION .....	2
1. FUEL AND THE NEED FOR A GREEN ALTERNATIVE .....	2
2. BIOMASS AS A SUSTAINABLE ALTERNATIVE .....	3
3. LIGNOCELLULOSE AS BIOMASS SOURCE.....	4
4. HEMICELLULOSE .....	6
5. XYLOSE .....	7
6. FURFURAL.....	9
6.1. PHYSICAL AND CHEMICAL PROPERTIES OF FURFURAL.....	9
6.2. REACTIONS AND USES OF FURFURAL.....	11
6.3. DERIVATIVES OF FURFURAL VIA HYDROGENATION.....	13
<i>Furfuryl Alcohol (FA)</i> .....	13
<i>Tetrahydrofurfuryl Alcohol (TFA)</i> .....	14
<i>1,5-Pentanediol (15PD)</i> .....	15
<i>1,2-Pentanediol (12PD)</i> .....	15
<i>2-Methylfuran (mFUR)</i> .....	18
<i>2-Methyltetrahydrofuran (mTHF)</i> .....	18
<i>Levulinic Acid (LA)</i> .....	19
<i>Furan (FUR)</i> .....	19
<i>Tetrahydrofuran (THF)</i> .....	20
7. CATALYSTS.....	21
7.1. CATEGORIES OF CATALYSTS.....	21
<i>Heterogeneous Catalysts</i> .....	21
<i>Monometallic Catalysts</i> .....	22
<i>Bimetallic Catalysts</i> .....	23
<i>Trimetallic Catalysts</i> .....	24
7.2. HOW DO HETEROGENEOUS CATALYSTS INTERACT WITH FURFURAL?.....	24
7.3. SUITABLE CATALYSTS FOR THE HYDROGENATION OF FURFURAL AND ITS DERIVATIVES	25
<i>Hydrogenation Of Furfural and Its Derivatives by Transition Metals Catalysts</i> .....	26
<i>Hydrogenation Of Furfural and Its Derivatives by Noble Metals Catalysts</i> .....	38
8. LAYERED DOUBLE HYDROXIDES (LDH) .....	49
8.1. DEFINITION OF LDH.....	50

<b>8.2 HT MATERIALS PROPERTIES</b> .....	51
<i>Cation-Exchangeable Brucite-Like Layer</i> .....	51
<i>Anion-Exchangeable Interlayer</i> .....	52
<i>The Memory Effects</i> .....	53
<i>Tunable basicity</i> .....	53
<i>Adsorption capacity</i> .....	53
<b>8.3. HT MATERIALS AS PROMISING CATALYSTS</b> .....	54
<b>9. THESIS OBJECTIVE AND STRUCTURE</b> .....	55
<b>10. REFERENCES</b> .....	58
<b>CHAPTER 2: MATERIALS AND METHODS</b> .....	81
<b>1. INTRODUCTION</b> .....	81
<b>2. SYNTHESIS OF THE CATALYSTS</b> .....	81
<b>3. CATALYST CHARACTERIZATION</b> .....	83
<b>4. CATALYST TESTING</b> .....	85
<b>5. REFERENCES</b> .....	92
<b>CHAPTER 3: NI-CU/AL<sub>2</sub>O<sub>3</sub> FROM LAYERED DOUBLE HYDROXIDES HYDROGENATES FURFURAL TO ALCOHOLS</b> .....	97
<b>1. INTRODUCTION</b> .....	97
<b>2. RESULTS AND DISCUSSION</b> .....	99
2.1. CATALYST CHARACTERIZATION .....	99
2.2. CATALYTIC ACTIVITY TESTS .....	109
<b>3. CONCLUSIONS</b> .....	114
<b>4. REFERENCES</b> .....	115
<b>CHAPTER 4: FURFURAL TO DIOLS OVER NI-CO/AL CATALYSTS</b> .....	122
<b>1. INTRODUCTION</b> .....	122
<b>2. RESULTS AND DISCUSSION</b> .....	125
2.1. CATALYST CHARACTERIZATION .....	125
2.2. CATALYTIC ACTIVITY TESTS .....	137
<b>3. CONCLUSIONS</b> .....	143
<b>4. REFERENCES</b> .....	144
<b>CHAPTER 5: NI-MG/AL PREPARED FROM DOUBLE LAYERED HYDROXIDES (LDHS) AS CATALYSTS FOR THE SELECTIVE CONVERSION OF FURFURAL TO TETRAHYDROFURFURYL ALCOHOL (TFA).</b> 150	
<b>1. INTRODUCTION</b> .....	150

<b>2. RESULTS AND DISCUSSION.....</b>	<b>154</b>
<b>2.1. CATALYST CHARACTERIZATION .....</b>	<b>154</b>
<b>2.2. CATALYTIC ACTIVITY TESTS .....</b>	<b>164</b>
<b>3. CONCLUSIONS .....</b>	<b>171</b>
<b>4. REFERENCES.....</b>	<b>173</b>
<b>CHAPTER 6: GENERAL CONCLUSIONS AND FUTURE WORK .....</b>	<b>180</b>
<b>1. GENERAL CONCLUSIONS .....</b>	<b>180</b>
<b>1.1. CONDITIONS.....</b>	<b>180</b>
<b>1.2. CATALYSTS .....</b>	<b>181</b>
<b>1.3. REACTORS.....</b>	<b>183</b>
<b>2. FUTURE WORK.....</b>	<b>184</b>
<b>3.REFERENCES .....</b>	<b>186</b>
<b>INDEXES.....</b>	<b>190</b>
<b>INDEX OF FIGURES:.....</b>	<b>190</b>
<b>CHAPTER 1.....</b>	<b>190</b>
<b>CHAPTER 2.....</b>	<b>191</b>
<b>CHAPTER 3.....</b>	<b>191</b>
<b>CHAPTER 4.....</b>	<b>192</b>
<b>CHAPTER 5.....</b>	<b>192</b>
<b>INDEX OF SCHEMES: .....</b>	<b>193</b>
<b>INDEX OF EQUATIONS: .....</b>	<b>194</b>
<b>INDEX OF TABLES:.....</b>	<b>194</b>
<b>CHAPTER 1.....</b>	<b>194</b>
<b>CHAPTER 2.....</b>	<b>195</b>
<b>CHAPTER 3.....</b>	<b>195</b>
<b>CHAPTER 4.....</b>	<b>195</b>
<b>CHAPTER 5.....</b>	<b>195</b>
<b>INDEX OF CATALYSTS:.....</b>	<b>196</b>
<b>INDEX OF ABBREVIATION: .....</b>	<b>197</b>
<b>1. COMPOUNDS.....</b>	<b>197</b>
<b>2. REACTORS.....</b>	<b>198</b>

<b>3. TECHNIQUES AND ANALYSIS METHODS .....</b>	<b>198</b>
<b>LIST OF EVENTS ATTENDED AND CONTRIBUTIONS.....</b>	<b>199</b>
<b>LIST OF THESIS OUTCOMES .....</b>	<b>200</b>

# Chapter one

---

# General Introduction

# Chapter 1: General introduction

## 1. Fuel and The Need for a Green Alternative

Over the last hundred years, fossil resources such as petroleum, natural gas, and coal have been the main energy sources for transportation fuels and chemicals production and have played a vital role in achieving economic growth [1,2]. Society's demand for energy had previously been dependent on plant biomass [3]. In the mid-1800s, for example, biomass satisfied over 90% of U.S. energy and fuel needs. In many developing countries, biomass still serves as a main energy source [4]. In the EU28 countries, the consumption of solid biofuel (all solid organic components to be used as fuels) has practically doubled since 2000 after accounting for over 100 Mtoe in 2019 [5].

By 2019, roughly 40.4% of the energy consumed worldwide came from oil resources while 16.4% came from natural gas [6] (Figure 1.1).

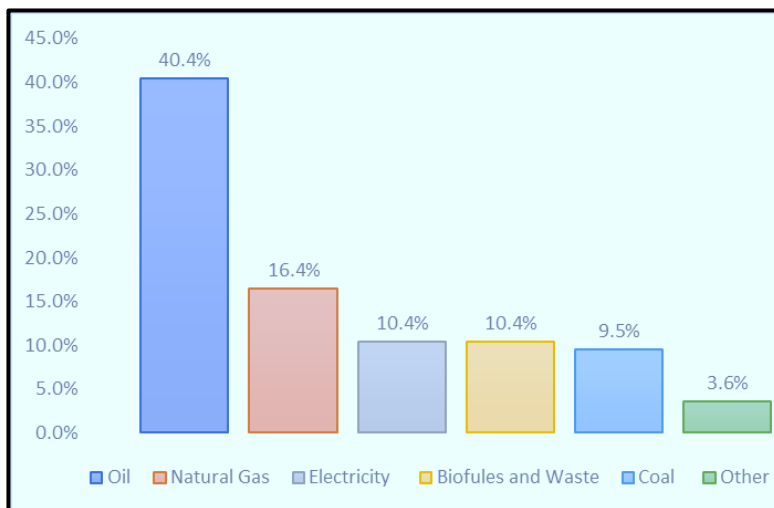


**Figure 1.1** The global consumption energy by 2019 [6]. Source: <https://www.iea.org/reports/key-world-energy-statistics-2021/final-consumption>

## General Introduction

Demand on energy sources has been rising in the last five decades. However, no remarkable changes in the amount of energy produced from oil or natural gas have been observed: oil consumption, for example, decreased from 48.5% in 1973 to 40.4% in 2019, while gas consumption ranged between 14.1% in 1973 and 16.4% in 2019 [6]. However, these resources are limited and their associated release of CO<sub>2</sub> into the atmosphere has led to climate change and global warming [3,7].

So, abrupt increases in global fossil CO<sub>2</sub> emissions [11], the growing shortage of fossil hydrocarbons, the rise in oil prices, concerns about greenhouse gas (GHG) emissions, and the projected mounting future demand for energy have encouraged society to search for new renewable resources that can replace fossil fuels in the current energy system [8].

At the same time, diminishing fossil fuel reservoirs and the ever-worsening environmental situation linked to worldwide fossil-fuel-based industries make the use of alternative feedstock imperative [3,9,10].

## 2. Biomass as a Sustainable Alternative

Solutions include replacing fossil fuel with renewable sources such as solar, wind, hydroelectric and geothermal power to produce heat and electricity. However, biomass is the only sustainable source of organic carbon on earth suggested as the perfect equivalent to petroleum for producing fuels, chemicals and carbon-based materials [12].

Thanks to its renewable capacity and vast reserves, biomass, which for thousands of years has been used directly via combustion to produce heat, is believed to have the capacity to satisfy our basic needs for the sustainable production of liquid transportation fuels and chemicals without threatening the needs of future generations [3,8].

## General Introduction

Since biomass has been considered a sustainable alternative to fossil resources, the efficient use of biomass has attracted significant interest from the scientific and industrial communities [13,15]. Biomass is an abundant, sustainable, non-edible material, and a cost-efficient source of organic chemicals and liquid biofuels [9, 16, 17]. Moreover, using biomass is environmentally less harmful than using fossil resources [3]. Biomass can form not only on agricultural land but also on forest, aquatic, and arid land. Though nature produces a wide range of structures from biomass, most biomass is built from a few basic monomer units [3].

Biomass as feedstock can be taken from the following sources: waste materials (agricultural waste, crop residues, wood waste, urban waste), forest products (wood, logging residues, trees, shrubs), energy crops (starch crops such as corn, wheat and barley; sugar crops; grasses; woody crops; vegetable oils; hydrocarbon plants), and aquatic materials (algae, water weeds, water hyacinths) [3]. Biomass can be transformed into chemicals and fuels by three different techniques, i.e., thermal, biochemical, or chemical.

### **3. Lignocellulose as Biomass Source**

Lignocellulose is the least expensive and most abundant source of biomass; for example, high-yield lignocellulosic energy crops such as switchgrass can be grown. A different approach is to use lignocellulosic biomass residues such as agricultural, industrial, and forest wastes. Biomass can be converted into liquid fuels via three primary routes (see Figure 1.2), i.e. syngas production by gasification, bio-oil production by pyrolysis or liquefaction, and hydrolysis of biomass to produce sugar monomer units and other high-value chemicals [21].

General Introduction

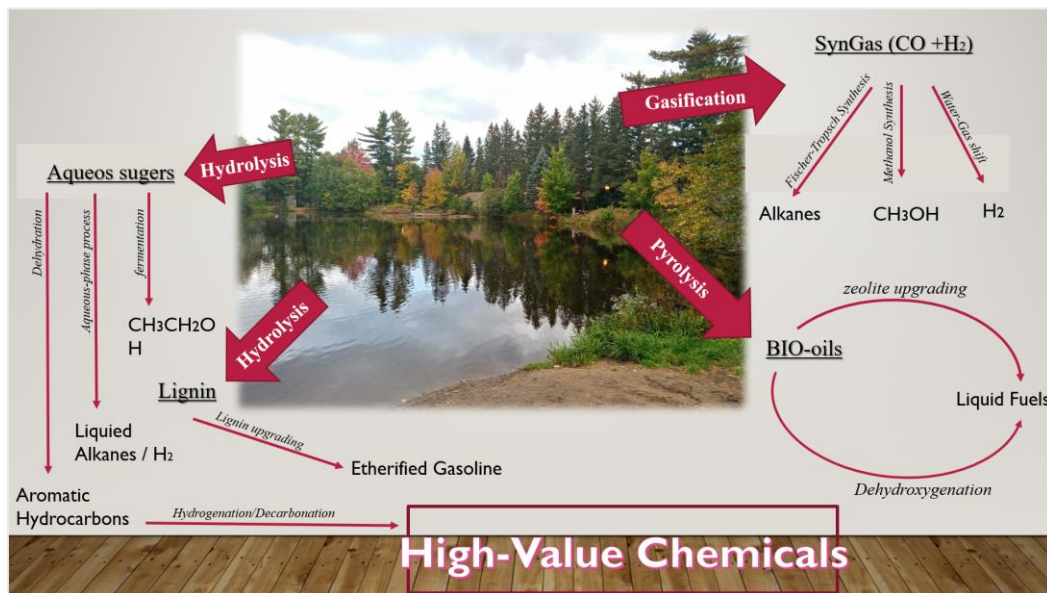


**Figure 1.2.** Process to produce fuel, hydrogen and high-value chemicals from biomass [21].

Lignocellulose is a polymeric material comprising three primary units (Figure 1.3): cellulose (30% to 50%), which is a crystalline polymer of glucose units; hemicellulose (20% to 35%), which is a highly branched polymer with a wide amorphous zone of five different C<sub>5</sub> and C<sub>6</sub> sugars; and lignin (10% to 25%), which is a three-dimensional polymer of propyl-phenol that surrounds the cellulose and hemicellulose [20,23].

## General Introduction

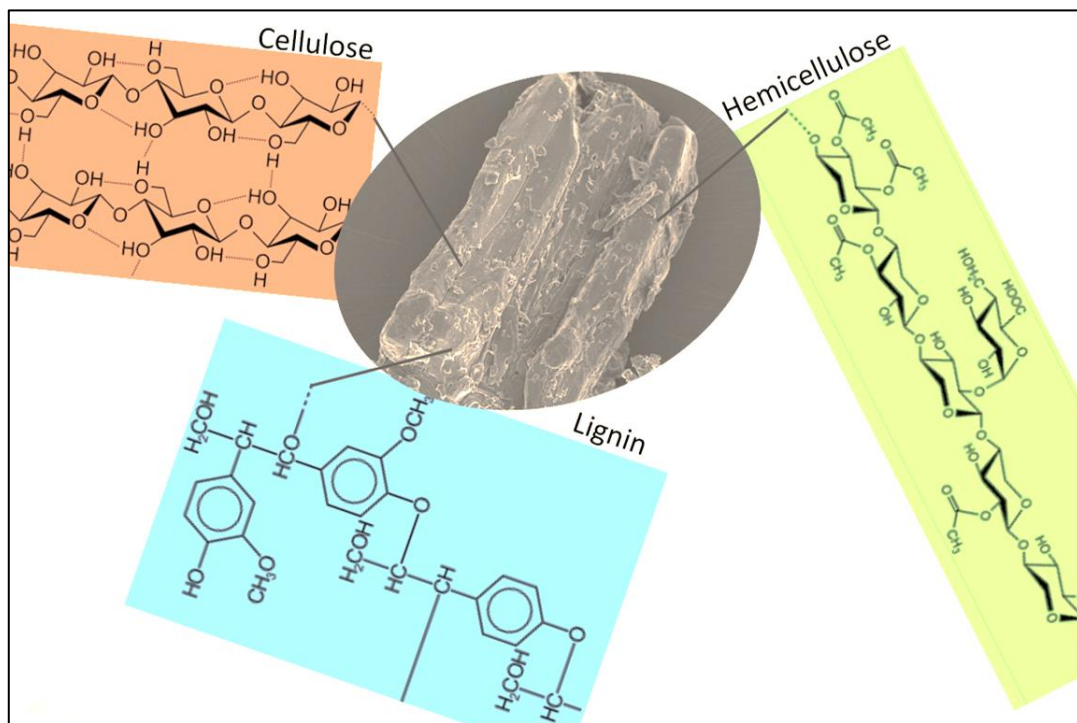


**Figure 1.3.** The three main components of lignocellulose; cellulose, hemicellulose and lignin [20].

## 4. Hemicellulose

The most interesting building block of hemicellulose is xylan (a sugar polymer that consists mainly of xylose and four other sugars linked to the [ $\beta$  (1 and 4 positions)] glycosidic bonds) [29].

Important  $C_5$  sugars can be formed from hemicellulose, the acidic hydrolysis can produce xylose via one-step hemicellulose deconstruction and xylose dehydration in the same reactor by cleavage of the C–O bonds present between adjacent sugar molecules (Figure 1.4) [20,42,46].

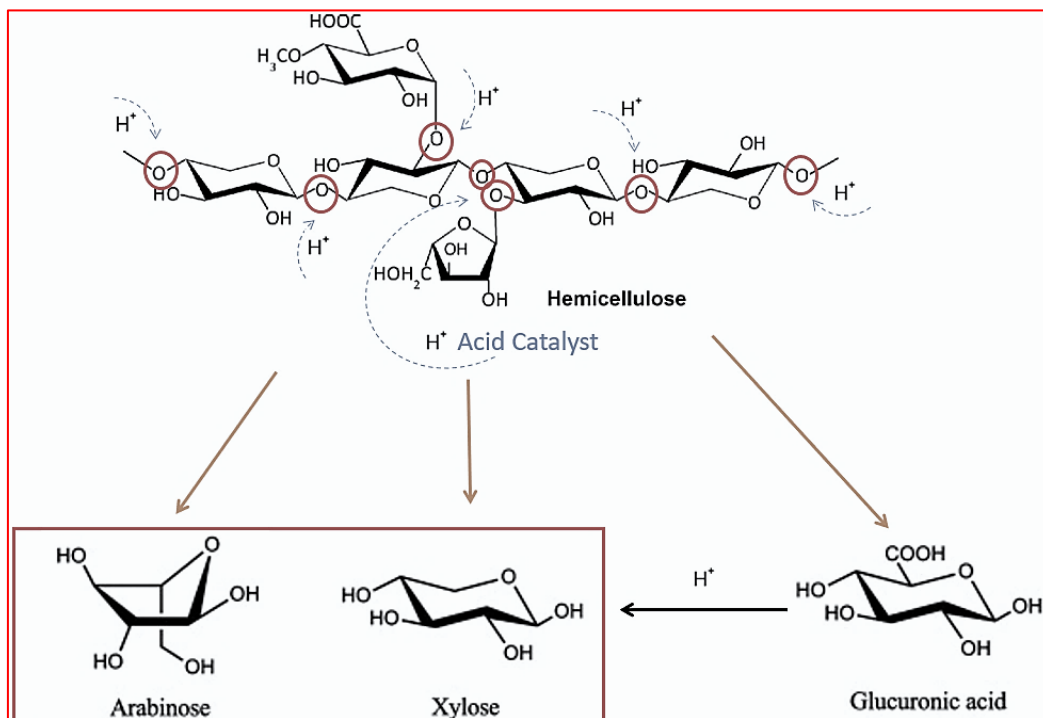


**Figure 1.4.** Sites of proton attack during the hemicellulose hydrolysis [20].

## 5. Xylose

Xylose ( $C_5H_{10}O_5$ ), or wood sugar, is a  $C_5$  monosaccharide of aldo-pentose type (Figure 1.5). It is the most abundant pentose sugar [47].

Many researchers have investigated its applications, especially those that involve converting xylose into added-value chemicals such as ethanol, furfural and xylitol.

General Introduction

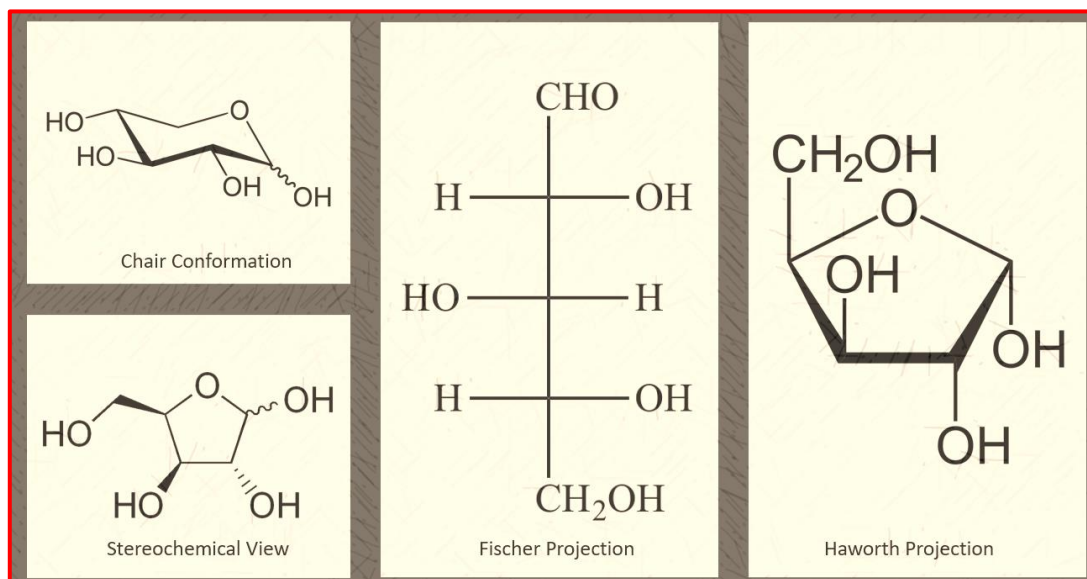


**Figure 1.5.** The different stereo-chemical structure of Xylose [272].

Xylose was first isolated from wood by the Finnish scientist Koch in 1881 [48]. It is also found in certain species of Chrysolina beetles, such as *Chrysolina coerulans*, which have cardiac glycosides (including xylose) in their defensive glands [49].

As a C<sub>5</sub> sugar, xylose is a valuable building block in the industry due to its leading role in various chemical and biological processes for producing chemicals such as furfural.

Furfural was synthesized via xylose dehydration under acidic conditions [54,55]. It is formed by the isomerization of xylose into its corresponding ketose (xylulose), which can play the intermediate role as it is believed to be more prone to dehydration [56]. This process can be achieved by both acid and base catalysis [57].

## 6. Furfural

### 6.1. Physical and Chemical Properties of Furfural

Furfural is a furan derivative produced from the hemicellulosic portion of lignocellulose [60]. It is a heterocyclic and aromatic aldehyde that consists of a furan ring with an aldehyde side group. It is also known as 2-furancarboxyaldehyde, furaldehyde, 2-furaldehyde, fural, and furfuraldehyde. Furfural is oily, has an almond-like odor, and is a colorless liquid that turns yellow to dark brown when exposed to air [60]. The physical properties of furfural are listed in Table 1.1.

**Table 1.1.** Physical properties of furfural Properties [60].

<i>Molecular formula</i>	<i>C<sub>5</sub>H<sub>4</sub>O<sub>2</sub></i>
<i>Molecular weight (gmol<sup>-1</sup>)</i>	96.1
<i>Boiling point (°C)</i>	161.7
<i>Melting point (°C)</i>	-37
<i>Density at 20°C (g/ml)</i>	1.16
<i>Solubility in water (g/L)</i>	83
<i>Vapor pressure (mmHg, 20°C)</i>	2

Thanks to its excellent physical properties, it is used as a selective extractant in various industries [61-63], for example to extract aromatics from lubricating oils, which improve their performance and to eliminate aromatics from diesel fuels that enhance the ignition properties [64,65]. To synthesis furfural more than one mechanism, based on several techniques and under different reaction conditions, have been reported.

The first mechanism can begin from the acyclic form of the pentose, followed by dehydration of a 1,2-enediol intermediate (Figure 1.6 - 1) [66]. A second mechanism is through direct dehydration, which can occur via a 2,3-( $\alpha,\beta$ ) unsaturated aldehyde (Figure 1.6 - 2) [67].

General Introduction

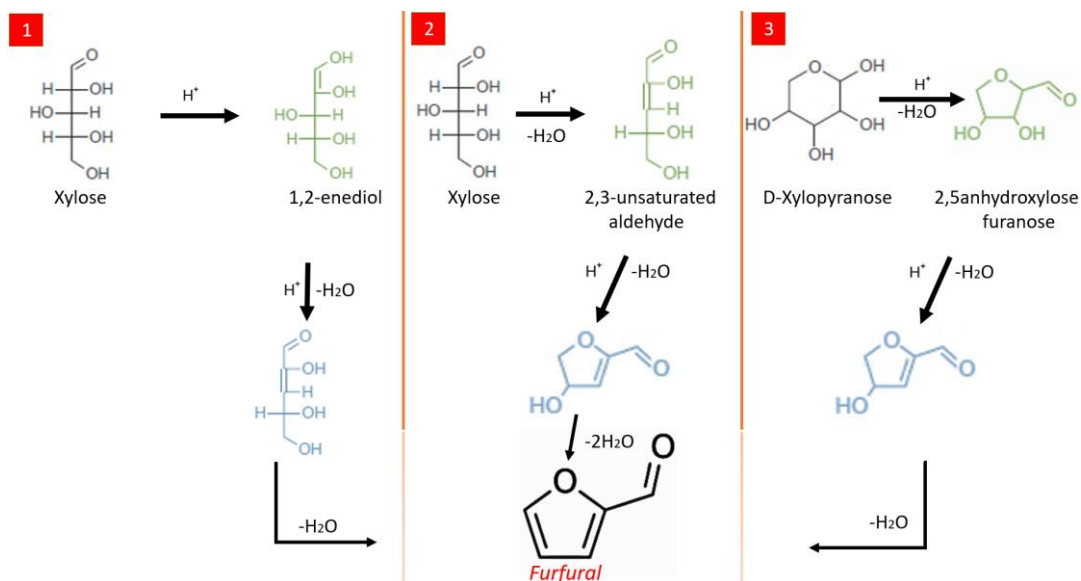


**Figure 1.6.** The three suggested mechanism of furfural production from xylose [66,67,68]. Green molecules: First phase intermediates, Blue molecules: Second phase intermediate.

With the last mechanism the reaction begins by producing an intermediate compound of 2,5-anhydroxylose furanose from the cyclic form of xylose (pyranose), which is formed by the action of  $H^+$  on the  $O^{-2}$  of the pyranose ring, and which is then dehydrated to produce furfural [68].

As Figure 1.7 shows, furfural has two major functional groups: an aldehyde group (CHO) and two olefin groups (CH=CH). It is a versatile compound for many applications.

## General Introduction

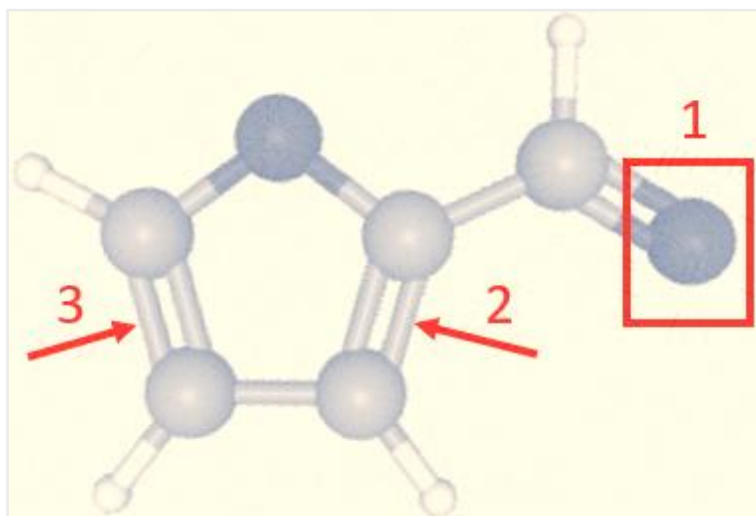


**Figure 1.7.** The reactive sites of furfural.

## 6.2. Reactions and Uses of Furfural

The reactions – including reductive amination to amines, reduction to alcohols, decarboxylation, oxidation to carboxylic acids, Grignard reactions, and aldol and Knoevenagel condensation – can occur in furfural through the aldehyde functional group ( $C=O$ ), while reactions such as alkylation, hydrogenation, oxidation, halogenation, open ring reactions, and nitration are enabled through the furan-ring system ( $C=C-C=C$ ) [69] (Figure 1.8).

One application of furfural is its use in the purification technology of  $C_4$  and  $C_5$  from hydrocarbons. It has been used in the purification of butadiene via the extractive distillation of butadiene with furfural, which separates it from other hydrocarbons. Butadiene is then ready to produce synthetic rubber [60,70].

Furfural is also used to manufacture inks, plastics, antacids, adhesives, nematicides, fungicides, fertilizers, flavoring compounds [71] and cross-linked polymers [64,65]. It is especially efficient in preventing the growth of wheat smut, which is eliminated by soaking the wheat for 3 h in a 0.05% aqueous solution of furfural [61-63]. It is reported that the industrial production of furfural was begun in 1921 by Quaker

General Introduction

Oats, which used various substrates [72]. Bozell et al., for their part, have proposed classifying furfural as one of the most promising chemicals for the sustainable production of fuels and chemicals in the 21st century [73].

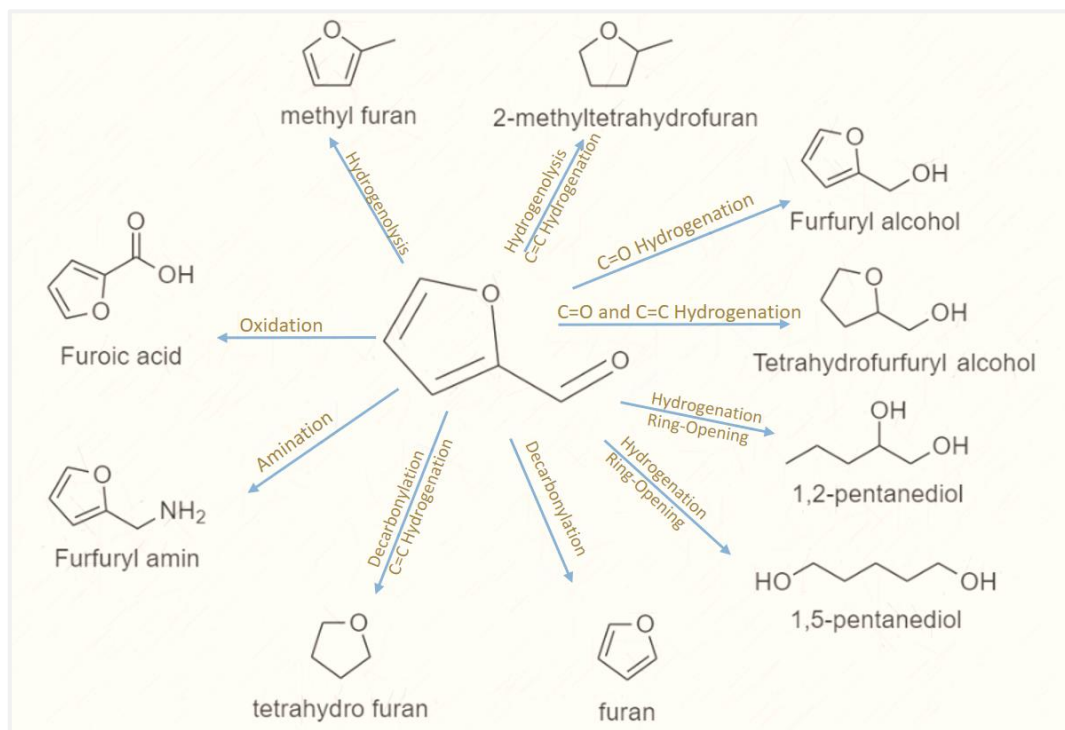


**Figure 1.8.** Reactions of furfural through aldehyde group and furan-rings' bonds [60].

In 2021, the furfural market was estimated at approximately 566 million U.S. dollars worldwide. By 2029, the global market value of this solvent is expected to increase to almost 731 million U.S. dollars (Figure 1.9) [74]. The compound annual growth rate (CAGR) for this chemical was 13.3% from 2014 to 2020 [74]. China, the main producer of furfural, accounts for 85% of global production capacity and 75% of world consumption [60]. Current environmental concerns highlighting the need to lower our use of conventional petrochemicals, as well as the emergence of novel furfural applications, are driving forces behind the global furfural market [60].

## General Introduction

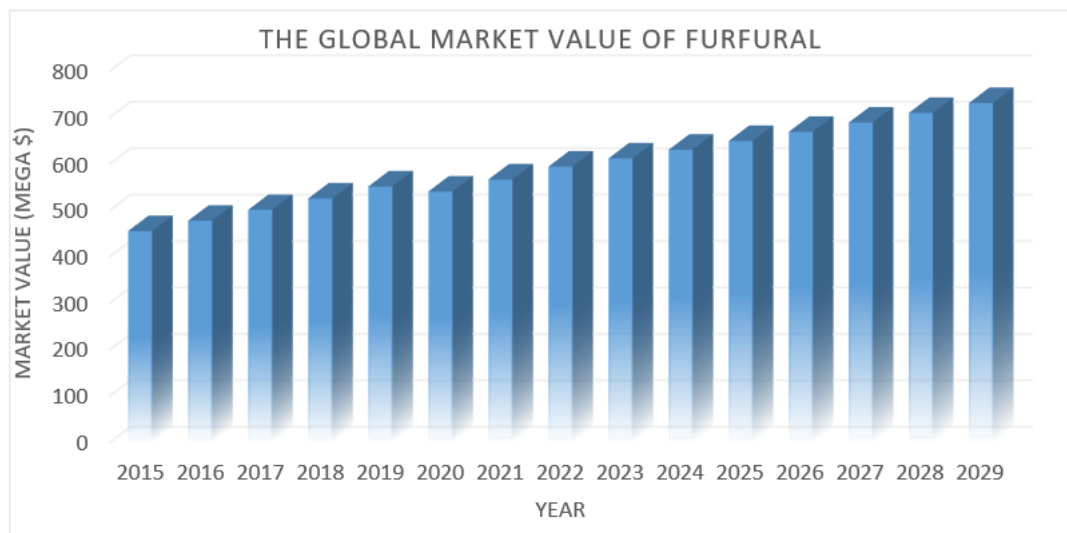


**Figure 1.9.** Furfural market value, adapted from reference [74].

### 6.3. Derivatives of Furfural Via Hydrogenation

Furfural can be converted via the hydrogenation process into different added-value chemicals. We are specifically interested in synthesizing Furfuryl Alcohol (FA), Tetrahydrofurfuryl Alcohol (TFA), 1,5-Pentanediol (15PD) and 1,2-Pentanediol (12PD) due to their great value and important role in the chemical industry (Table 1.2.)

#### Furfuryl Alcohol (FA)

Furfuryl alcohol (FA) is one of the most common compounds produced from the furfural hydrogenation process. Indeed, it has been speculated that roughly 62% of the global production of furfural is used to synthesize furfuryl alcohol each year [69].

The main application of furfuryl alcohol is in the manufacture of foundry resins, which are mostly produced through the cross-linked polymers of furfuryl alcohol with itself and with other products such as furfural, formaldehyde, phenolic compounds, and urea, etc. The resins obtained showed excellent chemical, thermal

## General Introduction

and mechanical properties. Furfuryl alcohol has also exhibited anti-corrosion and solvent-action properties [79]. For this reason, it has been used in the production of furan fiber-reinforced plastics in the piping industry and in high-performance chemical processes of chlorinated aromatics and oxygenated organic solvents [79]. It is also used as a precursor of ascorbic acid, levulinic acid, and lysine and in the industry of lubricants [76]. More applications summarized in Table. 1.2

In the last few decades, several varieties of catalysts and advanced methods have been developed for producing furfuryl alcohol through the hydrogenation of furfural. One of the most common catalysts for this is the copper/chromite-based catalyst [80-84]. The hydrogenation of furfural to furfuryl alcohol is relatively facile and has become more advanced in recent decades [69].

### **Tetrahydrofurfuryl Alcohol (TFA)**

Tetrahydrofurfuryl alcohol (TFA) has a molecular formula of  $C_5H_{10}O_2$  and a molecular weight of  $102 \text{ g}\cdot\text{mol}^{-1}$  [61,62]. It is a transparent, mobile, high-boiling liquid with mild odor that is completely miscible with water. It has many uses as a green solvent in, for example, agricultural applications, printing inks, industrial cleaners, and cleaners for electronics [69].

TFA can be utilized as raw material to produce important biofuels such as, tetrahydrofuran, 1,2-pentanediol and 1,5-pentanediol [77-78]. It has been considered as one of the advanced biofuels obtained from biomass which can play a significant role in reducing the fossil fuel consumption and the emissions of  $CO_2$  from Internal-combustion engine [102-106] (Table. 1.2).

It is produced industrially by Koatsu Chemical Industries in Japan with a production volume of roughly 30 tons per year. On the laboratory scale, tetrahydrofurfuryl alcohol can be directly produced from the hydrogenation of furfural or by forming

## General Introduction

furfuryl alcohol as intermediate product over distinct noble and non-noble metal catalysts [69,85,86].

### **1,5-Pentanediol (15PD)**

Two alcohol groups at both terminal positions provide 1,5-pentanediol with low viscosity and low glass transition temperatures, which make it a good candidate for use as a monomer in chemical processes such as the manufacture of polyester and polyurethane resins [90-92]. It has also been used to produce coatings, acrylates and adhesives [93] (Table. 1.2). Globally, the price of 1,5-pentanediol is 9,700 USD per ton and its market size in 2020 was nearly 133 million USD [94].

Because C<sub>5</sub> petroleum feedstocks are still not readily available, 1,5-pentanediol is still not produced on a large scale [91,92], which makes the unconventional selective production derived from bio-based C<sub>5</sub> feedstocks an alternative approach [93].

In 2009, selective hydrogenolysis of TFA was performed by the Tomishige group to synthesize 1,5-PD over heterogeneous noble bimetallic catalysts [95,96]. Also, many researchers have recently studied this synthesis through hydrogenolysis applied to furfural and furfuryl alcohol over several catalysts of monometallic, bimetallic, and trimetallic systems, including noble and non-noble metals [93].

### **1,2-Pentanediol (12PD)**

Like 15PD, 1,2-pentanediol is a high-value chemical that can be used as a monomer in the production of polyesters [115] and as an intermediate in the synthesis of fungicides [116]. It can also be used in the production of disinfectants, printing inks [117] and cosmetics [118] (Table. 1.2).

One conventional method for producing 1,2-pentanediol is via the oxidation of 1-pentene to 1,2-epoxypentene followed by a hydrolysis process to obtain 1,2-

## General Introduction

pentanediol that comprises a complex multistep system requiring sources of petroleum [115]. To address this, the need emerged for a new green sustainable synthesis of 1,2-Pentanediol from biomass-derived chemicals [119].

The synthesis of 1,2-Pentanediol from furanic compounds has been investigated over a few catalysts [120-122]. However, this synthesis still faces the problem of the low selectivity of 1,2-pentanediol, which drives researchers to discover an efficient catalytic system for producing it [123].

General Introduction

**Table 1.2.** Applications of Furfuryl Alcohol (FA), Tetrahydrofurfuryl Alcohol (TFA), 1,2-Pentenediol (12PD) and 1,5-Pentenediol (15PD) in the chemical industry.

<b>Compound</b>	<b>Uses and Industrial Applications</b>	<b>Reference</b>
<i>Furfuryl alcohol (FA)</i>	Piping industry	9,61,63,79
	Resins	79
	Pharmaceuticals	9,61,63
	Adhesive	61,63,9
	Anti-corrosion agent	79
	Fuel additives	273,274
	Solvent	273,274
<i>Tetrahydrofurfuryl alcohol (TFA)</i>	Wetting agent	63
	Green solvent	69
	Printing inks	69
	Electronics cleaners	69
	Biofuel	189
	Diesel additives	96
	Pyridine raw material	189
<i>1,2-Pentenediol (12PD)</i>	Dihydropyran raw material	189
	1,5- pentenediol raw material	189
	Intermediate in fungicides synthesis	116
	Production of polyesters	115
	Cosmetics	118
	Monomers of polyurethanes	253, 266
	Disinfectant	119
<i>1,5-Pentenediol (15PD)</i>	Printing ink	117
	Air care products	275
	Polishes, wax blends	275
	Production of polyester	90, 92
	Adhesives manufacturing	93
	Resins	90, 92
	Monomers of polyamides	253, 266
<i>1,5-Pentenediol (15PD)</i>	Monomer in coatings industry	93
	Monomers in acrylates production	93
	Polyurethane production	93
	Adhesives	93

## 2-Methylfuran (mFUR)

2-methylfuran (mFUR) is colorless mobile liquid with high solvent power [69]. The chemical properties of 2-methylfuran are usually comparable to conventional solvents like furan and THF, while their physical properties are compared with bioethanol and GVL [69].

It has recently been suggested that it is highly promising biofuel components [69]. Its performance is higher than other biofuels [111], and it can also be used directly in the process of the internal combustion engine [114].

One application of 2-methylfuran is its use as feedstock for the production of substances such as antimalarial drugs (chloroquine), methyl furfural, 2-Methyltetrahydrofuran, furan and sulfur heterocycles. It is also considered to be a good solvent [3,65,70,84,124].

Conducting reactions under high temperature and low pressure can selectively convert furfural into 2-methylfuran via the formation of an intermediate of furfuryl alcohol [127,128]. The temperature degree of the reaction should be gradually increased in order to avoid the coke deactivation over catalysts. [129]

## 2-Methyltetrahydrofuran (mTHF)

Like mFUR, 2-methyltetrahydrofuran (mTHF) is colorless mobile liquid with high solvent power compared to furan and THF [69].

One feature of 2-methyltetrahydrofuran is that it is inversely soluble in water, which means that its solubility decreases as the temperature increases [69]. mTHF is used as a solvent due to its high boiling temperature. It can also be used in electrolyte formulation for secondary lithium electrodes [65,84] and as a component of alternative fuels [3,75,124-126].

## General Introduction

Regarding the production of mTHF, is produced most efficiently via two routes: i.e. the hydrogenation of levulinic acid (LA) [136], or the hydrogenation of 2-methylfuran over different catalysts. [133-138].

### **Levulinic Acid (LA)**

$C_5H_8O_3$  is the chemical formula of the Levulinic Acid (LA), it is an organic acid derived from biomass [130]. Due to its high reactivity in hydrogenation, oxidation and esterification, it has been used in different industries like, the manufacture of drugs, fungicides, pesticides and fuel additives [131,132].

In 2004, It was classified among the most promising five-carbon compounds by the US Department of Energy and the US Department of Agriculture [132].

Although LA was synthesized for the first time by using fructose as feedstock and HCl as acidic catalyst, but it is produced most efficiently via the hydrogenation of furfural by forming furfuryl alcohol which further will be converted into Levulinic Acid [109, 130, 132].

### **Furan (FUR)**

Furan is synthesized by several methods. The first of these is the catalytic decarbonylation of furfural at high temperature as a side reaction during furfural hydrogenation, accompanied by a molecule of carbon monoxide (Figure 1.10.) [139, 141-144].

Another method is the Cannizzaro reaction, which produces the intermediate furoic acid, followed by decarboxylation [140]. A third, a commercial method, that produces furan at over 96% and is applied by heating furfural over Pd catalysts with potassium carbonate to facilitate the reaction [61].

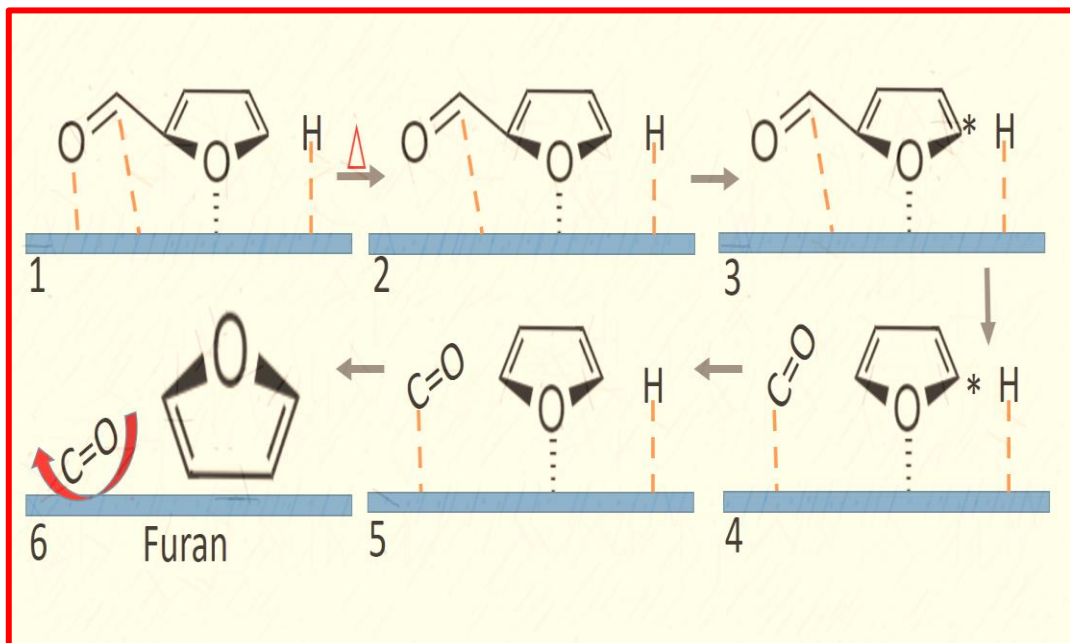


**Figure 1.10.** Furfural decarbonylation into furan [139].

## Tetrahydrofuran (THF)

Tetrahydrofuran is one of the most important solvents for chromatographic techniques such as gel phase chromatography and certain specialty syntheses of complex catalysts and Grignard reagents [2,3,14]. It is prepared via the hydrogenation of furan, which is one of its most attractive uses, and may be considered it as a promising alternative due to its renewable resources [61-63]. One of the main issues for THF production from furan today is the large amount of coke produced during the process, which diminishes catalytic activity and THF yield [69].

Another use of THF is as a precursor in anionic polymerization. For example, THF is the monomer polymerized under strongly acidic conditions for producing polytetramethylene ether glycol, which is involved in the manufacture of urethane elastomers and fibers [62,145]. Other reported applications of THF are as adhesives, PVC cement, vinyl films and cellophane [146,147].

Also, THF can be produced by the catalytic hydrogenation of maleic anhydride, via the cyclodehydration of 1,4-butanediol [148].

## 7. Catalysts

Like several other hydrogenation chemistries, using catalysts is imperative for maintaining balanced reaction activity and selectivity [149]. Below, we explained some of general definitions of catalysts.

### 7.1. Categories of Catalysts

The three main categories of catalysts are bio-catalysts, homogeneous catalysts and heterogeneous catalysts. Biocatalysts are natural, sensitive and selective catalysts that involve rapid reactions occurring under mild conditions [158,159]. Homogeneous catalysts exert their action in the same phase as the other reaction components (typically a liquid phase), while heterogeneous catalysts exert their action in a different phase to other components of the reaction mixture. Below, we give further details on Heterogeneous catalysts.

#### Heterogeneous Catalysts

Heterogeneous catalysis comprises two physical phases. The catalyst must be in a different phase from the reaction mixture, which limits the interaction between the reactant and the catalyst. Interaction with the catalyst merely involves temporary adsorption between the catalyst's surface and the substrate at active sites, where the desired transformation can be carried out. The products formed can then desorb from the catalyst's surface due to the weakness of the bond linkages created. [158].

Most commercial products of heterogeneous catalysts are often made by nanometer-sized particles supported on an inert material or metal oxide, such as

## General Introduction

TiO<sub>2</sub>, Al<sub>2</sub>O<sub>3</sub>, active carbon, etc. The catalyst can be designed by various methods to achieve high activity, good selectivity and long stability. These are crucial challenges when developing this type of catalyst. The advantages of heterogeneous catalysts are that they can be simple to handle, easy to recycle, and able to reuse their solid part, which minimizes waste and matches the 12 principles of Green Chemistry [164]. Additionally, heterogeneous catalysts have a broad commercial application in the production of inorganic chemicals and petrochemically derived compounds, as well as in novel green applications [165,166].

Heterogeneous catalysts can be classified according to principles such as the nature of the active center, the method used during the catalytic reaction, the metal content, etc. When classified by nature of their active center, they can be divided into metallic, acidic, or basic heterogeneous catalysts [167].

When classified by the process used, they can be divided into catalysts suitable for fixed-bed processes and slurry or fluidized-bed processes [168].

When classified by metallic content, they are known as monometallic, bimetallic, and trimetallic catalysts [89,159,169,170]. Below we explain the difference between the three types of metallic catalysts. Later, we list further details on noble and non-noble metal catalysts.

### **Monometallic Catalysts**

Monometallic catalysts are those that contain only a single metal species. They are based, for example, on just one noble metal, such as platinum, palladium, iridium, or just one transition metal, such as cobalt, nickel, copper, chromium, etc.

Monometallic materials have catalyzed many organic synthesis reactions and played an important role in producing numerous chemicals, for example,

hydrogenation reactions [89,99], coupling reactions of alkyl halides [171,172], ethanol steam reforming, and biogas reforming [170].

## **Bimetallic Catalysts**

Bimetallic catalysts contain two separately active metals. They may be prepared at the same or at different metal ratios, which may significantly influence the synergistic effect that makes them superior to monometallic catalysts [170].

In the 1960s, commercial production began to pay attention to bimetallic catalysts after new applications were found in the reformulation of hydrocarbon [173-175]. The surface of bimetallic catalysts typically demonstrates novel properties that are not provided on the surfaces of their parent metals [176-179]. The higher performance of bimetallic catalysts in comparison with monometallic catalysts can provide exceptional characteristics, including greater stability owing to the addition of the second metal, a longer catalyst life [169], a greater surface area, enhanced dispersion, and greater stability against coking [170].

Bimetallic catalysts create these characteristics thanks to two critical factors that affect the modification of the electronic and chemical properties of a metal on the surface. The first factor is the formation of heteroatom bonds that change the electronic nature and structure of the metal's surface. The second is the geometry of the bimetallic structure, which is different from that of the parent metals from which the bimetallic catalyst is derived [180]. The proportion of metal on the catalyst's surface is relatively higher than its proportion in bulk [170].

Moreover, adding a second metal to a monometallic alloy may decrease the reduction temperature, since the metal particles are more dispersed and can be reduced more easily than those in bulk [86,181]. Bimetallic components can catalyze and electro-catalyze numerous industrial applications, including

hydrogenation, dehydrogenation, reformulation, and oxidation reactions [182,185].

### **Trimetallic Catalysts**

Trimetallic catalysts are bimetallic catalysts that can obtain higher performance by adding a third metal onto their alloys [182]. Epron and colleagues, for example, attributed the greater stability of the catalysts and the higher selectivity when producing toluene from n-heptane to the addition of Sn onto the Pt–Ir bimetallic alloy [186].

In some cases, Trimetallic catalysts have shown significantly higher catalytic activities than the corresponding monometallic or bimetallic catalysts [187].

## **7.2. How Do Heterogeneous Catalysts Interact with Furfural?**

The heterogeneous catalysis process typically consists of a catalyst surface, which represents the solid phase, the substrates in the gas or liquid phase, and the bonds between them. The process may be regarded as a cycle involving the reactants' molecular adsorption, the reaction, and the products' molecular desorption, which occur on the catalyst surface. Certain circumstances, such as thermodynamics, mass transfer and heat transfer, can affect the reaction rate [159].

The hydrogenation of furan compounds derived from biomass was catalyzed by heterogeneous catalysts. See Figure 1.11 for a potential energy diagram suggested for the furfural hydrogenation at the catalyst surface.

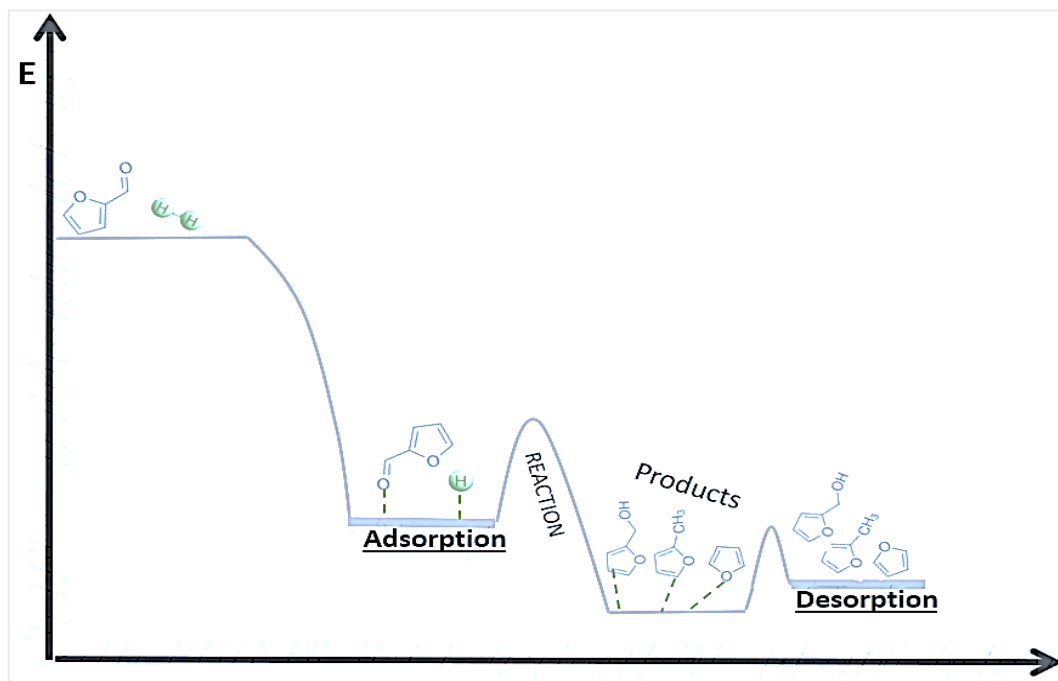


**Figure 1.11.** Potential energy diagram of the furfural hydrogenation over heterogeneous catalysts [159].

### 7.3. Suitable Catalysts for the Hydrogenation of Furfural and Its Derivatives

As aforementioned, furfural can be converted by hydrogenation into a wide range of high-value products with advantages comprising the sustainable production of fuel additives and the synthesis of chemicals. Chemicals such as furfuryl alcohol (FA), tetrahydrofurfuryl alcohol (TFA), 1,2-pentanediol (12PD), 1,5-pentanediol (15PD) and 2-methyl furan (mFUR) or tetrahydrofuran (THF) and furan (FUR) can be obtained from furfural [61-63,75-77].

The hydrogenation process requires catalytic promoting in order to improve the reaction activity and control the product's selectivity. Numerous studies have tested different metallic catalysts based on noble and non-noble metals. Below we

## General Introduction

summarize several studies that have investigated the hydrogenation of furfural over a wide range of catalysts.

### Hydrogenation Of Furfural and Its Derivatives by Transition Metals Catalysts

Transition metals are the elements in the d-block of the periodic table, which includes metals such as nickel, iron, cobalt, copper, chrome, zinc and others of groups 3 to 12 in the periodic table (Figure 1.12) [24,25].

The high cost of noble metals has made catalysts based on transition metals competitive and promising alternatives. Many studies have reported the hydrogenation of furfural over transition metals with a high reaction rate and the required selectivity towards the desired products. Copper, cobalt and nickel have recently gained great value in the manufacture of furan-derived compounds.

1 IA																		2 IIA										13 IIIA										14 IVA										15 VA										16 VIA										17 VIIA										18 VIIIA																																																																																																													
1 H																		2 He										3 B										4 C										5 N										6 O										7 F										8 Ne																																																																																																													
3 Li																		4 Be										5 Al										6 Si										7 P										8 S										9 Cl										10 Ar																																																																																																													
11 Na																		12 Mg										13 Al										14 Si										15 P										16 S										17 Cl										18 Ar																																																																																																													
19 K																		20 Ca										21 Sc										22 Ti										23 V										24 Cr										25 Mn										26 Fe										27 Co										28 Ni										29 Cu										30 Zn										31 Ga										32 Ge										33 As										34 Se										35 Br										36 Kr									
37 Rb																		38 Sr										39 Y										40 Zr										41 Nb										42 Mo										43 Tc										44 Ru										45 Rh										46 Pd										47 Ag										48 Cd										49 In										50 Sn										51 Sb										52 Te										53 I										54 Xe									
55 Cs																		56 Ba										57 La										58 Ce										59 Pr										60 Nd										61 Pm										62 Sm										63 Eu										64 Gd										65 Tb										66 Dy										67 Ho										68 Er										69 Tm										70 Yb										71 Lu																			
87 Fr																		88 Ra										89 Rf										90 Db										91 Sg										92 Bh										93 Hs										94 Mt										95 Ds										96 Rg										97 Cn										98 Uut										99 Fl										100 Uup										101 Lv										102 Uus										103 Uuo																			
89 La																		90 Ce										91 Pr										92 Nd										93 Pm										94 Sm										95 Eu										96 Gd										97 Tb										98 Dy										99 Ho										100 Er										101 Tm										102 Yb										103 Lu																																							
89 Ac																		90 Th										91 Pa										92 U										93 Np										94 Pu										95 Am										96 Cm										97 Bk										98 Cf										99 Es										100 Fm										101 Md										102 No										103 Lr																																							

Figure 1.12. The position of transition and noble metals in the periodic table of elements [272].

## General Introduction

Below we examine several noble metal-based catalytic systems that have been used for the reductive transformation of furfural.

### Cu-Based Catalysts

Due to the lower hydrogenation capability of copper in comparison to noble metals, Cu-based catalysts have been used as selective catalysts to hydrogenate the C=O bond and avoid the reduction of double bonds in the furan ring [128, 150]. Cu-based catalysts were the first catalytic systems used for the hydrogenation of furfural to produce chemicals and biofuels such as furfuryl alcohol, 2-methylfuran, cyclopentanone, and cyclopentanol [9].

Copper can have different numbers of valence ( $\text{Cu}^+$ ,  $\text{Cu}^{++}$  and  $\text{Cu}^0$ ). It was also demonstrated that the  $\text{Cu}^+/\text{Cu}^0$  species ratio on the catalyst surface can affect the catalytic activity. One accepted opinion has since suggested that the presence of both  $\text{Cu}^0$  and  $\text{Cu}^+$  is essential for the hydrogenation of furfural to furfuryl alcohol [189, 128, 20, 22, 27, 30].

Similarly, it was also proposed that  $\text{Cu}^0$  sites activate  $\text{H}_2$ , while  $\text{Cu}^+$  species act as Lewis acidic or electrophilic sites to polarize the C=O bond via the oxygen electron lone pair [31,32]. The  $\text{Cu}^+/\text{Cu}^0$  ratio is significantly related to factors such as the nature of support, the preparation procedure, the reduction, and the experimental conditions [189]. The deactivation of Cu-based catalysts is therefore what has largely limited their industrial use. Usual reasons for copper deactivation are loss of the  $\text{Cu}^+$  species by reduction, Cu particle sintering, and the poisoning of active Cu sites caused by the adsorption of reaction intermediates and coke formation/deposition [189].

Cu-based catalysts can adsorb the furfural molecule from the  $\eta^1\text{-(O)}$ -aldehyde configuration by only one interaction between the aldehyde group of furfural and

## General Introduction

the copper surface (Figure 1.13). It is reported that there are no additional interactions between the copper surface and the furan ring [189], which can be explained by the strong repulsion of the furan ring with the copper surface due to the partial overlap of the copper 3d band with the antibonding orbitals of the furan ring [190,191].

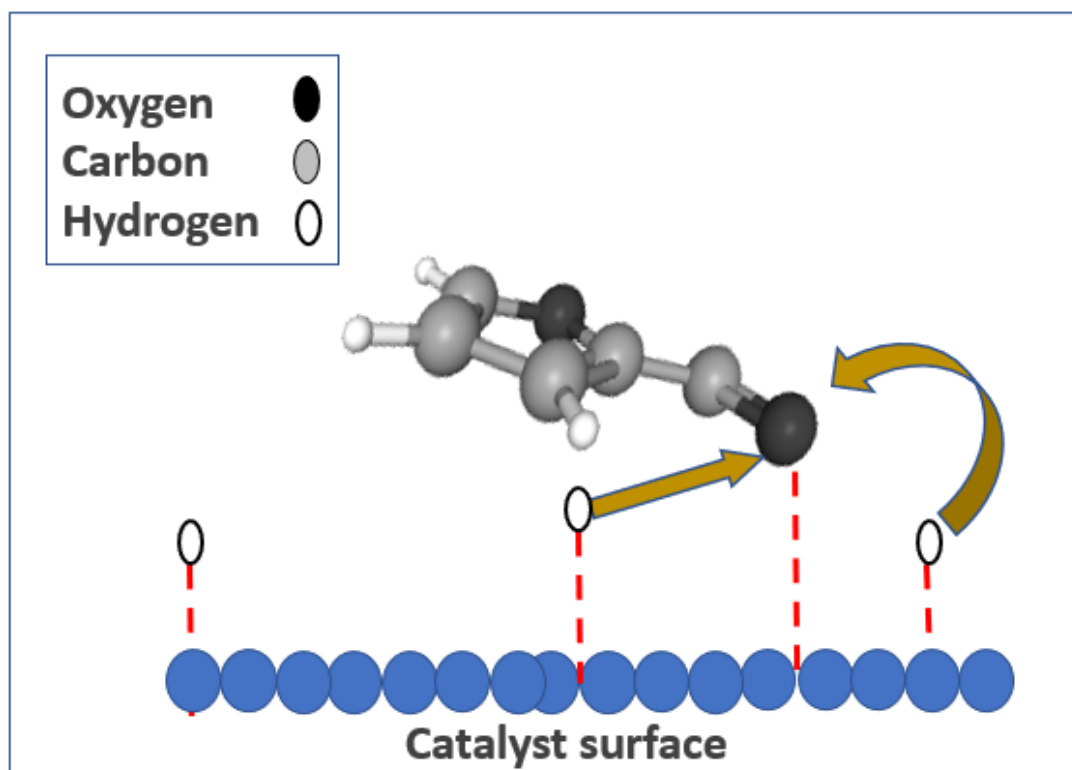


**Figure 1.13.** The adsorption of furfural at catalyst surface by  $\eta^1$ -(O)-Aldehyde configuration [189].

The  $\eta^1$ -(O)-aldehyde configuration did not show a flat adsorption position on the metal surface; only a tilted and a perpendicular adsorption were observed. However, this configuration over the Cu-based catalyst can only occur via the perpendicular adsorption, which is less stable than the tilted one (Figure 1.14) [189].

## General Introduction

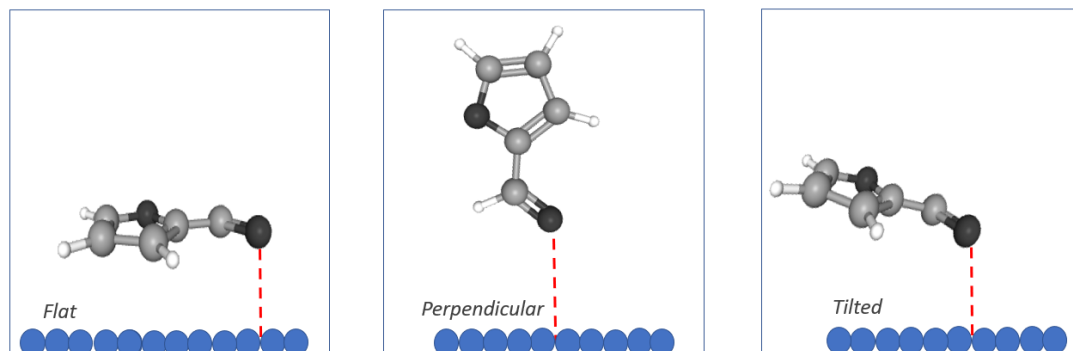


**Figure 1.14.** The three adsorption positions of furfural  $\eta^1$ -(O)-Aldehyde configuration [189].

**Practically speaking,** in the vapor phase and using a continuous reactor, Cu/MgO provides high activity to both furfural hydrogenation and the selective production of furfuryl alcohol. Production reached 97% of the total conversion of furfural with 95% selectivity to furfuryl alcohol was reported. The ratio of hydrogen to furfural was  $H_2/\text{Furfural} = 16$ , and the liquid hourly space velocity was set at  $1 \text{ h}^{-1}$ . The reaction temperature was 453 K, the pressure was adjusted to 0.1 MPa, and the reaction time was 4 h [160].

In another reaction, that was done over a catalyst of  $\text{Cu}_1\text{Ni}_1/\text{MgAlO}$ , furfuryl alcohol was produced at a yield of over 99% through the complete conversion of furfural at 373 K and 4 MPa. The reaction took 4 h and used methanol as a solvent [188]. Raising the reaction temperature from 373 K to 423 K and lowering the reaction time from 4 h to 3 h favored the production of tetrahydrofurfuryl alcohol as a dominant product rather than furfuryl alcohol. The synthesis took two hydrogenation pathways in a row. The first of these was the hydrogenation of the aldehyde group and the second was the hydrogenation of the furanic ring's double bonds. When Liu, H et al. used the same catalyst of  $\text{Cu}_1\text{Ni}_1/\text{MgAlO}$ , they achieved a selectivity of 95% to TFA at a near full conversion of furfural.

## General Introduction

In parallel with the production of TFA and FA (Table 1.3.), numerous studies have reported the use of Cu-based catalysts to produce 2-methyl furan from furfural. The Cu-Co/Al<sub>2</sub>O<sub>3</sub> catalyst prepared by impregnation formed 78% 2-methyl furan at a complete conversion of furfural. The reaction was conducted in a liquid phase of 2-propanol under 4 MPa, at 473 K, and after 4 h of reaction.

The production of cyclopentanone (CPO) and cyclopentanol (CPL) was also investigated over a Cu-based catalyst. A hydrogenation reaction of furfural into cyclopentanol was conducted in an aqueous solution using a catalyst of CuMgAl, under 4 MPa and 413 K. In this reaction, 98% of furfural was converted, 93% of which was to cyclopentanol [151]. Under similar conditions but using a different catalyst of CuZnAl, the conversion reached 100% but the selectivity of cyclopentanol fell to 84% [152]. Another study that used the same catalyst of CuZnAl to transform furfural into cyclopentanone provided a selectivity of 60% to cyclopentanone at 98% of total conversion [153].

Also reported is the synthesis of pentanediols from furfuryl alcohol and tetrahydrofurfuryl alcohol using Cu-based catalysts. Yoshida et al. suggest that Cu-ZnO synthesized by co-precipitation could provide a 1,5-pentanediol yield of 52.5% at 55.2% conversion of tetrahydrofurfuryl alcohol at 543 K and under 25 MPa after 5 hours of reaction [154].

Similarly, 10 wt % Cu-Mg<sub>3</sub>AlO<sub>4.5</sub> formed 1,2-pentanediol and 1,5-pentanediol at amounts of 51.2% and 28.8%, respectively, at almost complete conversion of furfuryl alcohol in ethanol under 413 K, 6 MPa, and a reaction time of 8 h [112].

## General Introduction

**Table 1.3.** Summary of relevant works on the conversion of furfural over different catalysts of Cu.

Catalyst	[C]	Solvent	P <sub>H2</sub> [MPa]	T [K]	t [h]	Conversion [%]	Selectivity of the main product (%)	Ref
Cu-Co/Al <sub>2</sub> O <sub>3</sub>	2.2 mol/L	2-propanol	4	473	4	>99	mFUR (78)	235
CuZnAl	0.63 mol/L	Water	4	423	10	100	CPL (84)	152
CuMgAl	0.63 mol/L	Water	4	413	10	98	CPL (93)	151
CuZnAl	0.33 mol/L	Water	4	423	6	98	CPO (60)	153
CuMgAlO	--	alcohol	6.0	423	6	>84	12PD (46.4), 15PD (25.0)	235
Cu <sub>1</sub> Ni <sub>1</sub> /MgAlO	0.25 mol/L	methanol	4.0	373	4	>99	FA (>99)	188
Cu <sub>1</sub> Ni <sub>1</sub> /MgAlO	0.25 mol/L	ethanol	4.0	423	3	>99	TFA (95)	188
Cu/MgO	--	--	0.1	453	200	97%	FA (95)	160
NiCu/ $\gamma$ -Al <sub>2</sub> O <sub>3</sub>	0.02 mol/L	2-propanol	4.5	473	4	95	FA (95)	40

## Ni-Based Catalysts

The excellent ability of nickel to hydrogenate the furanic derivatives leads to the production of a wide range of chemicals over Ni-based catalysts since not only are FA, mFUR, CPO, CPL, and TFA formed (as with the other transition metals) but also FUR, pentanediols, mTHF, and THF [87].

Nickel catalysts adsorb furfural not only via the aldehyde group, but also via the interaction with the furan ring. This adsorption is called the  $\eta^2(\text{C,O})$ -aldehyde configuration, which happens due to the strong interaction between the  $\pi$  bonds in furfural and the surface sites, resulting from the rehybridization of  $sp^2$ -to- $sp^3$  [192,196-198]. Figure 1.15. illustrates the two bonded centers – the C atom of the furan ring and the oxygen atom of the carbonyl group – which make it easy for furfural to be adsorbed on the nickel surface [87,88,149,192-195].

## General Introduction

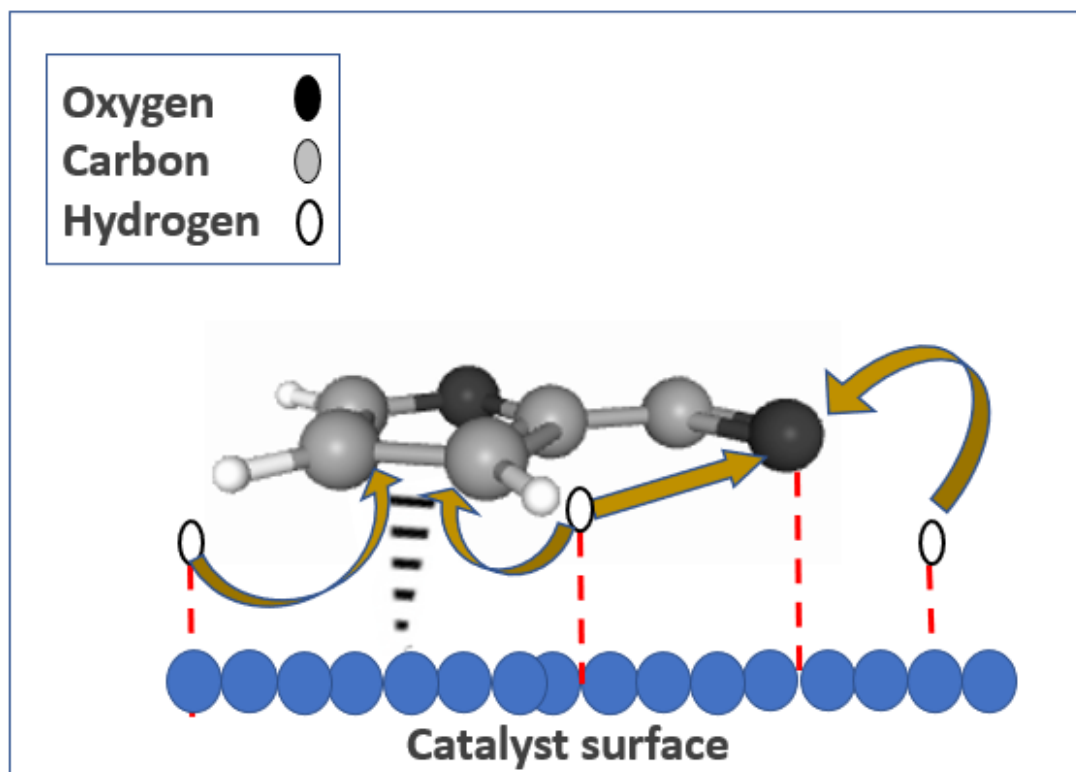


**Figure 1.15.** The adsorption of furfural at catalyst surface by  $\eta^2$ -(C,O)-Aldehyde configuration [189].

This configuration also occurs on Pt and Pd surfaces [189], while the interaction strength between furfural and metals follows this trend: Ni > Pd > Pt  $\gg$  Cu [87,199].

However, due to the non-selectivity of nickel, tetrahydrofurfuryl alcohol is formed in most furfural hydrogenation reactions [87, 88, 33]. To avoid this weak point and enhance the selectivity on nickel, three solutions are suggested in the literature. The first one is to precisely add and localize a specific amount of an oxophilic metal such as Fe, Mg, or Co [34]. The second is to use oxide supports that interact strongly with nickel, such as Al<sub>2</sub>O<sub>3</sub>,TiO<sub>2</sub> [51]. The third solution is to control the reaction conditions in order to prevent furfural hydrogenation into undesired products [35].

## General Introduction

Ni-based catalysts have also been used to produce furfuryl alcohol. The first research aimed at synthesizing furfuryl alcohol from furfural was conducted in 1906. The experiment was performed in the vapor phase under 463 K to facilitate the formation of furfuryl alcohol as the dominant product [36]. In one of the first studies published on the production of furfuryl alcohol in liquid phase from furfural, the yield was 95% over a catalyst of Ni/MgO [35]. Another reaction that used a catalyst of Ni-Sn/TiO<sub>2</sub> (Ni/ Sn = 1.5) prepared by hydrothermal treatment of solutions containing Ni and Sn species showed 99% furfuryl alcohol at 99% conversion of furfural. The reaction was conducted at 383 K under 3 MPa for 1.25 h (Table 1.4.) [37]. The deposition of (NH<sub>4</sub>)<sub>6</sub>Mo<sub>7</sub>O<sub>24</sub> over Ni also achieved a high performance for the formation of furfuryl alcohol in a reaction that used 2-propanol as solvent at a temperature of 333 K. After 6 h this produced 98% furfuryl alcohol when furfural conversion was close to 100% [38]. Finally, a trimetallic catalyst prepared from nickel with cerium and boron led the whole furfural conversion of 96.8% into furfuryl alcohol at 353 K and 1.0 MPa after 3 h [39]. The high selectivity may be attributed to the presence of Ce<sub>2</sub>O<sub>3</sub> in the catalyst, which favored the adsorption and polarization of the C=O bond on the acidic sites created on the surface [39]. In the same context, incorporating aluminum led to smaller particle sizes and a higher fraction of exposed surface sites that improved the hydrogenation performance. In a liquid phase reaction, a catalyst of Ni-Cu/ $\gamma$ -Al<sub>2</sub>O<sub>3</sub> transferred the whole amount of furfural converted (95%) into furfuryl alcohol after 4 h of reaction. The reaction temperature and pressure used were 473 K and 4.5 MPa [40].

To produce tetrahydrofurfuryl alcohol (TFA) from FA, industrial methods use a supported Ni catalyst under mild reaction temperatures [189]. TFA can also be directly synthesized from furfural in either vapor or liquid phase. In vapor phase,

## General Introduction

the hydrogenation of furfural to tetrahydrofurfuryl alcohol over Ni/SiO<sub>2</sub> yielded 94% TFA at 100% conversion at 413 K after 0.5 h [88]. Numerous studies have been published on the synthesis of TFA in liquid phase using different solvents of water, ethanol and 2-propanol. Normann, W. et al. detected a high selectivity to TFA (90%) at full conversion of furfural when the reaction was conducted over a catalyst of nickel chromate at 408 K, 4.5 MPa, and a reaction time of 4 h [41]. Similarly, Raney nickel catalysts have been used to produce tetrahydrofurfuryl alcohol. Some studies achieved a full transformation of furfural fed into tetrahydrofurfuryl alcohol. For example, reactions conducted for 3 h over a Raney Ni/tainiolite or Raney Ni/bentonite catalyst provided 100% furfural conversion and 100% TFA selectivity. The solvent was used in 2-propanol, the temperature was 393 K, and the pressure was 2 MPa [43].

2-methyl furan (mFUR) is also one of the main products formed over Ni-based catalysts from furfural. Catalysts modified with other metals are able to form mFUR in high amounts via the over-hydrogenation and decarbonylation of the furan ring [194]. An example of bimetallic Ni-based catalysts was presented in a study by Sitthisa et al., who used NiFe/SiO<sub>2</sub>. This catalyst afforded a mFUR yield of only 39% at 96% conversion in vapor phase at 523 K and 0.1 MPa [194], whereas furfural was totally converted and mFUR achieved 82% selectivity in liquid phase, over the NiCu/ $\gamma$ -Al<sub>2</sub>O<sub>3</sub> catalyst, at 473 K and 4 MPa [44].

Finally, furan was one of the desired products formed over Ni catalysts, when a catalyst of platinum and nickel supported on silica was used to produce furan, it provided 26% selectivity of furan at 43% of total furfural conversion after 1.5 h. The reaction was conducted under a low pressure of 0.69 MPa and a reaction temperature of 523 K [262].

## General Introduction

**Table 1.4.** Summary of relevant works on the conversion of furfural over different catalysts of Ni.

Catalyst	[C]	Solvent	P <sub>H2</sub> [MP]	T [K]	t [h]	Conversion [%]	Selectivity of the main product (%)	Ref
PVP-NiCoB	0.80 mol/L	ethanol	1.8	353	--	74	FA (72)	52
NiSn/TiO <sub>2</sub> (Ni/ Sn = 1.5)	0.36 mol/L	2-propanol	3	383	1.3	99	FA (99)	37
Raney Ni/ (NH <sub>4</sub> ) <sub>6</sub> Mo <sub>7</sub> O <sub>24</sub>	0.0042 mol/L	2-propanol	2.1	333	6	99.9	FA (98)	38
NiCeB	4 mol/L	ethanol	1	353	3	96.8	FA (96.8)	39
NiFe/SiO <sub>2</sub>	--	--	0.1	523	--	96	mFUR (39)	194
NiCu/ $\gamma$ -Al <sub>2</sub> O <sub>3</sub>	2.25 mol/L	2-propanol	4	473	4	100	mFUR (82)	44
Ni/SiO <sub>2</sub> -773	--	--	0.1	413	0.5	100	TFA (94)	88
nickel chromate	520 mmol	--	4.5	408	2.25	100	TFA (90)	41
Raney Ni/tainiolite	0.36 mol/L	2-propanol	2	393	3	100	TFA (100)	43
Raney Ni/bentonite	0.36 mol/L	2-propanol	2	393	3	100	TFA (100)	43
Ni@Pt/silica	0.4 mol/L	2-propanol	0.69	523	1.5	43	FUR (26)	262

## Co-Based Catalysts

Co bimetallic and trimetallic catalysts demonstrated high selectivity for the formation of furfuryl alcohol (FA) from furfural. One study that used PVP-CoNiB as the catalyst, achieved an FA selectivity of 72% at 74% conversion of furfural at a temperature of 353 K and a pressure of 1.8 MPa after 3 h [52]. In another study a complete conversion and selectivity were achieved when the reaction was catalyzed by a CoB catalyst. This reaction was carried out at 353 K and 1 Mpa, with a feed concentration of 4 mol/L [53].

Chen et al. studied the role of Mo as an additive metal in Co-based catalysts. They prepared a catalyst of CoMoB through chemical reduction in a solution of CoCl<sub>2</sub> and

## General Introduction

$\text{Na}_2\text{MoO}_4$  by  $\text{KBH}_4$ . The catalyst synthesized provided full conversion to furfuryl alcohol at 373 K in ethanol under 1 MPa after a 3 h reaction time [232]. Similarly, a CoFeAl metal catalyst prepared by co-precipitation was used to hydrogenate furfural into 2-methyl furan. Results showed that 90% of furfural was converted with a mFUR yield of 60% at 453 K and 0.1 MPa. The Co/Fe/Al ratio was 3/0.25/0.75 [233].

1,5-pentanediol (15PD) was also synthesized using a Co-based catalyst (Table 1.5.). For example, when  $\text{Co/TiO}_2$  was used at 413 K, the reaction formed 30% 15PD as well as a considerable amount of TFA (20%) at 99% furfural conversion [156]. When this catalyst was replaced with CoAlO, selectivity decreased to 30% and 62% for 15PD and TFA, respectively [110]. Finally, CoMgAlO increased the formation of 15PD and achieved 50% selectivity at full furfural conversion [157].

**Table 1.5.** Summary of relevant works on the conversion of furfural over different catalysts of Co.

Catalyst	[C]	Solvent	$P_{\text{H}_2}$ [MPa]	T [K]	t [h]	Conversion [%]	Selectivity of the main product (%)	Ref
CoB	4 mol/L	ethanol	1	353	--	100	FA (100)	53
CoMoB	0.91 mol/L	ethanol	1	373	3	100	FA (100)	234
CoFeAl	0.0015 mmol/mL	--	0.1	453	0.67	90	mFUR (60%)	235
Co/TiO <sub>2</sub> (5 wt.% Co)	2 wt.%	water	2.34	413	5.8	99.0	15PD (30.3), TFA (20.7)	156
CoAlO	10 g/L	2-propanol	3.0	423	8	100	15PD (30), TFA (62.2)	110
CoMgAlO	10 g/L	ethanol	5.0	443	4	100	15PD (49), TFA (14)	157

## Fe-Based Catalysts

Iron is abundant, cheap, eco-friendly, and easily recycled. It is usually used as an oxophilic metal additive to improve the hydrogenation/ hydrogenolysis activity of other metals [189]. Poor activity of monometallic Fe-based catalysts was exhibited in the reduction of furfural [234,200].

One process proposed to enhance hydrogenation activity is the addition of carbon or nitrogen promoters [189]. A study by Shi et al. presented  $\text{Fe}_3\text{C}@r\text{GO}/\text{CNT}$  prepared inside carbon nanotubes as a suitable catalyst for achieving full furfural conversion to furfuryl alcohol at 372 K in ethanol solvent under 2 MPa for 12 h [58]. Another study that used nitrogen species to optimize the performance of Fe-based catalysts reported a furfuryl alcohol amount of 83% at a furfural conversion of 92% using 5 wt % of Fe-N/C-800 as the catalyst at a temperature of 433 K in 2-butanol medium [59] (Table 1.6).

## Mo-Based Catalysts

Mo-based catalysts are normally presented in the form of molybdenum carbides ( $\text{Mo}_2\text{C}$ ), which are widely used for selectively removing oxygen from small oxygenates (e.g., ethanol and propanol), vegetable oils, stearic acid, and guaiacol. [189]

Few studies have reported that  $\text{Mo}_2\text{C}$  may be a suitable catalyst for the hydrogenation of furfural (Table 1.6). The main product resulting from this process is 2-methyl furan (mFUR). Almost 60% selectivity to mFUR was obtained at 423 K under atmospheric pressure after 36 h [45]. When Lee et al. also tested, in vapor phase, furfural conversion over an  $\text{Mo}_2\text{C}$  catalyst at a reaction temperature of 423 K and under ambient pressure, 60% 2-methylfuran selectivity was detected [201].

**Table 1.6.** Summary of relevant works on the conversion of furfural over different catalysts of Fe and Mo.

Catalyst	[C]	Solvent	P <sub>H<sub>2</sub></sub> [MPa]	T [K]	t [h]	Conversion [%]	Selectivity of the main product (%)	Ref
Fe <sub>3</sub> C@rGO/CNT	0.12 mol/L	ethanol	2	372	12	100	FA (100)	58
Fe-N/C-800	0.16 mol/L	2-butanol	--	433	15	92	FA (95)	59
Mo <sub>2</sub> C	--	--	1atm	423	36	--	mFUR(60)	45
Mo <sub>2</sub> C	--	--	1atm	423	6.1	7.5	mFUR(60)	201

## Hydrogenation Of Furfural and Its Derivatives by Noble Metals Catalysts

Noble metals are metallic chemical elements with outstanding oxidation resistance even at high temperatures. For example, metals in groups VIIb, VIIIb, and Ib of the second and third transition series of the periodic table (including rhenium, ruthenium, rhodium, palladium, silver, osmium, iridium, platinum and gold) are considered noble metals (Figure 1.12) [237]. These metals have excellent resistance to corrosive attack by a wide range of liquid and gaseous substances thanks mainly to their high thermodynamic stability [238].

Below we examine various noble metal-based catalytic systems that have been used for the reductive transformation of furfural and its derivatives.

### Pd-Based Catalysts

Palladium is widely known for its high activity in hydrogenation. Over Pd-based catalysts, furfural is converted through hydrogenation, hydrogenolysis and decarbonylation of the pendant aldehyde group into products such as furfuryl alcohol, tetrahydrofurfuryl alcohol, pentanediols, 2-methyl furan, and furan.

## General Introduction

To produce other add-value chemicals, hydrogenation on the palladium surface can be followed by various reactions, including the rearrangement of the furan ring, etherification and esterification, as well as oligomerization reactions or their combination, which may form 1-octanol, cyclopentanol, cyclopentanone, furfuryl methyl ether, furanic ester, and liquid fuels [189, 239].

Furfural can be strongly bonded onto the Pd surface via two different configurations, the first of which is the  $\eta^2$ -(C,O)-aldehyde configuration and the second is the  $\eta^1$ -(C)-acyl configuration. As was explained in the section on nickel catalysts, the  $\eta^2$ -(C,O)-aldehyde configuration occurs because of the strong interaction between the surface metal and the  $\pi$  bonds of the furan ring, while the  $\eta^1$ -(C)-acyl configuration occurs when the reaction temperature increases.

The high temperature favors the transformation of the  $\eta^2$ -(C,O)-aldehyde configuration into the  $\eta^1$ -(C)-acyl configuration (Figure 1.16) [189]. The main reaction with this configuration is the decarbonylation of furfural, which produces compounds such as furan and THF. The validity of this adsorption theory has been proven experimentally [189].

On the experimental side (Table 1.7.), the conversion of furfural into furfuryl alcohol on monometallic Pd-based catalysts suffers low selectivity because other reactions such as decarbonylation, hydrogenolysis and ring hydrogenation are preferred and difficult to avoid [189]. However, a furfural transformation experiment that used a palladium catalyst loaded over mesoporous silica converted 75% furfural and achieved 71% selectivity of furfuryl alcohol [240].

## General Introduction

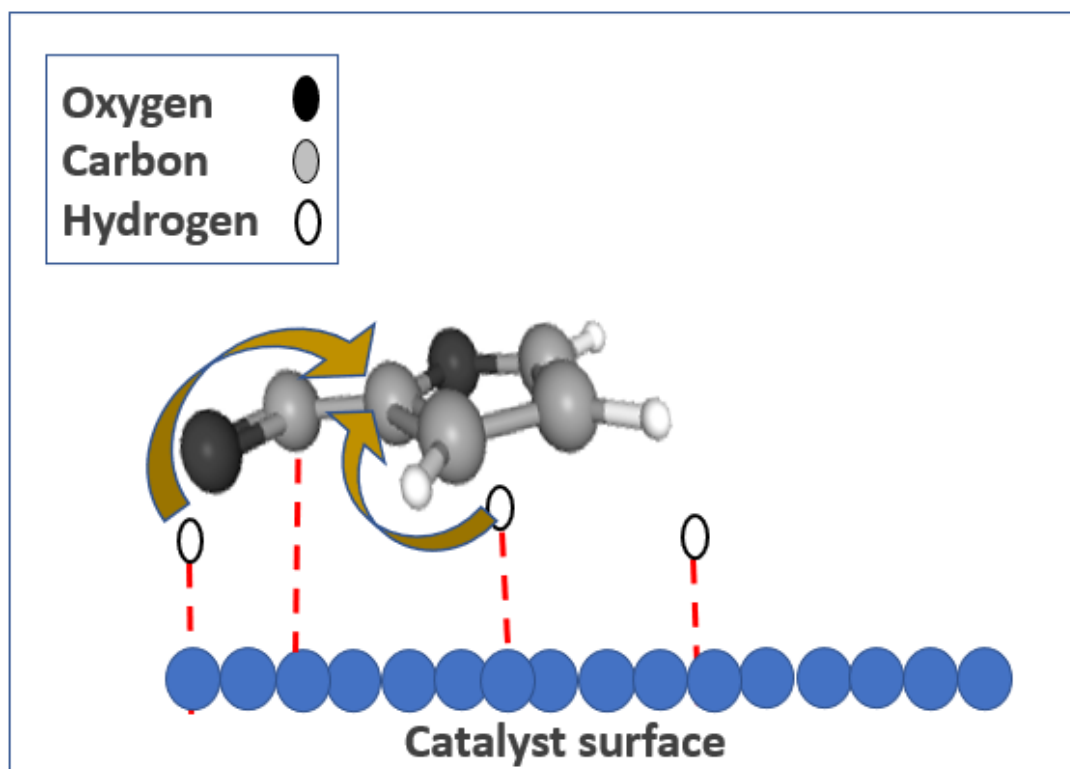


**Figure 1.16.** The adsorption of furfural at catalyst surface by  $\eta^1$ -(C)-acyl configuration [189].

Pd-based catalysts have been used to form tetrahydrofurfuryl alcohol in an aqueous medium (5 wt.% in water) from furfural. A bimetallic catalyst of palladium and iridium was prepared by impregnating  $\text{SiO}_2$  with a mixed aqueous solution of 1:1 Pd:Ir precursors. A 99% conversion of furfural into tetrahydrofurfuryl alcohol (94%) was achieved with high selectivity at 8 MPa of  $\text{H}_2$ , 275 K, and a reaction time of 6 h [241]. In another study, a monometallic catalyst of palladium has also shown high catalytic performance when supported on MFI, achieving 95% tetrahydrofurfuryl alcohol selectivity at 100% furfural conversion at a temperature of 493 K, a pressure of 3.4 MPa and a reaction time of 5 h [89].

## General Introduction

The use of Pd-based catalysts was extended to produce furfural-derived biofuel chemicals such as 2-methyl furan. Numerous studies reported the production of 2-methyl furan over palladium catalysts in the gas and liquid phases. For example, in the gas phase, a 65% yield of 2-methyl furan was detected at 99% furfural conversion when a Pd-Cu/SiO<sub>2</sub> catalyst was used at 0.1 MPa and 443 K [242]. In the liquid phase, on the other hand, 42% selectively to 2-methyl furan was observed at 98% conversion when Pd/TiO<sub>2</sub> was used as the catalyst at ambient temperature and 0.3 Mpa of H<sub>2</sub> [243]. In another study, the same catalyst (Pd/TiO<sub>2</sub>) and conditions were used in a synthesis reaction of 2-methyl furan but with furfuryl alcohol as the feed material rather than furfural. This reaction yielded 98% 2-methyl furan and full conversion after 1.5 h [244].

As mentioned earlier, the decarbonylation of furfural takes place on palladium catalysts at high temperature to produce furan (FUR) and tetrahydrofuran (THF) via the favorable formation of acyl species of furfural [87]. A 5 wt % Pd/C catalyst provided a furan yield of 98% at 100% conversion at 523 K [87]. In another research, a Pd/SiO<sub>2</sub> catalyst achieved 70% furan selectivity at 96% furfural conversion [195]. THF was also produced in large amounts since the Pd/C catalysts converted all the furfural to THF at 373 K, 5.5 MPa of H<sub>2</sub>, and a reaction time of one hour and 15 min [245].

## General Introduction

**Table 1.7.** Summary of relevant works on the conversion of furfural over different catalysts of Pd.

Catalyst	[C]	Solvent	P <sub>H2</sub> [MP]	T [K]	t [h]	Conversion [%]	Selectivity of the main product (%)	Ref
Pd-Cu/SiO <sub>2</sub>	--	--	0.1	443	--	99	mFUR (65)	242
Pd/TiO <sub>2</sub>	0.69 mol/L	Toluene	0.3	298	2	98	mFUR (42)	243
Pd/MFI	0.4 mol/L	2-propanol	3.4	493	5	100	TFA (95.0)	89
Pd/SiO <sub>2</sub>	5.0 mol/L	Octane	--	--	--	75	FA (71.0)	240
Pd/C	--	scCO <sub>2</sub>	--	523	--	100	FUR (98)	87
Pd/SiO <sub>2</sub>	--	--	0.1	523	0.15	96	FUR (70)	195
Pd/C	1.36 mol	--	5.5	373	1.15	100	THF (100)	245

## Ru-Based Catalysts

Ru-based catalysts are widely known for their effectiveness not only in reducing aromatics [246], nitriles [247], sugars [248], and polyols [248] but also in the reductive transformation of furanic compounds such as furfural under mild conditions [189]. These catalysts are also highly active for the hydrogenation of the pendant aldehyde group of furfural under moderate reaction conditions. Higher hydrogen pressures promote the formation of tetrahydrofurfuryl alcohol, while higher temperatures promote the formation of 2-methylfuran [189]. Ru-based catalysts were especially used to synthesize furfuryl alcohol from furfural (Table 1.8.) [189].

An Ru/C + AlCl<sub>3</sub> catalyst achieved 53% furfuryl alcohol selectivity after a reaction time of 3 hours at 433 K [250]. Ruthenium was also used to catalyze the production of tetrahydrofurfuryl alcohol from furfural. For example, an Ru-Fe/TiO<sub>2</sub> catalyst achieved 99.1% tetrahydrofurfuryl alcohol selectivity at 1 Mpa and 353 K [251]. An

## General Introduction

Ru/carbon foam catalyst was also able to form tetrahydrofurfuryl alcohol when the reaction started from xylose at 2.5 Mpa and 423 K. Global conversion was 67%, with a selectivity of 20% toward tetrahydrofurfuryl alcohol [252]. Another study reported that Ru/MgAlO<sub>4</sub> produced a tetrahydrofurfuryl alcohol yield of 84.3% at 99.9% conversion of furfuryl alcohol at 393 K and 6 MPa [253]. Also reported is the synthesis of 2-methylfuran from furfural using Ru-based catalysts. A catalyst based on Ru/C converted furfural to 2-methylfuran in liquid-phase with 61% selectivity and 95% conversion at 180 °C after 10 h [254].

Furthermore, the production of cyclopentanone from furfural was improved by Fang et al. It was done by preparing Ru catalyst on acidic MOF material (3 wt % Ru/MIL-101), it produced over 95% selectivity of cyclopentanone at full conversion in an aqueous medium at 4 MPa, 433 K and a reaction time of two and a half hours [255]. Finally, since pentanediol compounds are important in the chemical industry, Ru-based catalysts were used to enhance their production. In a previous study, a 1,2-pentanediol yield of 42.1% at full conversion of furfuryl alcohol was achieved at 423 K and 1.5 MPa in the aqueous phase [253].

**Table 1.8.** Summary of relevant works on the conversion of furfural over different Ru catalysts.

Catalyst	[C]	Solvent	P <sub>H<sub>2</sub></sub> [MPa]	T [K]	t [h]	Conversion [%]	Selectivity of the main product (%)	Ref
Ru/C+AlCl <sub>3</sub>	0.083mol/L	2-propanol	1.0(N <sub>2</sub> )	433	3	92	FA (53)	250
Ru-Fe/TiO <sub>2</sub>	--	--	1.0	353	--	99.9	TFA (99.1)	251
Ru/C	0.083mol/L	2-propanol	2.04 (N <sub>2</sub> )	453	10	95	mFUR(61)	254
Ru/MIL-101	--	H <sub>2</sub> O	4.0	433	2.5	>99	CPO (95)	255

## General Introduction

### Pt-Based Catalysts

Platinum is one of the most common metal used in the hydrogenation of  $\alpha,\beta$ -unsaturated aldehydes for producing a wide range of add-value chemicals and fuels from furfural [189,256]. Furfural can be hydrogenated over the Pt surface by providing a closer interaction with the furan ring and the aldehyde group via the  $\eta^2$ -(C,O) adsorption mode. This leads to reactions such as the hydrogenation of the aldehyde group, the hydrogenation of the furan ring, the opening-ring rearrangement, and decarbonylation [189].

Numerous Pt-based catalysts have been studied for the production of furfuryl alcohol from furfural in either the vapor phase or the liquid phase. In the vapor phase, a high catalytic performance was achieved with the PtSn@mSiO<sub>2</sub> catalyst, which provided 98% furfuryl alcohol at 100% conversion [257]. In the liquid phase, 95.7% furfuryl alcohol selectivity was achieved from furfural over a Pt/Re catalyst at 403 K and 5 MPa [258]. Another platinum catalyst derived from layered double hydroxide (LDH) enabled the whole amount of furfural to be converted into furfuryl alcohol (97%) in an experiment conducted at room temperature, 0.1 Mpa of hydrogenation, and a reaction time of 8 hours [259].

Another reaction that used platinum catalysts supported by hydrotalcite achieved the ring-opening reaction of the furan ring and produced a large amount of pentanediols (73% of 1,2-pentanediols and 8% of 1,5-pentanediols) at 423 K, 3 Mpa of hydrogen pressure, and a reaction time of 4 h [119]. Moreover, important results in the synthesis of pentanediols from furfural was achieved, 1,2-pentanediols selectivity was 65%, 46% and 41%, while 1,5-pentanediol selectivity was 8%, 6% and 4.5% when the platinum catalyst was supported by CeO<sub>2</sub>, MgO and La-Al<sub>2</sub>O<sub>3</sub>, respectively [260].

## General Introduction

A platinum-based catalyst was also used to promote the decarbonylation of furfural (Table 1.9.) when a Pt/Al<sub>2</sub>O<sub>3</sub> catalyst yielded 53% of furan from full furfural conversion at 513 K and 2 MPa [261].

**Table 1.9.** Summary of relevant works on the conversion of furfural over Pt catalysts.

Catalyst	[C]	Solvent	P <sub>H<sub>2</sub></sub> [MPa]	T [K]	t [h]	Conversion [%]	Selectivity of the main product (%)	Ref
Pt-Re/TiO <sub>2</sub> - ZrO <sub>2</sub>	2.1 mol/L	ethanol	5	403	8	100	FA (95.7)	258
PtSn@mSiO <sub>2</sub>	--	--	0.1	433	--	100	FA (98)	257
Pt <sub>3</sub> Ni/LDH	0.25 mol/L	ethanol	0.1	298	8	97	FA (97)	259
Pt/LDH	0.33 mol/L	2-propanol	3	423	4	>99	12PD (73) 15PD (8)	119
Pt/CeO <sub>2</sub>	0.4 mol/L	Water	1	443	1.5	100	12PD (65) 15PD (8)	260
Pt/MgO	0.4 mol/L	Water	1	443	1.5	100	12PD (46) 15PD (6)	260
Pt/La-Al <sub>2</sub> O <sub>3</sub>	0.4 mol/L	Water	1	443	1.5	100	12PD (41) 15PD (4.5)	260
Pt/Al <sub>2</sub> O <sub>3</sub>	0.51 mol/L	2-propanol	2.0	513	2	100	FUR (53)	261

## Rh-Based Catalysts

Using Rh-based catalysts provided high yields of pentanediols obtained from the hydrogenation of furfural. The M/Rh ratio played a key role, significantly impacting the activity and selectivity of the reaction [189]. Also, solvents had an important effect on pentanediol production, with water being reported in the literature as the best solvent for increasing the amount of pentanediols produced [189]. A lower reaction temperature and a longer reaction time can help to produce a larger amount of 1,5-pentanediol [189]. One study that used Rh Ir-ReOx/SiO<sub>2</sub> catalyst to

## General Introduction

achieve the whole conversion of furfural and led to the formation of 72.4% of 1,5-pentanediol under mild conditions [108].

Similarly, Rh-based catalysts are known for their high productivity in the formation of linear diols from tetrahydrofurfuryl alcohol [189]. In earlier studies (Table 1.10.), an Rh Ir-ReO<sub>x</sub>/SiO<sub>2</sub> catalyst converted 96.2% of tetrahydrofurfuryl alcohol with 77% selectivity of 1,5-pentanediol at 393 K and 8 MPa in the aqueous phase after a reaction time of 24 h [96].

A DFT study focusing on the ring-opening of tetrahydrofurfuryl alcohol on the Rh surface demonstrated that, due to lower steric hindrance, ring-opening via the primary C–O bond (Figure 1.17. (1)) required a lower activation barrier than that of the secondary C–O bond in Figure 1.17. (2) or that of the C–O bond from the side chain in Figure 1.17. (3) [263]. This led to a kinetic formation of 1,2-pentanediol rather than 1,5-pentanediol and 2-methyltetrahydrofuran [189].

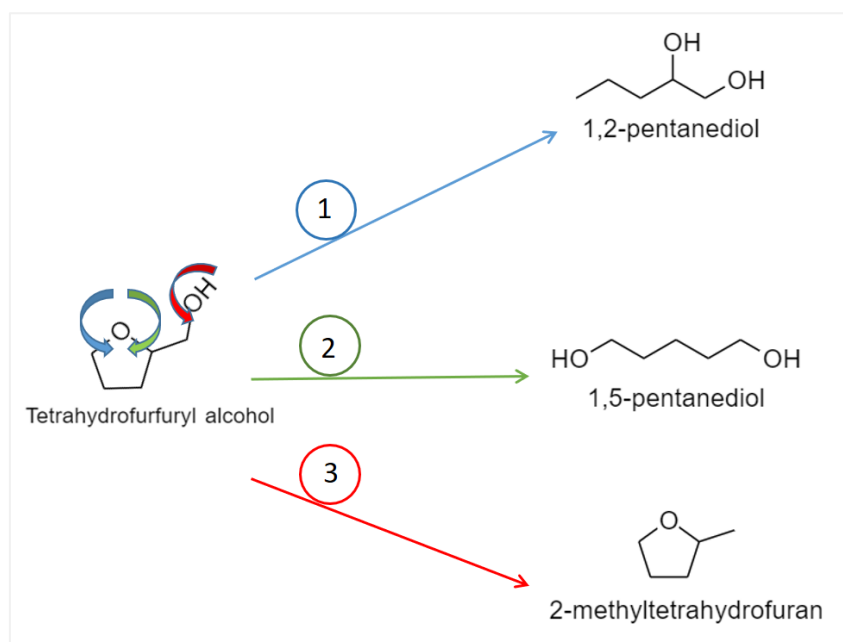


**Figure 1.17.** Pathways hydrogenolysis/deoxygenation of tetrahydrofurfuryl alcohol over Rh catalyst [189].

## Ir-Based Catalysts

Ir-based catalysts were reported as suitable catalysts for the hydrogenation of furanic derivatives. They can hydrogenate furfural into furfuryl alcohol at low temperature or even at room temperature. In aqueous phase, furfural was totally hydrogenated into furfuryl alcohol under a mild reaction using Ir-ReO<sub>x</sub>/SiO<sub>2</sub> [264]. Another reaction conducted for 18 hours at 373 K over an Ir@CN catalyst achieved 99% conversion of furfural into furfuryl alcohol via CTH reaction with formic acid [265].

Similarly, the production of 1,5-pentanediol from tetrahydrofurfuryl alcohol (TFA) may be considered one of the most valuable applications of Ir-based catalysts. A hydrogenation reaction of TFA over an Ir-MoO<sub>x</sub>/SiO<sub>2</sub> catalyst at 373 K and a hydrogen pressure of 8 MPa for 2 hours yielded 28% 1,5-pentanediol at a conversion of 31%. Conversion and selectivity increased to 60% and 57%, respectively, when the catalyst was replaced by Ir-ReO<sub>x</sub>/SiO<sub>2</sub>. On the other hand, when an Ir-WO<sub>x</sub>/SiO<sub>2</sub> catalyst was used, conversion fell to 5.1% with a slight selectivity of 4.9% toward 1,5-pentanediol [101].

The production of 1,5-pentanediol from furfural was studied by Liu, S et al. using a catalyst of Pd (0.66 wt.%) Ir-ReO<sub>x</sub>/SiO<sub>2</sub> and controlling the hydrogenation by two-step reaction conditions of 313 K for 8 h and 373 K for 72 h under a pressure of 6 MPa H<sub>2</sub>. Full conversion was acquired with high selectivity to 1,5-pentanediol (71.4%). In the same study but in another experiment, the selectivity of 1,5-pentanediol decreased to 63.6% when the reaction time was changed to 2 h for the first step and 24 h for the second (Table 1.10.) [107].

## Au-Based Catalysts

Due to the less effective activation/dissociation of Au with H<sub>2</sub>, Au has a lower activity in H<sub>2</sub>-mediated reactions than other noble metals [267]. Factors that can influence the hydrogenation activity of Au-based catalysts include the particle size, particle shape, and nature of the support [268]. However, it has been shown that smaller Au nanoparticles display more low-coordinated Au sites, such as edge and corner sites, and are more active for the dissociative adsorption of H<sub>2</sub> and the adsorption of C=O groups [269].

Another typical application of Au is in the selective hydrogenation to the aldehyde group over the hydrogenation of C=C functions, which guides the reaction to successful conversion of  $\alpha,\beta$ -unsaturated aldehydes to alcohols without saturating the furan ring double bonds. Au-based catalysts therefore have a strong ability to selectively transform furfural into furfuryl alcohol. [189]. For example, a solution of 25% of furfural in water was totally converted into furfuryl alcohol at 4 Mpa and 363 K for 4 hours when Au catalyst was supported on Rutile TiO<sub>2</sub> (Table 1.10.) [270]. Au-based catalysts have also been used to produce cyclopentanone. For instance, a 98% yield of cyclopentanone at 99% conversion was achieved over Au/anatase TiO<sub>2</sub> catalyst at 433 K, 4 MPa, and a reaction time of 1.2 h [271].

**Table 1.10.** Summary of relevant works on the conversion of furfural over different catalysts of Rh, Ir and Au.

Catalyst	[C]	Solvent	P <sub>H<sub>2</sub></sub> [MPa]	T [K]	t [h]	Conversion [%]	Selectivity of the main product (%)	Ref
Pd-Ir-ReOx/SiO <sub>2</sub>	10 wt %	water	6	313/373	2/24	>99.9	15PD (63.3)	107
Pd-Ir-ReOx/SiO <sub>2</sub>	10 wt %	water	6	313/373	8/72	>99.9	15PD (71.4)	107
Rh-Ir-ReOx/SiO <sub>2</sub>	10 wt %	water	6	313/373	8/24	>99.9	15PD (72.4)	108
Ir-ReOx/SiO <sub>2</sub>	1 mol/L	Water	8	303	6	>99	FA (>99)	264
Ir@CN	0.3 mol/L	Water	--	373	18	>99	FA (>99)	265
Au/rutile TiO <sub>2</sub>	0.13 mol/L	Water	4 (CO)	363	4	100	FA (100)	270
Au/anatase TiO <sub>2</sub>	--	Water	4	433	1.2	>99	>98	271

## 8. Layered Double Hydroxides (LDH)

Due to their features, LDH are considered versatile materials that can be used as support structure to obtain highly dispersed metal catalysts. Their surface metal species can cooperate with basic-acid sites on the surface of LDH to generate multifunctional catalysts [211].

Suitable heterogeneous catalysts for the hydrogenation reactions can be also obtained from LDH precursors by calcination at controlled conditions followed by reduction. In our work, we prepared a group of catalysts derived from Layered Double Hydroxides (LDH) for the hydrogenation of furfural, we therefore explained structure and properties of LDH in this section.

## 8.1. Definition of LDH

LDH is a hydrotalcite (HT), double hydroxide anionic-layered (LDH;  $[M^{2+}_{1-x} M^{3+}_x (OH)_2]^{x+} An^{-x/n} \cdot mH_2O$  ( $0 < x < 1$ )) clay [202-205]. It consists of a positively charged Brucite-like layer and negatively charged organic and inorganic anions.

Isomorphic divalent ions of  $Mg^{2+}$  with similar ionic radii of trivalent ions of  $Al^{3+}$  constitute the Brucite-like layers ( $[Mg^{2+}_{1-x} Al^{3+}_x (OH)_2]^{x+}$ ), while the anions ( $An^{-}$ ), which represent the negative part, are located between layers along with water. The typical HT,  $Mg_6Al_2(OH)_{16}CO_3 \cdot 4H_2O$ , contains  $CO_3^{2-}$  within the interlayer space (Figure 1.18).

The octahedra shape is formed by the coordination of six-fold coordinated  $Mg^{2+}$  with  $OH^{-}$  ions and shares edges with neighboring atoms to create two-dimensional Brucite-like layers. The partial substitution degree of  $Mg^{2+}$  by  $Al^{3+}$  is between 0.1 and 0.5.

HT-like materials can be synthesized by partial or full replacement of the  $Al^{3+}$  and  $Mg^{2+}$  of the Brucite-like layers by other metal ions or by changing the inorganic or organic anions within the interlayer space [206-210].

## General Introduction

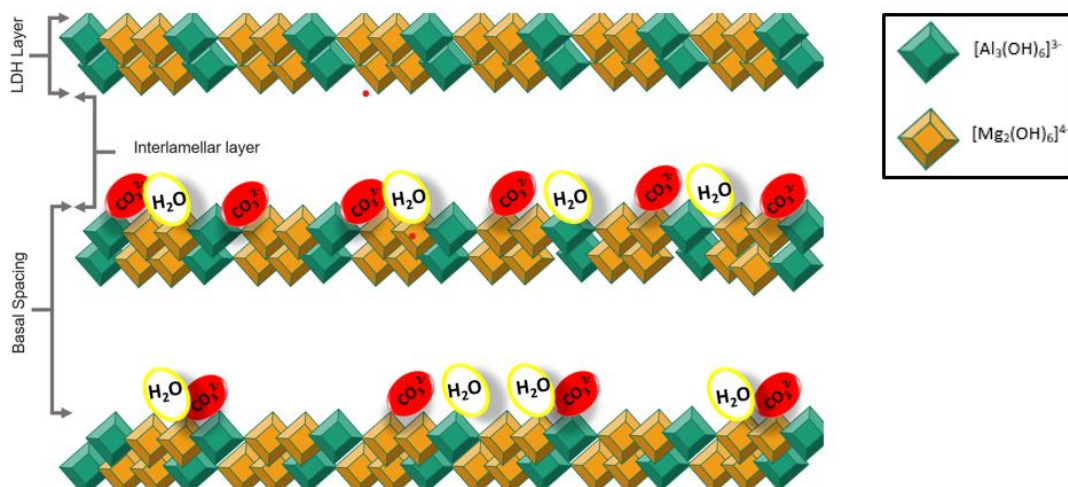


**Figure 1.18.** The structure of HT,  $Mg_6Al_2(OH)_{16}CO_3 \cdot 4H_2O$

## 8.2 HT Materials Properties

The characteristic crystalline, layered structure and compositional flexibility of HT materials afford numerous attractive properties [211], including a cation-exchangeable Brucite-like layer, an anion-exchangeable interlayer, memory effects, tunable basicity, and adsorption capacity.

### Cation-Exchangeable Brucite-Like Layer

Figure 1.19. illustrates the ability of  $Mg^{2+}$  or  $Al^{3+}$  to be exchanged in the Brucite-like layer with other divalent  $M^{2+}$  (Ma) and trivalent  $M^{3+}$  (Mb) ions with similar ionic radii to  $Mg^{2+}$  and  $Al^{3+}$ , respectively. This creates the Brucite-like layer composition expressed as  $[(MgMa)^{2+}_{1-x} (AlMb)^{3+}_x (OH)_2]^{x+}$  [211]. This substitution can be made not only with divalent and trivalent ions but also with monovalent ( $M^+$ ) and tetravalent ( $M^{4+}$ ) ions such as  $Li^+$  and  $Zr^{4+}$  [212-214], which facilitates the formation of a wide range of HT-like compounds [211].

General Introduction

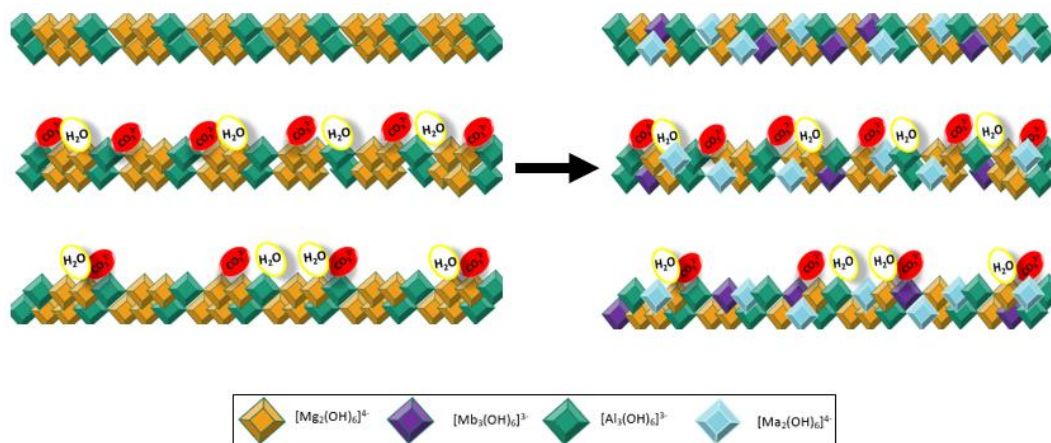


**Figure 1.19.** Schematic overview of partial cation exchange in the LDH structure.

### Anion-Exchangeable Interlayer

The negative charges of inorganic anions (e.g.  $\text{Cl}^-$ ,  $\text{F}^-$ ,  $\text{CO}_3^{2-}$ ,  $\text{NO}_3^-$ , etc.), organic anions (e.g. carboxylates, dicarboxylates, alkyl sulfates, alkane-sulfonates, etc.), complex anions (e.g.  $\text{Fe}(\text{CN})_6^{4-}$ ,  $\text{Fe}(\text{CN})_6^{3-}$ , metal-porphyrins, metal phthalocyanines, etc.), or polyoxometalates (e.g.  $\text{Mo}_7\text{O}_{24}^{6-}$ ,  $\text{W}_7\text{O}_{24}^{6-}$ ,  $\text{PMo}_{12}\text{O}_{40}^{3-}$ , etc.) [204,215-217] can compensate for the positive charges of the Brucite-like layers (Figure 1.20.) [206,207,218].

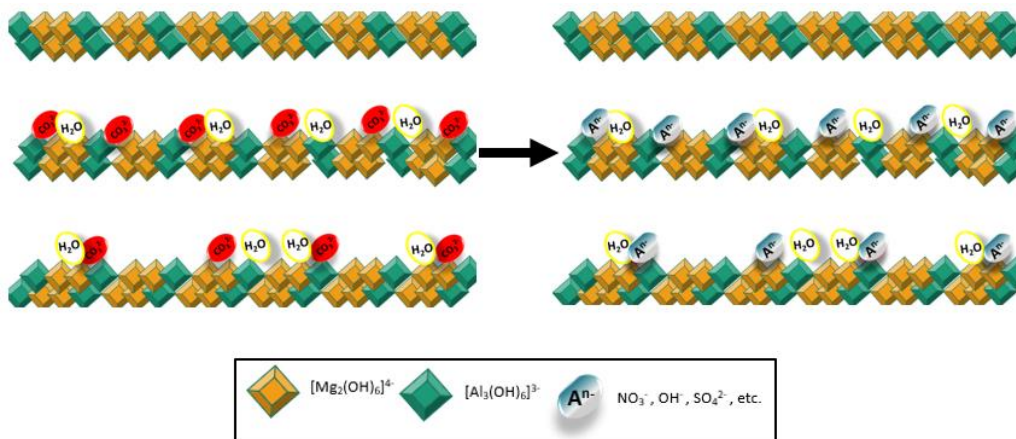


**Figure 1.20.** The anion exchange inside the Brucite-like layers.

## The Memory Effects

Memory effects occur when the mixed oxides generated by the thermal decomposition of HT are rehydrated by the aqueous solution of anionic species to obtain the new HT structure with the anions exchanged from the solution (Figure 1.21.) [211]. Large anions such as polyoxometalates can be introduced between the original Brucite-like layers during this reconstruction process [219,220].

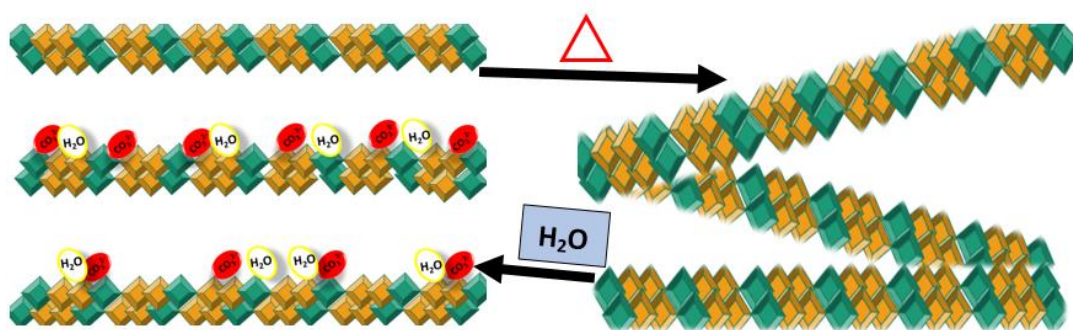


**Figure 1.21.** The memory effect via thermal and rehydration exposure.

## Tunable basicity

There are three ways of controlling basicity: (a) changing the ratio of  $M^{2+}$  to  $M^{3+}$ , (b) exchanging the cations themselves within the Brucite layer, and (c) exchanging anions within the interlayer and on the surface of the HT [211], which changes its chemical composition [208].

The typical HT contains  $CO_3^{2-}$  as an internal anionic species that is difficult to exchange. However, the calcination process after the rehydration of HT has the role of exchanging the  $CO_3^{2-}$  anions for another anionic species [211].

## Adsorption capacity

Due to the basicity of HT, inorganic and organic species such as arsenates [221], chromates [222] and anionic surfactants [223] can be adsorbed with alkali

adsorption centers. Adsorption can take place on the external surface and in the interlayer space [224]. The features of HT and HT-like compounds make them highly functionalized materials with numerous industrial applications, including as anti-acid drugs [225] and flame-retardant additives in polymeric materials [226,227], in the pharmaceutical and cosmetics industries [229,230], and as wastewater-treatment materials [228].

### **8.3. HT Materials as Promising Catalysts**

The use of HTs as catalysts makes them an up-and-coming field of research [218, 276, 277]. In the mid-1990s, the use of heterogeneous catalysis methods based on HT and HT-like compounds increased on account of their compatibility with the development of the “Green Chemistry” concept [164]. The characteristics of HTs make them flexible for designing high-performance multifunctional heterogeneous catalysts that act as catalytic bases or tailor-made metal catalysts with active species of divalent  $M^{2+}$  ( $M_A$ ) and/or trivalent  $M^{3+}$  ( $M_B$ ) ions at the octahedral sites. The active species are grafted by the high adsorption capacity of HTs and can be substituted for a wide range of transition metals to create various HT-like compounds. These compounds can be used as efficient heterogeneous catalysts in a series of organic synthesis and produced successfully in a single pot reaction [204,205,211,163]. Also, reduction of the grafted active species makes the HT materials a suitable solid for supporting metal nanoparticles (MNPs) [211].

In the catalyst structure, the cations and anions are exchanged and the memory effect can be used to modify the basicity of the HT surface.

Environmentally speaking, catalytic structures that use the HT method have significant advantages for achieving green organic syntheses because they use

nonpolluting reagents, have a high catalytic activity and selectivity, can be used with a wide range of substrates, and are simple to recover and reuse [211].

Moreover, solid-base HT catalysts are suitable for environmentally benign organic reactions [161,155] such as oxidation, epoxidation, esterification, and hydrogenation, etc. [211]. Several recent studies have used different HT materials to catalyze the hydrogenation reaction of furfural over Pt/HT [122], NiCoAl/HT [201], NiCuAl/HT [86], etc.

## 9. Thesis Objective and Structure

The current worldwide political scenario and lack of energy sources highlight the urgent need for sources of renewable energy.

The main aim of this thesis is to obtain a group of non-noble hydrogenation catalysts that are suitable for producing commodity chemicals for use as fuel and fuel additives from the biomass-derived platform chemical furfural.

To achieve this main aim, the following secondary objectives will be established:

- synthesize and characterize a group of catalysts suitable for the hydrogenation of furfural using layered double hydroxides (LDHs),
- assess the performance of the synthesized catalysts under a wide range of liquid-phase and gas-phase conditions, and
- select a small group of high-performance materials to conduct stability tests with extended time-on-stream under constant conditions.

## General Introduction

This thesis is divided into six chapters:

**Chapter 1** provides a general introduction to biomass materials and their structure; furfural and its reactions and derivatives; and catalysts used in furfural conversion, including those based on layered double hydroxide (LDH).

**Chapter 2** describes the materials used, the catalyst-preparation methods, the experimental procedures, and the reaction setups.

**Chapter 3** examines catalysts of Ni-Cu prepared from layered double hydroxides supported on aluminum oxide ( $\text{Al}_2\text{O}_3$ ) to hydrogenate furfural into alcohols. It also characterizes the catalytic materials in order to thoroughly explain the physical and chemical properties, assesses the performance of the catalysts in the conversion of furfural and the selectivity of the target products, and examines the effect of the Ni/Cu molar ratio on the range of products in two reactors, i.e. a high-batch slurry reactor (SSR) and a continuous packed-bed reactor (PBR).

**Chapter 4** describes the synthesis of mono and bimetallic catalysts of Ni and Co in different molar ratios of Ni:Co, i.e. 2:0, 1.5:0.5, 1:1, and 0.5:1.5, and conducts a comprehensive study of furfural's pathways during the hydrogenation reaction. To do so, an additional reductive catalytic reaction of either furfuryl alcohol and tetrahydrofurfuryl alcohol was performed and the results were compared with those obtained from furfural hydrogenation. A series of reactions over the  $\text{Ni}_1\text{Co}_1\text{Al}$  catalyst was also performed in order to explore the ideal reaction time. The strong influence of the Co/Ni ratio was reported via the hydrogenation of furfural in the liquid-phase using ethanol as a solvent in the batch reactor. As in Chapter 3, a broad physical characterization of the catalysts is made and the chemical content is analyzed.

## General Introduction

**Chapter 5** makes a comparative study based on the reaction variables of the furfural hydrogenation over  $\text{Ni}_2\text{Mg}_1\text{Al}$  as the catalyst. More specifically, three groups of furfural hydrogenation reactions were conducted under different conditions. Group one reactions were conducted in different time periods (1, 2, 4, 6 and 8 h), group two reactions were conducted under different pressures (1.0, 2.0, 3.0, 4.0 and 5.0 MPa.), and group three reactions were conducted at different temperatures (433 K, 463 K and 483 K). The hydrogenation of furfural was also performed over the three catalysts ( $\text{Ni}_2\text{Mg}_1\text{A}$ ,  $\text{Ni}_1\text{Mg}_1\text{A}$  and  $\text{Ni}_2\text{A}$ ) in two types of reactors: a high-batch slurry reactor (SSR) and a continuous packed-bed reactor (PBR). Also in this chapter the chemical and physical proprieties of the catalytic material were characterized.

**Chapter 6** provides a general conclusion for the thesis and suggests ideas for future work.

## 10. References

- [1] Chheda, J. N.; Dumesic, J. A. An Overview of Dehydration, Aldol-Condensation and Hydrogenation Processes for Production of Liquid Alkanes from Biomass-Derived Carbohydrates. *Catal. Today* 2007, 123, 59–70.
- [2] Serrano-Ruiz, J. C.; West, R. M.; Dumesic, J. A. Catalytic Conversion of Renewable Biomass Resources to Fuels and Chemicals. *Annu. Rev. Chem. Biomol. Eng.* 2010, 1, 79–100.
- [3] Huber, G. W.; Iborra, S.; Corma, A. Synthesis of Transportation Fuels from Biomass: Chemistry, Catalysts, and Engineering. *Chem. Rev.* 2006, 106, 4044–4098
- [4] Klass, D. L. Biomass for Renewable Energy, Fuels, and Chemicals. Academic Press, San Diego, CA, 1998, 1-651, Chapter 1, 1-27.
- [5] SOLID BIOFUELS BAROMETER - EurObserv'ER - DECEMBER 2020. <https://www.eurobserv-er.org/solid-biomass-barometer-2020/>
- [6] World total final consumption by source, 2019. <https://www.iea.org/reports/key-world-energy-statistics-2021/final-consumption>
- [7] Ravishankara, A. R.; Rudich, Y.; Pyle, J. A. Role of Chemistry in Earth's Climate. *Chem. Rev.* 2015, 115,3679–3681.
- [8] Yijun, Jiang.; Xicheng, Wang.; Quan, Cao.; Linlin, Dong.; Jing, Guan.; Xindong, Mu. Sustainable production of Bulk Chemicals. ISBN 978-94-017-7475-8
- [9] Mariscal, R.; Maireles-Torres, P.; Ojeda, M.; Sábada, I.; López-Granados, M. Furfural: a renewable and versatile platform molecule for the synthesis of chemicals and fuels. *Energy Environ Sci.* 2016, 9, 1144–1189.
- [10] Petrus, L.; Noordermeer, MA. Biomass to biofuels, a chemical perspective. *Green Chem.* 2006, 8:861–867.
- [11] [https://www.globalcarbonproject.org/global/images/carbonbudget/Infographic\\_Emissions2021.pdf](https://www.globalcarbonproject.org/global/images/carbonbudget/Infographic_Emissions2021.pdf)
- [12] Ragauskas, A. J.; Williams, C. K.; Davison, B. H.; G. Britovsek.; Cairney, J.; Eckert, C. A.; Frederick, W. J.; Hallett, J. P.; Leak, D. J.; Liotta, C. L.; Mielenz, J. R.; Murphy, R.; Templer, R.; Tschaplinski, T. The path forward for biofuels and biomaterials. *Science*, 2006, 311, 484–489
- [13] Cortright, R.C.; Davda, R.R.; Dumesic, J.A. Hydrogen from catalytic reforming of biomass-derived hydrocarbons in liquid water. *Nature* 2002, 418:964–967.13.
- [14] Mascal, M.; Nikitin, EB. Direct high-yield conversion of cellulose into biofuel. *Angew Chem Int Ed.* 2008 47:7924–7926.
- [15] Binder, J.B.; Raines, R.T. Simple chemical transformation of lignocellulosic biomass into furans for fuels and chemicals. *J Am Chem Soc.* 2009 131:1979–1985.

## General Introduction

- [16] Climent, M. J.; Corma, A.; Iborra, S. Conversion of Biomass Platform Molecules into Fuel Additives and Liquid Hydrocarbon Fuels. *Green Chem.* 2014, 16, 516.
- [17] Elliott, D. C. Historical Developments in Hydroprocessing Bio- Oils. *Energy Fuels* 2007, 21, 1792–1815.
- [18] Towler, G. P.; Oroskar, A. R.; Smith, S. Development of a sustainable liquid fuels infrastructure based on biomass E. *Environ. Prog.* 2004, 23, 334.
- [19] Lynd, L. R.; Wyman, C. E.; Gerngross. *Biocommodity Engineering. T. U. Biotechnol. Prog.* 1999, 1;15(5):777-793
- [20] Nagaraja, B.M.; Padmasri, A.H.; David Raju, B.; Rama Rao, K.S. Vapor Phase Selective Hydrogenation of Furfural to Furfuryl Alcohol over Cu–MgO Coprecipitated Catalysts. *J. Mol. Catal. A: Chem.* 2007, 265, 90–97.
- [21] Huber, G. W.; Dumesic. An Overview of Aqueous-Phase Catalytic Processes for Production of Hydrogen and Alkanes in a Biorefinery. *J. A. Catal. Today* 2006, 111, 119.
- [22] Liu, D.; Zemlyanov, D.; Wu, T.; Lobo-Lapidus, R. J.; Dumesic, J. A.; Miller, J. T.; Marshall, C. L. Deactivation Mechanistic Studies of Copper Chromite Catalyst for Selective Hydrogenation of 2-Furfuraldehyde. *J. Catal.* 2013, 299, 336–345.
- [23] F.H. Isikgor.; C.R. Becer. Lignocellulosic biomass: a sustainable platform for the production of biobased chemicals and polymers, *Polym. Chem.* 6, 2015, 4497–4559.
- [24] Petrucci, Ralph H.; Harwood, William S.; Herring, F. Geoffrey (2002). *General chemistry: principles and modern applications* (8th ed.). Publisher: Upper Saddle River, N.J: Prentice Hall. pp. 341–342. ISBN 978-0-13-014329-7.
- [25] Housecroft, C. E.; Sharpe, A. G. *Inorganic Chemistry*, 2nd ed, Pearson Prentice-Hall, 2005 pp. 20–21.
- [26] X. Liu.; F.P. Bouxin.; J. Fan.; V.L. Budarin.; C. Hu.; J.H. Clark. Recent Advances in the Catalytic Depolymerization of Lignin towards Phenolic Chemicals: A Review, *ChemSusChem* 13, 2020, 4296– 4317.
- [27] Zhang, H.; Canlas, C.; Jeremy Kropf, A.; Elam, J. W.; Dumesic, J. A.; Marshall, C. L. Enhancing the Stability of Copper Chromite Catalysts for the Selective Hydrogenation of Furfural with ALD Overcoating (II) – Comparison between TiO<sub>2</sub> and Al<sub>2</sub>O<sub>3</sub> Overcoatings. *J. Catal.* 2015, 326, 172–181.
- [28] Pratima Bajpai, Chapter 2 - Wood and Fiber Fundamentals, Pages 19-74, ISBN 9780128142400, Biermann's Handbook of Pulp and Paper (Third Edition), Elsevier, 2018.
- [29] P, Maki-Arvela.; T, Salmi.; B, Holmbom.; S, Willfor.; D. Y, Murzin, Chem. Selective Hydrolysis of Arabinogalactan into Arabinose and Galactose Over Heterogeneous Catalysts *Rev.* 2011, 111, 5638–5666.

## General Introduction

- [30] Nagaraja, B. M.; Siva Kumar, V.; Shasikala, V.; Padmasri, A. H.; Sreedhar, B.; David Raju, B.; Rama Rao, K. S. A Highly Efficient Cu/MgO Catalyst for Vapour Phase Hydrogenation of Furfural to Furfuryl Alcohol. *Catal. Commun.* 2003, 4, 287–293.
- [31] Dandekar, A.; Baker, R. T. K.; Vannice, M. A. Carbon-Supported Copper Catalysts. *J. Catal.* 1999, 184, 2, 421–439.
- [32] Boronat, M.; May, M.; Illas, F. Origin of Chemoselective Behavior of S-Covered Cu(111) towards Catalytic Hydrogenation of Unsaturated Aldehydes. *Surf. Sci.* 2008, 602, 3284–3290.
- [33] Liu, L.; Lou, H.; Chen, M. Selective Hydrogenation of Furfural to Tetrahydrofurfuryl Alcohol over Ni/CNTs and Bimetallic CuNi/CNTs Catalysts. *Int. J. Hydrogen Energy* 2016, 41, 14721–14731.
- [34] Sulmonetti, T. P.; Pang, S. H.; Claire, M. T.; Lee, S.; Cullen, D. A.; Agrawal, P. K.; Jones, C. W. Vapor Phase Hydrogenation of Furfural over Nickel Mixed Metal Oxide Catalysts Derived from Layered Double Hydroxides. *Appl. Catal., A* 2016, 517, 187–195.
- [35] Peters, J. F. N. Method for the Reduction of Furfural and Furan Derivatives. US1906873 A, May 2, 1933.
- [36] Ruelle, C.É. Bibliographie annuelle des études grecques. Review of Greek Studies 1906, 19, 420–484. [https://www.persee.fr/doc/reg\\_0035-2039\\_1888\\_num\\_1\\_4\\_7397](https://www.persee.fr/doc/reg_0035-2039_1888_num_1_4_7397)
- [37] Rudiansono, R.; Syahrul, K.; Takayoshi, H.; Nobuyuki, I.; Shogo, S. Highly Efficient and Selective Hydrogenation of Unsaturated Carbonylcompounds Using Ni–Sn Alloy Catalysts. *Catal. Sci. Technol.* 2012, 2, 2139–2149.
- [38] De Thomas, W. R.; Hort, E. V. Catalyst Comprising Raney Nickel With Adsorbed Molybdenum Compound. United States Patent, US4153578A, May 08, 1979.
- [39] Li, H.; Zhang, S.; Luo, H. A Ce-Promoted Ni–B Amorphous Alloy Catalyst (Ni–Ce–B) for Liquid-Phase Furfural Hydrogenation to Furfural Alcohol. *Mater. Lett.* 2004, 58, 2741–2746.
- [40] Reddy Kannapu, H. P.; Mullen, C. A.; Elkasabi, Y.; Boateng, A. A. Catalytic Transfer Hydrogenation for Stabilization of Bio-Oil Oxygenates: Reduction of p-Cresol and Furfural over Bimetallic Ni–Cu Catalysts Using Isopropanol. *Fuel Process. Technol.* 2015, 137, 220–228.
- [41] Normann, W.; Prückner, H. Process for Producing Tetrahydrofurfuryl Alcohol. United States Patent, US2071704, November 7, 1931. <https://patentimages.storage.googleapis.com/3d/88/0a/6cd4085367d18c/US2071704.pdf>
- [42] L. Lloyd. Handbook of Industrial Catalysts, 2011. Springer, US, ISBN : 978-0-387-24682-6.
- [43] Rodiansono, R.; Hara, T.; Shimazu, S. Total Hydrogenation of Biomass-derived Furfural over Raney Nickel-Clay Nanocomposite Catalysts. *Indones. J. Chem.* 2013, 13, 101–107.
- [44] Srivastava, S.; Jadeja, G. C.; Parikh, J. Synergism Studies on Alumina-Supported Copper-Nickel Catalysts towards Furfural and 5-Hydroxymethylfurfural Hydrogenation. *J. Mol. Catal. A: Chem.* 2017, 426, 244–256.

## General Introduction

- [45] Xiong, K.; Lee, W.-S.; Bhan, A.; Chen, J. G. Molybdenum Carbide as a Highly Selective Deoxygenation Catalyst for Converting Furfural to 2-Methylfuran. *ChemSusChem* 2014, 7, 2146–2149.
- [46] Chao, Zhong.; Chunming, Wang.; Fan, Huang.; Fengxue, Wang.; Honghua, Jia.; Hua, Zhou.; Ping, Wei. Selective hydrolysis of hemicellulose from wheat straw by a nanoscale solid acid catalyst, *Carbohydrate Polymers*, 131, 2015, 384-391, ISSN 0144-8617.
- [47] Andrea, Komesu.; Johnatt, Oliveira.; João, M. Neto.; Eduardo, D. Penteadó.; Anthony, A.R. Diniz.; Luiza, H.D.S, Martins. *Genetic and Metabolic Engineering for Improved Biofuel Production from Lignocellulosic Biomass*, Elsevier, Chapter 10, Xylose fermentation to bioethanol production using genetic engineering microorganisms, 143-154, 2020.
- [48] Hudson, Claude S.; Cantor, Sidney M.; Peat, Stanley; Stacey, Maurice. *Advances in Carbohydrate Chemistry*. eds. Vol. 5. Elsevier. ISBN 9780080562643, 1950.
- [49] Morgan, E. David. *Biosynthesis in Insects*. Royal Society of Chemistry. ISBN 9780854046911, 2004.
- [50] T. Werpy.; G. Petersen. *Top value added chemicals from biomass: Volume 1*, ed., US Department of Energy, 2004. 17.
- [51] Dandekar, A.; Vannice, M. A. Crotonaldehyde Hydrogenation on Pt/TiO<sub>2</sub> and Ni/TiO<sub>2</sub> SMSI Catalysts. *J. Catal.* 1999, 183, 344– 354.
- [52] Liaw, B. J.; Chiang, S. J.; Chen, S. W.; Chen, Y. Z. Preparation and Catalysis of Amorphous CoNiB and Polymer-Stabilized CoNiB Catalysts for Hydrogenation of Unsaturated Aldehydes. *Applied Catalysis A-general* . 346. 179-188. 10.1016/j.apcata.2008.05.025.
- [53] Li, H.; Chai, W. M.; Luo, H. S.; Li, H. X. Hydrogenation of Furfural to Furfuryl Alcohol over Co-B Amorphous Catalysts Prepared by Chemical Reduction in Variable Media. *Chin. J. Chem.* 2006, 24, 1704–1708.
- [54] C, Moreau.; R, Durand.; D, Peyron.; J, Duhamet.; P, Rivalier. Selective Preparation of Furfural from Xylose over Microporous Solid Acid Catalysts. *Ind.Crops Prod.*, 1998, 7, 95-99.
- [55] S, Lima.; M, Pillinger.; A.A, Valente. Dehydration of D-xylose into furfural catalysed by solid acids derived from the layered zeolite Nu-6(1). *Catal. Commun.*, 2008, 9,2144-2148.
- [56] C, Aellig.; D, Scholz.; P.Y, Dapsens.; C, Mondelli.; J, Pérez-Ramírez. When catalyst meets reactor: continuous biphasic processing of xylan to furfural over GaUSY/Amberlyst-36, *Catal. Sci. Technol.* 5, 2015 142–149.
- [57] I. Delidovich, R. Palkovits. Catalytic Isomerization of Biomass-Derived Aldoses: A Review, *Chem Sus Chem* 9, 2016, 547–561.
- [58] Shi, J. J.; Wang, Y. Y.; Du, W. C.; Hou, Z. Y. Iron Carbide Catalyst Wrapped by Graphene inside Carbon Nanotube for Aldehyde Hydrogenation and Preparation Method thereof. *CN105363482A*, 2015.

## General Introduction

- [59] Li, J.; Liu, J.; Zhou, H.; Fu, Y. Catalytic Transfer Hydrogenation of Furfural to Furfuryl Alcohol over Nitrogen-Doped Carbon-Supported Iron Catalysts. *Chem Sus Chem* 2016, 9, 1339–1347.
- [60] Anil, K. Mathew.; Amith, Abraham.; Kiran, K. Mallapureddy.; Rajeev, K. Sukumaran. Lignocellulosic Biorefinery Wastes, or Resources? *Waste Biorefinery*, 2018, Pages 267-297.
- [61] Zeitsch, K. J. The chemistry and technology of furfural and its many by-products. Elsevier; 2000, ISBN: 9780080528991.
- [62] William, J. McKillip.; Gerd, Collin.; Hartmut, Höke.; Karl, J. Zeitsch. Furan and derivatives. *Ullmann's encyclopedia of industrial chemistry* 2001.
- [63] Hoydonckx, H.E.; Van Rhijn, W.M.; Van Rhijn, W.; De Vos, D.E.; Jacobs, P.A. Furfural and Derivatives. In *Ullmann's Encyclopedia of Industrial Chemistry* 2007.
- [64] Wan Isahak, W.N.R.; Hisham, M.W.M.; Yarmo, M.A.; Hin, T.Y. A review on bio-oil production from biomass by using pyrolysis method. *Renew Sust Energy Rev* 2012, 16, 5910–23.
- [65] Aycock, D.F. Solvent applications of 2-methyltetrahydrofuran in organometallic and biphasic reactions. *Org Proc Res Dev* 2007; 11:156–9.
- [66] T, Ahmad.; L, Kenne.; K, Olsson.; O, Theander.; The formation of 2-furaldehyde and formic acid from pentoses in slightly acidic deuterium oxide studied by  $^1\text{H}$  NMR spectroscopy, *Carbohydr. Res.* 276, 1995, 309–320.
- [67] Bonner, W.A.; Roth, M.R.; The conversion of D-xylose-1- $\text{C}^{14}$  into 2-furaldehyde- $\alpha$ - $\text{C}^{14}$ , *J. Am. Chem. Soc.* 81, 1959, 5454–5456.
- [68] Nimlos, M.R.; Qian, X.; Davis, M.; Johnson, D.K.; Himmel, M.E. Energetics of xylose decomposition as determined using quantum mechanics, *J. Phys. Chem. A* 110, 2006, 11824–11838.
- [69] Yan, K.; Wu, G.; Lafleur, T.; Jarvis, C. Production, properties and catalytic hydrogenation of furfural to fuel additives and value-added chemicals, *Renew. Sustain. Energy Rev.* 38, 2014, 663–676.
- [70] Xiu, S.N.; Shahbazi, A. Bio-oil production and upgrading research: a review, *Renew. Sustain. Energy Rev.* 16, 2012, 4406–4414.
- [71] Raman, J.K.; Gnansounou, E. Furfural production from empty fruit bunch—a biorefinery approach, *Ind. Crop Prod.* 69, 2015, 371–377.
- [72] Ekpeni, L.E.N.; Benyounis, K.Y.; Nkem-Ekpeni, F.; Stokes, J.; Olabi, A.G. Energy diversity through renewable energy source (RES)—a case study of biomass, *Energy Procedia* 61, 2014, 1740-1747.
- [73] Bozell J J, Petersen GR. Technology development for the production of biobased products from biorefinery carbohydrates—the US Department of Energy's Top 10 revisited. *GreenChem* 2010; 12:539-54.

## General Introduction

- [74] Global furfural market value 2015-2029 - Statista. Source: © Statista 2022 <https://www.statista.com/statistics/1310467/furfural-market-value-worldwide/>
- [75] Corma, A.; Iborra, S.; Velty, A. Chemical routes for the transformation of biomass into chemicals, *Chemical reviews* 107, 2007, 2411–2502.
- [76] Millán, G.G.; Sixta, H. Towards the green synthesis of furfuryl alcohol in a one-pot system from xylose: A review. *Catalysts*. 2020; 10: 1101.
- [77] Tran, L.S.; Carstensen, H.H.; Lamoureux, N.; Foo, K.K.; Gosselin, S.; El Bakali, A.; Gasnot, L.; Desgroux, P. Exploring the flame chemistry of C<sub>5</sub> tetrahydrofuranic biofuels: Tetrahydrofurfuryl alcohol and 2-methyltetrahydrofuran. *Energy Fuels*. 2021; 35: 18699-18715.
- [78] Zhang, M.; Yang, J.H. Selective hydrogenation of furfural: Pure silica supported metal catalysts. *Chemistry Select*. 2022; 7: e202200013.
- [79] Barr, J.B.; Wallon, S.B. The chemistry of furfuryl alcohol resins. *J Appl Poly Sci* 1971, 15:1079-90.
- [80] Connor, R.; Folkers, K.; Adkins, H. The preparation of copper-chromium oxide catalysts for hydrogenation. *J Am Chem Soc* 1932, 54, 1138-1145.
- [81] Seo, G.; Chon, H. Hydrogenation of furfural over copper-containing catalysts. *J Catal* 1981, 67:424-9.
- [82] Lukes, R.M.; Wilson, C.L. Reactions of furan compounds. XI. side chain reactions of furfural and furfuryl alcohol over nickel-copper and iron-copper catalysts. *J Am Chem Soc* 1951, 73:4790-4.
- [83] Wojcik, B.H. Catalytic hydrogenation of furan compounds. *Ind Eng Chem* 1948, 40:210-6.
- [84] Brown, H.D.; Hixon, R.M. Vapor phase hydrogenation of furfural to furfuryl alcohol. *Ind Eng Chem* 1949, 41:1382-5
- [85] Stevens, J.G.; Bourne, R.A.; Twigg, M.V.; Poliakoff, M. Real-time product switching using a twin catalyst system for the hydrogenation of furfural in supercritical CO<sub>2</sub>. *Angew Chem Int Ed* 2010, 49:8856-9.
- [86] Aldureid, A.; Medina, F.; Patience G. S.; Montané, D. Ni-Cu/Al<sub>2</sub>O<sub>3</sub> from Layered Double Hydroxides Hydrogenates Furfural to Alcohols. *Catalysts* 2022, 12, 390.
- [87] Sitthisa, S.; Resasco, D.E. Hydrodeoxygenation of furfural over supported metal catalysts: a comparative study of Cu, Pd and Ni. *Catal Lett* 2011; 141: 784-91.
- [88] Nakagawa, Y.; Nakazawa, H.; Watanabe, H.; Tomishige, K. Total hydrogenation of furfural over a silica-supported nickel catalyst prepared by the reduction of a nickel nitrate precursor. *ChemCatChem* 2012; 4:1791-1797.

## General Introduction

- [89] Biradar, N.S.; Hengne, A.M.; Birajdar, S.N.; Niphadkar, P.S.; Joshi, P.N.; Rode, C.V. Single-pot formation of THFAL via catalytic hydrogenation of FFR over Pd/MFI catalyst. *ACS Sustainable Chem Eng* 2014; 2, 2 :272-81.
- [90] Werle, P.; Morawietz, M.; Lundmark, S.; Sörensen, K.; Karvinen, E.; Lehtonen, J. Alcohols, Polyhydric. In *Ullmann's Encyclopedia of Industrial Chemistry* 2008.
- [91] He, J.; Huang, K.; Barnett, K. J.; Krishna, S. H.; Alonso, D. M.; Brentzel, Z. J.; Burt, S. P.; Walker, T.; Banholzer, W. F.; Maravelias, C. T.; Hermans, I.; Dumesic, J. A.; Huber, G. W. New catalytic strategies for  $\alpha,\omega$ -diols production from lignocellulosic biomass. *Faraday Discuss.* 2017, 202, 247-267.
- [92] Huang, K. F.; Brentzel, Z. J.; Barnett, K. J.; Dumesic, J. A.; Huber, G. W.; Maravelias, C. T. Conversion of Furfural to 1,5-Pentanediol: Process Synthesis and Analysis. *ACS Sustainable Chem. Eng.* 2017, 5, 4699-4706.
- [93] Al-Yusufi, m.; Steinfeldt, N.; Eckelt, R.; Atia, H.; Lund H.; Bartling, S.; Rockstroh, N.; Köckritz, A. Efficient Base Nickel-Catalyzed Hydrogenolysis of Furfural-Derived Tetrahydrofurfuryl Alcohol to 1,5-Pentanediol. *ACS Sustainable Chemistry & Engineering* 2022, 10 ,15, 4954-4968.
- [94] MarketWatch. 1,5-Pentanediol Market Size In 2021 with 3.8% CAGR: Top Countries Data, What are the key growth impellers of the global 1,5-Pentanediol Industry, 2021; <https://www.marketwatch.com/press-release/global-15-pentanediol-market-2021-industry-growthand-key-countries-analysis-by-2027-2021-12-13>.
- [95] Koso, S.; Ueda, N.; Shinmi, Y.; Okumura, K.; Kizuka, T.; Tomishige, K. Promoting effect of Mo on the hydrogenolysis of tetrahydrofurfuryl alcohol to 1,5-pentanediol over Rh/SiO<sub>2</sub>. *J. Catal.* 2009, 267, 89-92.
- [96] Koso, S.; Furikado, I.; Shima, A.; Miyazawa, T.; Kunimori, K.; Tomishige, K. Chemo selective hydrogenolysis of tetrahydrofurfuryl alcohol to 1,5-pentanediol. *Chem. Commun.* 2009, 2035-2037.
- [97] Koso, S.; Watanabe, H.; Okumura, K.; Nakagawa, Y.; Tomishige, K. Comparative study of Rh-MoO<sub>x</sub> and Rh-ReO<sub>x</sub> supported on SiO<sub>2</sub> for the hydrogenolysis of ethers and polyols. *Appl. Catal. B: Environ.* 2012, 111-112, 27-37.
- [98] Chen, K. Y.; Koso, S.; Kubota, T.; Nakagawa, Y.; Tomishige, K. Chemoselective Hydrogenolysis of Tetrahydropyran-2-methanol to 1,6-Hexanediol over Rhenium-Modified Carbon-Supported Rhodium Catalysts. *ChemCatChem* 2010, 2, 547-555.
- [99] Chatterjee, M.; Kawanami, H.; Ishizaka, T.; Sato, M.; Suzuki, T.; Suzuki, A. An attempt to achieve the direct hydrogenolysis of tetrahydrofurfuryl alcohol in supercritical carbon dioxide. *Catal. Sci. Technol.* 2011, 1, 1466-1471.
- [100] Chia, M.; Pagán-Torres, Y. J.; Hibbitts, D.; Tan, Q.; Pham, H. N.; Datye, A. K.; Neurock, M.; Davis, R. J.; Dumesic, J. A. Selective Hydrogenolysis of Polyols and Cyclic Ethers over Bifunctional Surface Sites on Rhodium-Rhenium Catalysts. *J. Am. Chem. Soc.* 2011, 133, 12675-12689.

## General Introduction

- [101] Chen, K.; Mori, K.; Watanabe, H.; Nakagawa, Y.; Tomishige, K. C-O bond hydrogenolysis of cyclic ethers with OH groups over rhenium-modified supported iridium catalysts. *J. Catal.* 2012, 294, 171–183.
- [102] Transport & Environment. *Globiom: The Basis for Biofuel Policy Post-2020*; Transport & Environment: Brussels, Belgium, 2016; <https://www.transportenvironment.org/discover/globiom-basis-biofuel-policy-post-2020/>
- [103] Flach, B.; Lieberz, S.; Rossetti, A.; Phillips, S. *EU-28: Biofuels Annual*; United States Department of Agriculture (USDA): Washington, D.C., 2017.
- [104] Ternel, C.; Bouter, A.; Melgar, J. Life cycle assessment of midrange passenger cars powered by liquid and gaseous biofuels: Comparison with greenhouse gas emissions of electric vehicles and forecast to 2030. *Transp. Res. Part D: Transp. Environ.* 2021, 97, 102897.
- [105] Prussi, M.; Yugo, M.; Lonza, L.; De Prada, L.; Padella, M.; Edwards, R.; Lonza, L. *JEC Well-to-Tank Report V5*, EUR 30269 EN; Publications Office of the European Union: Luxembourg, 2020; ISBN: 978-92-76-19926-7, JRC119036,
- [106] Mathieu, F.; Reddemann, M.; Martin, D.; Kneer, R. Experimental investigation of fuel influence on atomization and spray propagation using an outwardly opening GDI-injector. *SAE Tech. Pap. Ser.* 2010
- [107] Liu, S. B.; Amada, Y.; Tamura, M.; Nakagawa, Y.; Tomishige, K. One-pot selective conversion of furfural into 1,5-pentanediol over a Pd added Ir-ReO<sub>x</sub>/SiO<sub>2</sub> bifunctional catalyst. *Green Chem.* 2014, 16, 617–626.
- [108] Liu, S. B.; Amada, Y.; Tamura, M.; Nakagawa, Y.; Tomishige, K. Performance and characterization of rhenium-modified Rh-Ir alloy catalyst for one-pot conversion of furfural into 1,5-pentanediol. *Catal. Sci. Technol.* 2014, 4, 2535–2549.
- [109] Viana, G.S.; Lau Bonfim, J.A.E.; Da Silva, G.P.; De Carvalho Filho, J.F.S.; Tokumoto, M.S.; Rangel, F.C.; Da Cruz, R.S. Design of Heterogeneous Catalysts for the Conversion of Furfural to C5 Derivatives: A Brief Review *Catalysis Research* 2022; 2(3),
- [110] Gavilá, L.; Lähde, A.; Jokiniemi, J.; Constanti, J.; Medina, F.; del Río, E.; Tichit, D.; Alvarez, M. G. Insights on the one-Pot formation of 1,5-Pentanediol from furfural with Co-Al spinel-based nanoparticles as an alternative to noble metal catalysts. *ChemCatChem* 2019, 11, 4944–4953.
- [111] Tuan, H.A.; Viet, P.V. 2-methylfuran (MF) as a potential biofuel: A thorough review on the production pathway from biomass, combustion progress, and application in engines. *Renew Sust Energ Rev.* 2021; 148: 111265.
- [112] Liu, H. L.; Huang, Z. W.; Zhao, F.; Cui, F.; Li, X. M.; Xia, C. G.; Chen, J. Efficient hydrogenolysis of biomass-derived furfuryl alcohol to 1,2- and 1,5-pentanediols over a non-precious Cu-Mg<sub>3</sub>AlO<sub>4</sub> bifunctional catalyst. *Catal. Sci. Technol.* 2016, 6, 668–671.
- [113] Gao, F. F.; Liu, H. L.; Hu, X.; Chen, J.; Huang, Z. W.; Xia, C. G. Selective hydrogenolysis of furfuryl alcohol to 1,5- and 1,2-pentanediol over Cu-LaCoO<sub>3</sub> catalysts with balanced Cu<sup>0</sup>-CoO sites. *Chinese J. Catal.* 2018, 39, 1711–1723.

## General Introduction

- [114] Zhou, P.; Chen, Y.; Luan, P.; Zhang, X.; Yuan, Z.; Guo, S.X. Selective electrochemical hydrogenation of furfural to 2-methylfuran over a single atom Cu catalyst under mild pH conditions. *Green Chem.* 2021; 23: 3028-3038.
- [115] Siegmeier, R.; Prescher, G.; Maurer, H.; Hering, G. Continuous Process for the Production of Pentanediol-1,2. U.S. Patent 4605795, August 12, 1986.
- [116] Date, N.S.; La Parola, V.; Rode, C.V.; Testa, M.L. Ti-Doped Pd-Au Catalysts for One-Pot Hydrogenation and Ring Opening of Furfural. *Catalysts* 2018, 8, 252.
- [117] Aoki, K.; Mukai, H. Ink-Jet Printing Method and Printed Products. JP Patent 2012245721, December 13, 2012.
- [118] Agostini, I.; Cupferman, S. Cosmetic Composition Comprising an Aqueous Dispersion of Film-Forming Polymer Particles Containing 1,2-Pentanediol. U.S. Patent 6296858, October 2, 2001.
- [119] Mizugaki, T.; Yamakawa, T.; Nagatsu, Y.; Maeno, Z.; Mitsudome, T.; Jitsukawa, K.; Kaneda, K. Direct transformation of furfural to 1,2-pentanediol using a hydrotalcite-supported platinum nanoparticle. *ACS Sustainable Chem. Eng.* 2014, 2, 2243-2247
- [120] Koch, O.; Koeckritz, A.; Kant, M.; Martin, A.; Schoening, A.; Armbruster, U.; Bartoszek, M.; Evert, S.; Lange, B.; Bienert, R. Method for Producing 1,2-Pentanediol. U.S. Patent Application 66666, March 6, 2014.
- [121] Kaufmann, W. E.; Adams, R. The use of platinum oxide as a catalyst in the reduction of organic compounds. IV. Reduction of furfural and its derivatives. *J. Am. Chem. Soc.* 1923, 45, 3029-3044.
- [122] Xu, W.; Wang, H.; Liu, X.; Ren, J.; Wang, Y.; Lu, G. Direct catalytic conversion of furfural to 1,5-pentanediol by hydrogenolysis of the furan ring under mild conditions over Pt/Co<sub>2</sub>AlO<sub>4</sub> catalyst. *Chem. Commun.* 2011, 47, 3924-3926.
- [123] Belskii, I. F.; Shuikin, N. I.; Shostakovskii, V. M. Effect of carbonyl and alkoxy carbonyl groups on the hydrogenolysis of the furan ring under the conditions of vapor-phase hydrogenation. *Bull. Acad. Sci. USSR* 1962, 11, 1727-1730.
- [124] Geilen, F.M.A.; Engendahl, B.; Hölscher, M.; Klankermayer, J.; Leitner, W. Selective homogeneous hydrogenation of biogenic carboxylic acids with [Ru (TriPhos) H]<sup>+</sup>: a mechanistic study. *J Am Chem Soc* 2011, 133:14349–58.
- [125] Yan, K.; Lafleu, T.; Wu, G.; Cheng, C.; Xie, X.M. Highly selective production of value-added  $\gamma$ -valerolactone from biomass-derived levulinic acid using the robust Pd nanoparticles. *Appl Catal A* 2013, 468:52-8.
- [126] Yan, K.; Lafleur, T.; Liao, J. Facile synthesis of palladium nanoparticles supported on multi-walled carbon nanotube for efficient hydrogenation of biomass-derived levulinic acid. *J Nanopart Res* 2013, 15(9):1-7.
- [127] Lange, J.P.; van der Heide, E.; van Buijtenen, J.; Price, R. Furfural-a promising platform for lignocellulosic biofuels. *ChemSusChem* 2012, 5:150–66.

## General Introduction

- [128] Rao, R.; Dandekar, A.; Baker, R.T.K.; Vannice, M.A. Properties of copper chromite catalysts in hydrogenation reactions. *J Catal* 1997, 171:406–19.
- [129] Bremner, J.G.M.; Keeys, R.K.F. The hydrogenation of furfuraldehyde to furfuryl alcohol and sylvan (2-methylfuran). *J Chem Soc* 1947: 1068–80.
- [130] Tian, Y.; Zhang, F.; Wang, J.; Cao, L.; Han, Q. A review on solid acid catalysis for sustainable production of levulinic acid and levulinate esters from biomass derivatives. *Bioresour Technol.* 2021; 342: 125977.
- [131] Xu, W.P.; Chen, X.F.; Guo, H.J.; Li, H.L.; Zhang, H.R.; Xiong, L. Conversion of levulinic acid to valuable chemicals: A review. *J Chem Technol Biotechnol.* 2021; 96: 3009-3024.
- [132] Dutta, S.; Bhat, N.S. Recent advances in the value addition of biomass-derived levulinic acid: A review focusing on its chemical reactivity patterns. *ChemCatChem.* 2021; 13: 3202-3222.
- [133] Mehdi, H.; Fabos, V.; Tuba, R.; Bodor, A.; Mika, L, T.; Horvath, I, T. Integration of homogeneous and heterogeneous catalytic processes for a multi-step conversion of biomass: from sucrose to levulinic acid,  $\gamma$ -valerolactone, 1,4- pentanediol, 2-methyltetrahydrofuran, and alkanes. *Topics in Catalysis*, 2008, 48, 49–54.
- [134] Geilen, F.M.A.; Engendahl, B.; Harwardt, B.E.; Marquardt, W.; Klankermayer, J.; Leitner, W. Selective and flexible transformation of biomass-derived platform chemicals by a multifunctional catalytic system. *Angew Chem Int Ed* 2010, 49:5510–4.
- [135] Upare, P.P.; Lee, J.M.; Hwang, Y.K.; Hwang, D.W.; Lee, J.H.; Halligudi, S.B.; Jin-Soo, Hwang.; Jong-San, Chang. Direct hydrocyclization of biomass-derived levulinic acid to 2-methyltetrahydrofuran over nanocomposite copper/silica catalysts. *ChemSusChem* 2011; 4:1749–52.
- [136] Du, X.L.; Bi, Q.Y.; Liu, Y.M.; Cao, Y.; He, H.Y.; Fan, K.N. Tunable copper-catalyzed chemoselective hydrogenolysis of biomass-derived  $\gamma$ -valerolactone into 1,4- pentanediol or 2-methyltetrahydrofuran. *Green Chem* 2012; 14:935–9.
- [137] Yang, Z.; Huang, Y.B.; Guo, Q.X.; Fu, Y. RANEYS Ni catalyzed transfer hydrogenation of levulinate esters to  $\gamma$ -valerolactone at room temperature. *Chem Commun* 2013; 49:5328–30.
- [138] Al-Shaal, M.G.; Dzierbinski, A.; Palkovits, R. Solvent-free  $\gamma$ -valerolactone hydrogenation to 2-methyltetrahydrofuran catalysed by Ru/C: a reaction network analysis. *Green Chem* 2014, 16:1358–64
- [139] Pang, S. H.; Medlin, J. W. Adsorption and Reaction of Furfural and Furfuryl Alcohol on Pd(111): Unique Reaction Pathways for Multifunctional Reagents. *ACS Catal.* 2011, 1, 1272–1283.
- [140] Mandalika, A.S. Enabling the development of furan-based biorefineries. (Master Thesis). University of Wisconsin–Madison; 2012.
- [141] Hurd, C.D.; Goldsby, A.R.; Osborne, E.N. Furan reaction. II. Furan From Furfural. *J Am Chem Soc* 1932, 54, 6, :2532–2536.

## General Introduction

- [142] Wilson, C.L.; Reactions of furan compounds. Part V. formation of furan from furfuraldehyde by the action of nickel or cobalt catalysts: importance of added hydrogen. *J Chem Soc* 1945:61–3.
- [143] P, Lejemble.; A, Gaset.; P, Kalck. From biomass to furan through decarbonylation of furfural under mild conditions. *Biomass* 1984, 4(4), 263–274.
- [144] Singh, H.; Prasad, M.; Srivastava, R.D. Metal support interactions in the palladium- catalysed decomposition of furfural to furan. *J Chem Tech Biotech* 1980; 30(1):293-6.
- [145] Gross, A.E. Vinylidene chloride copolymer coating for organic film.US Patents US3538029A, 1970.
- [146] Messori, M.; Vaccari, A. Reaction pathway in vapor phase hydrogenation of maleic anhydride and its esters to  $\gamma$ -butyrolactone. *J Catal* 1994, 150:177–85.
- [147] Kanetaka, J.; Asano, T.; Masamune, S. New process for production of tetrahy- drofuran. *Ind Eng Chem* 1970, 62(4):24–32.
- [148] Gilbert, W.W.; Hoke, B.W. Process of hydrogenating maleic anhydride with a nickel or cobalt molybdate catalyst. US Patent 2772293A, 1956.
- [149] Bin, Liu.; Lei, Cheng.; Larry, Curtiss.; Jeffrey, Greeley. Effects of van der Waals density functional corrections on trends in furfural adsorption and hydrogenation on close-packed transition metal surfaces. *Surface Science* 622, 2014, 51-59.
- [150] Moreno-Tost, R.; Santamaría-González, J.; Mérida-Robles, J.; Maireles-Torres, P. Gas-Phase Hydrogenation of Furfural over Cu/ CeO<sub>2</sub> Catalysts. *Catal. Today* 2017, 279, 327–338.
- [151] Zhou, M.; Zeng, Z.; Zhu, H.; Xiao, G.; Xiao, R. Aqueous-phase catalytic hydrogenation of furfural to cyclopentanol over Cu-Mg-Al hydrotalcites derived catalysts: model reaction for upgrading bio-oil. *J. Energy Chem.* 2014, 23, 91-96.
- [152] Wang, Y.; Zhou, M.; Wang, T.; Xiao, G. Conversion of Furfural to Cyclopentanol on Cu/Zn/Al Catalysts Derived from Hydrotalcite-Like Materials. *Catal. Lett.* 2015, 145, 1557-1565.
- [153] Guo, J.; Xu, G.; Han, A.; Zhang, Y.; Fu, Y.; Guo Q. Selective Conversion of Furfural to Cyclopentanone with CuZnAl Catalysts. *ACS Sustainable Chem. Eng.* 2014, 2, 2259-2266.
- [154] Yoshida, Y.; Hirotsu, K.; Fujimoto, R.; Katsura, R.; Fujitsu, S.; Doi, T.; Kashiwagi, K. Method for Producing High-Purity 1,5- Pentanediol. US8940946 B2, January 27, 2015.
- [155] G, Busca. Bases and basic materials in chemical and environmental processes. Liquid versus solid basicity. *Chem. Rev.* 2010, 110, 2217-2249.
- [156] Lee, J.; Burt, S. P.; Carrero, C. A.; Alba-Rubio, A. C.; Ro, I.; O'Neill, B. J.; Kim, H. J.; Jackson, D. H. K.; Kuech, T. F.; Hermans, I.; Dumesic, J. A.; Huber G. W. Stabilizing cobalt catalysts for aqueous-phase reactions by strong metal-support interaction. *J. Catal.* 2015, 330, 19–27.
- [157] Shao, Y.; Guo, M.; Wang, J.; Sun, K.; Zhang, L.; Zhang, S.; Hu, G.; Xu, L.; Yuan, X.; Hu, X. Selective Conversion of Furfural into Diols over Co-Based Catalysts: Importance of the

## General Introduction

- Coordination of Hydrogenation Sites and Basic Sites. *Ind. Eng. Chem. Res.* 2021, 60, 10393–10406
- [158] I, Chorkendorff.; J.W, Niemantsverdriet. *Concepts of Modern Catalysis and Kinetics*, John Wiley & Sons, 2003, 696 pp. ISBN 3-527-30574-2.
- [159] Gadi. Rothenberg. *Catalysis: concepts and green applications*. Weinheim [Germany]: Wiley VCH. ISBN 9783527318247. OCLC 213106542, 17 March 2008
- [160] Liu, H.; Hu, Q.; Fan, G.; Yang, L.; Li, F. Surface Synergistic Effect in Well-Dispersed Cu/MgO Catalysts for Highly Efficient Vapor-Phase Hydrogenation of Carbonyl Compounds. *Catal. Sci. Technol.* 2015, 5, 3960–3969.
- [161] H, Hattori. *Heterogeneous Basic Catalysis*. *Chem. Rev.*, 1995, 95, 537-550.
- [162] C, Moreau.; R, Durand.; D, Peyron.; J, Duhamet.; P, Rivalier. Selective preparation of furfural from xylose over microporous solid acid catalysts *Ind.Crops Prod.*, 1998, 7, 95.
- [163] K, Kaneda.; K, Ebitani.; T, Mizugaki.; K, Mori. Design of High-Performance Heterogeneous Metal Catalysts for Green and Sustainable Chemistry. *Bull. Chem. Soc. Jpn*, 2006, 79, 981-1016.
- [164] P.T, Anastas.; J.C, Warner. *Green Chemistry: Theory and Practice* Oxford University Press, Oxford, 1998.
- [165] S, Chassaing.; V, Bénétteau.; P, Pale. Green catalysts based on zeolites for heterocycle synthesis *Curr. Opin. Green Sustain. Chem.*, 2018, 10, 35-39.
- [166] Gabriele, Centi.; Siglinda, Perathoner. Catalysis and sustainable (green) chemistry *Catal. Today*, 2003, 77, 287–297.
- [167] Davor, Lončarević.; Željko, Čupić. Chapter 4 - The perspective of using nanocatalysts in the environmental requirements and energy needs of industry, In *Micro and Nano Technologies, Industrial Applications of Nanomaterials*, Elsevier, 2019, Pages 91-122, ISBN 9780128157497.
- [168] D, Greenhalgh. *Comprehensive Organic Synthesis (Second Edition)*, chapter: 8.16 Heterogeneous Hydrogenation of CC and CC Bonds, Elsevier, 2014, Pages 564-604, ISBN 9780080977430.
- [169] M, García-Diéguez.; I.S, Pieta.; M.C, Herrera.; M.A, Larrubia.; L.J, Alemany. Nanostructured Pt- and Ni-based catalysts for CO<sub>2</sub>-reforming of methane, *J. Catal.* 270, 2010, 136–145
- [170] Koehle, M.; Mhadeshwar, A. Chapter 3 - Nanoparticle Catalysis for Reforming of Biomass-Derived Fuels, *New and Future Developments in Catalysis*, Elsevier, 2013, Pages 63-93, ISBN 9780444538741. <https://doi.org/10.1016/B978-0-444-53874-1.00003-2>
- [171] Zhou, W.; Napoline, J.W.; Thomas, C.M. A Catalytic Application of Co/Zr Heterobimetallic Complexes: Kumada Coupling of Unactivated Alkyl Halides with Alkyl Grignard Reagents. *Eur. J. Inorg. Chem.* 2011, 2029–2033.

## General Introduction

- [172] Setty, V.N.; Zhou, W.; Foxman, B.M.; Thomas, C.M. Subtle Differences between Zr and Hf in Early/Late Heterobimetallic Complexes with Cobalt. *Inorg. Chem.* 2011, 50, 4647–4655.
- [173] Sinfelt, J. H. Acc. Catalysis by alloys and bimetallic clusters. *Chem. Res.* 1977, 10, 15.
- [174] Sinfelt, J. H. *Bimetallic Catalysts: Discoveries, Concepts and Applications*; John Wiley and Sons: New York, 1983.
- [175] Sinfelt, J. H.; Barnett, A. E.; Dembinski, G. W. U.S. patent, US3442973, 1969.
- [176] Campbell, C. T. Bimetallic Surface Chemistry. *Annual Rev. Phys. Chem.* 1990, 41, 775.
- [177] Rodriguez, J. A. Physical and chemical properties of bimetallic surfaces *Surf. Sci. Rep.* 1996, 24, 225.
- [178] Chen, J. G.; Menning, C. A.; Zellner, M. B. Monolayer bimetallic surfaces: Experimental and theoretical studies of trends in electronic and chemical properties *Surf. Sci. Rep.* 2008, 63, 201. 10.1016/j.surfrep.2008.02.001
- [179] Yu, W. T.; Barteau, M. A.; Chen, J. G. Glycolaldehyde as a probe molecule for biomass derivatives: reaction of C-OH and C=O functional groups on monolayer Ni surfaces. *J. Am. Chem. Soc.* 2011, 133, 20528.
- [180] Kitchin, J. R.; Norskov, J. K.; Barteau, M. A.; Chen, J. G. Role of Strain and Ligand Effects in the Modification of the Electronic and Chemical Properties of Bimetallic Surfaces. *Phys. Rev. Lett.* 2004, 93.
- [181] J, Zhang.; H, Wang.; A.K, Dalai. Development of stable bimetallic catalysts for carbon dioxide reforming of methane, *J. Catal.* 249, 2007, 300–310.
- [182] Weiting, Yu.; Marc.D, Porosoff.; Jinguang.G, Chen. Review of Pt-Based Bimetallic Catalysis: From Model Surfaces to Supported Catalysts. *Chem. Rev.* 2012, 112, 5780–5817
- [183] Bartholomew, C. H.; Farrauto, R. J. *Fundamentals of industrial catalytic processes*; Wiley Inter science: Hoboken, NJ, 2006. ISBN: 978-0-471-73007-1
- [184] Stamenkovic, V. R.; Fowler, B.; Mun, B. S.; Wang, G. F.; Ross, P. N.; Lucas, C. A.; Markovic, N. Improved oxygen reduction activity on Pt<sub>3</sub>Ni(111) via increased surface site availability *M. Science* 2007, 315, 493.
- [185] Zhang, J.; Sasaki, K.; Sutter, E.; Adzic, R. R. Stabilization of platinum oxygen-reduction electrocatalysts using gold clusters. *Science* 2007, 315, 220.
- [186] Epron, F.; Carnevillier, C.; Marecot, P. Catalytic properties in n-heptane reforming of Pt–Sn and Pt–Ir–Sn/Al<sub>2</sub>O<sub>3</sub> catalysts prepared by surface redox reaction. *Appl. Catal., A* 2005, 295, 157.
- [187] Aranishi, K.; Jiang, H. L.; Akita, T.; Haruta, M.; Xu, Q. One-step synthesis of magnetically recyclable Au/Co/Fe triple-layered core-shell nanoparticles as highly efficient catalysts for the hydrolytic dehydrogenation of ammonia borane. *Nano Res.* 2011, 4, 1233–1241.

## General Introduction

- [188] Liu, H.; Hu, Q.; Fan, G.; Yang, L.; Li, F. Surface Synergistic Effect in Well-Dispersed Cu/MgO Catalysts for Highly Efficient Vapor-Phase Hydrogenation of Carbonyl Compounds. *Catal. Sci. Technol.* 2015, 5, 3960–3969.
- [189] Chen, S.; Wojcieszak, R.; Dumeignil, F.; Marceau, E.; Royer, S. How catalysts and experimental conditions determine the selective hydroconversion of furfural and 5-hydroxymethylfurfural. *Chem. Rev.* 2018, 118, 11023–11117.
- [190] Shi, Y.; Zhu, Y.; Yang, Y.; Li, Y.-W.; Jiao, H. Exploring Furfural Catalytic Conversion on Cu(111) from Computation. *ACS Catal.* 2015, 5, 4020–4032.
- [191] Sitthisa, S.; Sooknoi, T.; Ma, Y.; Balbuena, P. B.; Resasco, D. E. Kinetics and Mechanism of Hydrogenation of Furfural on Cu/SiO<sub>2</sub> Catalysts. *J. Catal.* 2011, 277, 1–13.
- [192] Xiong, K.; Wan, W.; Chen, J. G. Reaction Pathways of Furfural, Furfuryl Alcohol and 2-Methylfuran on Cu(111) and NiCu Bimetallic Surfaces. *Surf. Sci.* 2016, 652, 91–97.
- [193] Medlin, J. W. Understanding and Controlling Reactivity of Unsaturated Oxygenates and Polyols on Metal Catalysts. *ACS Catal.* 2011, 1, 1284–1297.
- [194] Sitthisa, S.; An, W.; Resasco, D. E. Selective Conversion of Furfural to Methylfuran over Silica-Supported NiFe Bimetallic Catalysts. *J. Catal.* 2011, 284, 90–101.
- [195] Sitthisa, S.; Pham, T.; Prasomsri, T.; Sooknoi, T.; Mallinson, R. G.; Resasco, D. E. Conversion of Furfural and 2-Methylpentanal on Pd/SiO<sub>2</sub> and Pd–Cu/SiO<sub>2</sub> Catalysts. *J. Catal.* 2011, 280, 17–27.
- [196] Solomon, J. L.; Madix, R. J.; Stöhr, J. Orientation and Absolute Coverage of Furan and 2,5-dihydrofuran on Ag(110) Determined by near Edge X-ray Absorption Fine Structure and X-ray Photoelectron Spectroscopy. *J. Chem. Phys.* 1991, 94, 4012–4023.
- [197] Bradley, M. K.; Robinson, J.; Woodruff, D. P. The Structure and Bonding of Furan on Pd(111). *Surf. Sci.* 2010, 604, 920–925.
- [198] Ni, Z. M.; Xia, M.-Y.; Shi, W.; Qian, P.-P. Adsorption and Decarbonylation Reaction of Furfural on Pt(111) Surface. *Acta Phys.-Chim. Sin.* 2013, 29, 1916–1922.
- [199] Zhang, W.; Zhu, Y.; Niu, S.; Li, Y. A Study of Furfural Decarbonylation on K-Doped Pd/Al<sub>2</sub>O<sub>3</sub> Catalysts. *J. Mol. Catal. A: Chem.* 2011, 335, 71–81.
- [200] Manikandan, M.; Venugopal, A. K.; Nagpure, A. S.; Chilukuri, S.; Raja, T. Promotional Effect of Fe on the Performance of Supported Cu Catalyst for Ambient Pressure Hydrogenation of Furfural. *RSC Adv.* 2016, 6, 3888–3898.
- [201] Kristina, W. Golub.; Taylor, P. Sulmonetti.; Lalit, A. Darunte.; Michael, S. Shealy.; Christopher, W. Jones. Metal–Organic–Framework-Derived Co/Cu–Carbon Nanoparticle Catalysts for Furfural Hydrogenation. *ACS Applied Nano Materials* 2019, 2 (9), 6040–6056.
- [202] S. Miyata. *Physico-Chemical Properties of Synthetic Hydrotalcites in Relation to Composition Clays and Clay Minerals*, 1980, 28, 50–56.

## General Introduction

- [203] R. T. K. Baker.; Larry, L. Murrell. *Novel Materials in Heterogeneous Catalysis*, 1990, chapter 14, pp. 140-148. ISBN: 9780841218635
- [204] F. Cavani, F. Trifiro and A. Vaccari. *Hydrotalcite-Type Anionic Clays: Preparation, Properties and Applications Catal*, 1991, 11, 173-301.
- [205] A. Vaccari. Preparation and catalytic properties of cationic and anionic clays *Catal. Today* 1998, 41, 53-71.
- [206] A. I. Khan.; D. O'Hare. Intercalation chemistry of layered double hydroxides: recent developments and applications *J. Mater. Chem.*, 2002, 12, 3191-3198.
- [207] G. R. Williams.; D. O'Hare, *J. Mater. Towards understanding, control and application of layered double hydroxide chemistry. Chem.* 2006, 16, 3065 – 3074.
- [208] D. P. Debecker.; E. M. Gaigneaux.; G. Busca. Exploring, Tuning, and Exploiting the Basicity of Hydrotalcites for Applications in Heterogeneous Catalysis *Chem. Eur. J.*, 2009, 15, 3920-3935.
- [209] S. Nishimura.; A. Takagaki.; K. Ebitani. Characterization, synthesis and catalysis of hydrotalcite-related materials for highly efficient materials transformations. *Green Chem.*, 2013, 15, 2026.
- [210] E, Conterosito.; V, Gianotti.; L, Palin.; E, Boccaleri.; D, Viterbo.; M, Milanese. Facile preparation methods of hydrotalcite layered materials and their structural characterization by combined techniques. *Inorg. Chim. Acta*, 2018, 470, 36-50.
- [211] Kiyotomi, Kaneda.; Tomoo, Mizugaki. Design of high-performance heterogeneous catalysts using hydrotalcite for selective organic transformations. *Green Chemistry*, 2019, 21, No 6, p. 1361-1389
- [212] R. M. Taylor. The rapid formation of crystalline double hydroxy salts and other compounds by controlled hydrolysis. *Clay Miner*, 1984, 19, 591-603.
- [213] S, Velu.; V, Ramaswamy.; A, Ramani.; B. M, Chanda.; S, Sivasanker. New hydrotalcite-like anionic clays containing Zr<sup>4+</sup> in the layers *Chem. Commun.*, 1997, 2107-2108.
- [214] C. J, Serna.; J. L, Rendon.; J. E, Iglesias. Crystal-chemical study of layered [Al<sub>2</sub>Li(OH)<sub>6</sub>]<sup>+</sup> X<sup>-</sup> .nH<sub>2</sub>O. *Clay Miner*. 1982, 30, 180-184.
- [215] V, Rives.; M. A, Ulibarri. Layered double hydroxides (LDH) intercalated with metal coordination compounds and oxometalates. *Coord Chem. Rev.* 1999, 181, 61 – 120.
- [216] T, Li.; H, Miras.; Y.-F, Song. Polyoxometalate (POM)-Layered Double Hydroxides (LDH) Composite Materials: Design and Catalytic Applications *Catalysts*, 2017, 7, 260.14.
- [217] S. Omwoma.; W. Chen.; R. Tsunashima.; Y.-F. Song. Recent advances on polyoxometalates intercalated layered double hydroxides: From synthetic approaches to functional material applications. *Coord. Chem. Rev.* 2014, 258-259, 58-71.

## General Introduction

- [218] G, Fan.; F, Li.; D.G, Evans.; X, Duan. Catalytic applications of layered double hydroxides: recent advances and perspectives. *Chem. Soc. Rev.* 2014, 43, 7040-7066.
- [219] K. Takehira.; T. Shishido. Preparation of supported metal catalysts starting from hydrotalcites as the precursors and their improvements by adopting “memory effect” *Catal. Surv. Asia* ,2007, 11, 1-30.
- [220] K, Takehira. Recent development of layered double hydroxide-derived catalysts –Rehydration, reconstitution, and supporting, aiming at commercial application–*Appl. Clay Sci.* 2017, 136, 112-141. 10.1016/j.clay.2016.11.012
- [221] N.K, Lazaridis.; A, Hourzemanoglou.; K.A, Matis. Flotation of metal-loaded clay anion exchangers. Part II: the case of arsenates *Chemosphere*, 2002, 47, 319 – 324.
- [222] N. K, Lazaridis.; D. D, Asouhidou. Kinetics of sorptive removal of chromium(VI) from aqueous solutions by calcined Mg-Al-CO(3) hydrotalcite *Water Res.* 2003, 37, 2875-2882.
- [223] P.C, Pavan.; E.L, Crepaldi.; J.B.Valim, J. Sorption of Anionic Surfactants on Layered Double Hydroxides. *Colloid Interface Sci.* 2000, 229, 346-352.
- [224] Q.-L, Zhu.; Q, Xu. Liquid organic and inorganic chemical hydrides for high-capacity hydrogen storage. *Energy Environ. Sci.* 2015, 8, 478-512.
- [225] See the website <https://www.drugs.com/international/hydrotalcite.html>
- [226] Z, Matusinovic.; C.A, Wilkie. Fire retardancy and morphology of layered double hydroxide nanocomposites: a review. *J. Mater. Chem.* 2012, 22, 18701.
- [227] L.A, Utracki.; M, Sepehr.; E. Boccaleri, *Polym. Synthetic, layered nanoparticles for polymeric nanocomposites (PNCs).* *Adv. Technol.* 2007, 18, 1–37.
- [228] K.-H, Goh.; T.-T, Lim.; Z, Dong. Application of layered double hydroxides for removal of oxyanions: A review. *Water Res.* 2008, 42, 1343–1368.
- [229] V, Ambrogi.; G, Fardella.; G, Grandolini.; M, Nocchetti.; L, Perioli. Effect of hydrotalcite-like compounds on the aqueous solubility of some poorly water-soluble drugs. *J. Pharm. Sci.* 2003, 92, 1407-1418.
- [230] V, Ambrogi.; G, Fardella.; G, Grandolini.; L, Perioli. Intercalation compounds of hydrotalcite-like anionic clays with anti inflammatory agents-I. Intercalation and in vitro release of ibuprofen. *Int. J. Pharm.* 2001, 220, 23–32.
- [231] B. F, Sels.; D. E, De Vos.; P. A, Jacobs. Hydrotalcite-like anionic clays in catalytic organic reactions. *Catal. Rev. Sci. Eng.* 2001, 43, 443-488.
- [232] Chen, X.; Li, H.; Luo, H.; Qiao, M. Liquid Phase Hydrogenation of Furfural to Furfuryl Alcohol over Mo-doped Co- B Amorphous Alloy Catalysts. *Appl. Catal., A* 2002, 233, 13–20.

## General Introduction

- [233] Sulmonetti, T. P.; Hu, B.; Ifkovits, Z.; Lee, S.; Agrawal, P. K.; Jones, C. W. Vapor Phase Hydrogenolysis of Furanics Utilizing Reduced Cobalt Mixed Metal Oxide Catalysts. *ChemCatChem* 2017, 9, 1815–1823.
- [234] Li, H.; Luo, H.; Zhuang, L.; Dai, W.; Qiao, M. Liquid Phase Hydrogenation of Furfural to Furfuryl Alcohol over the Fe-promoted Ni-B Amorphous Alloy Catalysts. *J. Mol. Catal. A: Chem.* 2003, 203, 267–275.
- [235] Srivastava, S.; Jadeja, G. C.; Parikh, J. A Versatile Bi-Metallic Copper–Cobalt Catalyst for Liquid Phase Hydrogenation of Furfural to 2-Methylfuran. *RSC Adv.* 2016, 6, 1649–1658.
- [236] Fu, X.; Ren, X.; Shen, J.; Jiang, Y.; Wang, Y.; Orooji, Y.; Xu, W.; Liang, J. Synergistic catalytic hydrogenation of furfural to 1,2-pentanediol and 1,5-pentanediol with LDO derived from CuMgAl hydrotalcite. *Mol. Catal.* 2021, 499, 111298.
- [237] Britannica, T. Editors of Encyclopaedia. noble metal. *Encyclopedia Britannica*. <https://www.britannica.com/science/noble-metal>, 2021, May 6.
- [238] Lyon, S.B. Corrosion of noble metals. *Shreir's Corros.* 2010, 1, 2205–2223.
- [239] F.; Marceau, E.; Royer, S. How catalysts and experimental conditions determine the selective hydroconversion of furfural and 5-hydroxymethylfurfural. *Chem. Rev.* 2018, 118, 11023–11117
- [240] Zhao, Y. Facile Synthesis of Pd Nanoparticles on SiO<sub>2</sub> for Hydrogenation of Biomass-Derived Furfural. *Environ Chem.* 2014, 12, 185–190.
- [241] Nakagawa, Y.; Takada, K.; Tamura, M.; Tomishige, K Total Hydrogenation of Furfural and 5-Hydroxymethylfurfural over Supported Pd–Ir Alloy Catalyst. *ACS Catal.* 2014, 4, 2718–2726.
- [242] Dong, F.; Zhu, Y.; Ding, G.; Cui, J.; Li, X.; Li, Y. One-Step Conversion of Furfural into 2-Methyltetrahydrofuran under Mild Conditions. *ChemSusChem* 2015, 8, 1534–1537.
- [243] Aldosari, O. F.; Iqbal, S.; Miedziak, P. J.; Brett, G. L.; Jones, D. R.; Liu, X.; Edwards, J. K.; Morgan, D. J.; Knight, D. K.; Hutchings, G. J. Pd–Ru/TiO<sub>2</sub> Catalyst – an Active and Selective Catalyst for Furfural Hydrogenation. *Catal. Sci. Technol.* 2016, 6, 234–242.
- [244] King, G. M.; Iqbal, S.; Miedziak, P. J.; Brett, G. L.; Kondrat, S. A.; Yeo, B. R.; Liu, X.; Edwards, J. K.; Morgan, D. J.; Knight, D. K.; et al. An Investigation of the Effect of the Addition of Tin to 5%Pd/ TiO<sub>2</sub> for the Hydrogenation of Furfuryl Alcohol. *ChemCatChem*, 2015, 7, 2122–2129.
- [245] Godawa, C.; Rigal, L.; Gaset, A. Palladium Catalyzed Hydrogenation of Furan: Optimization of Production Conditions for Tetrahydrofuran. *Resour. Conserv. Recycl.* 1990, 3, 201–216.
- [246] Cui, X.; Surkus, A.-E.; Junge, K.; Topf, C.; Radnik, J.; Kreyenschulte, C.; Beller, M. Highly Selective Hydrogenation of Arenes Using Nanostructured Ruthenium Catalysts Modified with a Carbon–Nitrogen Matrix. *Nat. Commun.* 2016, 7, 11326.
- [247] Huang, Y.; Adeeva, V.; Sachtler, W. M. H. Stability of Supported Transition Metal Catalysts in the Hydrogenation of Nitriles. *Appl. Catal., A: General* 2000, 196, 73–85

## General Introduction

- [248] Wisnlak, J.; Simon, R. Hydrogenation of Glucose, Fructose, and Their Mixtures. *Ind. Eng. Chem. Prod. Res. Dev.* 1979, 18, 50–57
- [249] Chen, L.; Zhu, Y.; Zheng, H.; Zhang, C.; Zhang, B.; Li, Y. Aqueous-Phase Hydrodeoxygenation of Carboxylic Acids to Alcohols or Alkanes over Supported Ru Catalysts. *J. Mol. Catal. A: Chem.* 2011, 351, 217–227.
- [250] Panagiotopoulou, P.; Martin, N.; Vlachos, D. G. Liquid-Phase Catalytic Transfer Hydrogenation of Furfural over Homogeneous Lewis Acid–Ru/C Catalysts. *ChemSusChem* 2015, 8, 2046–2054.
- [251] Ning, J. B.; Liu, F.; Zhang, J. H.; Xu, W. J.; Fang, Y. Z.; Zhu, J.; Tang, T. X.; Pan, W. P.; Chen, X. Ruthenium catalyst, preparation method and application in synthesizing tetrahydrofurfuryl alcohol China Patent CN102489315 A, 2011.
- [252] Ordonsky, V. V.; Schouten, J. C.; van der Schaaf, J.; Nijhuis, T. A. Multilevel Rotating Foam Biphasic Reactor for Combination of Processes in Biomass Transformation. *Chem. Eng. J.* 2013, 231, 12–17.
- [253] Zhang, B.; Zhu, Y.; Ding, G.; Zheng, H.; Li, Y. Selective Conversion of Furfuryl Alcohol to 1,2-Pentanediol over a Ru/MnO<sub>x</sub> Catalyst in Aqueous Phase. *Green Chem.* 2012, 14, 3402–3409.
- [254] Panagiotopoulou, P.; Vlachos, D. G. Liquid Phase Catalytic Transfer Hydrogenation of Furfural over a Ru/C Catalyst. *Appl. Catal., A* 2014, 480, 17–24.
- [255] Fang, R.; Liu, H.; Luque, R.; Li, Y. Efficient and Selective Hydrogenation of Biomass-Derived Furfural to Cyclopentanone Using Ru Catalysts. *Green Chem.* 2015, 17, 4183–4188.
- [256] Kijeński, J.; Winiarek, P. Selective Hydrogenation of  $\alpha,\beta$ - Unsaturated Aldehydes over Pt Catalysts Deposited on Monolayer Supports. *Appl. Catal., A* 2000, 193, L1–L4.
- [257] Maligal-Ganesh, R. V.; Xiao, C.; Goh, T. W.; Wang, L. L.; Gustafson, J.; Pei, Y.; Qi, Z.; Johnson, D. D.; Zhang, S.; Tao, F.; et al. A Ship-in-a-Bottle Strategy to Synthesize Encapsulated Intermetallic Nanoparticle Catalysts: Exemplified for Furfural Hydrogenation. *ACS Catal.* 2016, 6, 1754–1763.
- [258] Chen, B.; Li, F.; Huang, Z.; Yuan, G. Tuning Catalytic Selectivity of Liquid-Phase Hydrogenation of Furfural via Synergistic Effects of Supported Bimetallic Catalysts. *Appl. Catal., A* 2015, 500, 23–29.
- [259] Ren, F.; Wang, Z.; Luo, L.; Lu, H.; Zhou, G.; Huang, W.; Hong, X.; Wu, Y.; Li, Y. Utilization of Active Ni to Fabricate Pt–Ni Nanoframe/NiAl Layered Double Hydroxide Multifunctional Catalyst through In Situ Precipitation. *Chem. - Eur. J.* 2015, 21, 13181–13185.
- [260] Ma, R.; Wu, X. P.; Tong, T.; Shao, Z. J.; Wang, Y.; Liu, X.; Xia, Q.; Gong, X. Q. The Critical Role of Water in the Ring Opening of Furfural Alcohol to 1,2-Pentanediol. *ACS Catal.* 2017, 7, 333–337.
- [261] Bhogeswararao, S.; Srinivas, D. Catalytic Conversion of Furfural to Industrial Chemicals over Supported Pt and Pd Catalysts. *J. Catal.* 2015, 327, 65–77.

## General Introduction

- [262] Zhang, C.; Lai, Q.; Holles, J. H. Bimetallic Overlayer Catalysts with High Selectivity and Reactivity for Furfural Hydrogenation. *Catal. Commun.* 2017, 89, 77–80.
- [263] Guan, J.; Li, J.; Yu, Y.; Mu, X.; Chen, A. DFT Studies of the Selective C–O Hydrogenolysis and Ring-Opening of Biomass Derived Tetrahydrofurfuryl Alcohol over Rh(111) Surfaces. *J. Phys. Chem. C* 2016, 120, 19124–19134.
- [264] Tamura, M.; Tokonami, K.; Nakagawa, Y.; Tomishige, K. Rapid Synthesis of Unsaturated Alcohols under Mild Conditions by Highly Selective Hydrogenation. *Chem. Commun.* 2013, 49, 7034–7036.
- [265] Wang, Z.; Huang, L.; Geng, L.; Chen, R.; Xing, W.; Wang, Y.; Huang, J. Chemoselective Transfer Hydrogenation of Aldehydes and Ketones with a Heterogeneous Iridium Catalyst in Water. *Catal. Lett.* 2015, 145, 1008–1013.
- [266] Sun, D.; Sato, S.; Ueda, W.; Primo, A.; Garcia, H.; Corma, A. Production of C4 and C5 Alcohols from Biomass-Derived Materials. *Green Chem.* 2016, 18, 2579–2597.
- [267] Fujitani, T.; Nakamura, I.; Akita, T.; Okumura, M.; Haruta, M. Hydrogen Dissociation by Gold Clusters. *Angew. Chem.* 2009, 121, 9679–9682.
- [268] Mohr, C.; Hofmeister, H.; Lucas, M.; Claus, P. Gold Catalysts for the Partial Hydrogenation of Acrolein. *Chem. Eng. Technol.* 2000, 23, 324–328.
- [269] Ohyama, J.; Esaki, A.; Koketsu, T.; Yamamoto, Y.; Arai, S.; Satsuma, A. Atomic-Scale Insight into the Structural Effect of a Supported Au Catalyst Based on a Size-distribution Analysis Using Cs-STEM and Morphological Image-Processing. *J. Catal.* 2016, 335, 24–35.
- [270] Dong, J.; Zhu, M.; Zhang, G.; Liu, Y.; Cao, Y.; Liu, S.; Wang, Y. Highly Selective Supported Gold Catalyst for CO-Driven Reduction of Furfural in Aqueous Media. *Chin. J. Catal.* 2016, 37, 1669–1675.
- [271] Zhang, G. S.; Zhu, M. M.; Zhang, Q.; Liu, Y. M.; He, H. Y.; Cao, Y. Towards Quantitative and Scalable Transformation of Furfural to Cyclopentanone with Supported Gold Catalysts. *Green Chem.* 2016, 18, 2155–2164.
- [272] Wikimedia foundation. [https://commons.wikimedia.org/wiki/File:Periodic\\_table\\_simple\\_et\\_bw.svg](https://commons.wikimedia.org/wiki/File:Periodic_table_simple_et_bw.svg)
- [273] Nakagawa, Y.; Tamura, M.; Tomishige, K. Catalytic Reduction of Biomass-Derived Furanic Compounds with Hydrogen. *ACS Catal.* 2013, 3, 2655–2668.
- [274] Li, X.; Jia, P.; Wang, T. Furfural: A Promising Platform Compound for Sustainable Production of C4 and C5 Chemicals. *ACS Catal.* 2016, 6, 7621–7640.
- [275] Products of biesterfeld, Biesterfeld Plastic GmbH.  
<https://www.biesterfeld.com/en/gb/product/12-pentenediol/#:~:text=1%2C2%2DPentenediol%20can%20be,wax%20blends%20and%20printing%20inks.>

## General Introduction

- [276] S, Kannan. Catalytic Applications of Hydrotalcite-like Materials and Their Derived Forms. *Catal. Surv. from Asia*, 2006, 10, 117-137.
- [277] Q, Wang.; D. O'Hare. Recent Advances in the Synthesis and Application of Layered Double Hydroxide (LDH) Nanosheets *Chem. Rev.* 2012, 112, 4124–4155.
- [278] Chemical formulas are obtained from: ChemDrawdirect and PubChem.

## General Introduction

## General Introduction

# Chapter Two

---

## Materials and methods

# Chapter 2: Materials and Methods

## 1. Introduction

As most catalysts are highly nonuniform materials combining multiple phases, with active centers on the surface playing a significant role in controlling the mechanism of chemical reactions. The catalyst design has become one of the challenges in the catalysis world. The catalyst must involve an oxide as an active phase, promoter, or support. Bulk oxides are usually vigorous and stable systems with crystallographic structures [1]. Supporting catalysts is usually done with solid materials that can increase the surface area of the catalyst. The typical supports are metals like alumina, silica and various kinds of carbon [2]. Different methods to prepare catalysts have been reported in the literature, for instance, precipitation and coprecipitation methods, sol-gel technique, solvothermal synthesis, solid-state reactions, aerosol flame, impregnation, chemical vapor deposition, physical vapor deposition, spray pyrolysis, etc [1]. Some of the aforementioned methods have been used to synthesize appropriate catalysts for the hydrogenation of furfural, such as liquid-feed flame spray pyrolysis (L-F FSP) [3], the impregnation method [4], preparing a Metal-Organic-Framework via the solvothermal synthesis method [5] and via co-precipitation method [6].

Our reactions were catalyzed by materials that were synthesized through the coprecipitation method, and then were calcined in order to construct a Layered Double Hydroxide (LDHs) structure to create a well-dispersed and porous mixed metal oxides, which upon reduction displayed high activity to hydrogenate furfural [7].

## 2. Synthesis of the catalysts

Layered Double Hydroxide materials (LDHs) were prepared by co-precipitation at constant pH. An aqueous solution with  $M(\text{NO}_3)_2 \cdot 6\text{H}_2\text{O}$ ,  $\text{Ni}(\text{NO}_3)_2 \cdot 6\text{H}_2\text{O}$  and  $\text{Al}(\text{NO}_3)_3 \cdot 9\text{H}_2\text{O}$ , adjusted to a total concentration of  $0.6 \text{ mol L}^{-1}$ , was added dropwise to a  $0.3 \text{ mol L}^{-1} \text{ Na}_2\text{CO}_3$  solution

## Materials and Methods

in a flat-bottom flask under vigorous stirring at room temperature. A pH sensor was placed in the solution to maintain a constant pH of 10 by the dropwise addition of  $1.0 \text{ mol L}^{-1}$  NaOH (Figure 2.1). Upon completion, the mixture was heated to 333 K and it was aged under vigorous stirring for 48 h. The solid was then filtered and washed with distilled water until the wash solution reached a pH of 7. The LDHs were dried at 378 K and calcined in air at 673 K for 4 h to form the mixed oxides. The calcined materials were labeled according to their nominal metal molar composition as  $\text{Ni}_x\text{M}_y\text{Al}_1$ , where M= Cu, Co, or Mg. The active forms of the catalysts were obtained by reduction of the calcined precursors at 773 K for 1 h with  $40 \text{ mL min}^{-1}$  at STP of pure hydrogen for the high-pressure slurry batch reactor (SSR), and  $60 \text{ mL min}^{-1}$  at STP in the continuous packed bed reactor (PBR). The suffix R in the label represents a reduced catalyst after calcination ( $\text{Ni}_x\text{M}_y\text{Al}_1\text{-R}$ ).

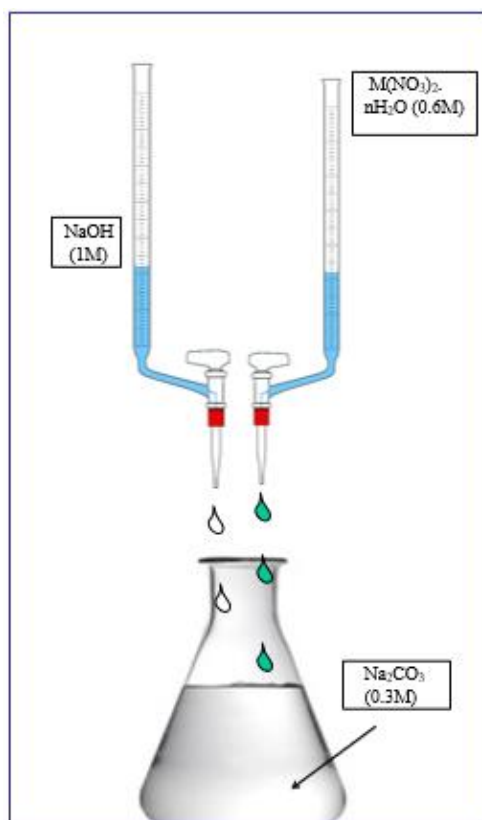


**Figure 2.1.** The synthesis of LDH materials by co-precipitation method.

### 3. Catalyst characterization

The chemical composition of the calcined precursors was determined by two distinct techniques, In chapter 3 the technique that was used is the Flame Atomic Absorption (FAA). Samples of ca. 5.2 mg were added to 10 mL of 69 wt.% nitric acid and digested in an ultrasonic shaker bath for 5 min. The digested solution was diluted with deionized water and analyzed in a Perkin Elmer PinAAcle 900 atomic adsorption spectrometer. While the measured chemical composition of the solids in chapter 4 and 5 was calculated by ICP-OES on a FHS16 spectrometer from Spectro Arcos. Samples of ca. 52 mg of calcined solids were dissolved with 10 mL of 69% HNO<sub>3</sub> in closed 50 mL vessels using an Ethos Easy microwave digester from Milestone. Digestions conditions were 15 min at 120 °C followed by 40 min at 220 °C and then a cooling period of 15 min, as in Table 2.1. The digested samples were then diluted with milli-Q ultrapure water at a 1:10 ratio.

**Table 2.1.** The microwave digester conditions of the catalyst (model: Ethos Easy)

Step Number	t (min)	MW (W)	T (°C)
1	10	700	120
2	5	700	120
3	25	1200	220
4	15	1000	220
5	15	Cooling	

The surface composition of the calcined precursors was determined by field emission scanning electron microscopy with energy dispersive X-ray spectroscopy (FESEM-EDX) in a Scios 2 Dual Beam (ThermoFisher) at 5kV with a resolution of 512 by 340 pixels and a pixel size of 0.01 µm. Surface composition was also analyzed by X-ray photoelectron spectroscopy (XPS) in VG ESCALAB 250Xi under Mono Al Ka ( $h\nu = 1486.6$  eV) X-ray source, and the binding energies were corrected using C (1s) at 284.6 eV.

The structure of the mixed oxides and the reduced catalysts of chapter 3 was assessed by X-ray diffraction on a Siemens D5000 diffractometer (Bragg-Brentano parafofocusing

## Materials and Methods

geometry and vertical  $\theta$ - $\theta$  goniometer) fitted with a curved graphite diffracted-beam monochromator, incident and diffracted-beam Soller slits, a  $0.06^\circ$  receiving slit and scintillation counter as a detector. The angular  $2\theta$  diffraction range was between  $5$  and  $80^\circ$ . The data were collected with an angular step of  $0.05^\circ$  at  $3$  s per step and sample rotation.  $\text{CuK}\alpha$  radiation was obtained from a copper X-ray tube operated at  $40$  kV and  $30$  mA. Diffraction data related to the oxides and metals was extracted from the Dfrac.Eva database (Bruker).

X-ray diffraction measurements of Bruker-AXS D8-Advance diffractometer was utilized to evaluate the mixed oxides and reduced catalysts resulted from chapter 4 and 5. The measurement was done at a vertical theta-theta goniometer, and diffracted-beam Soller slits of  $2.5^\circ$ , a fixed  $0.5^\circ$  receiving slit and an automatic Air-scattering knife on the sample surface. The angular  $2\theta$  range was between  $5$  and  $80^\circ$ . The data were collected with an angular step of  $0.02^\circ$  at a step time of  $0.5$  s.  $\text{CuK}\alpha$  radiation was obtained from a copper X-ray tube operated at  $40$  kV and  $40$  mA. Diffracted X-rays were detected with a PSD detector LynxEye-XE-T with an opening angle of  $2.94^\circ$ . The experimental diffractograms were fitted with the crystal structure (Rietveld analysis) [8] for the phases identified with the aid of TOPAS 6.0 software (Bruker AXS) [9]. With the same software, the cell parameters and the mean crystallite size of detected phases were determined using the Double Voigt approach [10]. We considered that the samples were free of micro strain as a secondary effect of the peak broadening in order to simplify the refinement. The wt.% of the phases involved was estimated by refining the Rietveld scale factor and applying the corresponding equations [11]. The instrumental contribution was obtained from a sample of LaB6 (SRM 660a) analyzed under the same conditions and was considered prior to establishing the crystallite size effect in the peak width.

The textural properties of the mixed oxides were determined from nitrogen adsorption-desorption isotherms at  $77$  K with a Quadrasorb SI Model 4.0 (Quantachrome Instruments). Samples of the calcined precursors were outgassed at  $423$  K for  $12$  h under vacuum ( $6$  mTorr) to eliminate chemisorbed volatiles before the adsorption isotherm was measured.

## Materials and Methods

Surface areas were calculated using the BET method, while the pore size distribution was calculated from the desorption wing of the isotherm according to the DFT method in chapter 4 and 5, and according to the BJH in chapter 3.

Temperature programmed reduction (TPR) of the calcined oxides was conducted on an AC2920 apparatus (Quantachrome Instruments) equipped with a TCD detector. Samples of ca. 100 mg of calcined oxides were treated at 473 K for 2 h under a constant flow of 20 mL min<sup>-1</sup> of He (Airgas, UHP) to remove pre-adsorbed species. The samples were then cooled to 323 K, and then heated to 1073 K at 5 K min<sup>-1</sup> under 20 mL min<sup>-1</sup> of 10 % H<sub>2</sub> in Ar.

The acidity of the catalysts was determined by temperature programmed desorption of ammonia (TPD- NH<sub>3</sub>) on an Autochem II 2920 analyzer (Micromeritics) equipped with a TCD detector. Samples of ca. 100 mg of the calcined oxides were reduced in situ by heating to 500 °C at 20 °C·min<sup>-1</sup> under 30 mL·min<sup>-1</sup> STP of 10% H<sub>2</sub> in Ar and kept at that temperature for 1 h. The reduced samples were then cooled down to 40 °C at 90 °C·min<sup>-1</sup> and stabilized for 10 min. Ammonia adsorption was performed with 30 mL·min<sup>-1</sup> STP of 2.5% NH<sub>3</sub> in helium during 60 min. Next, the samples were maintained at 45 °C under 30 mL·min<sup>-1</sup> STP of helium to remove the ammonia physically adsorbed. The TPD-NH<sub>3</sub> was then performed in helium heating the sample at 10 °C·min<sup>-1</sup> to 800 °C. The total amount of acidic sites was calculated from the area under the NH<sub>3</sub> desorption curve. Deconvolution of the desorption curve was used to estimate the amounts of weak ( $T_d < 220$  °C), middle strength ( $220$  °C <  $T_d < 500$  °C) and strong ( $T_d > 500$  °C) acidity sites. Calibration of the instrument was done using injections of a known volume of a calibration mixture (2.5% NH<sub>3</sub> in helium).

## 4. Catalyst testing

First, a packed bed reactor (Figure 2.2.) operating at atmospheric pressure was used in the gas-phase experiments [12]. The reactor was loaded with 500 mg of calcined oxides sieved to 100 – 200 μm, which were reduced in situ under 60 mLmin<sup>-1</sup> of H<sub>2</sub> (STP) at 773 K for 1 h. After the catalyst was reduced, the bed temperature was lowered to 463 K and the activity of the catalyst measured at that temperature for at least 4 h. Constant flow

## Materials and Methods

rates of  $80 \text{ mL min}^{-1}$  of  $\text{H}_2$  (STP) and  $0.6 \text{ mL min}^{-1}$  of a solution of  $0.05 \text{ g g}^{-1}$  of furfural in ethanol were used, equivalent to a WHSV of  $2.85 \text{ g}_{\text{FF}} \text{ g}_{\text{cat}}^{-1} \text{ h}^{-1}$ . During the experiment, samples of the reaction products were collected every hour in vials placed in a cold trap at  $268 \text{ K}$  installed at the exit of the reactor. The samples were stored in a freezer and analyzed later by gas chromatography (GC) as described below. A schematic diagram of the reactor setup is in Figure 2.3.

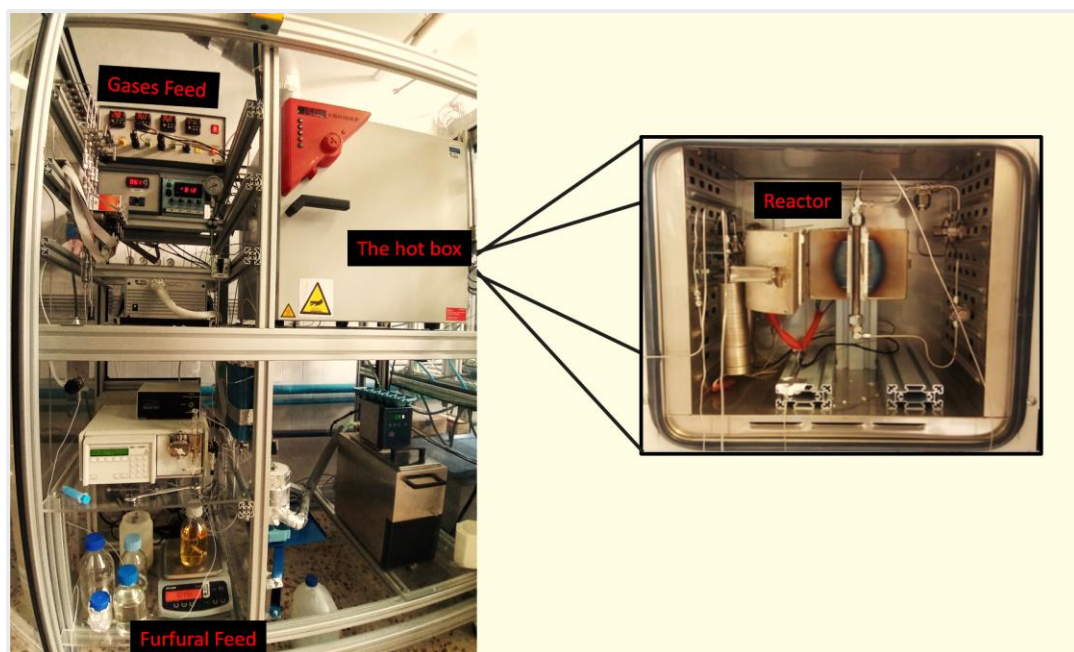


**Figure 2.2.** The packed bed reactor used for the hydrogenation reaction of furfural.

## Materials and Methods

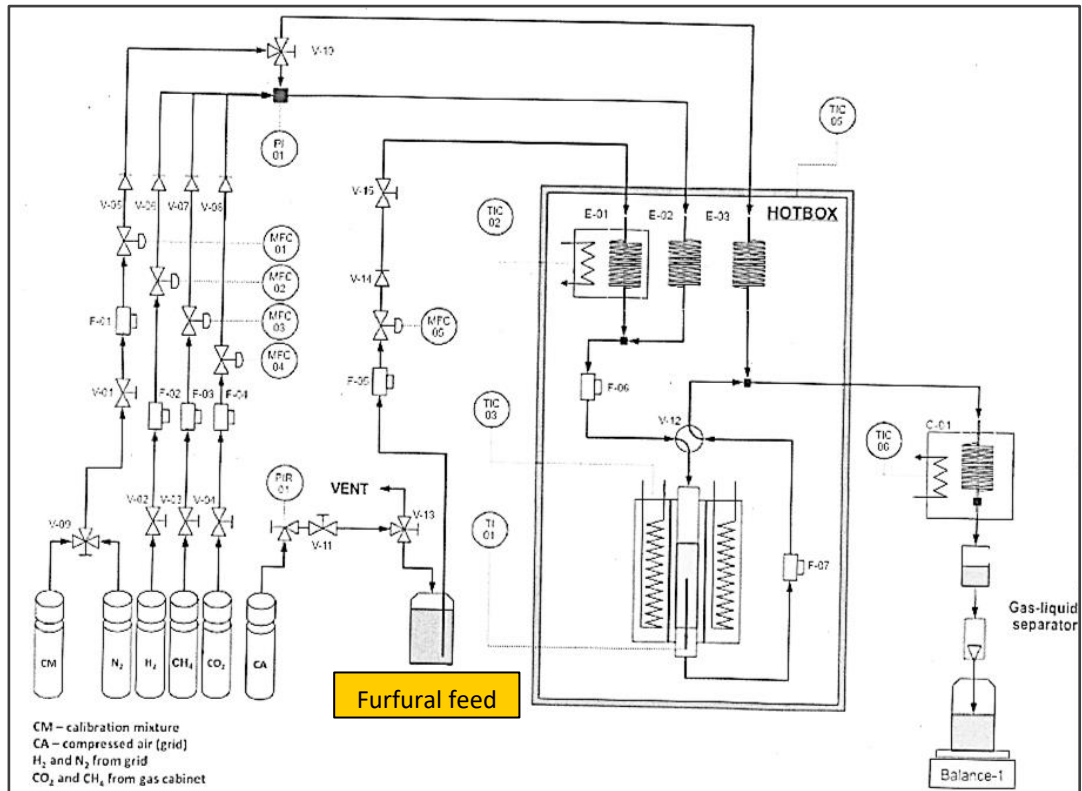


**Figure 2.3.** The scheme of the packed bed reactor which utilized for the hydrogenation reaction of furfural.

Second, the hydrogenation in liquid-phase was investigated on a high-pressure slurry batch reactor which appears in figures 2.4. and 2.5. (100 mL Mini Reactor, Autoclave Engineers).

## Materials and Methods

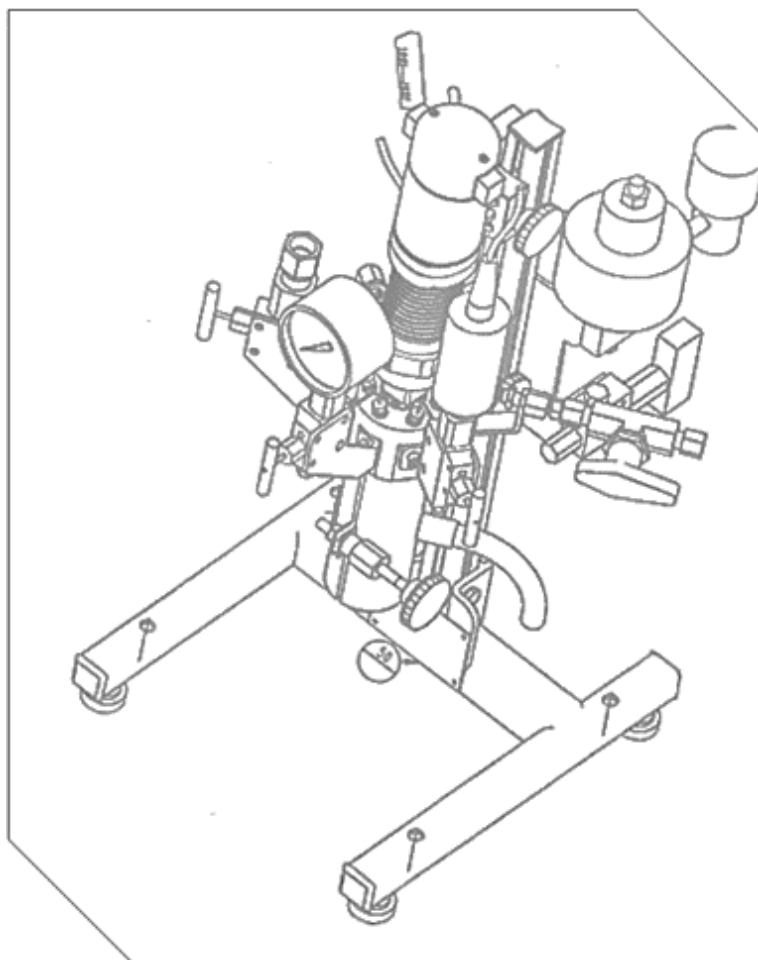


**Figure 2.4.** The slurry batch reactor which was used in the hydrogenation reaction of furfural (100 mL Mini Reactor, Autoclave Engineers).

Experiments were conducted with 30 mL of a  $0.05 \text{ g g}^{-1}$  solution of furfural in ethanol at a constant hydrogen pressure with 200 mg of catalyst sieved to 100-200  $\mu\text{m}$ , which gave a furfural-to-catalyst mass ratio of 7.44 g/g. A stirrer velocity of 1000 rpm minimized mass transfer resistances. Figure 2.4. shows the reactor from a vertical position, the capture was taken from the top.



## Materials and Methods

recover the catalyst, which was then washed with ethanol, air dried, and stored for further testing. A sample of the liquid was collected in a sealed vial and stored in a freezer until analyzed by GC. The performance of the catalysts was determined based on the fractional conversion of furfural ( $X_{FF}$ ) and the molar selectivity ( $S_j$ ) of the products was calculated by the equations (1) and (2).  $N_{FF,0}$  and  $N_{FF}$  were the initial and the final number of moles of furfural in the batch reactor,  $N_j$  was the number of moles of product  $j$  formed, and  $v_j$  was the stoichiometric number of moles of furfural required to form a molecule of  $j$ . In the tubular reactor,  $N_{FF,0}$ ,  $N_{FF}$  and  $N_j$  denote molar flows.

$$X_{FF} = \frac{N_{FF,0} - N_{FF}}{N_{FF,0}} \quad (1)$$

$$S_j = \frac{v_j N_j}{N_{FF,0} - N_{FF}} \quad (2)$$

The products were identified by GC-MS (Shimadzu GCMS-QP2010) with a TRB-5 column (Teknokroma, TR-120232; length: 30.0 m, film thickness: 0.25  $\mu\text{m}$ ; inner diameter: 0.25 mm). Analysis was conducted using a 3-stage temperature programming (5 min at 323 K, heating to 503 K at 5 K  $\text{min}^{-1}$  followed by 10 min at the latter temperature) with He as a carrier gas (47  $\text{mL min}^{-1}$ ). Sample injection was 1.0  $\mu\text{m}$  and the split ratio 300. The retention time and the mass spectra of the detected products were compared with those of pure standards, when available, to confirm the assignments. Routine quantification of the reaction products was conducted by GC-FID (Shimadzu GC-2010) using the same column and analysis conditions after calibration with standard solutions. Calibration standards were prepared with commercial samples dissolved in ethanol. Furfural (FF, 99%), furfuryl alcohol (FA, 98 %), tetrahydrofuran (THF, 99.9 %), 1,5-pentanediol (15-PD, 97 %), 1,2-pentanediol (12-PD, 96%), 1-pentanol (1PE, 99 %), furan (FUR, 99 %), and 1-butanol (1BU,

## Materials and Methods

99.8 %), cyclopentanone (CP, >99%) and cyclopentanol (CPO, 99%) were purchased from Sigma Aldrich. Tetrahydrofurfuryl alcohol (TFA, 98 %), 2-methylfuran (mFUR, 99 %) and 2-methyltetrahydrofuran (mTHF, 99.9 %) were acquired from Acros Organics. All chemicals were used as received without any further treatment. Response factors in the FID detector of the compounds that were not available commercially were estimated based on their structure [13,14]. In all cases, the samples were filtered with a nylon filter (Nylon 25 mm, 0.22  $\mu\text{m}$ , Sharlab) before injection.

## 5. References

- [1] Campbell, C. T. Bimetallic Surface Chemistry. *Annu. Rev. Phys. Chem.* 1990, 41, 775.
- [2] Ma, Zhen; Zaera, Francisco (2006). "Heterogeneous Catalysis by Metals". In: *Encyclopedia of Inorganic Chemistry*, John Wiley.
- [3] Gavilá, L.; Lähde, A.; Jokiniemi, J.; Constanti, J.; Medina, F.; del Río, E.; Tichit, D.; Alvarez, M. G. Insights on the one-Pot formation of 1,5-Pentanediol from furfural with Co-Al spinel-based nanoparticles as an alternative to noble metal catalysts. *ChemCatChem* 2019, 11, 4944–4953.
- [4] Mizugaki, T.; Yamakawa, T.; Nagatsu, Y.; Maeno, Z.; Mitsudome, T.; Jitsukawa, K.; Kaneda, K. Direct transformation of furfural to 1,2-pentanediol using a hydrotalcite-supported platinum nanoparticle. doi.org/10.1021/sc500325g | *ACS Sustainable Chem. Eng.* 2014, 2, 2243-2247
- [5] Kristina. W, Golub.; Taylor. P, Sulmonetti.; Lalit. A, Darunte.; Michael. S, Shealy.; Christopher. W, Jones. Metal–Organic–Framework–Derived Co/Cu–Carbon Nanoparticle Catalysts for Furfural Hydrogenation. *ACS Applied Nano Materials* 2019, 2 (9), 6040-6056.
- [6] Al-Yusufi, m.; Steinfeldt, N.; Eckelt, R.; Atia, H.; Lund H.; Bartling, S.; Rockstroh, N.; Köckritz, A. Efficient Base Nickel-Catalyzed Hydrogenolysis of Furfural-Derived Tetrahydrofurfuryl Alcohol to 1,5-Pentanediol. *ACS Sustainable Chemistry & Engineering* 2022, 10 ,15, 4954-4968.
- [7] Aldureid, A.; Medina, F.; Patience G. S.; Montané, D. Ni-Cu/Al<sub>2</sub>O<sub>3</sub> from Layered Double Hydroxides Hydrogenates Furfural to Alcohols. *Catalysts* 2022, 12, 390.
- [8] Rietveld, H. M. A profile refinement method for nuclear and magnetic structures. *J. Appl. Crystallogr.* 1969, 2(2), 65–71.
- [9] Coelho, A. A. TOPAS and TOPAS-Academic: An optimization program integrating computer algebra and crystallographic objects written in C++. *J. Appl. Crystallogr.* 2018, 51, 1–9.
- [10] Balzar, D. Voigt-function model in diffraction line-broadening analysis. In R. L. Snyder, J. Fiala, & H. J. Bunge (Eds.), *Defect and Microstructure Analysis by Diffraction*. International Union of Crystallography Monographs on Crystal. 1999, pp. 94–124. Oxford: Oxford University Press
- [11] Hill, R. J.; Howard, C. J. Quantitative phase analysis from neutron powder diffraction data using the Rietveld method. *J. Appl. Crystallogr.* 1987, 20(6), 467–474.
- [12] Abelló, S.; Bolshak, E.; Montané, D. Ni-Fe catalysts derived from hydrotalcite-like precursors for hydrogen production by ethanol steam reforming. *Appl. Catal. A: General* 2013, 450, 261-274.

## Materials and Methods

- [13] Jorgensen, A.D.; Picel, K.C.; Stamoudis, V.C. Prediction of gas chromatography flame ionization detector response factors from molecular structures. *Anal. Chem.* 1990, 62, 683–689.
  
- [14] De Saint Laumer, J.-Y.; Leocata, S.; Tissot, E.; Baroux, L.; Kampf, D.M.; Merle, P.; Boschung, A.; Seyfried, M.; Chaintreau, A. Prediction of response factors for gas chromatography with flame ionization detection: Algorithm improvement, extension to silylated compounds, and application to the quantification of metabolites. *J. Sep. Sci.* 2015, 38, 3209–3217.

## Materials and Methods

## Materials and Methods

**Ni-Cu/Al<sub>2</sub>O<sub>3</sub> from Layered Double Hydroxides  
Hydrogenates Furfural to Alcohols**

# Chapter Three

---

## **Ni-Cu/Al<sub>2</sub>O<sub>3</sub> from Layered Double Hydroxides Hydrogenates Furfural to Alcohols**

# Chapter 3: Ni-Cu/Al<sub>2</sub>O<sub>3</sub> from Layered Double Hydroxides Hydrogenates Furfural to Alcohols

## 1. Introduction

Furfural (FF) is one of the top value-added chemicals derived from biomass [1]. It is a versatile molecule that is produced in lignocellulosic biorefineries from biomass rich in xylan and other five-carbon polysaccharides [2, 3]. The activity of the aldehyde group and the furan ring facilitates the conversion of furfural into several valuable products. The first can be reduced to alcohol, decarbonylated, oxidized to carboxylic acid, reduced to amines, acetylated, and it gives aldol and Knoevenagel condensations and Grignard reactions. The furan ring can be transformed by halogenation, alkylation, oxidation, nitration, hydrogenation, and by ring-opening hydrogenolysis, which may involve the C–O–C bond or the C=C double bonds [4]. Hydrogenation produces several valuable chemicals, but furfuryl alcohol (FA) and tetrahydrofurfuryl alcohol (TFA) are the most common [5]. They find application as solvents and in the production of resins, fragrances, polyesters, agrochemicals, biofuels and fuel additives [3, 5-9]. Ring-opening hydrogenolysis of FF produces 1,2-pentanediol (12PD) and 1,5-pentanediol (15PD), which are monomers for polyesters, polyurethanes and polyamides, and as solvents and fuel additives [4]. Reduction of FF to FA within situ rearrangement yields cyclopentanone (CPO), which is a specialty chemical used in the synthesis of pharmaceuticals, fungicides, flavors and fragrances, and polyamides [3].

Furfural adsorption to the catalyst surface determines the hydrogenation and hydrogenolysis pathway. Copper surfaces adsorb FF molecules via the oxygen atom of the aldehyde group ( $\eta^1$ -(O)-aldehyde mode) [10, 11]. This directs the reaction towards the formation of FA by the hydrogenation of the aldehyde group [4]. Nickel surfaces tend to adsorb furfural via the  $\eta^2$ -(C,O)-aldehyde mode, where FF attaches to the surface by the

## Ni-Cu/Al<sub>2</sub>O<sub>3</sub> from Layered Double Hydroxides Hydrogenates Furfural to Alcohols

carbon and oxygen atoms of the aldehyde group leaving the furan ring parallel to the metal surface [10, 12-15]. This type of adsorption is stronger than the  $\eta^1$ -(O)-aldehyde due to the additional interaction between nickel and the  $\pi$  bonds in FF [15-17]. It promotes saturation of the furan ring and reduction of the aldehyde group, which mainly leads to TFA, but it may also favor ring-opening reactions. Temperature shifts the adsorption mode on nickel from  $\eta^2$ -(C,O)-aldehyde to  $\eta^1$ -(C)-acyl. The latter promotes the decarbonylation of furfural to furan (FUR) [4]. In general, the strength of the interaction of furfural with the surfaces of Ni, Pd, Pt, and Cu follows the order of Ni > Pd > Pt  $\gg$  Cu [18, 19]. Therefore, copper catalysts tend to be less active than those based on other metals are. Metal promoters such as Fe, Zn, Mg, or Co improve the activity of copper-based catalysts and modifies their selectivity to other products besides FA. Regardless of the metal, a high dispersion and a strong interaction of the metal particles with the support matrix enhance the activity of the catalyst and influence its selectivity [4]. Layered double hydroxides (LDHs) obtained by coprecipitation at controlled pH of salts of the active metals, are versatile materials that upon calcination and reduction yield catalysts with high metal dispersion and strong interaction with the support, which makes them active and resistant to sintering. FF hydrogenation has been reported on several catalysts based on LDHs. A CuMgAl catalyst converted 84 % of furfural with a 71 % selectivity to pentanediols (46 % 12PD and 25% 15PD) [20]. A spinel-based CoAlO catalyst gave complete conversion of FF and a selectivity to 15PD and TFA of 30 and 62 %, respectively [21], whereas a Cu-ZnO/Al<sub>2</sub>O<sub>3</sub> catalyst was highly selective to FA in the gas-phase hydrogenation of FF [22]. A CuNi/MgAlO catalyst prepared from a hydrotalcite precursor yielded FA with at an 89% selectivity and 93% conversion [23]. Copper-based bimetallic catalysts produced cyclopentanol (CuZnAl [24] and CuMgAl [25]) and cyclopentanone (CuZnAl [26] and CuNiAl [27]). 5-hydroxymethylfurfural (HMF), the furan analog to FF derived from six carbon monosaccharides, gave complete conversion and a selectivity of 64% to 1,2,6-hexanetriol on NiCoAl mixed oxide catalysts [28]. Modifying the calcination conditions of NiAl gave catalyst tailored to convert HMF selectively to 2,5-dimethylfuran (DMF), 2,5-dimethyltetrahydrofuran (DMTHF) or 2,5-dihydroxymethyltetrahydrofuran (DHMTHF) [29]. In this work, we synthesized Ni<sub>x</sub>Cu<sub>y</sub>Al<sub>1</sub>

## Ni-Cu/Al<sub>2</sub>O<sub>3</sub> from Layered Double Hydroxides Hydrogenates Furfural to Alcohols

catalysts from layered double hydroxides with Ni/Cu atomic ratios  $y/x$  of 1.5/0.5, 1/1 and 0.5/1.5. The catalysts were tested for furfural hydrogenation in vapor phase at atmospheric pressure, and in liquid phase at 5.0 MPa of hydrogen. The influence of the Ni/Cu ratio and the type of reactor on product selectivity is assessed, and the pathways leading to the formation of the major products are discussed.

## 2. Results and discussion

### 2.1. Catalyst characterization

The adsorption isotherms corresponded to mesoporous materials with type IV(a) isotherms and H3 hysteresis loops according to the IUPAC classification (Figure 3.1) [30, 31]. The pore size tended to decrease when the Ni/Cu atomic ratio increased (Figure 3.2). The average pore diameter increased from 7.0 nm in Ni<sub>1.5</sub>Cu<sub>0.5</sub>Al<sub>1</sub> to 7.4 nm in Ni<sub>0.5</sub>Cu<sub>1.5</sub>Al<sub>1</sub> (Table 3.1). Accordingly, surface area and pore volume were higher as lower was the average pore size. BET surface area grew from 127 m<sup>2</sup> g<sup>-1</sup> in Ni<sub>0.5</sub>Cu<sub>1.5</sub>Al<sub>1</sub> to 201 m<sup>2</sup> g<sup>-1</sup> in Ni<sub>1.5</sub>Cu<sub>0.5</sub>Al<sub>1</sub>. SEM imaging of the calcined LDHs confirmed that the surface morphology of the three samples were similar (Figure 3.3), although Ni<sub>1.5</sub>Cu<sub>0.5</sub>Al<sub>1</sub> had a slightly denser structure consisting of smaller particles

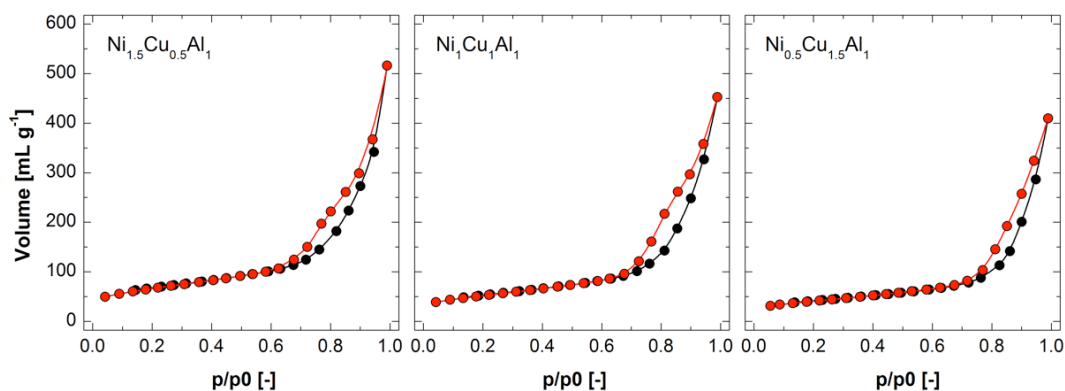


**Figure 3.1.** N<sub>2</sub> physisorption isotherms of the LDHs precursors calcined at 673 K for 4h.

## Ni-Cu/Al<sub>2</sub>O<sub>3</sub> from Layered Double Hydroxides Hydrogenates Furfural to Alcohols

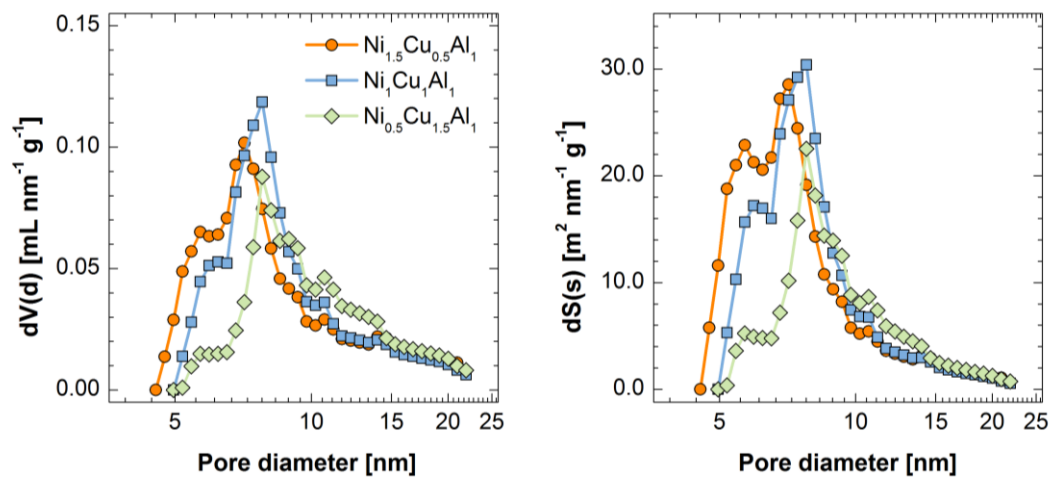


**Figure 3.2.** Pore volume (left) and surface (right) distributions of the LDHs calcined at 673 K for 4h, determined with the DFT model.

**Table 3.1.** Composition and textural properties of the calcined catalyst precursors.

Calcined material	BET Surface Area (m <sup>2</sup> g <sup>-1</sup> )	Pore volume (mL g <sup>-1</sup> )	Average pore diameter (nm)
Ni <sub>1.5</sub> Cu <sub>0.5</sub> Al <sub>1</sub>	201	0.53	7.0
Ni <sub>1</sub> Cu <sub>1</sub> Al <sub>1</sub>	162	0.52	7.3
Ni <sub>0.5</sub> Cu <sub>1.5</sub> Al <sub>1</sub>	127	0.48	7.4

## Ni-Cu/Al<sub>2</sub>O<sub>3</sub> from Layered Double Hydroxides Hydrogenates Furfural to Alcohols

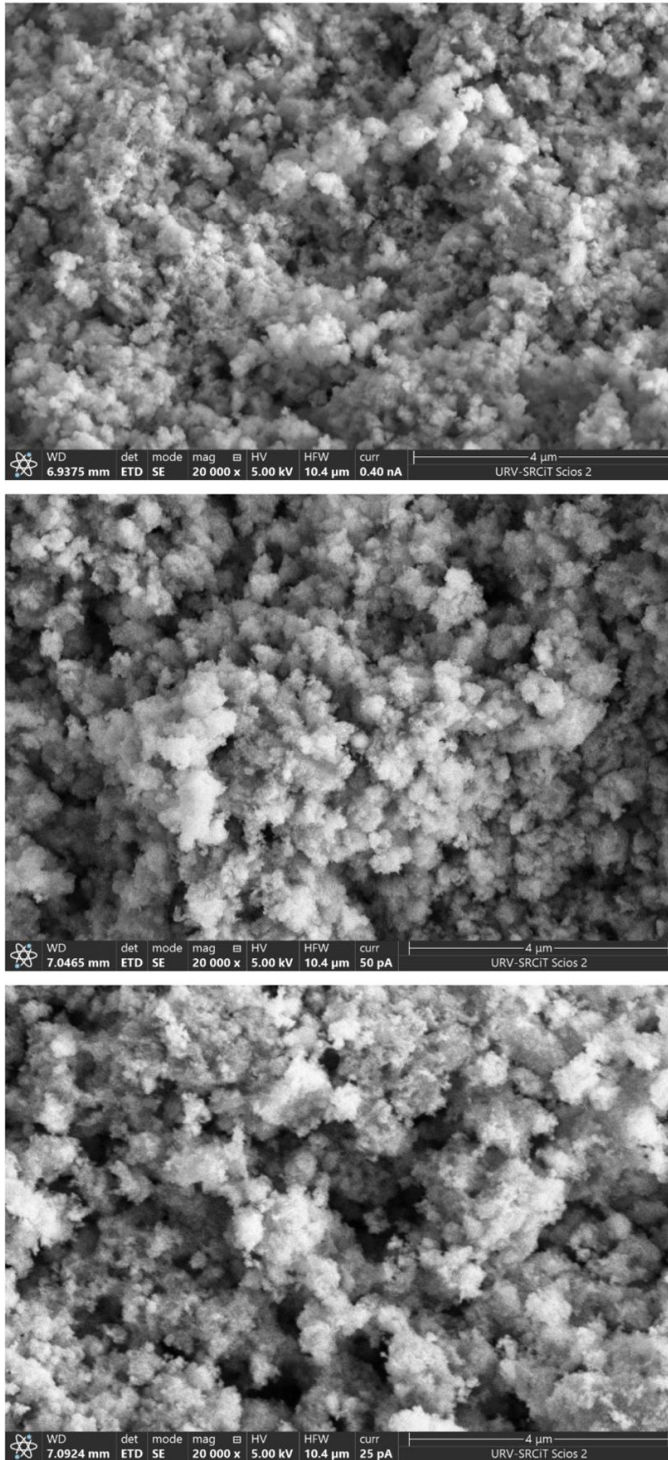


**Figure 3.3.** SEM imaging of the calcined materials (20 000 x magnification): Ni<sub>1.5</sub>Cu<sub>0.5</sub>Al<sub>1</sub> (top), Ni<sub>1</sub>Cu<sub>1</sub>Al<sub>1</sub> (center) and Ni<sub>0.5</sub>Cu<sub>1.5</sub>Al<sub>1</sub> (bottom)

## Ni-Cu/Al<sub>2</sub>O<sub>3</sub> from Layered Double Hydroxides Hydrogenates Furfural to Alcohols

The Ni/Al and Cu/Al atomic ratios of the calcined LDHs measured by FAA were close to the nominal values (Table 3.2), proving the suitability of the synthesis procedure. FESEM-EDX imaging showed a gradual change in composition among the three materials (Figure 3.4). The atomic ratios determined by this technique were higher than those measured by FAA, especially in Ni<sub>1.5</sub>Cu<sub>0.5</sub>Al<sub>1</sub>. High-resolution XPS also gave values above the nominal, although the Ni/Cu ratios were close to those determined by FAA. The higher Ni/Al and Cu/Al atomic ratios measured by XPS and FESEM-EDX were attributed to the formation of Cu and Ni oxides dispersed on top of aluminum oxides [32]. The oxides were identified and calculated by XPS in Table 3.3 (Figure 3.5 based on the binding energies of Ni 2p<sub>3</sub>, Cu 2p<sub>3</sub> and Al 2p).

**Table 3.2.** Metal atomic ratios in the materials calcined at 673 K for 4h, measured by FAA, FESEM-EDX, and XPS.

Calcined material	FAA		FESEM-EDX		XPS	
	Ni/Al	Cu/Al	Ni/Al	Cu/Al	Ni/Al	Cu/Al
Ni <sub>1.5</sub> Cu <sub>0.5</sub> Al <sub>1</sub>	1.43	0.53	1.86	0.64	1.60	0.66
Ni <sub>1</sub> Cu <sub>1</sub> Al <sub>1</sub>	0.98	1.04	0.90	0.91	1.19	1.27
Ni <sub>0.5</sub> Cu <sub>1.5</sub> Al <sub>1</sub>	0.49	1.47	0.47	1.48	0.67	1.57

## Ni-Cu/Al<sub>2</sub>O<sub>3</sub> from Layered Double Hydroxides Hydrogenates Furfural to Alcohols

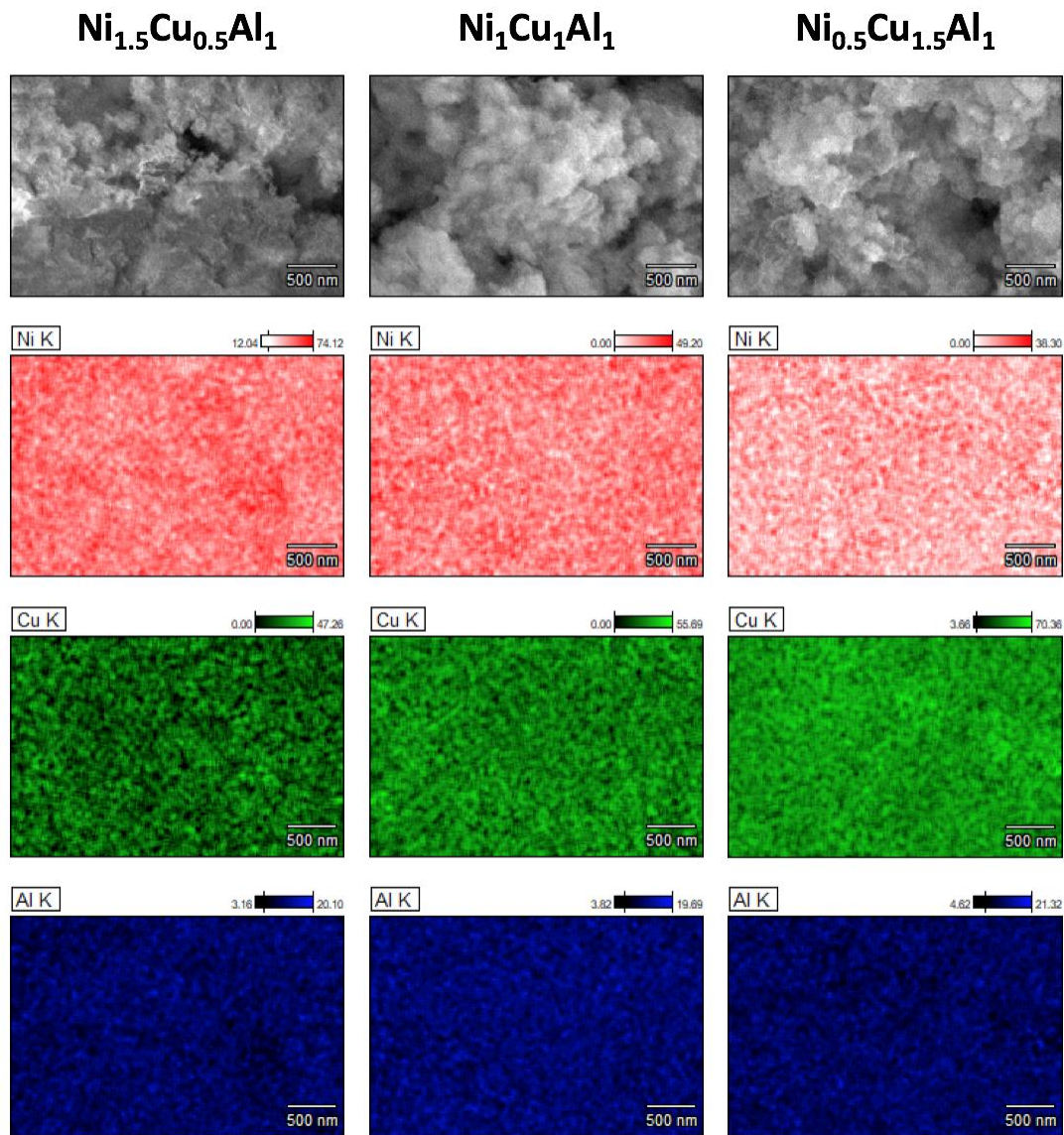


**Figure 3.4.** Surface composition of the LDHs precursors calcined at 673 K for 4h measured by EFSEM-EDX.

## Ni-Cu/Al<sub>2</sub>O<sub>3</sub> from Layered Double Hydroxides Hydrogenates Furfural to Alcohols

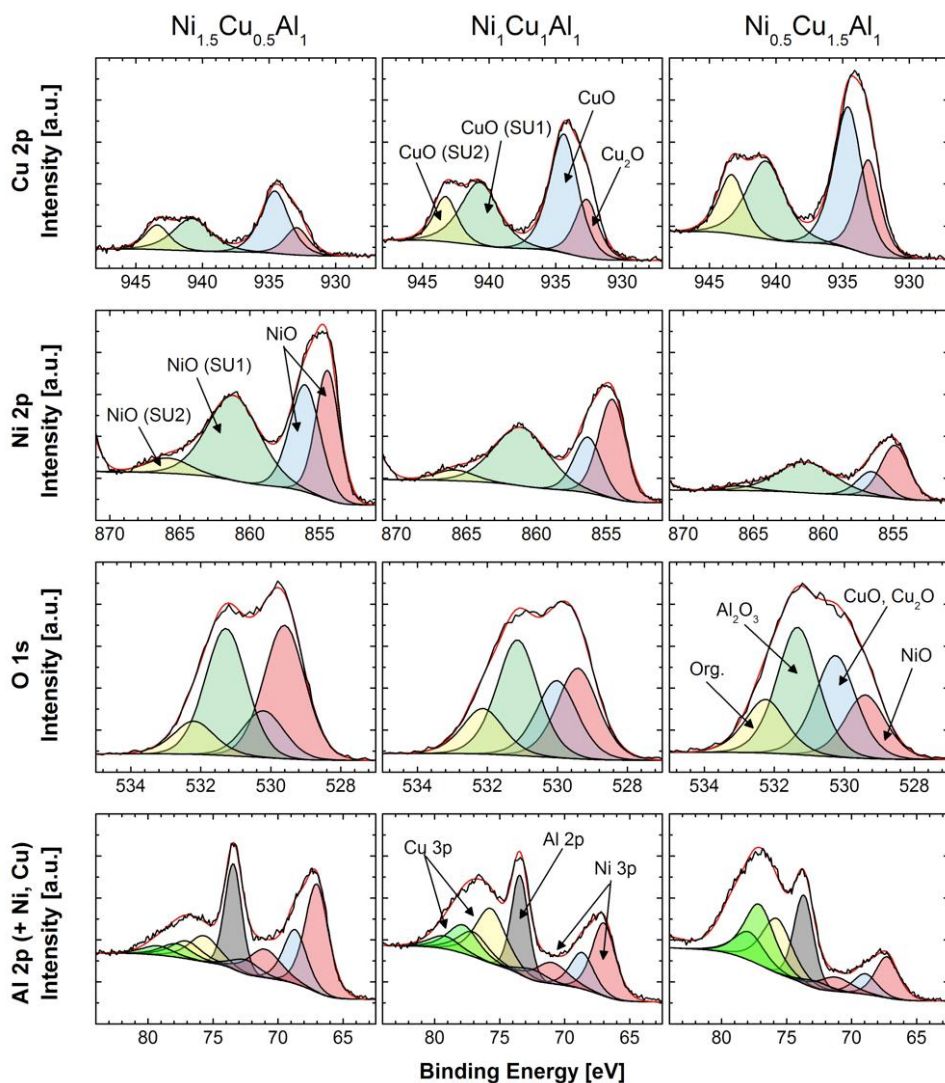


**Figure 3.5.** XPS spectra of Ni 2p, Cu 2p, and O 1s of the LDHs precursors calcined at 673 K for 4h.

Nickel formed NiO. Although, the binding energy at which Ni 2p was observed was higher than that expected for NiO and closer to that expected for Ni(OH)<sub>2</sub> [33], the shape of the shake up (SU) satellite peak was consistent with NiO [34]. The multiple splitting expected for NiO was not observed. This could be explained because the samples were under the form of powder, which tends to broaden the peaks and reduce energy resolution. Furthermore, the ratio of oxygen to nickel found was not consistent with nickel being predominantly in the form of Ni(OH)<sub>2</sub>. Copper formed CuO and Cu<sub>2</sub>O. An asymmetry and

## Ni-Cu/Al<sub>2</sub>O<sub>3</sub> from Layered Double Hydroxides Hydrogenates Furfural to Alcohols

slight shoulder on the low binding energy side of the Cu 2p<sub>3/2</sub> and Cu 2p<sub>1/2</sub> peaks indicated the presence of Cu<sub>2</sub>O. The shape and size of the SU satellite peak was consistent with CuO [34]. Nevertheless, only a weak SU was expected for Cu<sub>2</sub>O. The binding energy of the Cu 2p components of CuO and Cu<sub>2</sub>O was slightly higher than expected [33, 34]. As for nickel, the presence of a large amount of Cu(OH)<sub>2</sub> was ruled out because the ratio of oxygen to copper content was not large enough. The same argument applied to CuAl<sub>2</sub>O<sub>4</sub>. The binding energy of Cu 2p in this compound should be around 934.5 eV [35], consistent with the largest component observed here, but the oxygen to copper ratio was too low. Oxygen O 1s components were assigned to NiO [33, 36], CuO and Cu<sub>2</sub>O (internal reference) and Al<sub>2</sub>O<sub>3</sub> [34] based on binding energy and intensity to yield the proper metal/oxygen ratios. The Al 2p curve fitting had a high level of uncertainty as it overlapped with Ni 3p and Cu 3p. In the three materials, a single component of Al 2p was found at binding energies of 73.4 eV and 73.7 eV, which was consistent with the presence of Al<sub>2</sub>O<sub>3</sub>. The presence of CuAl<sub>2</sub>O<sub>4</sub> could not be confirmed because the binding energy of Al 2p in this compound, ca. 74 eV [35], was not significantly different from that of Al<sub>2</sub>O<sub>3</sub> when considering the overlap with Cu 3p.

**Table 3.3.** XPS analysis of the LDHs calcined at 673 K for 4h: binding energies of the metal oxides.

Calcined material	Binding energy (eV)							
	Ni 2p (NiO)	Ni 2p SU1 (NiO)	Ni 2p SU2 (NiO)	Cu 2p (Cu <sub>2</sub> O)	Cu 2p (CuO)	Cu 2p SU1 (CuO)	Cu 2p SU2 (CuO)	Al 2p (Al <sub>2</sub> O <sub>3</sub> )
Ni <sub>1.5</sub> Cu <sub>0.5</sub> Al <sub>1</sub>	856.0; 854.4	861.1	865.8	932.9	934.6	940.8	943.4	73.4
Ni <sub>1</sub> Cu <sub>1</sub> Al <sub>1</sub>	856.3; 854.6	861.1	865.8	932.7	934.4	940.7	943.3	73.4
Ni <sub>0.5</sub> Cu <sub>1.5</sub> Al <sub>1</sub>	856.6; 854.9	861.3	866.0	933.1	934.6	940.8	943.3	73.7

XRD of the calcined LDHs (Figure 3.6) gave three broad peaks at ca. 37°, 44° and 63° that were consistent with CuO, Cu<sub>2</sub>O and NiO. Overlapping of the signals of the three oxides could be caused by the smaller crystallite sizes and large dispersion of the oxides derived from LDH precursors [37, 38]. Noticeably, the signals attributable to NiO were more intense in Ni<sub>1.5</sub>Cu<sub>0.5</sub>Al<sub>1</sub>, whereas those of CuO were dominant in Ni<sub>0.5</sub>Cu<sub>1.5</sub>Al<sub>1</sub>.

Ni-Cu/Al<sub>2</sub>O<sub>3</sub> from Layered Double Hydroxides  
 Hydrogenates Furfural to Alcohols

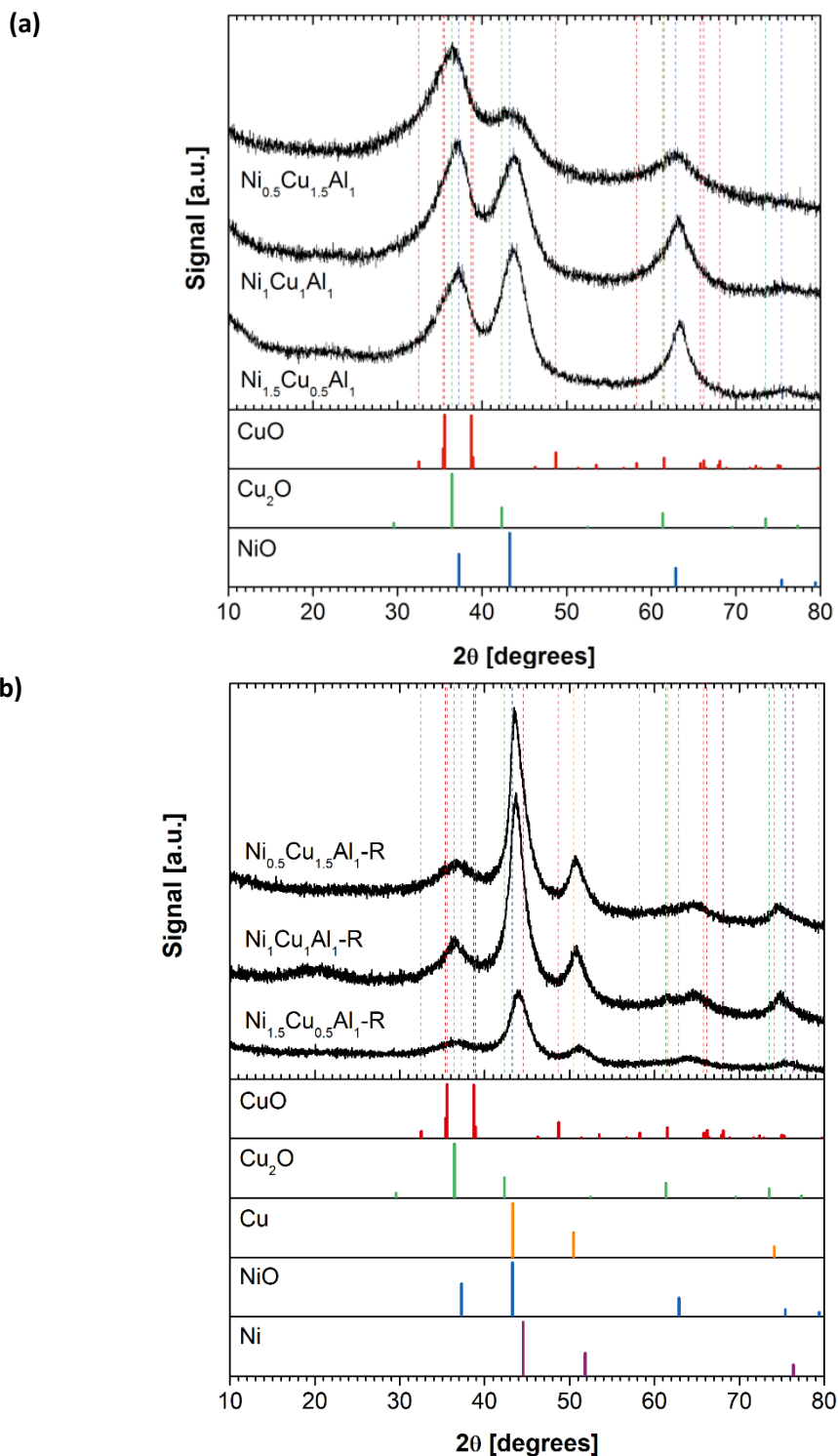


Figure 3.6. XRD patterns: (a) LDHs precursors calcined at 673 K for 4h; (b) reduced catalysts.

## Ni-Cu/Al<sub>2</sub>O<sub>3</sub> from Layered Double Hydroxides Hydrogenates Furfural to Alcohols

The reducibility of the calcined materials was studied by temperature-programmed reduction under 10 % hydrogen in argon (H<sub>2</sub>-TPR) from 375 to 1075 K (Figure 3.7). Two well-differentiated peaks of hydrogen consumption were observed. The peak at the lowest temperature corresponded to the reduction of highly dispersed particles of copper oxides to Cu<sup>0</sup> [39, 40], while the much broader peak at the highest temperature was attributed to the reduction of nickel oxide having strong interaction with aluminum oxides [41-44]. The Ni/Cu ratio influenced the temperature of each peak and their specific hydrogen consumption (Table 3.4). The hydrogen intake in the first peak raised with the content of copper in the sample, from 367 mL g<sup>-1</sup> of H<sub>2</sub> (STP) in Ni<sub>1.5</sub>Cu<sub>0.5</sub>Al<sub>1</sub> to 113 mL g<sup>-1</sup> of H<sub>2</sub> (STP) in Ni<sub>0.5</sub>Cu<sub>1.5</sub>Al<sub>1</sub>. The consumption of the second peak showed the opposite trend and it decreased from 85 mL g<sup>-1</sup> of H<sub>2</sub> (STP) in Ni<sub>1.5</sub>Cu<sub>0.5</sub>Al<sub>1</sub> to 19 mL g<sup>-1</sup> of H<sub>2</sub> (STP) in Ni<sub>0.5</sub>Cu<sub>1.5</sub>Al<sub>1</sub>. However, Ni<sub>1</sub>Cu<sub>1</sub>Al<sub>1</sub> had the highest total consumption and the lowest temperature of nickel oxide reduction. This suggests that the nickel oxides had a slightly weaker interaction with the alumina matrix in this material, thus resulting on a better reducibility.

Nickel and copper metal were present in the three catalysts after reduction at 773 K (Figure 3.6 b) and CuO and Cu<sub>2</sub>O diminished. The three catalysts gave the signal of Cu<sup>0</sup> at 50.4° and its intensity grew with the contents of copper. The main signal of Cu<sup>0</sup> at 43.3° overlapped with that of NiO at the same angle, but the presence of NiO was confirmed by its secondary band at 37.2°. Concerning Ni<sup>0</sup>, its main signal at 44.5° was observed, especially in Ni<sub>1.5</sub>Cu<sub>0.5</sub>Al<sub>1</sub>-R, although it overlapped with the signals of NiO and Cu<sup>0</sup> at 43.3°. Overall, the crystalline phases detected after reduction at 773 K agreed with the TPR. Most copper was reduced to its metal form whereas nickel was only reduced partially and a significant fraction remained as NiO.

Ni-Cu/Al<sub>2</sub>O<sub>3</sub> from Layered Double Hydroxides  
 Hydrogenates Furfural to Alcohols

**Table 3.4.** Specific hydrogen consumptions during TPR of the calcined LDHs samples.

Calcined material	Peak 1		Peak 2		Total
	T (K)	H <sub>2</sub> (mL g <sup>-1</sup> STP)	T (K)	H <sub>2</sub> (mL g <sup>-1</sup> STP)	H <sub>2</sub> (mL g <sup>-1</sup> STP)
Ni <sub>1.5</sub> Cu <sub>0.5</sub> Al <sub>1</sub>	474	37	738	85	121
Ni <sub>1</sub> Cu <sub>1</sub> Al <sub>1</sub>	484	84	714	70	155
Ni <sub>0.5</sub> Cu <sub>1.5</sub> Al <sub>1</sub>	525	113	757	19	132

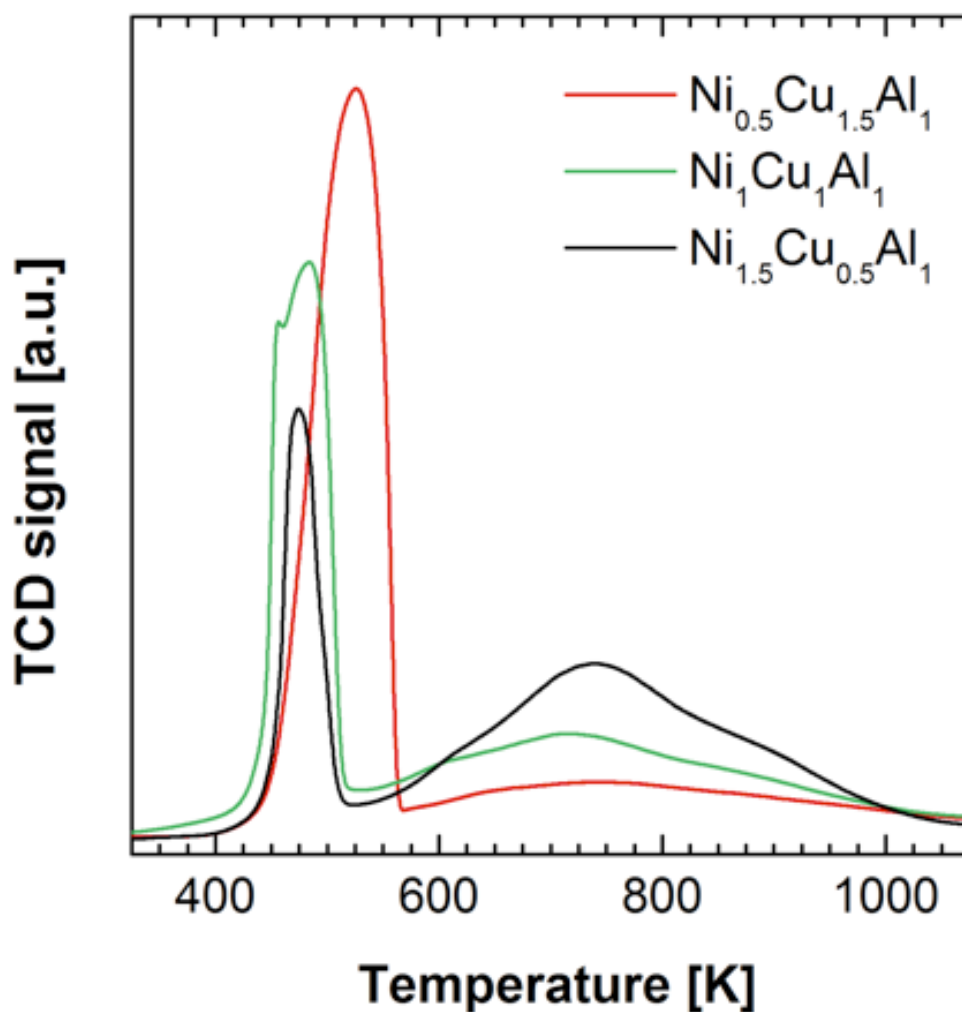


**Figure 3.7.** H<sub>2</sub>-TPR of the LDHs precursors calcined at 673 K for 4h.

## Ni-Cu/Al<sub>2</sub>O<sub>3</sub> from Layered Double Hydroxides Hydrogenates Furfural to Alcohols

### 2.2. Catalytic activity tests

The activity of the catalysts was tested in gas phase on a continuous packed bed reactor at atmospheric pressure (PBR), and in liquid-phase on a high-pressure stirred slurry reactor (SSR). All catalysts gave complete conversion of furfural (FF) during the tests performed in the SSR at 5.0 Mpa of H<sub>2</sub>. The Ni/Cu metal ratio of the catalyst influenced the distribution of products significantly (Figure 3.8 and Table 3.5).

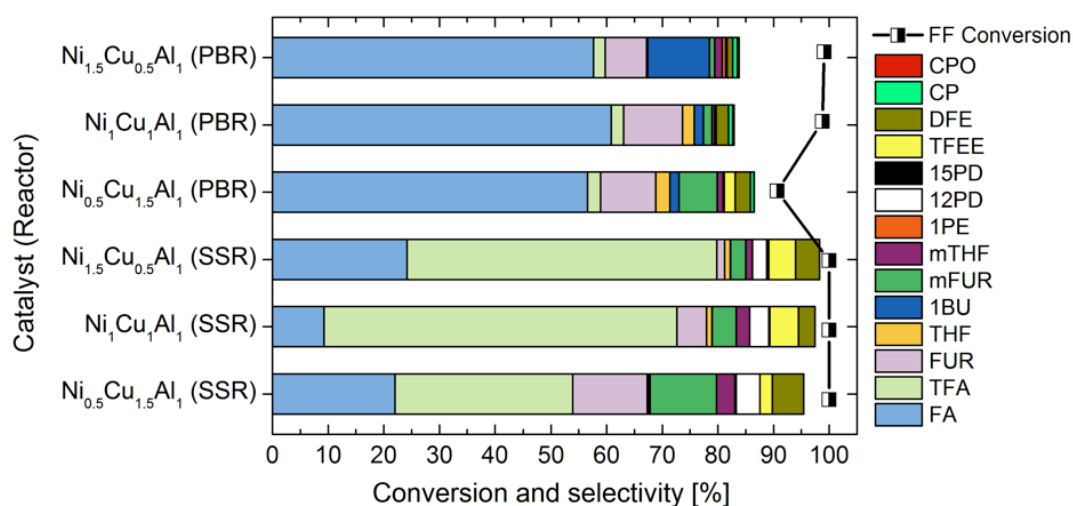


**Figure 3.8.** Furfural conversion and product selectivity of the three catalysts in the atmospheric PBR and the SSR at 5.0 MPa H<sub>2</sub>. All experiments at 463 K.

Tetrahydrofurfuryl alcohol (TFA) was the main product on Ni<sub>1</sub>Cu<sub>1</sub>Al<sub>1</sub>-R with a selectivity of 63%, together with furfuryl alcohol (FA 9.2%), furan (FUR 5.3%), 2-methylfuran (mFUR 4.3%), 2-methyltetrahydrofuran (mTHF 2.4%) and 1,2-pentanediol (12PD 3.4%). In addition, two products that could not be formed by direct hydrogenation/hydrogenolysis of furfural were present, ethyl tetrahydrofurfuryl ether (TFEE 5.2%) and difurfuryl ether (DFE 3.0%). Shifting to a higher copper content (Ni<sub>0.5</sub>Cu<sub>1.5</sub>Al<sub>1</sub>-R) reduced the formation of TFA to 32% and augmented the selectivity to FA (22%), FUR (14%), mFUR (12%), 12PD (4.3%) and mTHF (3.3%). However, on Ni<sub>1.5</sub>Cu<sub>0.5</sub>Al<sub>1</sub>-R the selectivity to TFA diminished (56%), that of FA augmented (24%) and the formation of FUR, mFUR, 12PD and mTHF was

## Ni-Cu/Al<sub>2</sub>O<sub>3</sub> from Layered Double Hydroxides Hydrogenates Furfural to Alcohols

lower than that on Ni<sub>1</sub>Cu<sub>1</sub>Al<sub>1</sub>-R. Trace amounts of 1-butanol (1BU) and 1,5-pentaneanediol (15PD) and significant amounts of TFEE and DFE were always formed with the Ni/Cu atomic ratio shifting selectivity towards more TFEE and less DFE.

**Table 3.5.** Selectivity and conversion during furfural hydrogenation in the pressurized SSR and atmospheric PBR reactors.

Conversion (%)	Stirred slurry reactor (SSR)			Tubular reactor (PBR)		
	Ni <sub>0.5</sub> Cu <sub>1.5</sub> Al <sub>1</sub> -R	Ni <sub>1</sub> Cu <sub>1</sub> Al <sub>1</sub> -R	Ni <sub>1.5</sub> Cu <sub>0.5</sub> Al <sub>1</sub> -R	Ni <sub>0.5</sub> Cu <sub>1.5</sub> Al <sub>1</sub> -R	Ni <sub>1</sub> Cu <sub>1</sub> Al <sub>1</sub> -R	Ni <sub>1.5</sub> Cu <sub>0.5</sub> Al <sub>1</sub> -R
	100.	100.	100.	91	99	99
FA	22	9.2	24	57	61	58
FUR	13	5.3	1.4	9.9	11	7.4
mFUR	12	4.3	2.7	6.9	1.5	1.0
TFA	32	63	56	2.3	2.3	2.1
THF	0.3	0.9	1.0	2.6	2.1	0.2
mTHF	3.3	2.4	1.2	1.0	0.5	1.3
12PD	4.3	3.4	2.6	-	-	-
15PD	-	0.2	0.4	-	-	-
1PE	0.2	-	-	0.2	0.3	0.6
1BU	0.2	0.1	0.1	1.6	1.6	11
CP	-	-	-	0.1	0.2	0.3
CPO	-	-	-	0.6	0.8	0.8
TFEE	2.3	5.2	4.8	1.9	-	-
DFE	5.6	3.0	4.3	2.8	2.2	1.0
Other	4.6	2.6	1.7	14	17	16

Three competing pathways were involved in the conversion of FF on the SSR (Scheme 3.1). The first route started with the hydrogenation of the carbonyl group of FF to form FA., followed by the hydrogenation of the alcohol group in FA to form mFUR (which can be further hydrogenated to mTHF), or the direct hydrogenation of the double bonds ( $\pi$  bonds) in FA to form TFA. The second route was the decarbonylation of FF to FUR, which was followed by the hydrogenation of the  $\pi$  bonds in the furan ring of FUR to produce THF, or by the ring-opening hydrogenolysis of FUR to form 1BU. TFEE and DFE evolved through the formation of acetals on acidic sites of the catalyst surface by reversible nucleophilic



## Ni-Cu/Al<sub>2</sub>O<sub>3</sub> from Layered Double Hydroxides Hydrogenates Furfural to Alcohols

product with a selectivity of 61% in the Ni<sub>1</sub>Cu<sub>1</sub>Al<sub>1</sub>-R catalyst, followed by FUR (11%) and lower amounts of TFA (2.3%), THF (2.1%) and mFUR (1.5%), 1BU (1.6%) and mTHF (0.5%). In addition, selectivity to DFE was 2.2%, but TFEE was not formed. Pentanediols were not detected among the reaction products but trace amounts of 1PE together with cyclopentanone (CP) and cyclopentanol (CPO) were produced by the rearrangement of FA. When the Ni/Cu ratio was lower (Ni<sub>0.5</sub>Cu<sub>1.5</sub>Al<sub>1</sub>-R), the selectivity of FA decreased to 57% and that of mFUR raised to 6.9%. The other products were not affected substantially except for TFEE, which was formed on this catalyst. On the other hand, when the Ni/Cu ratio was augmented (Ni<sub>1.5</sub>Cu<sub>0.5</sub>Al<sub>1</sub>-R), selectivity to FA diminished to 57 % but now 1BU (11 %) was the main secondary product. FUR was lower (7.4%) and TFEE was not formed. The selectivity to DFE was lower than in the SSR and it tended to decrease with the Ni/Cu atomic ratio in the catalyst. Overall, nickel favored the paths leading to FUR and 1BU, whereas Cu favored the hydrogenation of the alcohol group in FA to mFUR and did not promote the ring opening hydrogenolysis of FUR or mFUR to linear alcohols. The three catalysts presented little activity on the hydrogenation of the  $\pi$  bonds of the furan ring, at least at the short contact time of these experiments, which explains the low yields of TFA, THF and mTHF.

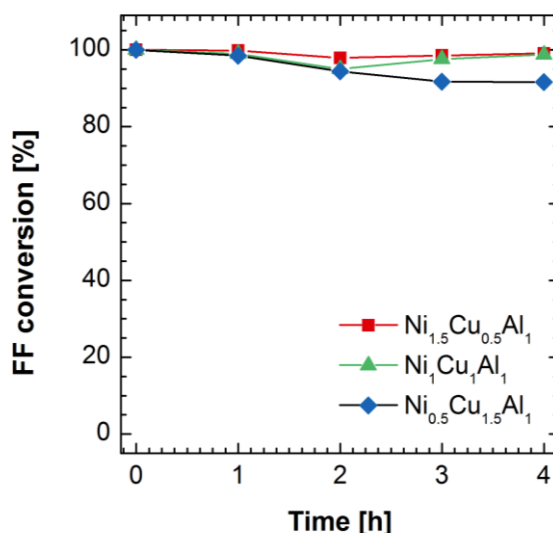


**Figure 3.9.** FF conversion in the atmospheric PBR at 463 K and a WHSV of 2.85 g<sub>FF</sub> g<sub>cat</sub><sup>-1</sup> h<sup>-1</sup>.

## Ni-Cu/Al<sub>2</sub>O<sub>3</sub> from Layered Double Hydroxides Hydrogenates Furfural to Alcohols

Hydrogen availability was different in both reactor systems and this could influence selectivity. The effective hydrogen-to-furfural molar ratio in the liquid phase of the SSR was low because of the small solubility of hydrogen in ethanol, even with a high operation pressure and optimized stirring to avoid mass transfer limitations. An estimation of the equilibrium composition of the liquid and gas phases at the beginning of the reaction in the SSR was obtained with ASPEN Plus using the Peng-Robinson equation of state. The model was first validated by comparing equilibrium calculations of ethanol-hydrogen mixtures at saturation at high pressure and temperature with published data [50]. The equilibrium molar concentrations of hydrogen, furfural and ethanol in the liquid at 5.0 MPa and 463 K were 0.190, 0.419 and 11.3 mol L<sup>-1</sup>, respectively. This means that in the SSR, the initial molar ratio between hydrogen and furfural in the bulk of the liquid was ca. 0.45 mol<sub>H<sub>2</sub></sub>/mol<sub>FF</sub> at the most. In the initial stages of the reaction FF was converted to FA, which given the extended contact time (4 h in these experiments), was subsequently transformed to TFA, FUR and several hydrogenolysis products, including 1,2-pentanediol. The low availability of hydrogen and the huge excess of ethanol made possible the nucleophilic addition between FF and ethanol/FA that led to TFEE and DFE.

Given the feed flowrates of FF solution and hydrogen used in the PBR, the catalyst particles at the beginning of reactor were exposed to concentrations of hydrogen, furfural and ethanol of 9.35 10<sup>-3</sup>, 7.36 10<sup>-4</sup> and 2.92 10<sup>-2</sup> mol L<sup>-1</sup>, respectively (an absolute pressure of 0.15 MPa was assumed to compensate for pressure drop across the packed bed and accessories downstream of the reactor). These conditions corresponded to a molar ratio of 12.7 mol<sub>H<sub>2</sub></sub>/mol<sub>FF</sub>. Even with the large excess of hydrogen, the short contact time in the PBR allowed FA to be the main product and reduced its subsequent hydrogenation to TFA and other hydrogenolysis products. However, the large excess of hydrogen probably promoted the conversion of FF and FA to FUR and 1BU on the Ni<sub>1.5</sub>Cu<sub>0.5</sub>Al<sub>1</sub> catalyst. The higher availability of hydrogen also reduced the occurrence of the addition reactions, thus lowering the selectivity towards TFEE and DFE. The inhibition of this pathway was promoted by a higher Ni/Cu ratio. With further optimization of the reaction conditions, the Ni<sub>x</sub>Cu<sub>y</sub>Al<sub>1</sub> catalysts could be used to produce furfuryl alcohol with high selectivity by the

## Ni-Cu/Al<sub>2</sub>O<sub>3</sub> from Layered Double Hydroxides Hydrogenates Furfural to Alcohols

gas-phase hydrogenation of furfural, but also to explore the co-production of tetrahydrofurfuryl alcohol and high-value products such as 1,2-pentanediol by the liquid-phase hydrogenolysis in slurry or trickle-bed type reactors.

### 3. Conclusions

NiCuAl catalysts derived from layered double hydroxides showed high activity in the hydrogenation and hydrogenolysis of furfural, both in the gas phase at atmospheric pressure and in the liquid phase in a slurry batch reactor. Furfural was converted through three competing paths: decarbonylation to furan, hydrogenation to furfuryl alcohol and nucleophilic addition with alcohols (ethanol, the solvent, and furfuryl alcohol) to form acetals, which were subsequently converted to DFE and TFEE. These primary products were further converted by saturation of the furan ring and/or ring opening to alcohols. In all cases, sequential hydrogenation to furfuryl alcohol and tetrahydrofurfuryl alcohol was the main route, but the selectivity was influenced by the Ni/Cu ratio of the catalysts and by the different hydrogen availability in both reactors

## Ni-Cu/Al<sub>2</sub>O<sub>3</sub> from Layered Double Hydroxides Hydrogenates Furfural to Alcohols

### 4. References

- [1] Bozell, J.J.; Petersen, G.R. Technology development for the production of biobased products from biorefinery carbohydrates—the US Department of Energy’s “Top 10” revisited. *Green Chem.* 2010, 12, 539-554.
- [2] Wettstein, S.G.; Martin Alonso, D.; Gürbüz, E.I.; Dumesic, J.A. A roadmap for conversion of lignocellulosic biomass to chemicals and fuels. *Chem. Eng.* 2012, 1, 218-224.
- [3] Mariscal, R.; Maireles-Torres, P.; Ojeda, M.; Sádaba, I.; López Granados. Furfural: a renewable and versatile platform molecule for the synthesis of chemicals and fuels. *Energy Environ. Sci.* 2016, 9, 1144-1189.
- [4] Chen, S.; Wojcieszak, R.; Dumeignil, F.; Marceau, E.; Royer, S. How Catalysts and Experimental Conditions Determine the Selective Hydroconversion of Furfural and 5-Hydroxymethylfurfural. *Chem. Rev.* 2018, 118, 11023-11117.
- [5] Hoydonckx, H.E.; Van Rhijn, W.M.; Van Rhijn, W.; De Vos, D.E.; Jacobs, P.A. Furfural and Derivatives. In *Ullmann’s Encyclopedia of Industrial Chemistry*; Wiley-VCH Verlag GmbH & Co. KGaA: Weinheim, Germany, 2012; Volume 16, pp. 285-313.
- [6] Serrano-Ruiz, J. C.; Luque, R.; Sepulveda-Escribano, A. Transformations of biomass-derived platform molecules: from high added-value chemicals to fuels via aqueous-phase processing. *Chem. Soc. Rev.* 2011, 40, 5266-5281.
- [7] Lange, J.-P.; van der Heide, E.; van Buijtenen, J.; Price, R. Furfural - A Promising Platform for Lignocellulosic Biofuels. *ChemSusChem* 2012, 5, 150-166.
- [8] Climent, M.J.; Corma, A.; Iborra, S. Conversion of biomass platform molecules into fuel additives and liquid hydrocarbon fuels. *Green Chem.* 2014, 16, 516-547.
- [9] Jiang, Y.; Wang, X.; Cao, Q.; Dong, L.; Guan, J.; Mu, X. Chemical Conversion of Biomass to Green Chemicals. In *Sustainable Production of Bulk Chemicals*; Xian, M., Ed.; Springer: Dordrecht, The Netherlands, 2016; pp 19-49.
- [10] Sitthisa, S.; Pham, T.; Prasomsri, T.; Sooknoi, T.; Mallinson, R.G.; Resasco, D.E. Conversion of Furfural and 2-Methylpentanal on Pd/SiO<sub>2</sub> and Pd-Cu/SiO<sub>2</sub> Catalysts. *J. Catal.* 2011, 280, 17-27.
- [11] Shi, Y.; Zhu, Y.; Yang, Y.; Li, Y.-W.; Jiao, H. Exploring Furfural Catalytic Conversion on Cu(111) from Computation. *ACS Catal.* 2015, 5, 4020-4032.
- [12] Medlin, J.W. Understanding and Controlling Reactivity of Unsaturated Oxygenates and Polyols on Metal Catalysts. *ACS Catal.* 2011, 1, 1284-1297.
- [13] Ni, Z.-M.; Xia, M.-Y.; Shi, W.; Qian, P.-P. Adsorption and Decarbonylation Reaction of Furfural on Pt (111) Surface. *Acta Phys.-Chim. Sin.* 2013, 29, 1916-1922.

## Ni-Cu/Al<sub>2</sub>O<sub>3</sub> from Layered Double Hydroxides Hydrogenates Furfural to Alcohols

- [14] Liu, B.; Cheng, L.; Curtiss, L.; Greeley, J. Effects of van Der Waals Density Functional Corrections on Trends in Furfural Adsorption and Hydrogenation on Close-Packed Transition Metal Surfaces. *Surf. Sci.* 2014, 622, 51-59.
- [15] Xiong, K.; Wan, W.; Chen, J.G. Reaction Pathways of Furfural, Furfuryl Alcohol and 2-Methylfuran on Cu(111) and NiCu Bimetallic Surfaces. *Surf. Sci.* 2016, 652, 91-97.
- [16] Bradley, M.K.; Robinson, J.; Woodruff, D.P. The Structure and Bonding of Furan on Pd(111). *Surf. Sci.* 2010, 604, 920-925.
- [17] Jenness, G.R.; Vlachos, D.G. DFT Study of the Conversion of Furfuryl Alcohol to 2-Methylfuran on RuO<sub>2</sub> (110). *J. Phys. Chem. C* 2015, 119, 5938-5945.
- [18] Sitthisa, S.; Resasco, D.E. Hydrodeoxygenation of Furfural over Supported Metal Catalysts: A Comparative Study of Cu, Pd and Ni. *Catal. Lett.* 2011, 141, 784-791.
- [19] Zhang, W.; Zhu, Y.; Niu, S.; Li, Y. A Study of Furfural Decarbonylation on K-Doped Pd/Al<sub>2</sub>O<sub>3</sub> Catalysts. *J. Mol. Catal. A: Chem.* 2011, 335, 71-81.
- [20] Fu, X.; Ren, X.; Shen, J.; Jiang, Y.; Wang, Y.; Orooji, Y.; Xu, W.; Liang, J. Synergistic catalytic hydrogenation of furfural to 1,2-pentanediol and 1,5-pentanediol with LDO derived from CuMgAl hydrotalcite. *Molecular Catalysis* 2021, 499, 111298.
- [21] Gavilà, L.; Lahde, A.; Jokiniemi, J.; Constantí, M.; Medina, F.; del Río, E.; Tichit, D.; Álvarez, M.G. Insights on the One-Pot Formation of 1,5-Pentanediol from Furfural with Co-Al Spinel-based Nanoparticles as an Alternative to Noble Metal Catalysts. *ChemCatChem* 2019, 11, 4944-4953.
- [22] Bertolini G.R.; Jiménez-Gómez C.P.; Cecilia J.A.; Maireles-Torres P. Gas-Phase Hydrogenation of Furfural to Furfuryl Alcohol over Cu-ZnO-Al<sub>2</sub>O<sub>3</sub> Catalysts Prepared from Layered Double Hydroxides. *Catalysts* 2020, 10, 486.
- [23] Herbois, R.; Noël, S.; Léger, B.; Bai, L.; Roucoux, A.; Monflier, E.; Ponchel, A. Cyclodextrins as growth controlling agents for enhancing the catalytic activity of PVP-stabilized Ru(0) nanoparticles. *Chem. Commun.* 2012, 48, 3451-3453.
- [24] Wang, Y.; Zhou, M.; Wang, T.; Xiao, G. Conversion of Furfural to Cyclopentanol on Cu/Zn/Al Catalysts Derived from Hydrotalcite-Like Materials. *Catal. Lett.* 2015, 145, 1557-1565.
- [25] Zhou, M.; Zeng, Z.; Zhu, H.; Xiao, G.; Xiao, R. Aqueous-phase catalytic hydrogenation of furfural to cyclopentanol over Cu-Mg-Al hydrotalcites derived catalysts: model reaction for upgrading bio-oil. *J. Energy Chem.* 2014, 23, 91-96.
- [26] Guo, J.; Xu, G.; Han, A.; Zhang, Y.; Fu, Y.; Guo Q. Selective Conversion of Furfural to Cyclopentanone with CuZnAl Catalysts. *ACS Sustainable Chem. Eng.* 2014, 2, 2259-2266.
- [27] Zhu, H.; Zhou, M.; Zeng, Z.; Xiao, G.; Xiao, R. Selective hydrogenation of furfural to cyclopentanone over Cu-Ni-Al hydrotalcite-based catalysts. *Korean J. Chem. Eng.* 2014, 31, 593-597.

## Ni-Cu/Al<sub>2</sub>O<sub>3</sub> from Layered Double Hydroxides Hydrogenates Furfural to Alcohols

- [28] Yao, S.; Wang, X.; Jiang, Y.; Wu, F.; Chen, X.; Mu, X. One-Step Conversion of Biomass-Derived 5-Hydroxymethylfurfural to 1,2,6-Hexanetriol Over Ni-Co-Al Mixed Oxide Catalysts Under Mild Conditions. *ACS Sustainable Chem. Eng.* 2014, 2, 173-180.
- [29] Kong, X.; Zheng, R.; Zhu, Y.; Ding, G.; Zhu, Y.; Lia, Y.-W. Rational design of Ni-based catalysts derived from hydrotalcite for selective hydrogenation of 5-hydroxymethylfurfural. *Green Chem.* 2015, 17, 2504-2514.
- [30] Thommes, M.; Kaneko, K.; Neimark, A.V.; Olivier, J.P.; Rodriguez-Reinoso, F.; Rouquerol, J.; Sing, K.S.W. Physisorption of gases, with special reference to the evaluation of surface area and pore size distribution (IUPAC Technical Report). *Pure Appl. Chem.* 2015, 87, 1051-1069.
- [31] Bardestani R.; Patience G.S.; Kaliaguine S. Experimental methods in chemical engineering: specific surface area and pore size distribution measurements - BET, BJH, and DFT. *Can J Chem Eng.* 2019, 97, 2781-2791.
- [32] Yi, Y.; Liu, H.; Chu, B.; Qin, Z.; Donga, L.; He, H.; Tang, C.; Fan, M.; Bin, L. Catalytic removal NO by CO over LaNi<sub>0.5</sub>M<sub>0.5</sub>O<sub>3</sub> (M=Co, Mn, Cu) perovskite oxide catalysts: Tune surface chemical composition to improve N<sub>2</sub> selectivity. *Chem. Eng. J.* 2019, 369, 511-521.
- [33] McIntyre, N.S.; Cook, M.G. X-ray photoelectron studies on some oxides and hydroxides of cobalt, nickel, and copper. *Anal. Chem.* 1975, 47, 2208-2213.
- [34] Moulder, J.F.; Stickle, W.F.; Sobol, P.E.; Bomben, K.D. *Handbook of X-ray Photoelectron Spectroscopy: A Reference Book of Standard Spectra for Identification and Interpretation of XPS Data.* Physical Electronics Division, Perkin-Elmer Corporation: Eden Prairie (MN), USA, 1992. ISBN-10: 096481241X
- [35] Zhidkov, I.S.; Belik, A.A.; Kukharensko, A.I.; Cholakh, S.O.; Taran, L.S.; Fujimori, A.; Streltsov, S.V.; Kurmaev, E. Z. Cu-Site Disorder in CuAl<sub>2</sub>O<sub>4</sub> as Studied by XPS Spectroscopy. *JETP Letters* 2021, 114, 556-560.
- [36] Monaco, L.; Sodhi, R.N.S.; Palumbo, G.; Erb, U. XPS study on the passivity of coarse-grained polycrystalline and electrodeposited nanocrystalline nickel-iron (NiFe) alloys. *Corrosion Science* 2020, 176, 108902.
- [37] Li, D.; Wang, L.; Koike, M.; Nakagawa, Y.; Tomishige K. Steam reforming of tar from pyrolysis of biomass over Ni/Mg/Al catalysts prepared from hydrotalcite-like precursors. *Appl. Catal. B: Environmental* 2011, 102, 528-538.
- [38] Yu, X.; Zhang, F.; Chu, W. Effect of a second metal (Co, Cu, Mn or Zr) on nickel catalysts derived from hydrotalcites for the carbon dioxide reforming of methane. *RSC Adv.* 2016, 6, 70537.
- [39] Gao, P.; Li, F.; Zhan, H.; Zhao, N.; Xiao, F.; Wei, W.; Zhong, L.; Wang, H.; Sun, Y. Influence of Zr on the performance of Cu/Zn/Al/Zr catalysts via hydrotalcite-like precursors for CO<sub>2</sub> hydrogenation to methanol. *J. Catal.* 2013, 298, 51-60.
- [40] Liu, C.; Guo, X.; Guo, Q.; Mao, D.; Yu, J.; Lu, G. Methanol synthesis from CO<sub>2</sub> hydrogenation over copper catalysts supported on MgO-modified TiO<sub>2</sub>. *J. Mol. Catal. A Chem.* 2016, 425, 86-93.

## Ni-Cu/Al<sub>2</sub>O<sub>3</sub> from Layered Double Hydroxides Hydrogenates Furfural to Alcohols

- [41] Abelló, S.; Verboekend, D.; Bridier, B.; Pérez-Ramírez, J. Activated takovite catalysts for partial hydrogenation of ethyne, propyne, and propadiene. *J. Catal.* 2008, 259, 85-95.
- [42] Puxley, D.C.; Kitchener, I.J.; Komodromos, D.; Parkyns, N.D. The Effect of Preparation Method upon the Structures, Stability and Metal/Support Interactions in Nickel/Alumina Catalysts. In *Studies in Surface Science and Catalysis*; Poncelet, G., Grange, P., Jacobs, P.A. Eds.; Elsevier: Amsterdam, The Netherlands, 1983; Volume 16, pp. 237-271.
- [43] Clause, O.; Coelho, M.G.; Gazzano, M.; Matteuzzi, D.; Trifirò, F.; Vaccari, A. Synthesis and thermal reactivity of nickel-containing anionic clays. *Appl. Clay Sci.* 1993, 8, 169-186.
- [44] Abelló, S.; Berruoco, C.; Gispert-Guirado, F.; Montané, D. Synthetic natural gas by direct CO<sub>2</sub> hydrogenation on activated takovites: effect of Ni/Al molar ratio. *Catal. Sci. Technol.* 2016, 6, 2305-2317.
- [45] Wang, Y.; Cui, Q.; Guan, Y.; Wu, P. Facile synthesis of furfuryl ethyl ether in high yield via the reductive etherification of furfural in ethanol over Pd/C under mild conditions. *Green Chem.* 2018, 20, 2110-2117.
- [46] Selishcheva S.A.; Smirnov A.A.; Fedorov A.V.; Bulavchenko O.A.; Saraev A.A.; Lebedev M.Y.; Yakovlev V.A. Highly Active CuFeAl-containing Catalysts for Selective Hydrogenation of Furfural to Furfuryl Alcohol. *Catalysts* 2019, 9, 816.
- [47] He, J.; Nielsen, M.R.; Hansen, T.W.; Yang, S.; Riisager, A. Hierarchically constructed NiO with improved performance for catalytic transfer hydrogenation of biomass-derived aldehydes. *Catal. Sci. Technol.* 2019, 9, 1289-1300.
- [48] Ramos, R.; Peixoto, A.F.; Arias-Serrano, B.I.; Soares, O.S.G.P.; Pereira, M.F.R.; Kubicka, D.; Freire, C. Catalytic Transfer Hydrogenation of Furfural over Co<sub>3</sub>O<sub>4</sub>-Al<sub>2</sub>O<sub>3</sub> Hydrotalcite-derived Catalyst. *ChemCatChem* 2020, 12, 1467-1475.
- [49] Jorge, E.Y.; Lima, T.D.M.; Lima, C.G.; Marchini, L.; Castelblanco, W.N.; Rivera, D.G.; Urquieta-Gonzalez, E.A.; Varma, R.S.; Paixão, M.W. Metal-exchanged magnetic  $\beta$ -zeolites: valorization of lignocellulosic biomass-derived compounds to platform chemicals. *Green Chem.* 2017, 19, 3856-3868.
- [50] d'Angelo J.V.H.; Francesconi, A.Z. Gas-Liquid Solubility of Hydrogen in *n*-Alcohols ( $1 \leq n \leq 4$ ) at Pressures from 3.6 MPa to 10 MPa and Temperatures from 298.15 K to 525.15 K. *J. Chem. Eng. Data* 2001, 46, 671-674.

## Ni-Cu/Al<sub>2</sub>O<sub>3</sub> from Layered Double Hydroxides Hydrogenates Furfural to Alcohols

## Ni-Cu/Al<sub>2</sub>O<sub>3</sub> from Layered Double Hydroxides Hydrogenates Furfural to Alcohols

# Chapter Four

---

## Furfural to diols over Ni-Co/Al catalysts

# Chapter 4: Furfural to diols over Ni-Co/Al catalysts

## 1. Introduction

Furfural is produced from the C-5 carbohydrate fraction of lignocellulosic biomass and constitutes one of the key platform chemicals in biorefinery [1-3]. Selective hydrogenation and hydrogenolysis of furfural give a variety of building blocks for the chemical industry and the synthesis of fuel additives [4, 5]. For instance, furfuryl alcohol (FA) is used in the production of thermostatic resins, tetrahydrofurfuryl alcohol (TFA) is a solvent used industrially [6], and pentanediols (PDs) are finding new applications. 1,2-pentanediol (12PD) can be used to synthesize polyesters, polyurethanes and polyamides, with applications in printing inks, cosmetics and pharmaceutical intermediates [7, 8]. 1,5-pentanediol (15PD) is as a monomer for polyesters and polyurethanes [9-12] and it can be esterified or etherified to produce liquid biofuels. For example, by combining 15PD with valeric acid – also a renewable molecule obtained by hydrogenation of levulinic acid – to form pentyl divalerate [3].

Numerous catalysts have been studied to produce diols from FF. Direct hydrogenolysis of FF to PDs remains a challenge due to the large number of competitive reactions that FF can suffer and, therefore, a two-step process is usually proposed. The first step involves the selective hydrogenation of FF to FA or TFA, which are then converted to PDs in the second reaction stage. To maximize the overall yield of the process, each stage should use tailored catalysts and optimized process conditions. Relevant works on the production of PDs from furfural are summarized in Table 4.1.

Furfural to diols over Ni-Co/Al catalysts

**Table 4.1.** Summary of relevant works on the conversion of FF to PDs.

Catalyst	Reactant and solvent	$p_{H_2}$ (MPa)	T (°C)	Time (h)	R/C ratio ( $\frac{g_{\text{reactant}}}{g_{\text{cat}}}$ )	Conversion (%)	Main product and (selectivity %)	Ref.
Rh–ReO <sub>x</sub> /SiO <sub>2</sub> (Re/Rh = 0.5)	TFA (5 wt.% in water)	8.0	120	4	20.0	56.9	15PD (94.2)	9
Rh–MoO <sub>x</sub> /SiO <sub>2</sub> (Mo/Rh = 0.13)	TFA (5 wt.% in water)	8.0	120	4	20.0	50.1	15PD (95.5)	10
Rh–ReO <sub>x</sub> /SiO <sub>2</sub> (Re/Rh = 0.5)	TFA (20 wt.% in water)	8.0	100	2	6.67	53.6	15PD (97.2)	12
Ir–ReO <sub>x</sub> /SiO <sub>2</sub> (Re/Ir = 2)	TFA (20 wt.% in water)	8.0	100	2	6.67	58.2	15PD (95.8)	12
Pd–Ir/SiO <sub>2</sub> (Pd/Ir = 1)	FF (5 wt.% in water)	8.0	2	6	3.20	>99	TFA (94.0)	13
Pd (0.66 wt.%) Ir–ReO <sub>x</sub> /SiO <sub>2</sub>	FF (10 wt.% in water)	6.0	40/120	2/24	10.0	>99.9	15PD (63.2)	14
Rh (0.66 wt.%) Ir–ReO <sub>x</sub> /SiO <sub>2</sub>	FF (10 wt.% in water)	6.0	40/100	8/24	10.0	>99.9	15PD (72.4)	15
Pt/HT (1.9 wt.%)	FF (0.33 mol/L in 2-propanol)	3.0	150	4	0.96	>99.9	12PD (73.0)	16
Cu <sub>1</sub> Ni <sub>1</sub> /MgAlO	FF (0.25 mol/L in methanol)	4.0	100	4	48.0	>99	FA (>99)	17
Cu <sub>1</sub> Ni <sub>1</sub> /MgAlO	FF (0.25 mol/L in ethanol)	4.0	150	3	9.61	>99	TFA (95)	17
CuMgAlO	FF (unspecified, alcohol)	6.0	150	6	n.a.	>84	12PD (46.4), 15PD (25.0)	18
Co/SBA-15 (10 wt.% Co)	FF (50 wt.% in ethanol)	2.0	150	2	2.0	90	FA (78)	19
Co/TiO <sub>2</sub> (5 wt.% Co)	FA (2 wt.% in water)	2.34	140	5.8	-	99.0	15PD (30.3), TFA (20.7)	20
CoAlO	FF (10 g/L in 2-propanol)	3.0	150	8	10.0	100	15PD (30), TFA (62.2)	21
CoMgAlO	FF (10 g/L in ethanol)	5.0	170	4	1.92	100	15PD (49), TFA (14)	22

Catalysts based on noble metal catalysts are more active and require milder process conditions than their non-noble metal counterparts. Nakagawa and coworkers [13] reported on a Pd–Ir/SiO<sub>2</sub> catalyst that achieved complete conversion of aqueous FF with a

## Furfural to diols over Ni-Co/Al catalysts

94% selectivity to TFA. Rh-ReO<sub>x</sub>/SiO<sub>2</sub> [9, 12], Ir-ReO<sub>x</sub>/SiO<sub>2</sub> [12] and Rh-MoO<sub>x</sub>/SiO<sub>2</sub> [10] demonstrated excellent selectivity at moderate conditions in the hydrogenolysis of TFA to 15PD using water as solvent. The conversion of TFA, however, had to be limited to ca. 50-60% to optimize the yield of 15PD and prevent its further hydrogenation to pentanol (PE), or even pentane. Catalysts based on Ir-ReO<sub>x</sub>/SiO<sub>2</sub> with 0.66% of added Pd [14] or Rh [15] achieved complete conversion of aqueous FF with a selectivity to 15PD of 63.2% and 72.4%, respectively. However, the reaction process consisted of two consecutive steps performed at low (40 °C) and high temperature (100 or 120 °C). In the first step, FF was hydrogenated to TFA, which was then transformed to 15PD during the second step. The total reaction time required to achieve those optimal values was close to 30 h. Concerning the production of 12PD, the processing of FF in 2-propanol with a catalyst based on platinum supported on hydrotalcite (Pt/HT) gave complete conversion with a selectivity of 73% in a single step of only 4 h [16].

Catalysts based on transition metals such as Cu, Ni and Co have been investigated for FF hydrogenation as well. A Cu-Ni/MgAlO catalyst with a Cu/Ni ratio of 1.0 was able to fully convert FF with a selectivity to FA above 99% when methanol was used as solvent. The same catalyst gave a selectivity of 95% to TFA when ethanol was used instead of methanol [17]. Production of PDs from FF was achieved in a single step on a CuMgAlO catalyst with an 84% conversion of FF and a total selectivity to PDs of 71.4% (46.4% 12PD and 25.0% 15PD) [18]. Similar results were reported with cobalt-based materials. A catalyst consisting of 10 wt.% of cobalt supported on mesoporous silica (Co/SBA-15) produced a 90% conversion of concentrated FF (50 wt.% in ethanol) and gave a 78% selectivity to FA with only 2 h of reaction at 150 °C and 2 MPa of H<sub>2</sub> [19], which are suitable conditions for industrial operation. On the contrary, 5% Co supported on TiO<sub>2</sub> provided complete conversion of aqueous FA at a GHSV of 5.8 h<sup>-1</sup> on a continuous packed bed reactor and gave 30.3% selectivity to 15PD and a 20.7% to TFA. Many unidentified byproducts were formed as well, which comprised ca. 24% of the carbon contained in the FA [20]. A CoAlO spinel achieved complete conversion of FF in 2-propanol with a selectivity to 15PD and TFA

## Furfural to diols over Ni-Co/Al catalysts

of 30 % and 62.2%, respectively [21]. Combination of Co and Mg in a CoMgAlO catalyst improved the basicity of the surface and promoted a stronger adsorption of C–O–C and C=C groups, which benefited the conversion of FA into diols [22].

Concerning Ni-Co bimetallic catalysts, Yao and coworkers [23] tested  $Ni_xCo_yAl$  mixed oxide catalysts derived from a hydrotalcite precursors in the conversion of 5-hydroxymethylfurfural (HMF) to 1,2,6-hexanetriol (126-HT). At optimal reaction conditions  $Ni_{0.5}Co_{2.5}Al$  gave total conversion of HMF and a yield of 126-HT of 64.5%. Furthermore, testing of  $Co_3Al$  or  $Ni_3Al$  at the same conditions for 4 h did not produce significant amounts of 126-HT;  $Co_3Al$  gave an 89.4% conversion and 83% selectivity to 2,5-dihydroxymethylfuran (25-DHF), while  $Ni_3Al$  achieved 95.4% conversion and an 80.1% selectivity to 2,5-tetrahydrofuran-dimethanol (THFDM). Nickel-cobalt bimetallic catalysts prepared from layered double hydroxides seem therefore to offer good potential for the hydrogenolysis of furfural. In this work we synthesized and characterized  $Ni_xCo_{(2-x)}Al$  catalysts with different Co/Ni atomic ratios. The effect of the addition of cobalt on the conversion of furfural and the selectivity to intermediate and final products has been assessed, and the existence of competing reaction pathways has been established.

## 2. Results and discussion

### 2.1. Catalyst characterization

The surface and bulk composition of the oxides obtained by calcination of the LDHs precursors was measured by FESEM-EDX and ICP-OES, respectively. The change in the composition of the three materials was demonstrated by ESEM-EDX imaging in Figure 4.1. The atomic Ni/Al ratio of  $Ni_2Al$  was 2.05 on the surface (EDX) and 1.83 of the total content of the catalyst (ICP), close to the intended value (Table 4.2).

Furfural to diols over Ni-Co/Al catalysts

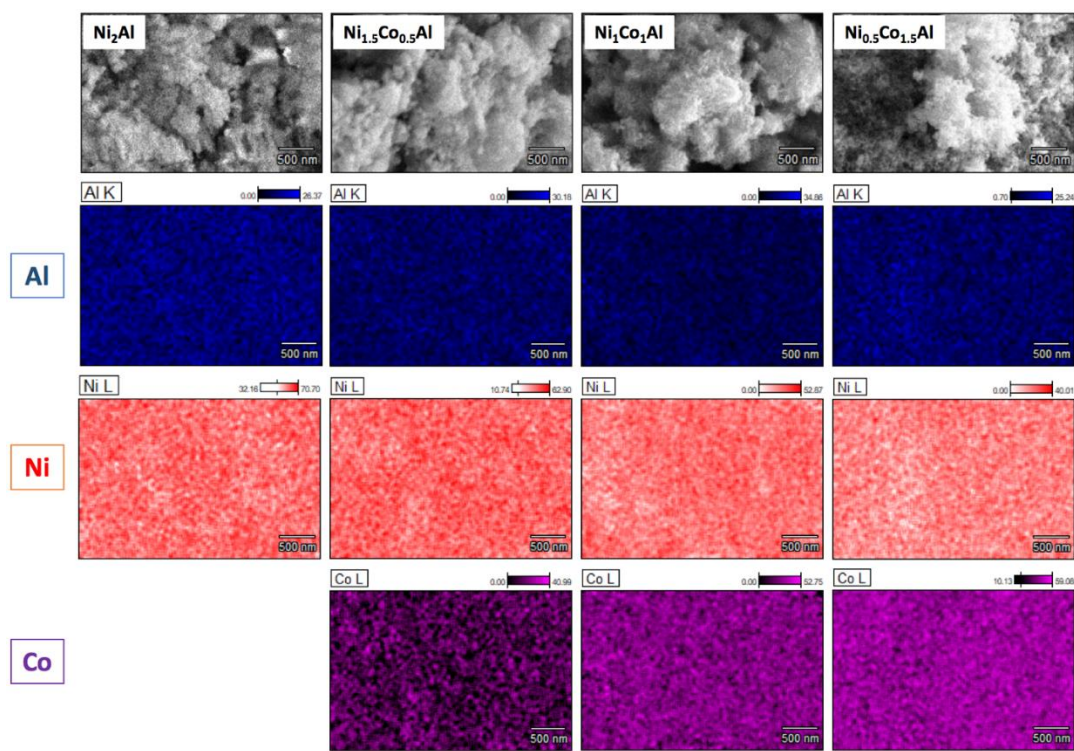


**Figure 4.1.** FESEM-EDX imaging of the LDH precursors calcined at 400 °C for 4h.

In the materials containing Co, the Ni/Al ratios measured by FESEM-EDX, were higher than the nominal values, especially in the case of Ni<sub>0.5</sub>Co<sub>1.5</sub>Al, whereas ICP-EOS gave values closer to the nominal. In contrast, the Co/Al ratios determined by both techniques were always close to those intended.

**Table 4.2.** Metal ratios in the calcined samples determined by FESEM-EDX and ICP-OES

Calcined Material	ICP-OES		FESEM-EDX	
	Ni/Al	Co/Al	Ni/Al	Co/Al
Ni <sub>2</sub> Al	1.83	-	2.05	-
Ni <sub>1.5</sub> Co <sub>0.5</sub> Al	1.32	0.48	1.86	0.42
Ni <sub>1</sub> Co <sub>1</sub> Al	1.05	1.06	1.33	1.09
Ni <sub>0.5</sub> Co <sub>1.5</sub> Al	0.48	1.40	0.99	1.56

## Furfural to diols over Ni-Co/Al catalysts

SEM imaging of the calcined materials (Figure 4.2) show a change in morphology with the amount of cobalt. Ni<sub>2</sub>Al had a granular structure that was also observed on Ni<sub>1.5</sub>Co<sub>0.5</sub>Al, but it changed to superficial flake-like aggregates in Ni<sub>1</sub>Co<sub>1</sub>Al and even more clearly in Ni<sub>0.5</sub>Co<sub>1.5</sub>Al.

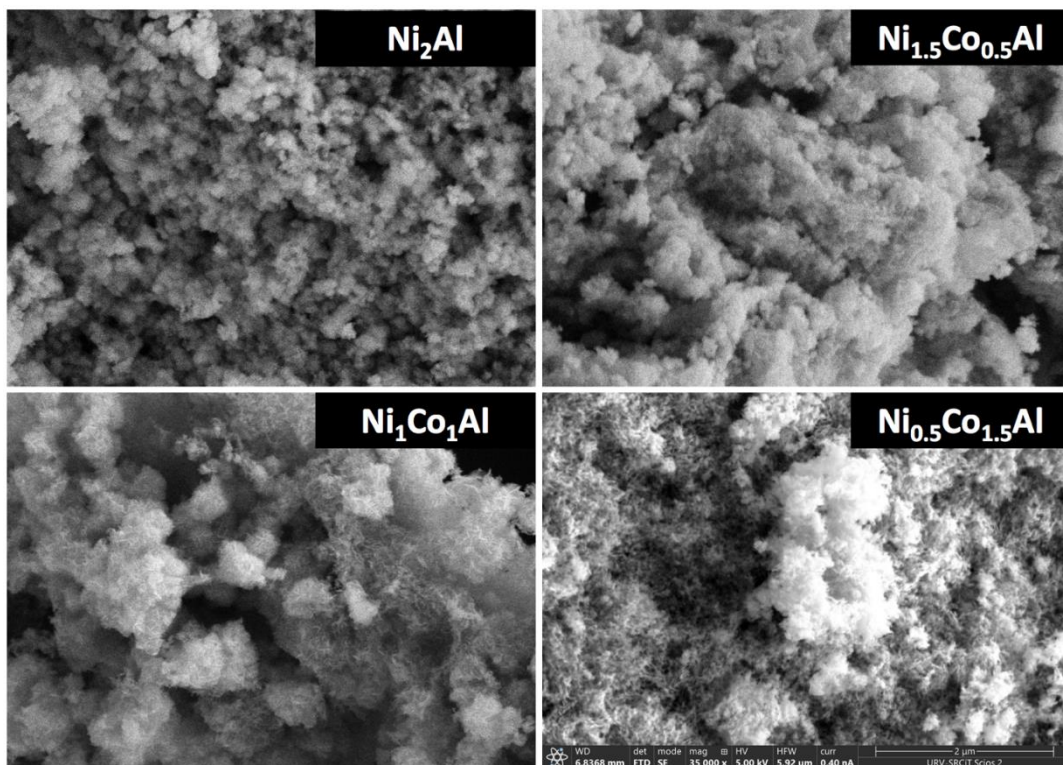


**Figure 4.2.** SEM imaging of the LDH precursors calcined at 400 °C for 4h (35 000 × magnification).

The N<sub>2</sub> physisorption isotherms (Figure 4.3) corresponded to mesoporous materials with type IV(a) isotherms and H2(b) hysteresis loops, according to the IUPAC classification [24, 25]. Surface areas and pore volumes (Table 4.3) and the surface and pore size distributions (Figure 4.4) were calculated with the BET and BJH models.

Furfural to diols over Ni-Co/Al catalysts

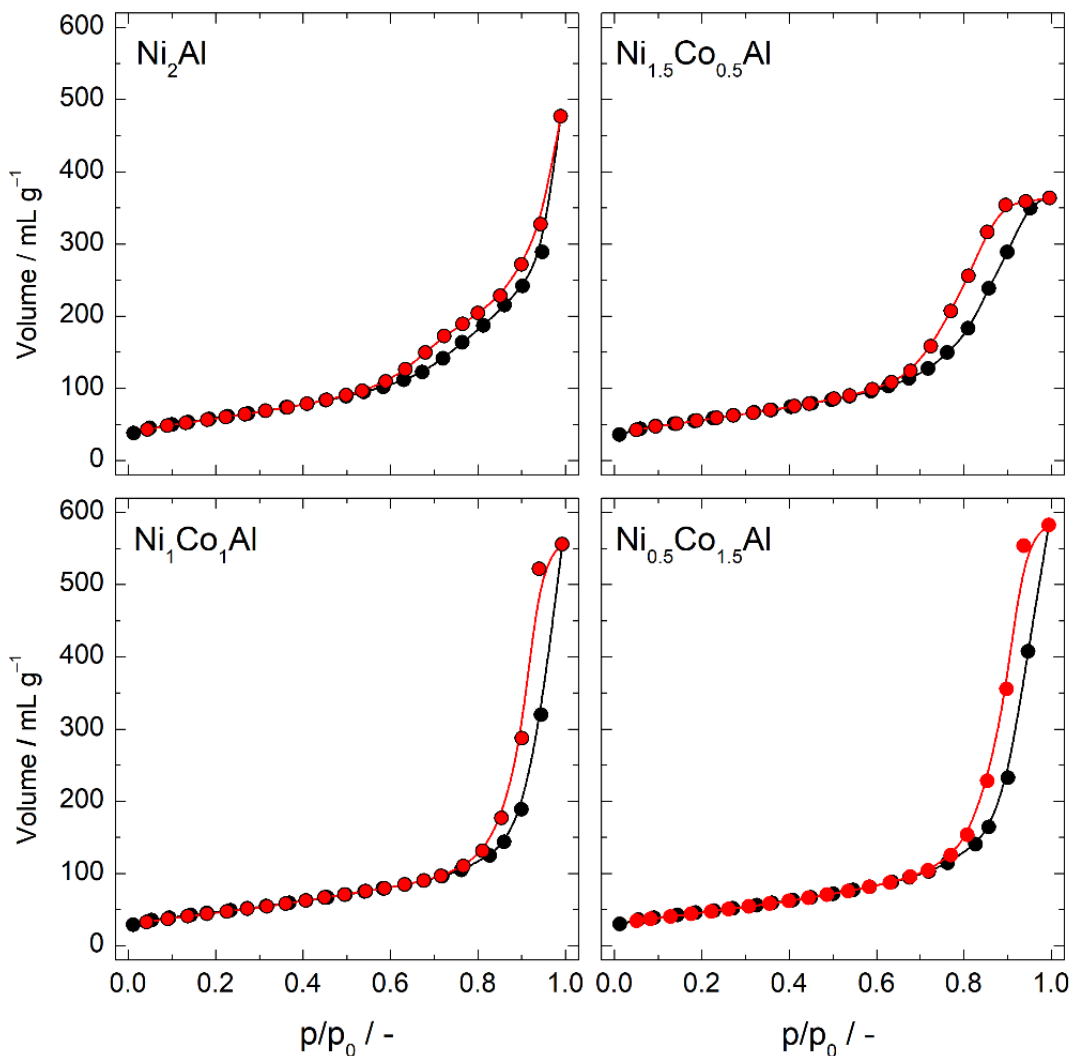


**Figure 4.3.** N<sub>2</sub> physisorption isotherms of the LDHs precursors calcined at 400 °C for 4h (Black line: adsorption branch; red line: desorption branch)

The presence of cobalt did not modify the surface area substantially in Ni<sub>1.5</sub>Co<sub>0.5</sub>Al (201 m<sup>2</sup>·g<sup>-1</sup>) when compared to Ni<sub>2</sub>Al (210 m<sup>2</sup>·g<sup>-1</sup>) but formed larger pores (8.5 nm vs. 6.2 nm in Ni<sub>2</sub>Al) with a lower total pore volume. A higher Co/Ni ratio had more impact on the textural properties. In Ni<sub>1</sub>Co<sub>1</sub>Al the surface area was lower (167 m<sup>2</sup>·g<sup>-1</sup>) and the average pore diameter and the pore volume were larger (28 nm and 0.86 mL·g<sup>-1</sup>, respectively) than in

Furfural to diols over Ni-Co/Al catalysts

Ni<sub>2</sub>Al and Ni<sub>1.5</sub>Co<sub>0.5</sub>Al. Further increasing the Co/Ni ratio in Ni<sub>0.5</sub>Co<sub>1.5</sub>Al resulted on a smaller average pore size (17 nm), no remarkable change was noticed on the surface area (168 m<sup>2</sup>·g<sup>-1</sup>), the shapes of the surface and pore size distributions were similar (Figure 4.3).

**Table 4.3.** Textural properties of the calcined samples determined from N<sub>2</sub> physisorption

Calcined Material	BET Surface Area (m <sup>2</sup> ·g <sup>-1</sup> )	Pore volume (mL·g <sup>-1</sup> )	Average pore diameter (nm)
Ni <sub>2</sub> Al	210	0.74	6.2
Ni <sub>1.5</sub> Co <sub>0.5</sub> Al	201	0.57	8.5
Ni <sub>1</sub> Co <sub>1</sub> Al	167	0.86	28
Ni <sub>0.5</sub> Co <sub>1.5</sub> Al	168	0.92	17

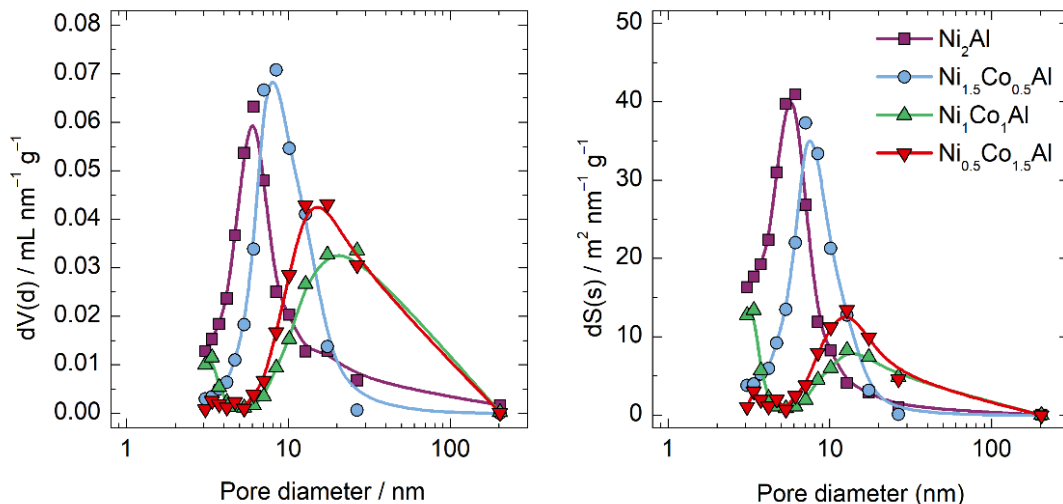


**Figure 4.4.** Pore volume (left) and surface (right) distributions of LDHs calcined at 400 °C for 4h, determined with the BJH model.

The X-ray diffractograms of the LDHs calcined at 400 °C for 4 h (Figure 4.5) presented very broad peaks produced by small crystallites, which made the elucidation of the structure

Furfural to diols over Ni-Co/Al catalysts

difficult. The phases detected were NiO, a spinel-type structure (A)[B]<sub>2</sub>O<sub>4</sub> (Fd3m) with the tetrahedral position (A) and the octahedral position [B] occupied by Ni, Co and Al, and a small fraction of Ni(OH)<sub>2</sub>NiOOH (Jamborite, ICSD entry 076650). The distribution of cations inside the spinel structure was adjusted manually in such a way that the following rules were fulfilled: i) minimum difference between the elemental composition of the sample measured by SEM and that calculated from the Rietveld analysis; ii) minimum electrical charge of the spinel structure-type calculated with the Bond Valence Theory [26]; iii) minimum R<sub>wp</sub> (conventional Rietveld agreement factor); and iv) complete occupation of the tetrahedral position (A) and the octahedral position [B] by the cations. A detailed quantification of the detected phases and their crystallite sizes is given in Table 4 of the supplementary material. Calcined Ni<sub>2</sub>Al was formed by equivalent amounts of NiO and spinel, and a small amount of Jamborite. Addition of Co promoted the formation of the spinel structure, suppressed Jamborite and decreased the amount of NiO, which accounted only for 3.4 wt.% in Ni<sub>0.5</sub>Co<sub>1.5</sub>Al. The spinel peaks shifted to higher 2θ angles (lower interplanar spacing) with the amount of Co, and the crystallite sizes were larger.

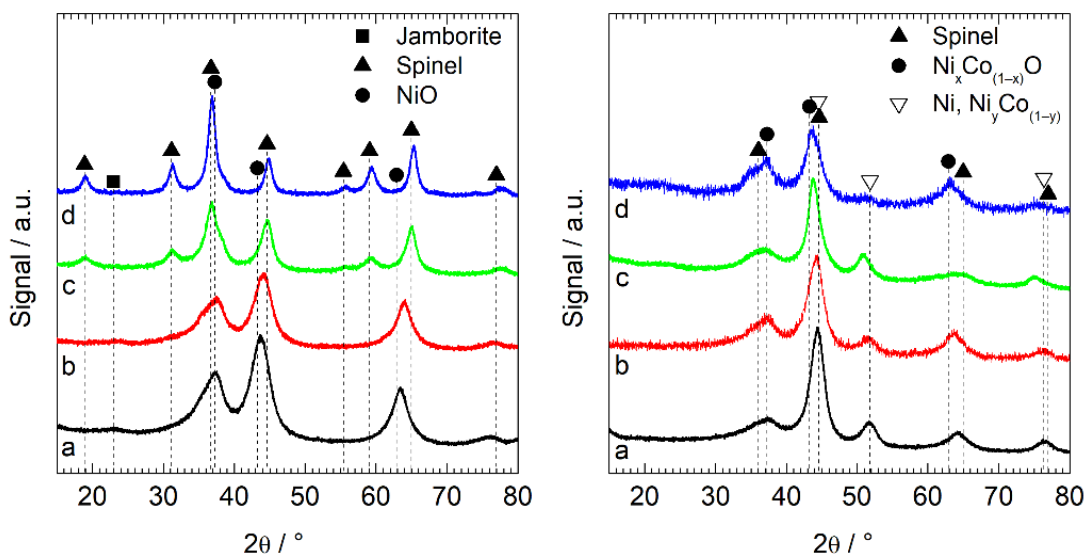


**Figure 4.5.** XRD patterns of the LDH precursors calcined at 400 °C for 4 h (left) and the catalysts reduced at 500 °C for 1 h (right) (a: Ni<sub>2</sub>Al; b: Ni<sub>1.5</sub>Co<sub>0.5</sub>Al; c: Ni<sub>1</sub>Co<sub>1</sub>Al; d: Ni<sub>0.5</sub>Co<sub>1.5</sub>Al)

## Furfural to diols over Ni-Co/Al catalysts

The signals of the X-ray diffractograms of the catalysts reduced at 500 °C for 1 h (Figure 4.5) were broader than those of the calcined samples, which made the interpretation of the diffraction patterns even more difficult. Besides the (A)[B]<sub>2</sub>O<sub>4</sub> spinel structure present in the calcined materials, Ni<sub>x</sub>Co<sub>(1-x)</sub> alloys (Fd3m) and Ni<sub>x</sub>Co<sub>(1-x)</sub>O mixed oxides (Fm-3m) were formed. The composition of the Ni<sub>x</sub>Co<sub>(1-x)</sub>O oxides was estimated from the refined cell parameter applying the empirical Vegard law [27], taking as extreme values the cell parameters of NiO (a = 4.1771Å, ICDD card 47-1049) and CoO (a = 4.26120Å, ICDD card 48-1719). We chose this method to estimate the composition because it was not possible to refine the substitution Ni ↔ Co in the structure by X-ray diffraction due to the similar X-ray scattering power of these atoms. The samples with more Co displayed a shoulder at 2θ ≈ 34.5° that coincided with the most intense peak of the spinel. This shoulder was less evident at lower Co contents but always the (111) peak of Ni<sub>x</sub>Co<sub>(1-x)</sub>O presented an asymmetry at lower angles that could only be explained by the presence of the spinel. The Ni<sub>2</sub>Al-R catalyst had a 29 wt.% of reduced nickel and a 35 wt.% of NiO forming highly dispersed crystallites of 3.4 and 1.8 nm, respectively (Table 4.4). The spinel-type phase was 35 wt.% and had a Ni/Al ratio significantly lower than that of the unreduced material. Ni<sub>1.5</sub>Co<sub>0.5</sub>Al-R contained a 17 wt.% of metallic nickel, a 52 wt.% of Ni<sub>0.66</sub>Co<sub>0.44</sub>O and a 30 wt.% of spinel, although the latter consisted only of Al and Ni. The Ni<sub>1</sub>Co<sub>1</sub>Al-R catalyst had a 29 wt.% of reduced Ni<sub>0.2</sub>Co<sub>0.8</sub> alloy forming 3.7 nm crystallites, together with a 34 wt.% of NiO and a 33 wt.% of spinel. The latter also had lower Co/Al and Ni/Al ratios than the unreduced material. In contrast, Ni<sub>0.5</sub>Co<sub>1.5</sub>Al-R had only a 3 wt.% of Ni<sub>0.7</sub>Co<sub>0.3</sub> alloy, a 46 wt.% of Ni<sub>0.5</sub>Co<sub>0.5</sub>O and a 42 wt.% of spinel phase that was enriched in Al as in the other catalysts (Table 4.4).

Furfural to diols over Ni-Co/Al catalysts

**Table 4.4.** Phase composition and average crystallite sizes of the calcined LDHs precursors and the reduced catalysts.

	Elemental composition (SEM, wt.%)			Calculated composition (DRX, wt.%)			Phases		
	Al	Co	Ni	Al	Co	Ni	Identified	wt.%	Crystal lite size (nm)
Ni <sub>2</sub> Al	12.4	-	55.3	13.6	-	57.6	(Al <sub>0.85</sub> Ni <sub>0.15</sub> )[Al <sub>0.55</sub> Ni <sub>0.45</sub> ] <sub>2</sub> O <sub>4</sub>	46.1	1.32
							NiO	48.6	2.24
							Jamborite	5.3	2.2
Ni <sub>1.5</sub> Co <sub>0.5</sub> Al	11.5	10.5	46.5	12.1	12.0	47.8	(Co <sub>0.25</sub> Al <sub>0.75</sub> )[Co <sub>0.25</sub> Al <sub>0.45</sub> Ni <sub>0.30</sub> ] <sub>2</sub> O <sub>4</sub>	51.2	1.35
							NiO	47.4	2.34
							Jamborite	1.4	6.0
Ni <sub>1</sub> Co <sub>2</sub> Al	11.0	26.2	31.9	12.2	27.1	32.4	(Co <sub>0.25</sub> Al <sub>0.50</sub> Ni <sub>0.25</sub> )[Co <sub>0.53</sub> Al <sub>0.37</sub> Ni <sub>0.10</sub> ] <sub>2</sub> O <sub>4</sub>	72.3	3.07
							NiO	27.6	3.3
Ni <sub>0.5</sub> Co <sub>1.5</sub> Al	10.7	36.6	23.2	10.5	36.6	23.2	(Co <sub>0.35</sub> Al <sub>0.30</sub> Ni <sub>0.35</sub> )[Co <sub>0.51</sub> Al <sub>0.28</sub> Ni <sub>0.21</sub> ] <sub>2</sub> O <sub>4</sub>	96.6	4.99
							NiO	3.4	9.0
Ni <sub>2</sub> Al-R	12.4	-	55.3	18.3	-	59.0	(Al <sub>0.90</sub> Ni <sub>0.10</sub> )[Al <sub>0.99</sub> Ni <sub>0.01</sub> ] <sub>2</sub> O <sub>4</sub>	35	1.27
							NiO	35	1.8
							Ni	29	3.36
Ni <sub>1.5</sub> Co <sub>0.5</sub> Al-R	11.5	10.5	46.5	10.4	14.9	53.1	(Al <sub>0.80</sub> Ni <sub>0.20</sub> )[Al <sub>0.80</sub> Ni <sub>0.20</sub> ] <sub>2</sub> O <sub>4</sub>	30	1.27
							Ni <sub>0.66</sub> Co <sub>0.44</sub> O	52	1.9
							Ni	17	3.6
Ni <sub>1</sub> Co <sub>2</sub> Al-R	11.3	26.2	31.9	13.9	24.0	40.0	(Co <sub>0.10</sub> Al <sub>0.90</sub> )[Al <sub>0.80</sub> Ni <sub>0.20</sub> ] <sub>2</sub> O <sub>4</sub>	33	1.27
							NiO	34	1.4
							Ni <sub>0.2</sub> Co <sub>0.8</sub>	29	3.7
							Jamborite	3.0	2.2
Ni <sub>0.5</sub> Co <sub>1.5</sub> Al-R	10.7	36.6	23.2	11.2	35.8	25.0	(Co <sub>0.30</sub> Al <sub>0.70</sub> )[Co <sub>0.45</sub> Al <sub>0.55</sub> ] <sub>2</sub> O <sub>4</sub>	42	1.27
							Ni <sub>0.5</sub> Co <sub>0.5</sub> O	46	1.9
							Ni <sub>0.7</sub> Co <sub>0.3</sub>	3.0	3.7
							Jamborite	7.5	2.2

Furfural to diols over Ni-Co/Al catalysts

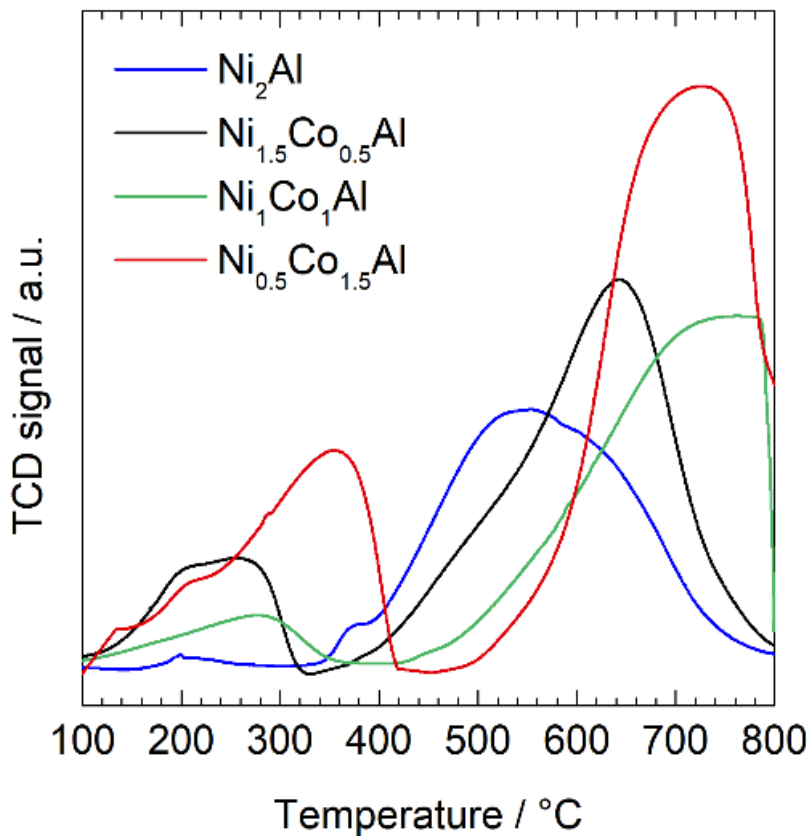


Figure 4.6. H<sub>2</sub>-TPR of LDH precursors calcined at 400 °C for 4h

The reducibility of the calcined materials was studied by temperature-programmed reduction (H<sub>2</sub>-TPR) between 100 and 800 °C under 10% hydrogen in argon. Ni<sub>2</sub>Al had a small shoulder at 380 °C and a larger peak at 554 °C (Figure 4.6). The first was consistent with the reduction of a small fraction of NiO that had little interaction with the spinel, while the second corresponded to nickel oxide that had stronger interaction and the transformation of the spinel structure itself [28-30]. Addition of Co caused the formation of two broad peaks that were displaced to higher temperature with the Co/Ni ratio of the sample. The peak in the low temperature range (200 to 400 °C) resulted from the reduction of Co<sup>3+</sup> to Co<sup>2+</sup> and the transformation of the spinel structure, while the peak in the high temperature range (500 to 800 °C) corresponded to the reduction of mixed nickel and cobalt oxides to

## Furfural to diols over Ni-Co/Al catalysts

form NiCo alloys dispersed on the aluminum-enriched spinel. Specific hydrogen consumption increased with the Co/Ni ratio, but reduction temperature shifted to higher values (Table 4.5).

**Table 4.5.** TPR of the LDH precursors calcined at 400 °C for 4h. Peaks detected and specific hydrogen consumption

Calcined Material	Peak 1		Peak 2		Total
	T (°C)	H <sub>2</sub> , mL·g <sup>-1</sup> (STP)	T (°C)	H <sub>2</sub> , mL·g <sup>-1</sup> (STP)	H <sub>2</sub> , mL·g <sup>-1</sup> (STP)
Ni <sub>2</sub> Al	388	3.4	554	136	139
Ni <sub>1.5</sub> Co <sub>0.5</sub> Al	254	35	643	168	203
Ni <sub>1</sub> Co <sub>1</sub> Al	276	17	762	219	236
Ni <sub>0.5</sub> Co <sub>1.5</sub> Al	354	90	726	246	336

The acidity of the catalysts was determined by temperature programmed desorption of ammonia (Figure 4.7). The desorption peaks of all the materials had broad temperature ranges, implying wide distributions in the strength of the acid sites. Multiple overlapped peaks were apparent in Ni<sub>2</sub>Al-R below 350 °C resulting from the desorption of ammonia from weak and moderate strength sites, together with a peak of strong acidic sites at ca. 600 °C. The presence of Co on Ni<sub>1.5</sub>Co<sub>0.5</sub>Al-R increased the area of the low temperature peaks pointing to an increase in weak acidity sites. Co on Ni<sub>1</sub>Co<sub>1</sub>Al-R promoted a new maximum at 120 °C associated to weak sites and increased the area of the high temperature peak, pointing to an increase on the concentration of strong sites. Finally, adding more Co on Ni<sub>0.5</sub>Co<sub>1.5</sub>Al-R tended to reduce the acidity of the material since the area of the peaks was lower, especially in strong acidity region.

Furfural to diols over Ni-Co/Al catalysts

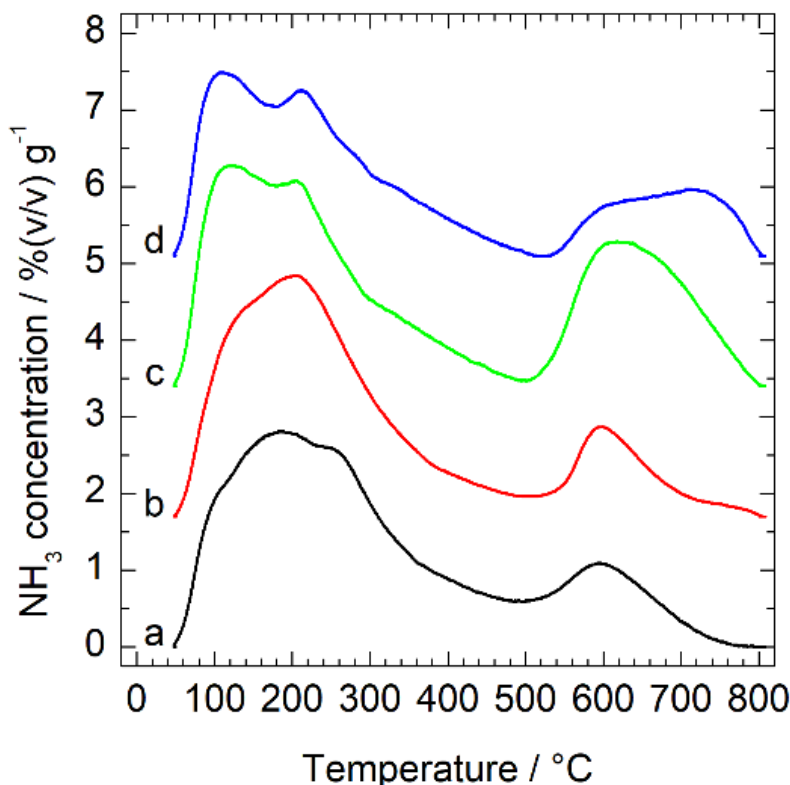


**Figure 4.7.** Temperature programmed desorption of ammonia (TPD-NH<sub>3</sub>): ammonia concentration normalized to the amount of catalyst vs. the desorption temperature (a: Ni<sub>2</sub>Al-R; b: Ni<sub>1.5</sub>Co<sub>0.5</sub>Al-R; c: Ni<sub>1</sub>Co<sub>1</sub>Al-R; d: Ni<sub>0.5</sub>Co<sub>1.5</sub>Al-R).

Signal deconvolution (Figure 4.8) was used to quantify the amounts of weak ( $\alpha$ ,  $T_d < 220$  °C), intermediate ( $\beta$ ,  $220$  °C  $< T_d < 500$  °C) and strong ( $\gamma$ ,  $T_d > 500$  °C) sites and the total acidity of the catalysts (Table 4.6). Overall, the addition of cobalt increased the amount of  $\alpha$  sites from  $0.34$  mmol NH<sub>3</sub> g<sup>-1</sup> in Ni<sub>2</sub>Al-R to ca.  $0.60$  mmol NH<sub>3</sub> g<sup>-1</sup> in Ni<sub>1.5</sub>Co<sub>0.5</sub>Al-R and Ni<sub>1</sub>Co<sub>1</sub>Al-R, and decreased to  $0.54$  mmol NH<sub>3</sub> g<sup>-1</sup> in Ni<sub>0.5</sub>Co<sub>1.5</sub>Al-R. The amount of  $\beta$  sites diminished with the content of Co in the catalyst, from  $0.66$  to  $0.20$  mmol NH<sub>3</sub> g<sup>-1</sup> in Ni<sub>2</sub>Al-R and Ni<sub>0.5</sub>Co<sub>1.5</sub>Al-R, respectively. Finally, the presence of  $\gamma$  sites was close to  $0.20$  mmol NH<sub>3</sub> g<sup>-1</sup> for all the materials except for Ni<sub>1</sub>Co<sub>1</sub>Al-R, which had  $0.43$  mmol NH<sub>3</sub> g<sup>-1</sup>. The total acidity of the catalysts was high, from  $0.96$  mmol NH<sub>3</sub> g<sup>-1</sup> in Ni<sub>0.5</sub>Co<sub>1.5</sub>Al-R to  $1.3$  in Ni<sub>1</sub>Co<sub>1</sub>Al-R.

Furfural to diols over Ni-Co/Al catalysts

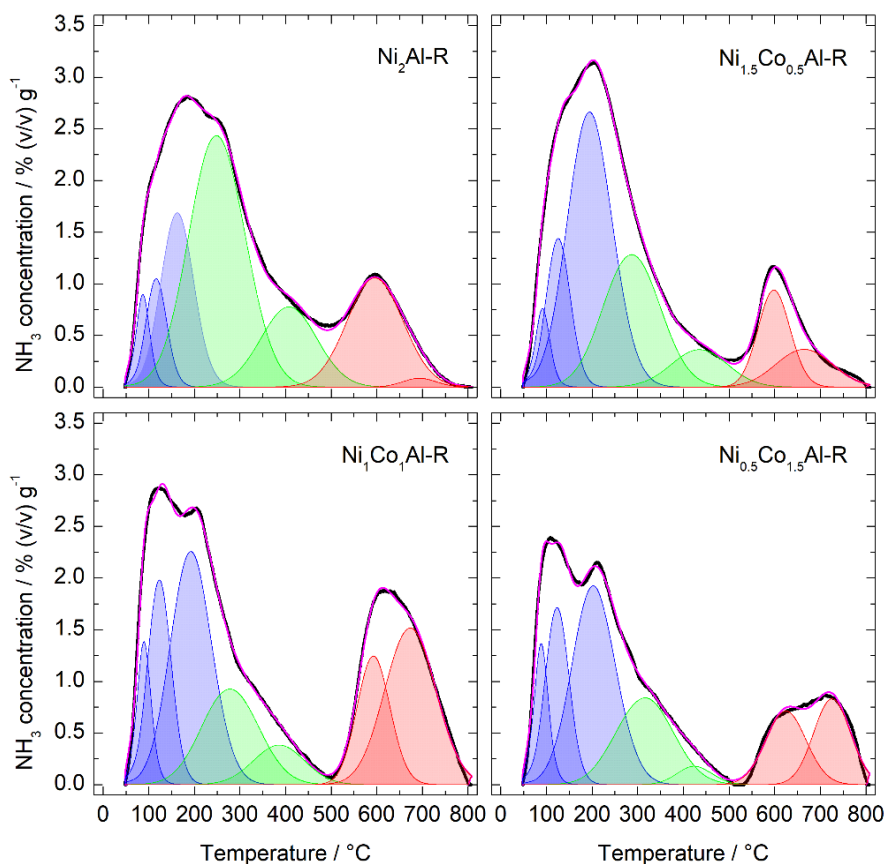


**Figure 4.8.** Temperature programmed desorption of ammonia (TPD-NH<sub>3</sub>): deconvolution of the ammonia concentration normalized to the amount of catalyst vs. the desorption temperature (Blue peaks: α-weak sites; Green peaks: β-intermediate strength sites; Red peaks: γ-strong sites. Blue line: recorded signal; Cyan line: deconvoluted signal).

**Table 4.6.** total concentration of acidic sites and estimation of weak, intermediate, and strong acidic sites based on signal deconvolution by TPD-NH<sub>3</sub>.

Catalyst	Concentration of acidic sites (mmol NH <sub>3</sub> g <sup>-1</sup> )			Total
	Weak (α) T <sub>d</sub> < 220 °C	Intermediate (β) 220 °C < T <sub>d</sub> < 500 °C	Strong (γ) T <sub>d</sub> > 500 °C	
Ni <sub>2</sub> Al-R	0.34	0.66	0.23	1.2
Ni <sub>1.5</sub> Co <sub>0.5</sub> Al-R	0.62	0.34	0.19	1.2
Ni <sub>1</sub> Co <sub>1</sub> Al-R	0.60	0.26	0.43	1.3
Ni <sub>0.5</sub> Co <sub>1.5</sub> Al-R	0.54	0.20	0.22	0.96

Furfural to diols over Ni-Co/Al catalysts

2.2. Catalytic activity tests

The effect of reaction time on the FF hydrogenation activity was evaluated on the Ni<sub>1</sub>Co<sub>1</sub>Al-R catalyst at 190 °C and 5.0 MPa of H<sub>2</sub> for up to 8 h. Conversion of furfural was already higher than 99.5% after only one hour of reaction and a wide variety of products were formed (Figure 4.9). Three primary products that reached their maximum selectivity after 1 h of reaction were identified: furfuryl alcohol (FA, 25.7%), 2-furaldehyde diethyl acetal (FDA, 31.0%) and di-furfuryl ether (DFE, 9.4%).

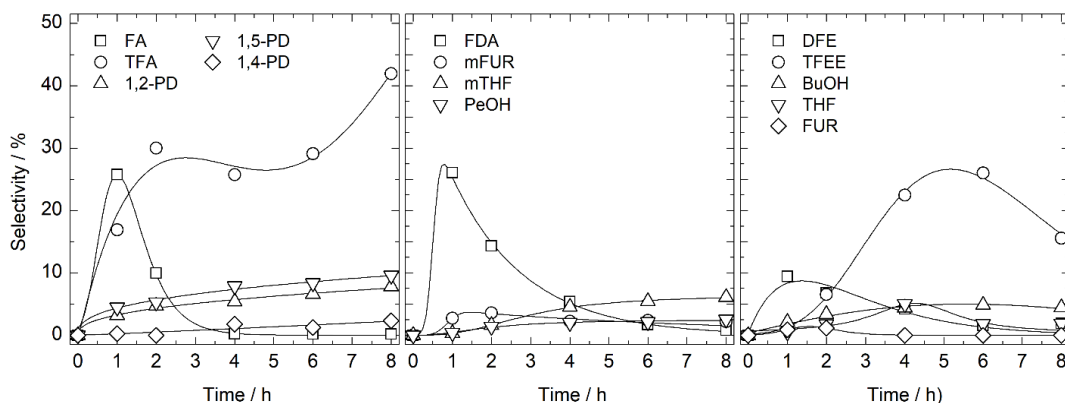


Figure 4.9. Product selectivity of furfural hydrogenolysis on the Ni<sub>1</sub>Co<sub>1</sub>Al-R catalyst at at 190 °C, 5.0 MPa H<sub>2</sub>. Furfural conversion was >99.5% after 1 h.

FA was formed by the hydrogenation of the aldehyde group of FF, which was subsequently converted to tetrahydrofurfuryl alcohol (TFA) by hydrogenation of the double bonds in the furan ring. The selectivity to TFA was 17% after 1 h. Hydrogenolysis of FA, and eventually of TFA, opened the furan rings to form pentanediols as schematized in the reaction pathway shown in Scheme 4.1. A 4.5% selectivity to 1,5-pentanediol (15PD) and a 3.2% to 1,2-pentanediol (12PD) were obtained after 1 h, together with trace amounts of 1,4-pentanediol (14PD). Extending the reaction time caused the selectivity to FA to decrease and only trace amounts of this product could be detected after 6 h. Selectivity to TFA was nearly constant at ca. 29% from 2 to 6 h but grew to 42% after 8 h. This was due to the

## Furfural to diols over Ni-Co/Al catalysts

formation of additional TFA by the hydrogenolysis of FDA, as explained below. Selectivity to pentanediols increased steadily as reaction time was extended. After 8 h it reached 9.6%, 7.8% and 2.3% for 15PD, 12PD and 14PD, respectively, thus reaching a combined selectivity to pentanediols of ca. 20%.

The reversible nucleophilic addition of ethanol or FA with FF on the acidic sites of the catalyst produced FDA and DFE, a conversion pathway that has been reported during FF hydrogenation. TPD-NH<sub>3</sub> results showed that all catalysts have a significant amount of acidic sites which is one of the factors causing this reversible nucleophilic addition, among others. The formation of FDA from FF and ethanol on a Pd/C catalyst under mild hydrogenation conditions was identified as the key intermediate step in the production of furfuryl ethyl ether (FEE) and TFE [31]. The formation of 2-(diisopropoxymethyl) furan – the analogous to FDA resulting from acetylation of FF with 2-propanol – was reported on Pt/Al<sub>2</sub>O<sub>3</sub> [32], NiO [33], NiO-Al<sub>2</sub>O<sub>3</sub> and ZnAl<sub>2</sub>O<sub>4</sub>-Al<sub>2</sub>O<sub>3</sub> [34], and on Pd-exchanged  $\beta$ -zeolite catalysts [35] during the catalytic transfer hydrogenation of FF with 2-propanol. Recently, FDA and DFE were also observed during the hydrogenation of FF in ethanol solution with NiCuAl catalysts [36]. On the Ni<sub>1</sub>Co<sub>1</sub>Al-R catalyst, FDA reached its maximum selectivity at 1 h and decreased afterwards (Figure 4.9). Hydrogenolysis of FDA led to the formation of tetrahydrofurfuryl ethyl ether (TFEE) which reached a maximum selectivity of 26% after 6 h and started to decrease afterwards due to its subsequent conversion to TFA. A similar trend was observed for DFE, whose selectivity started to decrease after reaching a maximum at 1 h. The intermediate compounds ethoxy(furan-2-yl)methanol (EFm) and 2((ethoxy(furan-2-yl)methoxy)methyl)furan (FEFA) could not be identified in the reaction mixture, which suggest that they were rapidly converted to FDA and DFE. In addition, hydrogenolysis of DBE should lead to the formation of furfuryl-tetrahydrofurfuryl ether and ditetrahydrofurfuryl ether (not shown in Scheme 4.1), but those compounds could not be identified in our samples. Subsequent hydrogenolysis of DBE should form 2-methyl tetrahydrofurane (mTHF) and additional TFA, as shown in Scheme 4.1.

## Furfural to diols over Ni-Co/Al catalysts

Hydrogenation of the alcohol group in FA led to 2-methylfuran (mFUR) which was subsequently converted to mTHF and PE. FA was completely consumed after 4 h thus preventing the formation of additional mFUR by this route. From 4 to 8 h the selectivity of mFUR decreased while that of PE increased in an equivalent extent, but the selectivity to mTHF grew continuously until it doubled that of PE. This was consistent with mTHF being also formed by the hydrogenolysis of DFE. Minor amounts of furan (FUR) were detected up to 2 h of reaction, which could be formed by decarbonylation of furfural or the hydrogenolysis of FA. FUR was further converted to BU as main product – 4.5% selectivity at 8 h – and hydrogenated to tetrahydrofuran (THF) as byproduct (1.9% selectivity at 8 h).

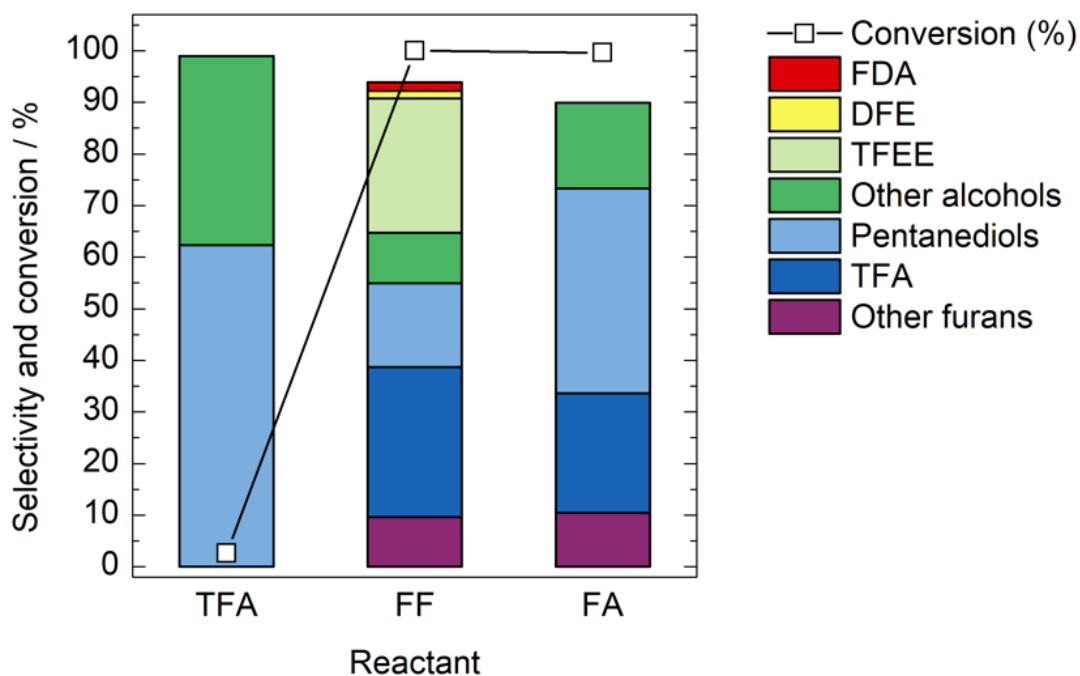


**Figure 4.10.** Conversion and product selectivity of furfural (FF), furfuryl alcohol (FA) and tetrahydrofurfuryl alcohol (TFA) hydrogenolysis on the Ni<sub>1</sub>Co<sub>1</sub>Al-R catalyst at 190 °C, 5.0 MPa H<sub>2</sub> and 6 h.

## Furfural to diols over Ni-Co/Al catalysts

It was worth mentioning that the relatively fast grow in the selectivity to TFA after 6 h at the expense of FDA consumption was not accompanied by a similar rise in the selectivity towards pentanediols, which posed the question whether the Ni<sub>1</sub>Co<sub>1</sub>Al-R catalyst was able to open the saturated ring in furans such as TFA, mTHF or THF. To address this issue, additional experiments were conducted with the Ni<sub>1</sub>Co<sub>1</sub>Al-R catalyst at the same conditions of temperature and pressure (190 °C and 5.0 MPa of H<sub>2</sub>) for 6 hours but using FA or TFA at 5 wt.% concentration in ethanol as reactant. Conversion barely reached 2.6% when TFA was used (Figure 4.10). The only quantifiable products derived from TFA were pentanediols, with a total selectivity of 62.3%, and a 36.7% of other alcohols (mainly propanediol). This shows that the catalyst had little activity towards the opening of the saturated furan rings. Concerning FA, conversion was higher than 99.5% and it produced pentanediols (39.7%), TFA (23.2%), other alcohols (16.7%) – basically BU (7.5%) and PE (4.9%) – and other furans, which were mFUR (2.5%), mTHF (7.5%) and trace amounts of FUR and THF. With FA, the selectivity to pentanediols was almost twice the selectivity to TFA, whereas it was the opposite when FF was used as feed. This supports the existence of a competing path towards TFA formation through the DFE and FDA in the case of furfural. In fact, FDA and DFE were not formed from FA or TFA, which confirms that they evolve from FF through its nucleophilic addition with ethanol and FA. In addition, TFEE was not detected in either case, which confirms that it evolves from the hydrogenolysis of FDA.

Furfural to diols over Ni-Co/Al catalysts

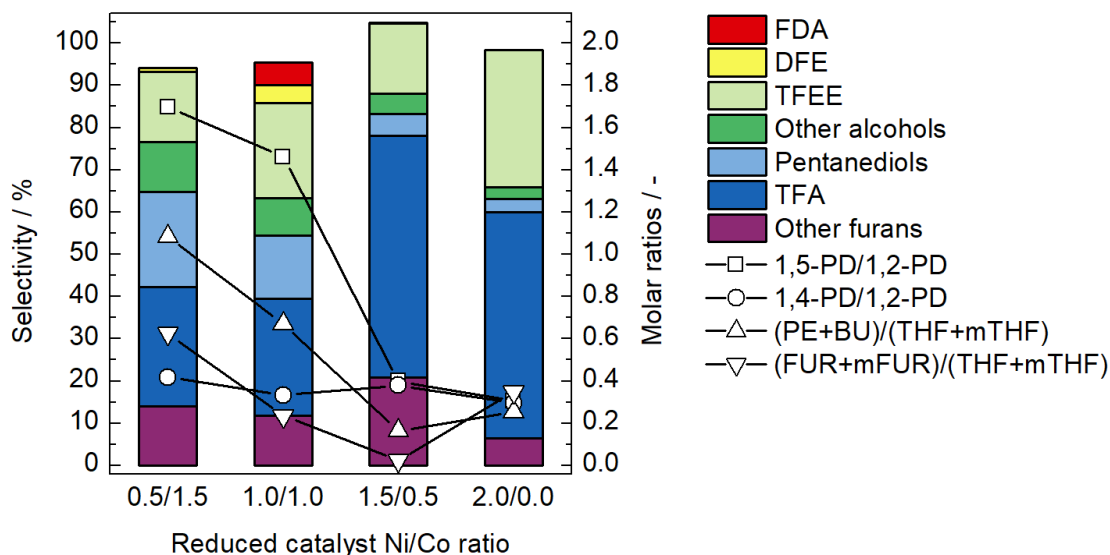


**Figure 4.11.** Product selectivity during furfural hydrogenolysis on the four catalysts at 190 °C, 5.0 MPa H<sub>2</sub> and 4 h. Furfural conversion was always higher than 99.5%.

The Co/Ni ratio of the catalyst had a strong influence on selectivity (Figure 4.11). Furfural conversion after 4 h at 190 °C and 5.0 MPa of H<sub>2</sub> was always higher than 99.5%. The Ni<sub>2</sub>Al-R and Ni<sub>1.5</sub>Co<sub>0.5</sub>Al-R catalysts had the lowest capacity to activate ring-opening hydrogenolysis reactions when compared to the catalysts having a higher Co/Ni ratio but exhibited good activity for the saturation of the furan ring. In Ni<sub>2</sub>Al-R, TFA was the main product (53.5%), followed by a 32.3% of TFEE. Selectivity to pentanediols was only 3.1%. Ni<sub>1.5</sub>Co<sub>0.5</sub>Al-R gave similar results. TFA was again the main product with a selectivity of 57.2%, together with a 16.5% of TFEE, 14.2% of mTHF and 6.3% THF, while the combined selectivity to pentanediols and to other alcohols were only 5.1% and 4.8%, respectively. Small amounts of FDA (<0.3%) and DBE (<0.1%) were observed, thus supporting the reaction pathway proposed for the formation of TFEE. The Ni<sub>0.5</sub>Co<sub>1.5</sub>Al-R catalyst had the highest capacity for the formation of pentanediols (22.4% combined selectivity) and other alcohols (12%), but TFA was still the most abundant product with a 28.3% selectivity, virtually identical to that on Ni<sub>1</sub>Co<sub>1</sub>Al-R. Compared to the latter catalyst, the selectivity to TFEE on Ni<sub>0.5</sub>Co<sub>1.5</sub>Al-R was lower (16.5%), and that to the combined amounts of other furans



### 3. Conclusions

The effect of the Co/Ni atomic ratio on the selectivity of  $\text{Ni}_x\text{Co}_{(2-x)}\text{Al}$  catalysts during the liquid-phase hydrogenolysis of furfural in ethanol has been studied at 190 °C and 5.0 MPa of  $\text{H}_2$ . Two competing pathways were inferred. The first involved the hydrogenation of FF to FA and its subsequent conversion by hydrogenolysis to pentanediols and by hydrogenation to TFA. The second pathway took place by nucleophilic addition on the acidic sites of the catalyst surface; FF reacted with ethanol to form FDA, and with FA to produce DFE. Hydrogenolysis of the addition products lead to TFEE and TFA in the first case, and to TFA and mTHF in the second. Additional experiments with TFA and FA as feedstocks instead of FF revealed that the primary products of nucleophilic addition were not formed when FF was not present. Also, TFA was not converted substantially, thus showing that the  $\text{Ni}_x\text{Co}_{(2-x)}\text{Al}$  catalysts had little capacity to open the saturated furan rings in TFA, THF and mTHF. The presence of  $\text{Ni}_x\text{Co}_y$  metal alloys on the reduced catalysts seems to promote ring-opening reactions of the unsaturated furans over ring hydrogenation, thus favoring the production of alcohols and diols.

## Furfural to diols over Ni-Co/Al catalysts

# 4. References

- [1] Werpy, T.; Petersen, G.; Aden, A.; Bozell, J.; Holladay, J.; White, J.; Manheim, A.; Eliot, D.; Lasure, L.; Jones, S; Top Value Added Chemicals from Biomass, Vol. 1: Results of Screening for Potential Candidates from Sugars and Synthesis Gas; U.S. Department of Energy: Washington, DC, 2004.
- [2] Bozell, J. J.; Petersen, G. R. Technology development for the production of biobased products from biorefinery carbohydrates - the US Department of Energy's "Top 10" revisited. *Green Chem.* 2010, 12, 539–554.
- [3] Mariscal, R.; Maireles-Torres, P.; Ojeda, M.; Sábada, I.; López-Granados, M. Furfural: a renewable and versatile platform molecule for the synthesis of chemicals and fuels. *Energy Environ Sci.* 2016, 9, 1144–1189.
- [4] Nakagawa, Y.; Tamura, M.; Tomishige, K. Catalytic Reduction of Biomass-Derived Furanic Compounds with Hydrogen. *ACS Catal.* 2013, 3, 2655–2668.
- [5] Chen, S.; Wojcieszak, R.; Dumeignil, F.; Marceau, E.; Royer, S. How Catalysts and Experimental Conditions Determine the Selective Hydroconversion of Furfural and 5-Hydroxymethylfurfural. *Chem. Rev.* 2018, 118, 11023–11117.
- [6] Li, X.; Jia, P.; Wang, T. Furfural: A Promising Platform Compound for Sustainable Production of C4 and C5 Chemicals. *ACS Catal.* 2016, 6, 7621–7640.
- [7] Xu, W.; Wang, H.; Liu, X.; Ren, J.; Wang, Y.; Lu, G. Direct catalytic conversion of furfural to 1,5-pentanediol by hydrogenolysis of the furan ring under mild conditions over Pt/Co<sub>2</sub>AlO<sub>4</sub> catalyst. *Chem. Commun.* 2011, 47, 3924–3926.
- [8] Tong, T.; Liu, X.; Guo, Y.; Banis, M. N.; Hu, Y.; Wang, Y. The critical role of CeO<sub>2</sub> crystal-plane in controlling Pt chemical states on the hydrogenolysis of furfuryl alcohol to 1,2-pentanediol. *J. Catal.* 2018, 365, 420–428.
- [9] Koso, S.; Furikado, I.; Shimao, A.; Miyazawa, T.; Kunimori, K.; Tomishige, K. Chemoselective hydrogenolysis of tetrahydrofurfuryl alcohol to 1,5-pentanediol. *Chem. Commun.* 2009, 2035–2037.
- [10] Koso, S.; Ueda, N.; Shinmi, Y.; Okumura, K.; Kizuka, T.; Tomishige, K. Promoting effect of Mo on the hydrogenolysis of tetrahydrofurfuryl alcohol to 1,5-pentanediol over Rh/SiO<sub>2</sub>. *J. Catal.* 2009, 267, 89–92.
- [11] Chia, M.; Pagán-Torres, Y. J.; Hibbitts, D.; Tan, Q.; Pham, H. N.; Datye, A. K.; Neurock, M.; Davis, R. J.; Dumesic, J. A. Selective Hydrogenolysis of Polyols and Cyclic Ethers over Bifunctional Surface Sites on Rhodium-Rhenium Catalysts. *J. Am. Chem. Soc.* 2011, 133, 12675–12689.
- [12] Chen, K.; Mori, K.; Watanabe, H.; Nakagawa, Y.; Tomishige, K. C–O bond hydrogenolysis of cyclic ethers with OH groups over rhenium-modified supported iridium catalysts. *J. Catal.* 2012, 294, 171–183.

## Furfural to diols over Ni-Co/Al catalysts

- [13] Nakagawa, Y.; Takada, K.; Tamura, M.; Tomishige, K. Total Hydrogenation of Furfural and 5-Hydroxymethylfurfural over Supported Pd–Ir Alloy Catalyst. *ACS Catal.* 2014, 4, 2718–2726.
- [14] Liu, S.; Amada, Y.; Tamura, M.; Nakagawa, Y.; Tomishige, K. One-pot selective conversion of furfural into 1,5-pentanediol over a Pd-added Ir–ReO<sub>x</sub>/SiO<sub>2</sub> bifunctional catalyst. *Green Chem.* 2014, 16, 617–626.
- [15] Liu, S.; Amada, Y.; Tamura, M.; Nakagawa, Y.; Tomishige, K. Performance and characterization of rhenium-modified Rh–Ir alloy catalyst for one-pot conversion of furfural into 1,5-pentanediol. *Catal. Sci. Technol.* 2014, 4, 2535–2549.
- [16] Mizugaki, T.; Yamakawa, T.; Nagatsu, Y.; Maeno, Z.; Mitsudome, T.; Jitsukawa, K.; Kaneda, K. Direct Transformation of Furfural to 1,2-Pentanediol Using a Hydrotalcite-Supported Platinum Nanoparticle Catalyst. *ACS Sustainable Chem. Eng.* 2014, 2, 2243–2247.
- [17] Wu, J.; Gao, G.; Li, J.; Sun, P.; Long, X.; Li, F. Efficient and versatile CuNi alloy nanocatalysts for the highly selective hydrogenation of furfural. *Appl. Catal. B Environ.* 2017, 203, 227–236.
- [18] Fu, X.; Ren, X.; Shen, J.; Jiang, Y.; Wang, Y.; Orooji, Y.; Xu, W.; Liang, J. Synergistic catalytic hydrogenation of furfural to 1,2-pentanediol and 1,5-pentanediol with LDO derived from CuMgAl hydrotalcite. *Mol. Cataly.* 2021, 499, 111298.
- [19] Audemar, M.; Ciotonea, C.; De Oliveira Vigier, K.; Royer, S.; Ungureanu, A.; Dragoi, B.; Dumitriu, E.; Jérôme, F. Selective Hydrogenation of Furfural to Furfuryl Alcohol in the Presence of a Recyclable Cobalt/SBA-15 Catalyst. *ChemSusChem* 2015, 8, 1885–1891.
- [20] Lee, J.; Burt, S. P.; Carrero, C. A.; Alba-Rubio, A. C.; Ro, I.; O'Neill, B. J.; Kim, H. J.; Jackson, D. H. K.; Kuech, T. F.; Hermans, I.; Dumesic, J. A.; Huber, G. W. Stabilizing cobalt catalysts for aqueous-phase reactions by strong metal-support interaction. *J. Catal.* 2015, 330, 19–27.
- [21] Gavilà, L.; Lähde, A.; Jokiniemi, J.; Constantí, M.; Medina, F.; del Río, E.; Tichit, D.; Álvarez, M. G. Insights on the One-Pot Formation of 1,5-Pentanediol from Furfural with Co–Al Spinel-based Nanoparticles as an Alternative to Noble Metal Catalysts. *ChemCatChem* 2019, 11, 4944–4953.
- [22] Shao, Y.; Guo, M.; Wang, J.; Sun, K.; Zhang, L.; Zhang, S.; Hu, G.; Xu, L.; Yuan, X.; Hu, X. Selective Conversion of Furfural into Diols over Co-Based Catalysts: Importance of the Coordination of Hydrogenation Sites and Basic Sites. *Ind. Eng. Chem. Res.* 2021, 60, 10393–10406.
- [23] Yao, S.; Wang, X.; Jiang, Y.; Wu, F.; Chen, X.; Mu, X. One-Step Conversion of Biomass-Derived 5-Hydroxymethylfurfural to 1,2,6-Hexanetriol Over Ni–Co–Al Mixed Oxide Catalysts Under Mild Conditions. *ACS Sustainable Chem. Eng.* 2014, 2, 173–180.
- [24] Thommes, M.; Kaneko, K.; Neimark, A.V.; Olivier, J. P.; Rodriguez-Reinoso, F.; Rouquerol, J.; Sing, K. S. W. Physisorption of gases, with special reference to the evaluation of surface area and pore size distribution (IUPAC Technical Report). *Pure Appl. Chem.* 2015, 87, 1051–1069.
- [25] Bardestani, R.; Patience, G. S.; Kaliaguine, S. Experimental methods in chemical engineering: specific surface area and pore size distribution measurements – BET, BJH, and DFT. *Can. J. Chem. Eng.* 2019, 97, 2781–2791.

**Furfural to diols over Ni-Co/Al catalysts**

- [26] Brown, I. D. Bond Valence Theory. In I. Brown & K. Poeppelmeier (Eds.), *Bond Valences. Structure and Bonding*. Springer Berlin Heidelberg. 978-3-642-54968-7 (2013).
- [27] Vegard, L. *Z.phys* 5 1921 17.
- [28] Clause, O.; Coelho, M. G.; Gazzano, M.; Matteuzzi, D.; Trifirò, F.; Vaccari A. Synthesis and thermal reactivity of nickel-containing anionic clays. *Appl. Clay Sci.* 1993, 8, 169–186.
- [29] Mas, V.; Baronetti, G.; Amadeo, N.; Laborde, M. Ethanol steam reforming using Ni(II)-Al(III) layered double hydroxide as catalyst precursor. *Kinetic study. Chem. Eng. J.* 2008, 138, 602–667.
- [30] Abelló, S.; Berruoco, C.; Gispert-Guirado, F.; Montané D. Synthetic natural gas by direct CO<sub>2</sub> hydrogenation on activated talcovites: effect of Ni/Al molar ratio. *Catal. Sci. Technol.* 2016, 6, 2305–2317.
- [31] Wang, Y.; Cui, Q.; Guan, Y.; Wu, P. Facile synthesis of furfuryl ethyl ether in high yield via the reductive etherification of furfural in ethanol over Pd/C under mild conditions. *Green Chem.* 2018, 20, 2110–2117.
- [32] Agote-Arán M, Alijani S, Coffano C, Villa A, Ferri D. Effect of Pt Particle Size and Phosphorous Addition on Furfural Hydrogenation Over Pt/Al<sub>2</sub>O<sub>3</sub>. *Catal Lett* 2022, 152:980. doi.10.1007/s10562-021-03685-7
- [33] He, J.; Nielsen, M. R.; Hansen, T. W.; Yang, S.; Riisager, A. Hierarchically constructed NiO with improved performance for catalytic transfer hydrogenation of biomass-derived aldehydes. *Catal. Sci. Technol.* 2019, 9, 1289–1300.
- [34] Ramos, R.; Peixoto, A. F.; Arias-Serrano, B. I.; Soares, O. S. G. P.; Pereira, M. F. R.; Kubička, D.; Freire, C. Catalytic Transfer Hydrogenation of Furfural over Co<sub>3</sub>O<sub>4</sub>-Al<sub>2</sub>O<sub>3</sub> Hydrotalcite-derived Catalyst. *ChemCatChem* 2020, 12, 1467–1475.
- [35] Jorge, E. Y.; Lima, T. D. M.; Lima, C. G.; Marchini, L.; Castelblanco, W. N.; Rivera, D. G.; Urquieta-Gonzalez, E. A.; Varma, R. S.; Paixão, M. W. Metal-exchanged magnetic  $\beta$ -zeolites: valorization of lignocellulosic biomass-derived compounds to platform chemicals. *Green Chem.* 2017, 19, 3856–3868.
- [36] Aldureid, A.; Medina, F.; Patience G. S.; Montané, D. Ni-Cu/Al<sub>2</sub>O<sub>3</sub> from Layered Double Hydroxides Hydrogenates Furfural to Alcohols. *Catalysts* 2022, 12, 390.

## Furfural to diols over Ni-Co/Al catalysts

## **Furfural to diols over Ni-Co/Al catalysts**

# Chapter five

---

## **Ni-Mg/Al prepared from double layered hydroxides (LDHs) as catalysts for the selective conversion of furfural to TFA**

# Chapter 5: Ni-Mg/Al prepared from double layered hydroxides (LDHs) as catalysts for the selective conversion of furfural to tetrahydrofurfuryl alcohol (TFA).

## 1. Introduction

Furfural is produced by the acid-catalyzed dehydration of the C-5 carbohydrates forming hemicellulose and it has been identified as a key biomass-derived platform chemical [1-3]. Furfural is a versatile chemical due to the presence of an aldehyde group and the  $\alpha,\beta$  unsaturation of the furan ring. These functionalities make furfural an excellent starting molecule for the synthesis of many value-added chemicals since it can be converted by dehydration, oxidation, hydrogenation, decarbonylation, decarboxylation, condensation or ring opening reactions [4,5]. Furfural hydrogenation can produce several industrially useful chemicals, such as furfuryl alcohol, tetrahydrofurfuryl alcohol, or tetrahydrofuran, among others. Tetrahydrofurfuryl alcohol in particular is used as a high-boiling point solvent for dyes, pesticides and herbicides, inks, specialty chemicals, and in the synthesis of some pharmaceuticals [6].

The established industrial process to produce tetrahydrofurfuryl alcohol (TFA) uses supported Ni catalysts to hydrogenate furfuryl alcohol (FA) at low temperature (typically below 100 °C) in either vapor or liquid phase. The direct synthesis of TFA from furfural has attracted considerable interest, but it is challenging since it requires catalysts that activate both the furan ring and the carbonyl group. Heterogeneous catalysts based on noble metals supported on a variety of materials have been studied in detail for this reaction, since they have good C=C reduction activity. Palladium supported on a Si-MFI molecular sieve (3% Pd/MFI) gave a 95% selectivity to TFA after 10 h at 220 °C and 35.5 bar H<sub>2</sub> using isopropanol as solvent [7]. Milder conditions were required to reach similar selectivity with other supports such as hydroxyapatite (100% TFA, Pd-HAP, isopropanol, 40 °C, 10 bar H<sub>2</sub>, 3 h) [8]

## Mg/Al prepared from double layered hydroxides (LDHs) as catalysts the selective conversion of furfural to TFA

or metal organic frameworks (100% TFA, Pd/UiO-66, water, 60 °C, 10 bar H<sub>2</sub>, 4 h) [9]. Addition of platinum to palladium using titania as support (PdPt/TiO<sub>2</sub>) gave a 95% selectivity to TFA at lower pressure and temperature (isopropanol, 30 °C, 3 bar H<sub>2</sub>, 4 h) [10]. A platinum-nickel alloy supported on activated carbon (PtNi/C) gave a 93% TFA yield at 35 °C and 20 bar H<sub>2</sub> using water as solvent for 12 h, close to yield with Pd/C [11], and also similar to the performance of a commercial Rh/C catalyst (93% TFA, water, 30 °C, 10 bar H<sub>2</sub> and 12h) [12]. Due to the relatively high cost of noble metals, catalysts based on non-noble metals such as nickel have been studied widely. Nakagawa et al. [13] reported a 94% yield of TFA in the gas phase hydrogenation of FF at 130 °C on Ni/SiO<sub>2</sub> prepared by impregnation. TFA was formed through the sequential transformation of FF to FA to TFA. The presence of FF inhibited the second step because FF adsorption on the surface was stronger than that of FOL. This step was also very sensitive to the structure of the catalyst. The highest activity was reached with small Ni crystallites (< 4 nm). Yang et al. [14] reached a 99% selectivity to TFA at 140 °C, 40 bar H<sub>2</sub> and 4h using water as solvent with nickel supported on alumina modified with barium (Ni/Ba-Al<sub>2</sub>O<sub>3</sub>). Barium enhanced the selectivity to TFA by giving more basicity to the surface, thus inhibiting furfural polymerization and secondary reactions on acidic sites. A bimetallic Ni-Co supported on mesoporous silica (SBA-15) gave catalysts with highly dispersed Ni-CoO<sub>x</sub> sites (5-8 nm crystallites) that were responsible for the high selectivity to TFA (90 %) during the hydrogenation of FF in isopropanol at 210 °C and 70 bar H<sub>2</sub> for 6 h [15]. Mesoporous clays modified with MgO to reduce acidity were used as support for Ni catalysts (Ni/MgO/montmorillonite MK-10) that achieved a complete conversion of FF to TFA in aqueous-phase at 140 °C, 40 bar H<sub>2</sub> and 4h [16]. Kumar et al. [17] reported a ca. 90% selectivity to TFA with 10% nickel supported on a CuFe spinel (Ni/CuFe<sub>2</sub>O<sub>4</sub>) at 150 °C and 10 bar H<sub>2</sub> with ethanol as solvent. High metal dispersion, small crystallite size and a strong interaction with the support increase the hydrogenation activity of the catalysts. An efficient way to achieve a high dispersion is by introducing the metal directly into the composition of the support. This is feasible when using precursors based on layered double hydroxides [18].

**Mg/Al prepared from double layered hydroxides (LDHs) as catalysts the selective conversion of furfural to TFA**

Layered double hydroxides (LDH) are clays consisting of hydroxide layers having positive charge, balanced by mobile anions and water located in the interlayer region, according to the general molecular formula  $[M^{2+}_{1-x}N^{3+}_x(OH)_2]^{x+}[A^{n-}_{x/n}\cdot\gamma H_2O]^{x-}$  ( $0 < x < 1$ ) [19] (Figure 5.1). This particular structure makes LDH versatile materials that can be used as heterogeneous catalysis. The basicity of the LDH surface can be modified by varying the  $M^{2+}/N^{3+}$  ratio or by changing the anionic species in the interlayer space. Therefore, surface metal species can cooperate with basic-acid sites on the surface of LDH to generate multifunctional catalysts. The anionic species in the interlayer region can be modified by ion-exchange or by calcination and rehydration (memory effect), to introduce catalytically active species into the structure. Furthermore, LDH can be used as support structure for highly dispersed metal nanoparticles [19-21]. Heterogeneous catalysts can be also obtained from LDH precursors by calcination at controlled conditions followed by partial reduction. This produces mixed oxide structures containing small and highly dispersed metal crystallites that have strong interaction with the oxides, which provides active catalysts with good resistance to sintering [22-24]. Catalysts derived from LDHs have demonstrated good performance in the hydrogenation of furfural. Sulmonetti et al. [25] tested various nickel mixed metal oxides derived from Ni-Mg-Al and Ni-Co-Al LDHs in the gas-phase hydrogenation of FF at 155 °C and atmospheric pressure. FA was the main product followed by TFA, but variable amounts of FUR, mFUR, BU and 12PD were obtained. Selectivity to TFA was only 21% with  $Ni_2Al$  and 13.1% with  $Ni_{1.9}Mg_1Al$ . Improved selectivity to TFA was achieved in liquid phase hydrogenation. Wu et al. [26] reported a 95% selectivity to TFA in the hydrogenation of furfural in ethanol at 150 °C, 40 bar  $H_2$  and 3 h using a supported CuNi alloy catalyst (CuNi/MgAlO) obtained from a LDH precursor. The dispersion of the alloy crystallites and the basicity of the surface was determined by the temperature of calcination of the LDH. A 99% selectivity to TFA using Ni supported on mixed metal oxides prepared from Ni-Al LDHs having carbonate as interlayer anion was attained in isopropanol at 110 °C, 30 bar  $H_2$  and 3 h [27]. Similarly, a 98% yield of TFA was achieved at 160 °C, 30 bar  $H_2$  and 4 h using 2-butanol as solvent with an equimolar NiCu alloy supported on mixed oxides ( $NiO$ ,  $CuO$ ,  $CuAl_2O_4$  and  $NiAl_2O_4$  spinel) derived from Ni(Cu)Al-LDH [28]. Recently,

**Mg/Al prepared from double layered hydroxides (LDHs) as catalysts the selective conversion of furfural to TFA**

Stepanova [29] explored the Ni(Mg)AlO<sub>x</sub> catalysts obtained by calcination of Ni(Mg)Al-LDH. Tests were conducted using water as solvent at 90 °C and 20 bar H<sub>2</sub>. FA tended to be the main product, but Ni<sub>1.5</sub>Mg<sub>3.5</sub>Al gave a 44% selectivity to TFA.

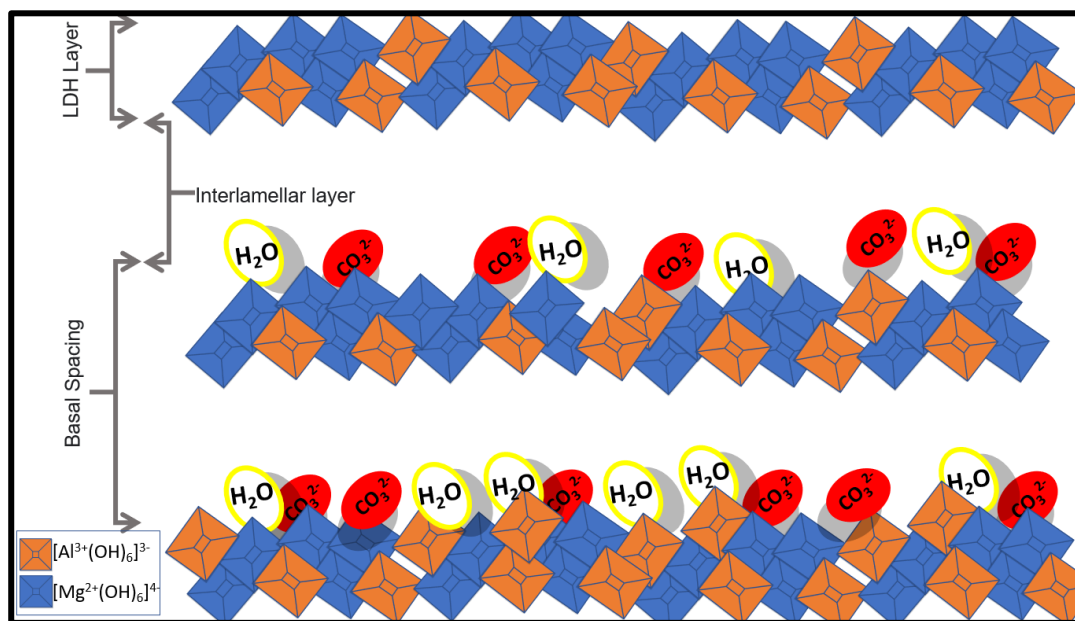


**Figure. 5.1.** The LDH structure, color code for atoms in blocks representation:  $M^{2+}= Mg^{2+}$ : blue blocks,  $M^{3+}= Al^{3+}$ : orange blocks.

In this work, we synthesized Ni<sub>x</sub>Mg<sub>y</sub>Al catalyst from LDH precursors with Ni/Mg atomic ratios x/y of 2/0, 2/1 and 1/1. The catalysts were characterized and tested for the total hydrogenation of furfural to TFA, both in liquid phase under hydrogen pressure in a batch slurry reactor, and in gas phase at atmospheric pressure on a continuous packed bed. The influence on product selectivity of the process conditions, the Ni/Mg ratio of the catalysts and the type of reactor was assessed, and the pathways leading to the formation of the major products were discussed.

## 2. Results and discussion

### 2.1. Catalyst characterization

The bulk chemical composition of the calcined oxides was measured by ICP-OES (Table 5.1). The Ni/Al atomic ratios obtained for  $\text{Ni}_2\text{Mg}_1\text{Al}$  and  $\text{Ni}_1\text{Mg}_1\text{Al}$  were 1.90 and 0.90, respectively, closer to the intended values than the ratio of 1.83 in  $\text{Ni}_2\text{Al}$ . Similarly, the Mg/Al ratios were close to the nominal, with values of 1.11 in  $\text{Ni}_2\text{Mg}_1\text{Al}$  and 0.98 in  $\text{Ni}_1\text{Mg}_1\text{Al}$ . The surface compositions determined by FESEM-EDX (Table 5.1) gave values similar to those of the bulk composition determined by ICP-OES, except on the case of  $\text{Ni}_2\text{Mg}_1\text{Al}$ , where both the Ni/Al and Mg/Al were lower.

**Table 5.1.** Atomic ratios of the LDH precursors calcined at 400 °C for 4 h, measured by ICP-OES and FESEM-EDX.

Calcined material	ICP-OES		FESEM-EDX	
	Ni/Al	Mg/Al	Ni/Al	Mg/Al
$\text{Ni}_2\text{Mg}_1\text{Al}$	1.90	1.11	1.27	0.82
$\text{Ni}_1\text{Mg}_1\text{Al}$	0.90	0.98	0.96	1.02
$\text{Ni}_2\text{Al}$	1.83	-	2.05	-

The change in the composition of the three materials was demonstrated by ESEM-EDX imaging in Figure 5.2.

**Mg/Al prepared from double layered hydroxides (LDHs) as catalysts the selective conversion of furfural to TFA**

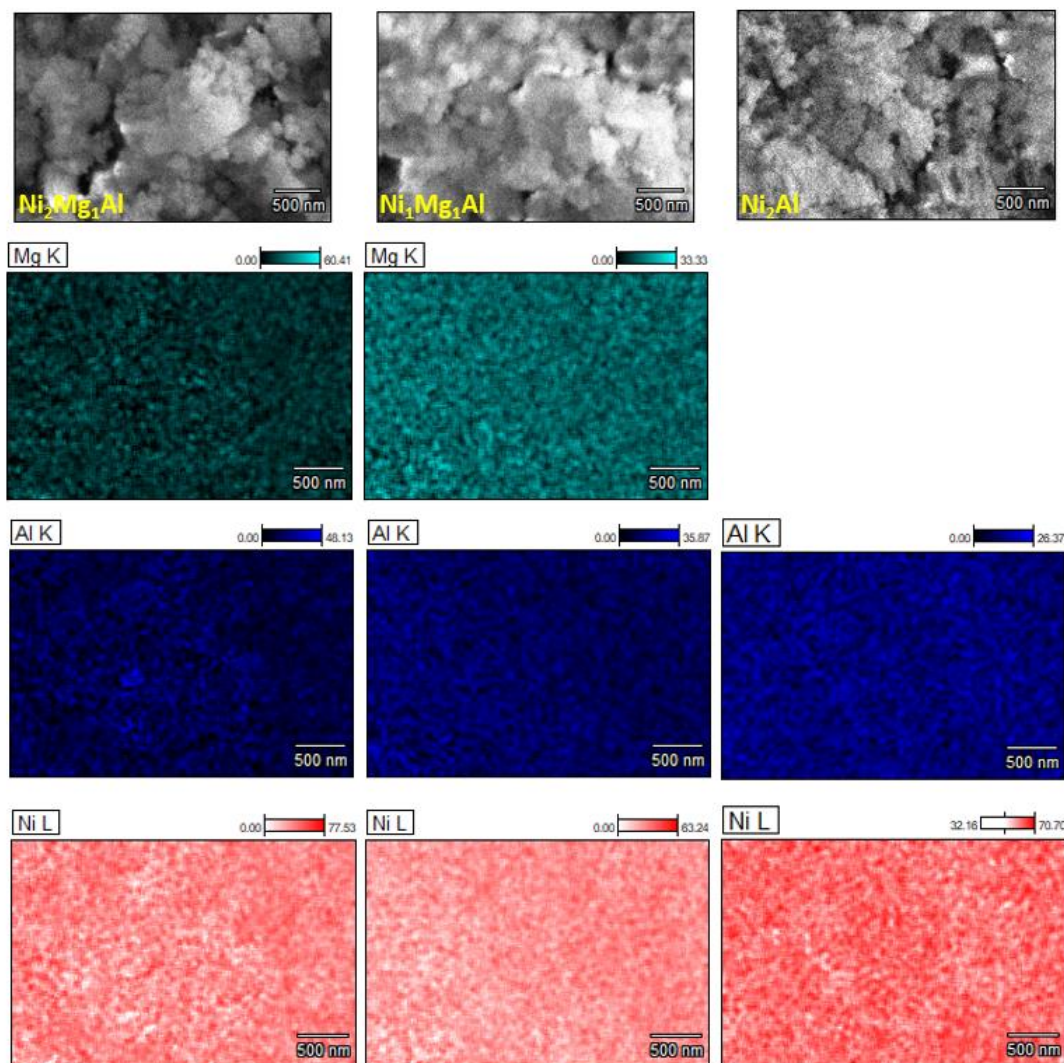


**Figure 5.2.** FESEM-EDX imaging of the LDH precursors calcined at 400 °C for 4h. Green color for Magnesium, blue color for Aluminum and red color for Nickel.

SEM imaging of the calcined materials (Figure 5.3) showed a slight change in morphology with the addition of magnesium. The three calcined materials consisted of aggregates of spherical granules, which were slightly larger in  $\text{Ni}_2\text{Mg}_1\text{Al}$  and  $\text{Ni}_1\text{Mg}_1\text{Al}$ .

**Mg/Al prepared from double layered hydroxides (LDHs) as catalysts the selective conversion of furfural to TFA**

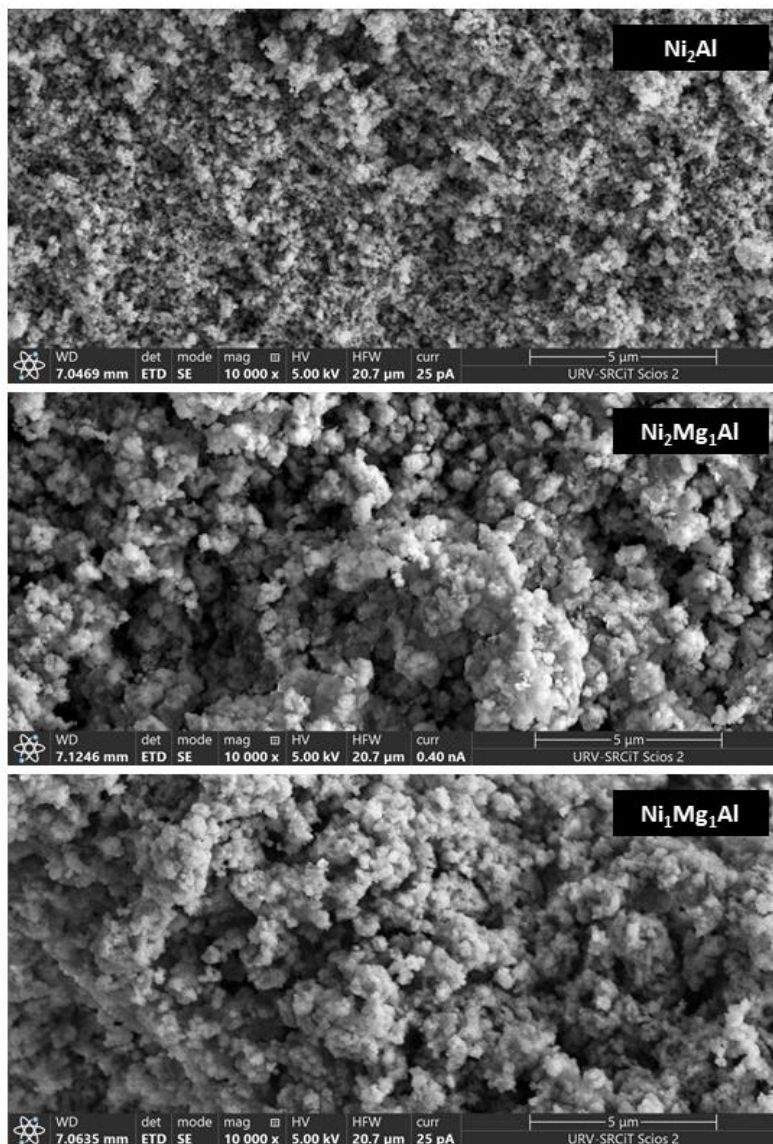


**Figure 5.3.** SEM imaging of the LDH precursors calcined at 400 °C for 4 h (10000  $\times$  magnification).

The  $N_2$  physisorption isotherms of the calcined LDH precursors (Figure 5.4) were characteristic of mesoporous materials with type II isotherms and H3 hysteresis loops, according to the IUPAC classification [30, 31].

**Mg/Al prepared from double layered hydroxides (LDHs) as catalysts the selective conversion of furfural to TFA**

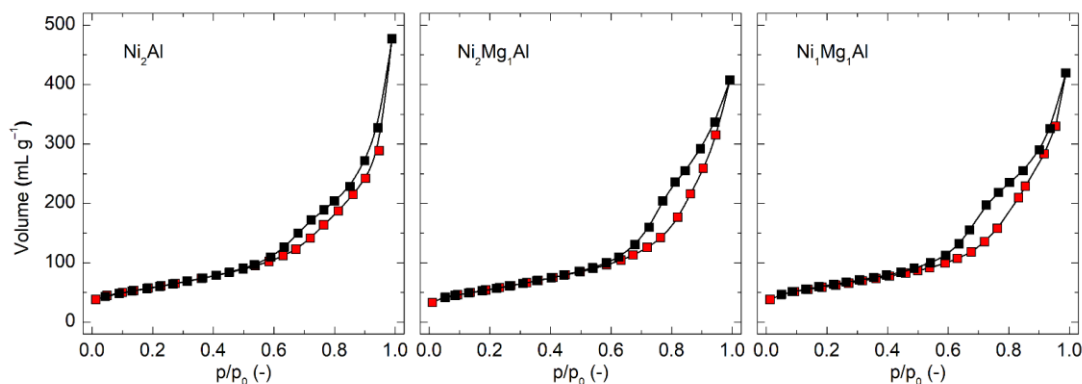


**Figure 5.4.** N<sub>2</sub> physisorption isotherms of the LDH precursors calcined at 400 °C for 4 h. The red symbols are the adsorption branch, and the black symbols represent the desorption branch of the isotherm.

The BET surface area of the three materials was similar. It was ca. 210 m<sup>2</sup> g<sup>-1</sup> in Ni<sub>2</sub>Al, 212 m<sup>2</sup> g<sup>-1</sup> in Ni<sub>1</sub>Mg<sub>1</sub>Al and 200 m<sup>2</sup> g<sup>-1</sup> in Ni<sub>2</sub>Mg<sub>1</sub>Al. The pore size and surface distributions (Figure 5.5) and the specific volume and average pore diameter (Table 5.2) calculated with the DFT model followed a similar trend. The pore volume and surface area were ca. 0.49 mL g<sup>-1</sup> and 5.4 nm in both Ni<sub>2</sub>Al and Ni<sub>1</sub>Mg<sub>1</sub>Al. Ni<sub>2</sub>Mg<sub>1</sub>Al had the same pore volume but a larger pore size (7.1 nm).

**Table 5.2.** Textural properties of the LDH precursors calcined at 400 °C for 4 h.

Calcined material	BET Surface Area (m <sup>2</sup> g <sup>-1</sup> )	DFT pore volume (mL g <sup>-1</sup> )	DFT pore diameter (nm)
Ni <sub>2</sub> Al	210	0.49	5.4
Ni <sub>2</sub> Mg <sub>1</sub> Al	200	0.50	7.1
Ni <sub>1</sub> Mg <sub>1</sub> Al	212	0.48	5.4

Overall, the textural properties and the surface composition changed with the (Ni+Mg)/Al atomic ratio of the calcined material.

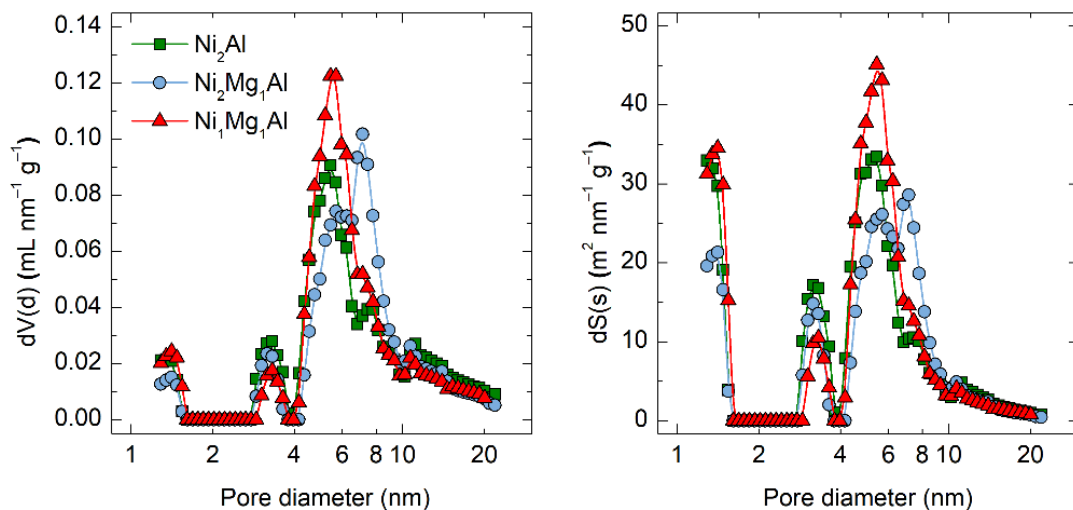


**Figure 5.5.** Pore volume (left) and surface (right) distributions of the LDH precursors calcined at 400 °C for 4 h, determined with the DFT model.

The XRD diffraction patterns of the calcined catalyst precursors (Figure 5.6) had wide overlapping peaks characteristic of structures with small crystallites, which complicated the elucidation of the phases present in the materials. The Rietveld analysis of the diffractograms revealed combinations of several structures, with compositions and proportions that depended on the Ni/Al and Mg/Al ratio. In general, these comprised a spinel-type structure  $(\text{A})[\text{B}]_2\text{O}_4$  (Fd3m) with the tetrahedral position [A] and the octahedral [B] position occupied by Ni, Mg and Al oxides, NiO or  $\text{Ni}_x\text{Mg}_{(1-x)}\text{O}$  oxides, and in some cases minor amounts of Jamborite ( $\text{Ni}(\text{OH})_2\text{NiOOH}$ , ICSD entry 076650).

**Mg/Al prepared from double layered hydroxides (LDHs) as catalysts the selective conversion of furfural to TFA**

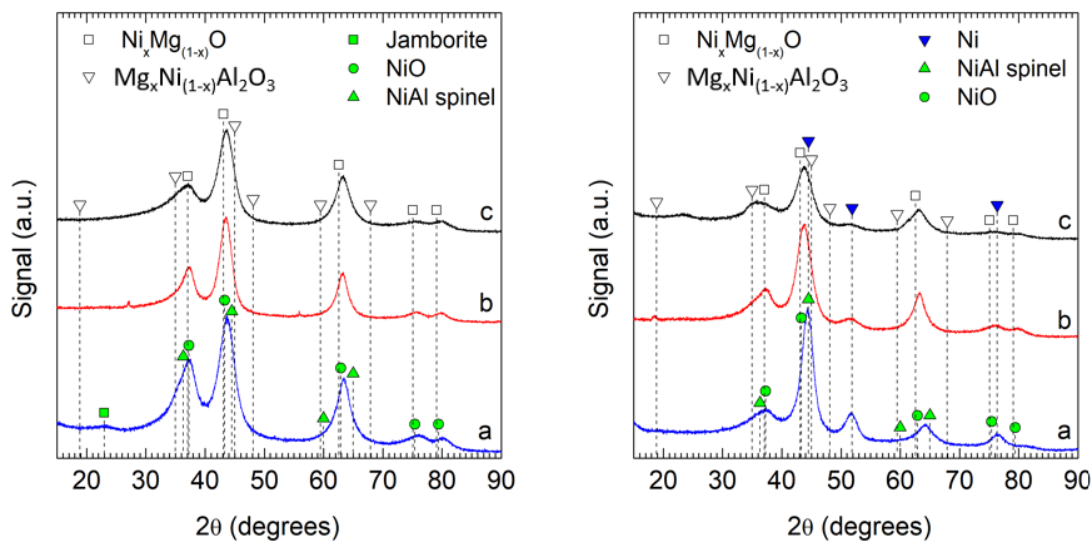


**Figure 5.6.** XRD patterns of the LDH precursors calcined at 400 °C for 4 h (left), and the catalysts after reduction at 500 °C for 1h (right). a: Ni<sub>2</sub>Al; b: Ni<sub>2</sub>Mg<sub>1</sub>Al; c: Ni<sub>1</sub>Mg<sub>1</sub>Al

The distribution of cations in the spinel structure was adjusted manually to fulfill these rules:

i) minimum difference between the elemental composition of the sample measured by SEM and that calculated from the Rietveld analysis; ii) minimum electrical charge of the spinel structure calculated with the Bond Valence Theory [32]; iii) minimum conventional Rietveld agreement factor ( $R_{wp}$ ); and iv) complete occupation of the tetrahedral position (A) and the octahedral position [B] by the cations. The  $Ni_xMg_{(1-x)}O$  structure was estimated from its refined cell parameter (Vegard's law) [33]. Calcined Ni<sub>2</sub>Al consisted of 48.6 wt.% of NiO and 46.1 wt.% of spinel (Table 5.3) together with a small amount of Jamborite. In Ni<sub>2</sub>Mg<sub>1</sub>Al, the main structures were comprised of a ca. 58.1 wt.% of mixed nickel-magnesium oxide (Ni<sub>0.49</sub>Mg<sub>0.51</sub>O) with a 41.9 wt.% of the Mg<sub>0.7</sub>Ni<sub>0.3</sub>[Al]<sub>2</sub>O<sub>4</sub> spinel. Similarly, Ni<sub>1</sub>Mg<sub>1</sub>Al contained Ni<sub>0.31</sub>Mg<sub>0.69</sub>O and Mg<sub>0.5</sub>Ni<sub>0.5</sub>[Al]<sub>2</sub>O<sub>4</sub> by 53.5 wt.% and 46.5 wt.%, respectively. Reduction with hydrogen at 500 °C for 1 h altered the diffraction patterns of the three materials substantially (Figure 5.6). In Ni<sub>2</sub>Al-R, the amounts of spinel and NiO phases decreased, the spinel was enriched in aluminum and contained little nickel, and a 29.0 wt.% of metallic nickel phase (Fd3m) having an average crystallite size of 3.4 nm was

Mg/Al prepared from double layered hydroxides (LDHs) as catalysts the selective conversion of furfural to TFA

formed (Table 5.3). The reduction transformed the Ni<sub>2</sub>Mg<sub>1</sub>Al phases into additional Mg[Al]<sub>2</sub>O<sub>4</sub> spinel (39.6 %), Ni<sub>0.51</sub>Mg<sub>0.49</sub>O (47.9 %), and also a 12.6% of metallic nickel with an average crystallite size of 2.8 nm. Likewise, reduction of Ni<sub>1</sub>Mg<sub>1</sub>Al led to form a mixture spinel and mixed nickel-magnesium oxide and a 6.2 wt.% of metallic nickel (Table 5.3.).

**Table 5.3.** Crystalline phases detected and average crystallite sizes calculated from the XRD diffraction patterns of the calcined and reduced samples.

Samples	Composition (XRD, wt.%)			Phases		
	Al	Mg	Ni	Identified	wt.%	Crystallite size (nm)
Ni <sub>2</sub> Al	13.6	-	57.6	(Al <sub>0.85</sub> Ni <sub>0.15</sub> )[Al <sub>0.55</sub> Ni <sub>0.45</sub> ] <sub>2</sub> O <sub>4</sub>	46.1	1.3
				NiO	48.6	2.2
				Jamborite	5.3	2.2
Ni <sub>2</sub> Mg <sub>1</sub> Al	10.5	13.6	33.0	Mg <sub>0.7</sub> Ni <sub>0.3</sub> [Al] <sub>2</sub> O <sub>4</sub>	41.9	1.2
				Ni <sub>0.49</sub> Mg <sub>0.51</sub> O	58.1	2.8
Ni <sub>1</sub> Mg <sub>1</sub> Al	7.7	13.0	18.8	Mg <sub>0.5</sub> Ni <sub>0.5</sub> [Al] <sub>2</sub> O <sub>4</sub>	46.5	0.7
				Ni <sub>0.31</sub> Mg <sub>0.69</sub> O	53.5	2.1
Ni <sub>2</sub> Al-R	18.3	-	59.0	(Al <sub>0.90</sub> Ni <sub>0.10</sub> )[Al <sub>0.99</sub> Ni <sub>0.01</sub> ] <sub>2</sub> O <sub>4</sub>	35.0	1.3
				NiO	35.0	1.8
				Ni	29.0	3.4
Ni <sub>2</sub> Mg <sub>1</sub> Al-R	15.08	16.8	37.1	Mg[Al] <sub>2</sub> O <sub>4</sub>	39.6	1.3
				Ni <sub>0.51</sub> Mg <sub>0.49</sub> O	47.9	2.8
				Ni	12.3	2.8
Ni <sub>1</sub> Mg <sub>1</sub> Al-R	16.5	18.8	30.3	Mg[Al] <sub>2</sub> O <sub>4</sub>	43.6	1.3
				Ni <sub>0.44</sub> Mg <sub>0.66</sub> O	45.3	1.5
				Ni	6.2	3.6
				Jamborite	4.9	2.5

The reducibility of the calcined materials was studied by temperature-programmed reduction (H<sub>2</sub>-TPR) between 100 and 800 °C under 10% hydrogen in argon (Figure 5.7). The

Mg/Al prepared from double layered hydroxides (LDHs) as catalysts the selective conversion of furfural to TFA

three materials presented two peaks above 300 °C, which shifted to higher temperature with the magnesium content (Table 5.4). In Ni<sub>2</sub>Al, the low temperature shoulder at 387 °C was attributed to the reduction of small fraction of NiO that had little interaction with the spinel, while the largest and broader peak at 554 °C comprised the transformation of the spinel and the partial reduction of NiO [34-36]. Ni<sub>2</sub>Mg<sub>1</sub>Al and specially Ni<sub>1</sub>Mg<sub>1</sub>Al were less reducible than Ni<sub>2</sub>Al. The high temperature peak was also very broad and was attributed to the transformation of multiple structures of nickel with magnesium and aluminum [37]. The peak maxima shifted to higher temperature and the hydrogen consumption decreased with the amount of magnesium, which was consistent with the formation of unreducible Mg[Al]<sub>2</sub>O<sub>4</sub> spinel, mixed Ni<sub>x</sub>Mg<sub>(1-x)</sub>O oxides and the lower formation of reduced nickel that was inferred from XRD.

**Table 5.4.** Specific hydrogen consumption during the TPR of the LDH precursors calcined at 400 °C for 4 h.

Calcined Material	Peak 1		Peak 2		Total
	T (°C)	H <sub>2</sub> (mL g <sup>-1</sup> )	T (°C)	H <sub>2</sub> (mL g <sup>-1</sup> )	H <sub>2</sub> (mL g <sup>-1</sup> )
Ni <sub>2</sub> Al	387	3	554	136	139
Ni <sub>2</sub> Mg <sub>1</sub> Al	392	7	630	127	134
Ni <sub>1</sub> Mg <sub>1</sub> Al	420	13	705	96	109

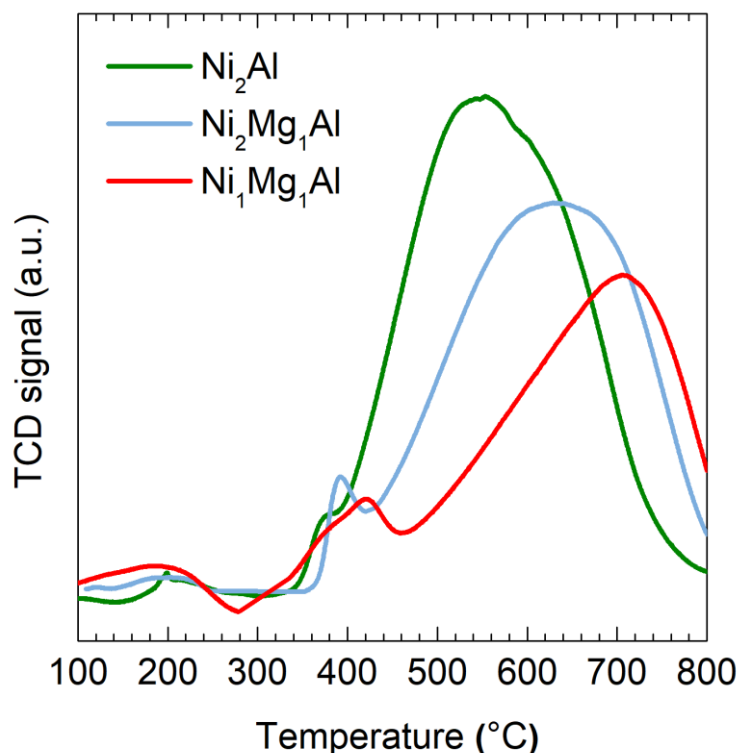


**Figure 5.7.** H<sub>2</sub>-TPR of the LDH precursors calcined at 400 °C for 4 h.

The acidity of the catalysts was determined by temperature programmed desorption of ammonia (Figure 5.8). The desorption peaks of all the materials had broad temperature peaks areas, indicating wide distributions in the strength of the acid sites. Multiple overlapped peaks were observed in Ni<sub>2</sub>Al-R below 350 °C forming from the desorption of ammonia from weak and moderate strength sites, together with a peak of strong acidic sites at ca. 600 °C. A decrease in the area of the low temperature peaks was found, pointing to the effect of Mg addition on Ni<sub>2</sub>Mg<sub>1</sub>Al-R and Ni<sub>1</sub>Mg<sub>1</sub>Al-R in reducing the weak and intermediate acidity sites. This may be attributed to the role that magnesium can play as an Alkaline earth metal. In addition to this, the high temperature peak area grew, the samples of Ni<sub>2</sub>Mg<sub>1</sub>Al-R and Ni<sub>1</sub>Mg<sub>1</sub>Al-R have higher peaks than the peaks of Ni<sub>2</sub>Al-R.

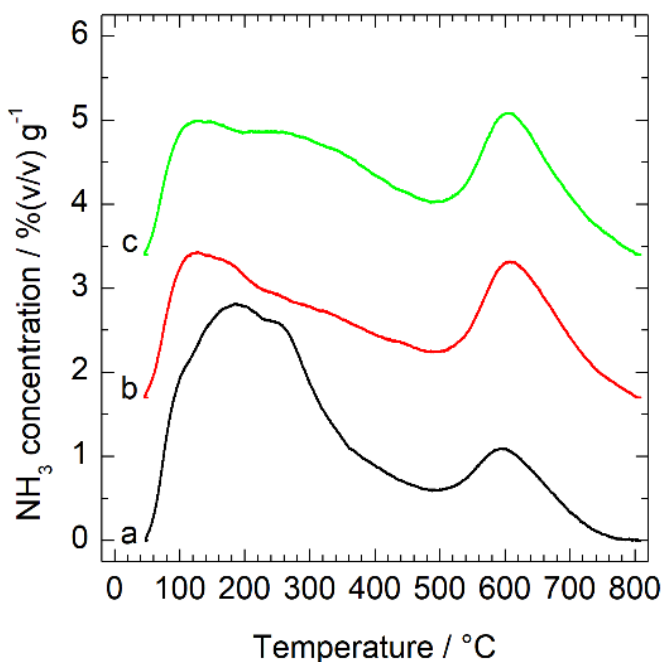


**Figure 5.8.** Temperature programmed desorption of ammonia (TPD-NH<sub>3</sub>): ammonia concentration normalized to the mass of catalyst vs. the desorption temperature (a: Ni<sub>2</sub>Al-R; b: Ni<sub>2</sub>Mg<sub>1</sub>Al-R; c: Ni<sub>1</sub>Mg<sub>1</sub>Al-R).

Signal deconvolution (Figure 5.9) was used to quantify the amounts of weak ( $\alpha$ ,  $T_d < 220$  °C), intermediate ( $\beta$ ,  $220$  °C  $< T_d < 500$  °C) and strong ( $\gamma$ ,  $T_d > 500$  °C) sites and the total acidity of the catalysts (Table 5.5). Overall, the addition of magnesium raised the amount of  $\alpha$  sites from  $0.34$  mmol NH<sub>3</sub> g<sup>-1</sup> in Ni<sub>2</sub>Al-R to ca.  $0.36$  mmol NH<sub>3</sub> g<sup>-1</sup> and  $0.41$  mmol NH<sub>3</sub> g<sup>-1</sup> in Ni<sub>2</sub>Mg<sub>1</sub>Al-R and Ni<sub>1</sub>Mg<sub>1</sub>Al-R, respectively. The amount of  $\beta$  sites was reduced according to the influence of Mg content on the catalyst, from  $0.66$  in Ni<sub>2</sub>Al-R to  $0.31$  mmol NH<sub>3</sub> g<sup>-1</sup> in Ni<sub>2</sub>Mg<sub>1</sub>Al-R and to  $0.33$  mmol NH<sub>3</sub> g<sup>-1</sup> in Ni<sub>1</sub>Mg<sub>1</sub>Al-R. Finally, the presence of  $\gamma$  sites increased from  $0.23$  mmol NH<sub>3</sub> g<sup>-1</sup> in the sample without magnesium (Ni<sub>2</sub>Al-R) to  $0.32$  mmol NH<sub>3</sub> g<sup>-1</sup> in both magnesium samples.

**Mg/Al prepared from double layered hydroxides (LDHs) as catalysts the selective conversion of furfural to TFA**

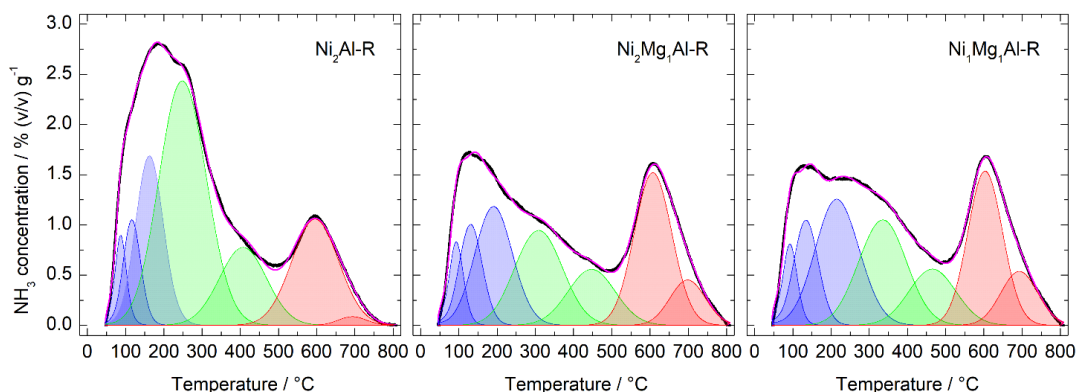


**Figure 5.9.** Temperature programmed desorption of ammonia (TPD-NH<sub>3</sub>): deconvolution of the ammonia concentration normalized to the mass of catalyst vs. the desorption temperature (Blue peaks:  $\alpha$ -weak sites; Green peaks:  $\beta$ -intermediate strength sites; Red peaks:  $\gamma$ -strong sites. Blue line: recorded signal; Cyan line: deconvoluted signal).

The total acidity of the catalysts was high, 1.2 mmol NH<sub>3</sub> g<sup>-1</sup> in Ni<sub>2</sub>Al-R, decreased to 1.0 mmol NH<sub>3</sub> g<sup>-1</sup> in Ni<sub>2</sub>Mg<sub>1</sub>Al-R and 1.1 mmol NH<sub>3</sub> g<sup>-1</sup> in Ni<sub>1</sub>Mg<sub>1</sub>Al-R (Table.5.X).

**Table 5.5.** Total concentration of acidic sites and estimation of the weak, intermediate, and strong acidic sites based on signal deconvolution by (TPD-NH<sub>3</sub>).

Catalyst	Concentration of acidic sites (mmol NH <sub>3</sub> g <sup>-1</sup> )			Total
	Weak ( $\alpha$ ) T <sub>d</sub> < 220 °C	Intermediate ( $\beta$ ) 220 °C < T <sub>d</sub> < 500 °C	Strong ( $\gamma$ ) T <sub>d</sub> > 500°C	
Ni <sub>2</sub> Al-R	0.34	0.66	0.23	1.2
Ni <sub>2</sub> Mg <sub>1</sub> Al-R	0.36	0.31	0.32	1.0
Ni <sub>1</sub> Mg <sub>1</sub> Al-R	0.41	0.33	0.32	1.1

## 2.2. Catalytic activity tests

The influence of process conditions on the conversion of furfural and the selectivity to its main hydrogenation products was studied in detail with the Ni<sub>2</sub>Mg<sub>1</sub>Al-R catalyst. Experiments were performed in a stirred slurry reactor (SSR) considering

**Mg/Al prepared from double layered hydroxides (LDHs) as catalysts the selective conversion of furfural to TFA**

temperature (160 °C, 190 °C and 210 °C), time (1, 2, 4, 6 and 8 hours) and hydrogen pressure (10, 20, 30, 40 and 50 bar). In all the experiments, 30 mL of a 5.0 wt% FF solution in ethanol and 200 mg of reduced catalyst were used.

The effect of hydrogen pressure was studied at 190 °C and 4 h. Furfural conversion was 90.6% at 10 bar, 99.4% at 30 bar and complete above that (Figure 5.10). A variety of products with selectivity that changed with hydrogen pressure were identified.

At 10 bar, furfural was hydrogenated to furfuryl alcohol (FA, 32%) as the main product and 2-methylfuran (mFUR, 21.6%), but it was also decarbonylated to furane (FUR, 22%). Minor hydrogenation products included tetrahydrofurfuryl alcohol (TFA, 4.9%) from the hydrogenation of FA, and n-butanol (BU, 5.1%) from the ring-opening hydrogenolysis of FUR. Also, difurfuryl ether (DFE, 9.9%) and 2-(diethoxymethyl)furan (FDA, 0.9%) were obtained. Both evolved through the formation of acetals on acidic sites of the catalyst surface by reversible nucleophilic addition of FF with FA or ethanol (Scheme 5.1), a reaction path that has been previously observed on different catalysts [42]. The formation of FDA from FF and ethanol was reported under mild hydrogenation conditions on Pd/UiO-66 [9] and on a Pd/C catalyst, where it was identified as the key intermediate in the production of tetrahydrofurfuryl ethyl ether (TFEE) [38]. Similarly, 2-(diisopropoxymethyl)furan resulting from acetylation of FF with isopropanol was reported on NiO [39], NiO-Al<sub>2</sub>O<sub>3</sub> and ZnAl<sub>2</sub>O<sub>4</sub>-Al<sub>2</sub>O<sub>3</sub> [40], and on Pd-exchanged  $\beta$ -zeolites [41] during the catalytic transfer hydrogenation of FF with 2-propanol. During FF hydrogenation under mild conditions over Pd/HPA, 2-(isopropoxymethyl)furan was formed as an intermediate compound in weak acidic sites that was then converted to TFA on basic sites [8]. Increasing the hydrogen pressure of the reaction over Ni<sub>2</sub>Mg<sub>3</sub>Al-R promoted the formation of FA and lowered the selectivity to FUR and mFUR. FA selectivity was maximum at 20 bar (58%) but decreased at higher pressure and it was not detected significantly at 50 bar. Pressure favored the hydrogenation of FA to tetrahydrofurfuryl alcohol (TFA), which reached a selectivity of 78.5% at 50 bar. In addition, pressure shifted the selectivity of the addition reactions to the formation of FDA instead of DFE, which was subsequently hydrogenated to TFEE (Scheme 5.1). The selectivity to 1,2- and 1,5-pentanediol (12PD and 15PD), formed by the

**Mg/Al prepared from double layered hydroxides (LDHs) as catalysts the selective conversion of furfural to TFA**

hydrogenolysis of FA and TFA, grew continuously with the hydrogen pressure and reached a selectivity of 7.0% (12PD) and 4.5% (15PD), at 50 bar, respectively. Concerning FUR and mFUR, hydrogen pressure promoted their hydrogenation to tetrahydrofuran (THF) and 2-methyltetrahydrofuran (mTHF). The hydrogenation of FUR to THF was promoted over its hydrogenolysis to BU as hydrogen pressure was increased. Overall, a pressure of 50 bar was the most adequate to favor the selectivity to TFA and to lower the formation of byproducts such as DFE, TFEE and FDA, and it was selected to study the effect of the other variables.

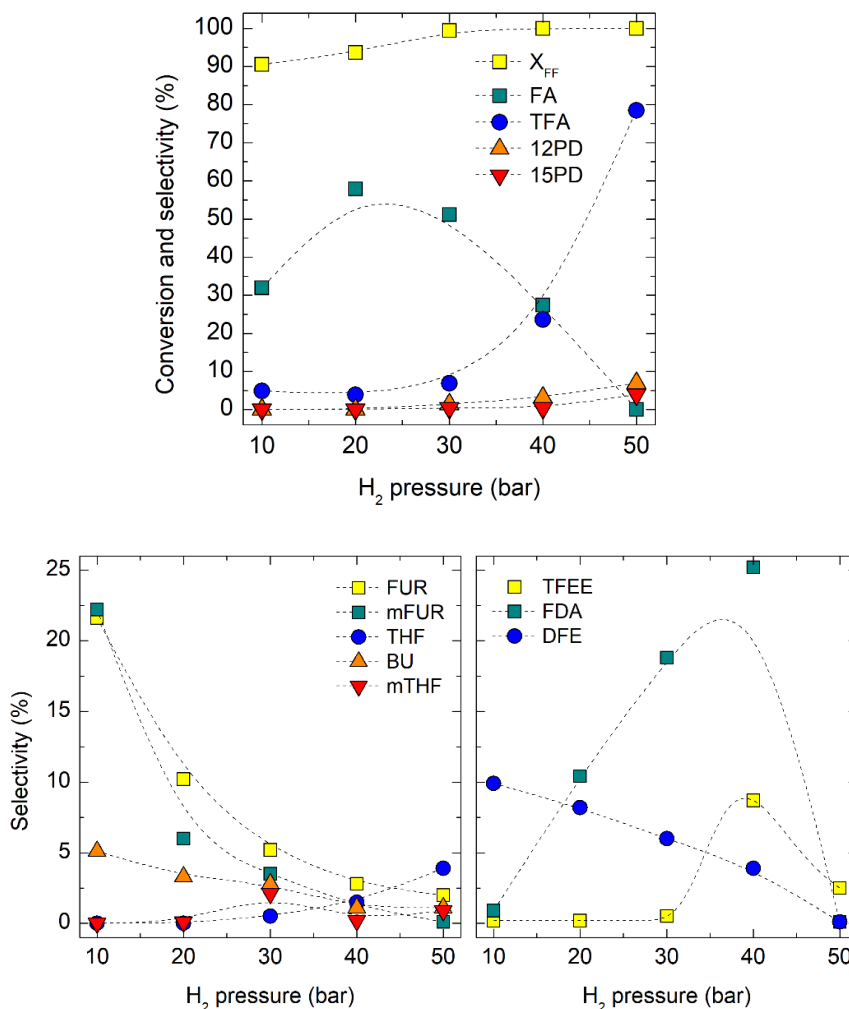


**Figure 5.10.** FF conversion and product selectivity over Ni<sub>2</sub>Mg<sub>1</sub>Al-R: effect of hydrogen pressure at 4 h and 190 °C using 5 wt% FF in ethanol (the dashed lines only indicate trends).

**Mg/Al prepared from double layered hydroxides (LDHs) as catalysts the selective conversion of furfural to TFA**

The effect of reaction time was investigated with the Ni<sub>2</sub>Mg<sub>1</sub>Al-R catalyst at 190 °C and 50 bar of hydrogen for up to 8 h. FF conversion was 93.4% after 1 h and the main products were FA (50%) and TFA (36%), together with FUR (4.7%), 12PD (3.2%) and minor amounts of the other products (Figure 5.11). FF conversion was complete after 2 h. After 4 h, FA was not present and TFA reached a selectivity of 78.5%, with a 7.0% of 12PD, a 4.5% of 15PD and 3.9% of THF. Extending the reaction time to 8 h had little impact on the composition of the product mixture. Selectivity to TFA was constant at ca. 80% and 12PD and 15PD only increased marginally reaching 9.0% and 4.8% after 8 h, respectively, showing that the catalyst was not significantly active for the hydrogenolysis of TFA, and producing pentanediol through the opening of the furan rings.

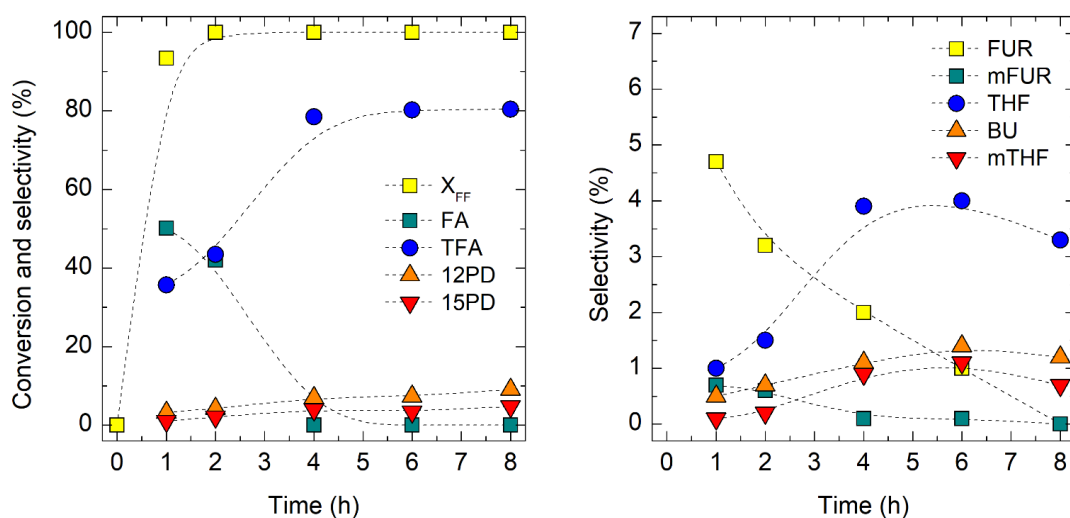


**Figure 5.11.** Furfural conversion and product selectivity over Ni<sub>2</sub>Mg<sub>1</sub>Al-R: effect of reaction time at 50 bar of H<sub>2</sub> and 190 °C using 5 wt% FF in ethanol (the dashed lines only indicate trends).

The effect of temperature was tested at 160, 190 and 210 °C, with the Ni<sub>2</sub>Mg<sub>1</sub>Al-R catalyst at 50 bar and 2 h. FF conversion was 92.7% at 160 °C, and it was complete at higher temperature (Figure 5.12). Results show that temperature favored the decarbonylation of FF to FUR, which grew from 1.5% at 160 °C to 7.4% at 210 °C, even if FA was always the

**Mg/Al prepared from double layered hydroxides (LDHs) as catalysts the selective conversion of furfural to TFA**

main primary product (51.5% and 54.3% at 160 °C and 210 °C, respectively). Similarly, the selectivity to mFUR and BU also grew with temperature. It is worth mentioning that the effectivity of the catalyst to hydrogenate the double bonds ( $\pi$  bonds) in furan rings decreased with temperature. The selectivity to TFA was actually lower at 210 °C (26.4%) than at 190 °C (43.6%), while that of FA was higher. In addition, the selectivity to THF and mTHF was virtually unchanged from 190 to 210 °C, even if the amount of FUR and mFUR increased. Finally, rising the temperature from 190 to 210 °C had no impact on the selectivity to 12PD and 15PD.

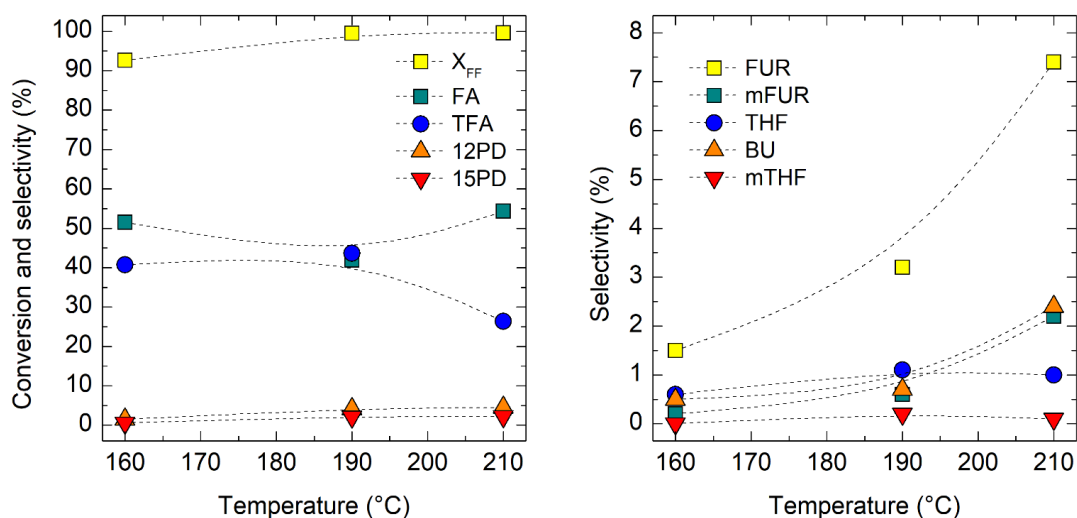


**Figure 5.12.** Furfural conversion and product selectivity over  $Ni_2Mg_1Al-R$ : effect of temperature at 2 h of reaction and 50 bar of  $H_2$  using 5 wt% FF in ethanol (the dashed lines only indicate trends).

Based on the previous results, the effect of the Mg/Ni ratio in the catalyst was tested by conducting the hydrogenation of furfural over three different catalysts,  $Ni_2Al-R$ ,  $Ni_2Mg_1Al-R$  and  $Ni_1Mg_1Al-R$ , at 190 °C, 50 bar of  $H_2$  and 4 h of reaction time (Figure 5.13). The conversion of FF was complete in the three catalysts ( $Ni_2Al-R$ ,  $Ni_2Mg_1Al-R$  and  $Ni_1Mg_1Al-R$ ) and the selectivity to minor products such as FUR, mFUR, THF, mTHF and BU was practically independent of the catalyst composition. TFA was the main product in all

**Mg/Al prepared from double layered hydroxides (LDHs) as catalysts the selective conversion of furfural to TFA**

cases, but significant differences were observed. FA was not produced in Ni<sub>2</sub>Al-R, which had the lowest selectivity to TFA (51%) and a 35% selectivity to TFEE thus showing a high capacity to catalyze the formation of acetals through addition reactions. On the other hand, TFEE in Ni<sub>1</sub>Mg<sub>1</sub>Al-R was only 0.4% showing that addition of Mg inhibited this reaction route by decreasing the acidity sites of the catalyst, as exhibited in TPD-NH<sub>3</sub> results. This catalyst formed less TFA (62%) than Ni<sub>2</sub>Mg<sub>1</sub>Al-R (78.5%) while it still gave a 7.3% of unconverted FA. Furthermore, it was the catalyst that gave the highest selectivity to 12PD (12%) and 15PD (8.2%).

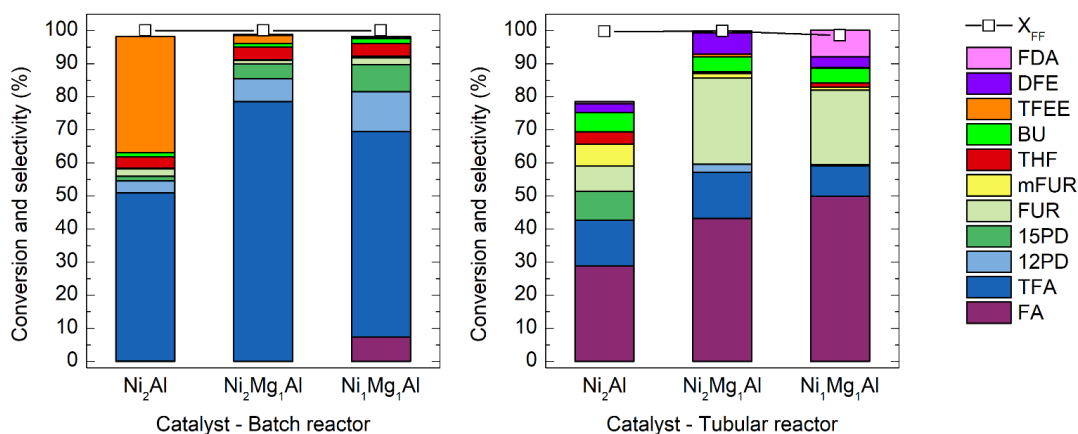
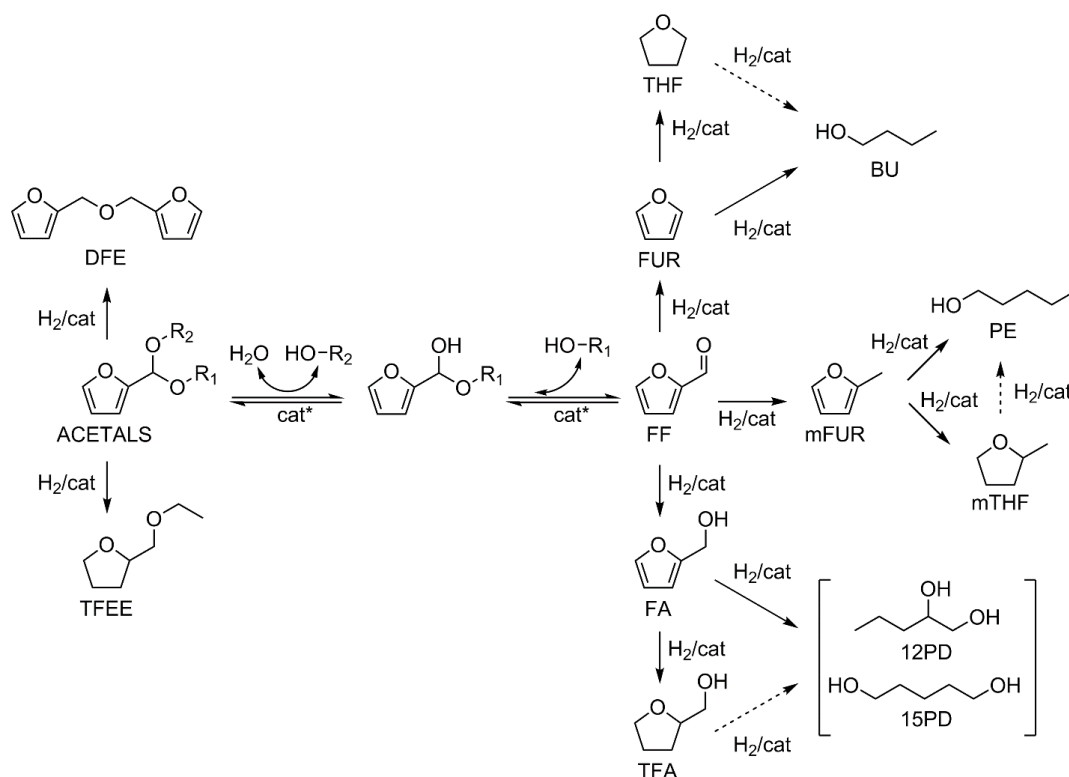


**Figure 5.13.** Furfural conversion and product selectivity using 5 wt% FF in ethanol at 190 °C: influence of the catalyst composition and the reactor type. Left: batch reactor at 50 bar of H<sub>2</sub> for 4 h. Right: tubular reactor at atmospheric pressure using a WHSV of 2.85 g<sub>FF</sub> g<sub>cat</sub><sup>-1</sup> h<sup>-1</sup> and a hydrogen-to-furfural molar ratio of 12.7:1.0.

The three catalysts were also tested at 190 °C on a continuous packed bed reactor at atmospheric pressure. Important differences on the behavior of the catalysts were observed when the reaction was conducted in gas phase (Figure 5.13). Unlike the SSR, FA was always the main product in the atmospheric PBR. FF conversion was complete on Ni<sub>2</sub>Al-R and it gave a selectivity to FA and THF of 30% and 14%, respectively, accompanied by smaller amounts of 15PD, FUR, mFUR, THF, BU and DFE. Overall, the selectivity of the

## Mg/Al prepared from double layered hydroxides (LDHs) as catalysts the selective conversion of furfural to TFA

products that were identified only accounted for 79% of the converted furfural. The unidentified fraction consisted of a complex mixture of species with apparent high molar masses that were observed in the gas chromatograms at high retention time but could not be identified by GC/MS. The formation of these compounds by condensation reactions involving FF and FA seems consistent with the capacity exhibited by this catalyst to promote the formation of acetals in liquid phase at high H<sub>2</sub> pressure. In Ni<sub>2</sub>Mg<sub>1</sub>Al-R the selectivity to FA was 43%, followed in decreasing order by FUR (26%), TFA (14%) and DFE (6.5%). In fact, these values are qualitatively closer to those obtained with this catalyst in the SSR reactor at 10 bar than to those measured at 50 bar. Finally, FF conversion was only 98.6% on Ni<sub>1</sub>Mg<sub>1</sub>Al-R, although it gave more FA (50%) and less FUR and TFA than Ni<sub>2</sub>Mg<sub>1</sub>Al-R. It is worth mentioning that pentanediols were not formed significantly in Ni<sub>2</sub>Mg<sub>1</sub>Al-R and Ni<sub>1</sub>Mg<sub>1</sub>Al-R at atmospheric pressure, in contrast with the situation in the slurry reactor at 50 bar of H<sub>2</sub>. Also, both catalysts produced significant amounts of condensation products at atmospheric pressure, with a 6.5% of DFE in Ni<sub>2</sub>Mg<sub>1</sub>Al-R and a 8.0% of FDA in Ni<sub>1</sub>Mg<sub>1</sub>Al-R.



**Scheme 5.1.** Reaction pathways involved in the hydrogenation of furfural on Ni-Mg/Al catalysts. (FDA is the acetal compound when R<sub>1</sub>=R<sub>2</sub>=CH<sub>2</sub>CH<sub>3</sub>)

### 3. Conclusions

Ni-Mg/Al catalysts derived from layered double hydroxides were synthesized and tested in the production of TFA from FF in liquid-phase hydrogenation. After calcination and reduction, the catalysts contained small nickel crystallites (ca < 4 nm) dispersed on a solid matrix consisting of nickel-magnesium mixed oxides and a Mg[Al]<sub>2</sub>O<sub>4</sub> spinel. Furfural conversion took place by a competing set of reactions. A low hydrogen pressure favored FA as the main hydrogenation product together with FUR and mFUR, and also promoted addition reactions that formed acetals that eventually led to DFE and TFEE as identified final products. Higher hydrogen pressures promoted the hydrogenation of the furan rings and reduced the extension of the condensation reactions, thus favoring TFA as the main

## Mg/Al prepared from double layered hydroxides (LDHs) as catalysts the selective conversion of furfural to TFA

product. Temperature reduced the selectivity to TFA and increased that to FA. Pentanediols (12PD and 15PD) were formed as minor products, but their selectivity increased with the Mg/Ni ratio of the catalyst. Testing of the catalysts in gas-phase hydrogenation conditions at atmospheric pressure revealed a poorer performance with FA and FUR as the main products. Even if the  $\text{Ni}_2\text{Mg}_1\text{Al}$  catalysts achieved complete conversion of FF and a selectivity to TFA of 80% after 6 h at 190 °C and 50 bar  $\text{H}_2$ , a large variety of coproducts were present at low concentration. Further optimization of the catalysts (Mg/Ni ratio and synthesis parameters) and reaction conditions is required to obtain a catalyst selective enough for the total hydrogenation of FF to TFA at industrial level.

## 4. References

- [1] Bozell, J.J.; Petersen, G.R. Technology development for the production of biobased products from biorefinery carbohydrates—the US Department of Energy’s “Top 10” revisited. *Green Chem.* 2010, 12, 539 – 554
- [2] Lange, J.-P.; van der Heide, E.; van Buijtenen, J.; Price, R. Furfural - A Promising Platform for Lignocellulosic Biofuels. *ChemSusChem* 2012, 5, 150-166.
- [3] Mariscal, R.; Maireles-Torres, P.; Ojeda, M.; Sádaba, I.; López Granados. Furfural: a renewable and versatile platform molecule for the synthesis of chemicals and fuels. *Energy Environ. Sci.* 2016, 9, 1144 – 1189.
- [4] Zeitsch, K.J. The chemistry and technology of furfural and its many by-products. Elsevier, Ney Work, eBook ISBN: 9780080528991, 2000
- [5] Yan, K.; Wu, G.; Lafleur, T.; Jarvis, C. Production. Properties and catalytic hydrogenation of furfural to fuel additives and value-added chemicals. *Renew Sustain Energy Rev* (2014) 38:663–676
- [6] Hoydonckx, H.E.; Van Rhijn, W.M.; Van Rhijn, W.; De Vos, D.E.; Jacobs, P.A. Furfural and Derivatives. In *Ullmann’s Encyclopedia of Industrial Chemistry*; Wiley-VCH Verlag GmbH & Co. KGaA: Weinheim, Germany, 2012; Volume 16, pp. 285-313.
- [7] Biradar, N.S.; Hengne, A.M.; Birajdar, S.N.; Niphadkar, P.S.; Joshi, P.N.; Rode, C.V. Single- pot formation of THFAL via catalytic hydrogenation of FFR over Pd/MFI catalyst. *ACS Sustainable Chem Eng* 2014; 2, 2 :272-81.
- [8] C, Li.; G, Xu.; X, Liu.; Y, Zhang.; Y, Fu. Hydrogenation of Biomass-Derived Furfural to Tetrahydrofurfuryl Alcohol over Hydroxyapatite-Supported Pd Catalyst under Mild Conditions. *Ind. Eng. Chem. Res.* 2017, 56, 8843–8849.
- [9] C, Wang.; A, Wang.; Z, Yu.; Y, Wang.; Z, Sun.; V.M, Kogan.; Y.-Y, Liu. Aqueous phase hydrogenation of furfural to tetrahydrofurfuryl alcohol over Pd/UiO-66. *Catalysis Communications.* 2021, 148 106178.
- [10] R,Albilali.; M, Douthwaite.; Q, Heb.; S, H, Taylor. The selective hydrogenation of furfural over supported palladium nanoparticle catalysts prepared by sol-immobilisation: effect of catalyst support and reaction conditions. *Catal. Sci. Technol.* 2018, 8, 252–267.
- [11] J, Wu.; X, Zhang.; Q, Chen.; L, Chen.; Q, Liu.; C, Wang.; L, Ma. One-Pot Hydrogenation of Furfural into Tetrahydrofurfuryl Alcohol under Ambient Conditions over PtNi Alloy Catalyst. *Energy Fuels* 2020, 34, 2178–2184.
- [12] B. M, Matsagar.; C.-Y, Hsu.; S. S, Chen.; T, Ahamad.; S. M, Alshehri.; D. C. W, Tsang.; Kevin C.-W, Wu. Selective hydrogenation of furfural to tetrahydrofurfuryl alcohol over a Rh-loaded carbon catalyst in aqueous solution under mild conditions. *Sustainable Energy Fuels*, 2020, 4, 293–301.

Mg/Al prepared from double layered hydroxides (LDHs) as catalysts the selective conversion of furfural to TFA

- [13] Y, Nakagawa.; H, Nakazawa.; H, Watanabe.; K, Tomishige. Total Hydrogenation of Furfural over a Silica-Supported Nickel Catalyst Prepared by the Reduction of a Nickel Nitrate Precursor. *ChemCatChem* 2012, 4, 1791 – 1797.
- [14] Y, Yang.; J, Ma.; X, Jia.; Z, Du.; Y, Duan.; J, Xu. Aqueous phase hydrogenation of furfural to tetrahydrofurfuryl alcohol on alkaline earth metal modified Ni/Al<sub>2</sub>O<sub>3</sub>. *RSC Adv.*, 2016, 6, 51221–51228.
- [15] J, Parikh.; S, Srivastava.; G. C, Jadeja. Selective Hydrogenation of Furfural to Tetrahydrofurfuryl Alcohol Using Supported Nickel–Cobalt Catalysts. *Ind. Eng. Chem. Res.* 2019, 58, 16138–16152.
- [16] C, Sunyol.; R, English, Owen.; M.D, González.; P, Salagre.; Y, Cesteros. Catalytic hydrogenation of furfural to tetrahydrofurfuryl alcohol using competitive nickel catalysts supported on mesoporous clays. *Applied Catalysis A, General* 611 (2021) 117903.
- [17] A, Kumar.; A, Shivhare.; R, Bal.; R, Srivastava. Metal and solvent-dependent activity of spinel-based catalysts for the selective hydrogenation and rearrangement of furfural. *Sustainable Energy Fuels*, 2021, 5, 3191–3204.
- [18] F, Cavani.; F, Trifirò.; A, Vaccari. Hydrotalcite-type anionic clays: Preparation, properties and applications. *Catalysis Today* 11, 1991, 173-301.
- [19] K, Kaneda.; T, Mizugaki. Design of high-performance heterogeneous catalysts using hydrotalcite for selective organic transformations. *Green Chem.* 2019, 21, 1361-1389
- [20] B.F, Sels.; D.E, De Vos.; P.A, Jacobs. Hydrotalcite-like anionic clays in catalytic organic reactions. *Catal. Rev. Sci. Eng.*, 2001, 43, 443–488.
- [21] K, Kaneda.; K, Ebitani.; T, Mizugaki.; K, Mori. Design of High-Performance Heterogeneous Metal Catalysts for Green and Sustainable Chemistry. *Bull Chem. Soc. Jpn.*, 2006, 79, 981–1016.
- [22] S, Kannan. Catalytic applications of hydrotalcite-like materials and their derived forms. *Catal. Surv. Asia*, 2006, 10, 117–137.
- [23] G, Fan.; F, Li.; D. G, Evans.; X, Duan. Catalytic applications of layered double hydroxides: recent advances and perspectives. *Chem. Soc. Rev.*, 2014, 43, 7040–7066.
- [24] J, Feng.; Y, He.; Y, Liu.; Y, Du.; D, Li. Supported catalysts based on layered double hydroxides for catalytic oxidation and hydrogenation: general functionality and promising application prospects *Chem. Soc. Rev.*, 2015, 44, 5291–5319.
- [25] T.P, Sulmonetti.; S.H, Pang.; M.T, Claire.; S, Lee.; D.A, Cullen.; P.K, Agrawal.; C.W, Jones. Vapor phase hydrogenation of furfural over nickel mixed metal oxide catalysts derived from layered double hydroxides. *Applied Catalysis A: General* 517 (2016) 187–195.
- [26] J, Wu.; G, Gao.; J, Li.; P, Sun.; X, Long.; F, Li. Efficient and versatile CuNi alloy nanocatalysts for the highly selective hydrogenation of furfural. *Applied Catalysis B: Environmental* 203 (2017) 227–236.

Mg/Al prepared from double layered hydroxides (LDHs) as catalysts the selective conversion of furfural to TFA

- [27] X, Meng.; Y, Yang.; L, Chen.; M, Xu.; X, Zhang.; M, Wei. A Control over Hydrogenation Selectivity of Furfural via Tuning Exposed Facet of Ni Catalysts. *ACS Catal.* 2019, 9, 4226–4235.
- [28] T.U, Rao.; S.,Suchada.; C, Choi.; H, Machida.; Z, Huo.; K, Norinaga. Selective hydrogenation of furfural to tetrahydrofurfuryl alcohol in 2-butanol over an equimolar Ni-Cu-Al catalyst prepared by the co-precipitation method. *Energy Conversion and Management* 265, 2022, 115736.
- [29] L.N, Stepanova.; O.B, Belskaya.; N.N, Leonteva.; E.O, Kobzar.; A.N, Salanov.; T.I, Gulyaeva.; M.V, Trenikhin.; V.A, Likholobov. Study of the properties of the catalysts based on Ni(Mg)Al-Layered Hydroxides for the reaction of furfural hydrogenation. *Materials Chemistry and Physics* 263, 2021, 124091.
- [30] Thommes, M.; Kaneko, K.; Neimark, A.V.; Olivier, J. P.; Rodriguez-Reinoso, F.; Rouquerol, J.; Sing, K. S. W. Physisorption of gases, with special reference to the evaluation of surface area and pore size distribution (IUPAC Technical Report). *Pure Appl. Chem.* 2015, 87, 1051–1069.
- [31] Bardestani, R.; Patience G. S.; Kaliaguine S. Experimental methods in chemical engineering: specific surface area and pore size distribution measurements – BET, BJH, and DFT. *Can. J. Chem. Eng.* 2019, 97, 2781-2791.
- [32] Brown, I.D.; Poeppelmeier, K. Bond Valences, Vol. 3, (Springer Berlin, Heidelberg, Germany, 2014).
- [33] Vegard, L. *Z.phys* 5 1921 17.
- [34] Clause, O.; Coelho, M. G.; Gazzano, M.; Matteuzzi, D.; Trifirò, F.; Vaccari A. Synthesis and thermal reactivity of nickel-containing anionic clays. *Appl. Clay Sci.* 1993, 8, 169–186.
- [35] Mas, V.; Baronetti, G.; Amadeo, N.; Laborde, M. Ethanol steam reforming using Ni(II)-Al(III) layered double hydroxide as catalyst precursor. Kinetic study. *Chem. Eng. J.* 2008, 138, 602–667.
- [36] S, Abelló.; C, Berruoco.; F, Gispert-Guirado.; D, Montané. Synthetic natural gas by direct CO<sub>2</sub> hydrogenation on activated takovites: effect of Ni/Al molar ratio *Catal. Sci. Technol.*, 2016, 6, 2305–2317
- [37] D.C, Puxley.; I.J, Kitchener.; C, Komodromos.; N.D, Parkyns. in *Preparation of Catalysts III*, Stud. Surf. Sci. Catal., ed. G. Poncelet, P. Grange and P. A. Jacobs, Elsevier Science, 1983, vol. 16, pp. 237–271.
- [38] Wang, Y.; Cui, Q.; Guan, Y.; Wu, P. Facile synthesis of furfuryl ethyl ether in high yield via the reductive etherification of furfural in ethanol over Pd/C under mild conditions. *Green Chem.* 2018, 20, 2110–2117.
- [39] He, J.; Nielsen, M. R.; Hansen, T. W.; Yang, S.; Riisager, A. Hierarchically constructed NiO with improved performance for catalytic transfer hydrogenation of biomass-derived aldehydes. *Catal. Sci. Technol.* 2019, 9, 1289–1300.

Mg/Al prepared from double layered hydroxides (LDHs) as catalysts the selective conversion of furfural to TFA

- [40] Ramos, R.; Peixoto, A. F.; Arias-Serrano, B. I.; Soares, O. S. G. P.; Pereira, M. F. R.; Kubička, D.; Freire, C. Catalytic Transfer Hydrogenation of Furfural over Co<sub>3</sub>O<sub>4</sub>-Al<sub>2</sub>O<sub>3</sub> Hydrotalcite-derived Catalyst. *ChemCatChem* 2020, 12, 1467–1475.
- [41] Jorge, E. Y.; Lima, T. D. M.; Lima, C. G.; Marchini, L.; Castelblanco, W. N.; Rivera, D. G.; Urquieta-Gonzalez, E. A.; Varma, R. S.; Paixão, M. W. Metal-exchanged magnetic  $\beta$ -zeolites: valorization of lignocellulosic biomass-derived compounds to platform chemicals. *Green Chem.* 2017, 19, 3856–3868.
- [42] Aldureid, A.; Medina, F.; Patience G. S.; Montané, D. Ni-Cu/Al<sub>2</sub>O<sub>3</sub> from Layered Double Hydroxides Hydrogenates Furfural to Alcohols. *Catalysts* 2022, 12, 390.

**Mg/Al prepared from double layered hydroxides (LDHs) as catalysts the selective conversion of furfural to TFA**

Mg/Al prepared from double layered hydroxides (LDHs) as catalysts the selective conversion of furfural to TFA

# Chapter Six

---

# General Conclusions And Future Work

# Chapter 6: General Conclusions and Future Work

## 1. General Conclusions

The main objective of this research was to obtain a group of suitable non-noble hydrogenation catalysts for converting biomass-derived platform chemicals such as furfural into commodity chemicals such as pentanediols, tetrahydrofurfuryl alcohol and furfuryl alcohol. We designed a series of catalysts based on transition metal (Ni, Cu, Co) and alkaline earth metal (Mg). We supported all catalysts with the layered double hydroxide structure of aluminum. This research has helped to develop certain conditions for controlling furfural conversion.

### 1.1. Conditions

Since hydrogen is a reactant in our process, hydrogen pressure is one of the main parameters that affect the performance of the reaction. Also, since hydrogen solubility is related to hydrogen pressure, this influences the amount of available hydrogen capable of reacting with the other reactant (furfural) in the reaction medium.

In our experiments we found that, to guide the reaction towards the preferred products (TFA, FA, 12PD, 15PD) and avoid consumption of the substrate (furfural) in the formation of by-products, the conversion reaction should be performed at 5 MPa of hydrogen pressure. This enables a suitable amount of hydrogen to be in contact with furfural in the reaction medium.

The by-products are probably formed because the reaction took the nucleophilic addition route on acidic sites of the catalyst surface, in which furfural reacts with

## General Conclusions and future Work

either ethanol or furfuryl alcohol to form some other undesired products whose presence has been shown to decrease the reaction rates.

Conducting the furfural conversion at low hydrogen pressure led to form FA as the main product and may produce other chemicals such as FUR through the decarbonylation, or mFUR through the hydrogenation. Also, other reactions that formed acetals which finally produced DFE and TFEE as final products may occur.

Furthermore, since activation energy is needed to carry out the hydrogenation of furfural, suitable thermal conditions, among other factors, are crucial for directing furfural conversion towards the desired compounds. In general, we found that a temperature of 463 K led to a high conversion of furfural and the formation of the desired products. Performing the reaction at lower temperatures would not achieve the expected results and may synthesize undesired products.

With regard to reaction time, two hours was the minimum recorded time in which the reaction completed 100% conversion with most catalysts. This short time produced only simple alcohols such as furfuryl alcohol. The hydrogenolysis process for forming linear C5 di-alcohols required a longer time (at least four hours). The impact of the catalyst and the economic concerns of energy consumption notwithstanding, reaction time played a highly significant role, with reactions lasting four hours achieving the best results.

### 1.2. Catalysts

Our approach focused on heterogeneous catalysts that after the reaction are easily separated from the mixture, easily prepared, available from abundant elements, and cheaper than most other catalysts in the literature that use noble metals.

## General Conclusions and future Work

All our catalysts contained nickel and aluminum and were derived from layered double hydroxides (LDHs). Three catalysts contained cobalt, while copper was added to another three, a pair of catalysts were modified by magnesium and a catalyst that consisted only of aluminum and nickel as a reference for the activity.

Our catalysts can be divided into three groups based on their activity to hydrogenate furfural. The first group comprises catalysts that promote the hydrogenation of the aldehyde group into alcohols. The second group comprises catalysts that are capable of opening the furan ring. The third group comprises catalysts that support hydrogenation by other routes such as the cleavage of C=O and/or the decarbonylation of furfural.

The first group comprises Cu-based and Mg-based catalysts due to their high capacity to direct furfural hydrogenation into the reduction of the aldehyde group and produce high yields of furfuryl alcohol and tetrahydrofurfuryl alcohol (cyclic alcohol).

The second group contains Co-based catalysts because of the greater amount of pentanediols it obtained compared to the other catalysts. This shows that cobalt is necessary in the catalyst structure to drive furfural hydrogenation into a ring-opening route and produce pentanediols in large amounts.

The third group consists of Cu-based catalysts, which led to the formation of valued compounds such as 2-methyl furan, 2-methyl Tetrahydrofuran, Furan, and THF. These compounds were produced in all reactions but higher selectivities were obtained in reactions done over catalysts based on copper than in those based on cobalt and magnesium.

## General Conclusions and future Work

In other words:

- **Cu-based** catalysts were suitable for forming furfuryl alcohol. Compared to the other catalysts, a slight amount of furfuryl alcohol was produced when Mg-based catalysts were used but no furfuryl alcohol was produced when Co-based catalysts were used. The highest amount of furfuryl alcohol was obtained with the copper catalysts.
- **Mg-based** catalysts were not very active in ring-opening. However, since they were the most active catalysts in both the aldehyde group hydrogenation and the furanic ring's double bond, they became the catalysts of choice for producing tetrahydrofurfuryl alcohol.
- **Co-based** catalysts appear to be more active than the other catalysts when it comes to opening the furan ring and generating two groups of alcohols to form pentanediols. Since the production of pentanediols is not yet on a large scale, this characteristic may make cobalt a promising candidate for designing catalysts to produce 1,5-pentanediol and 1,2-pentanediol in up-scale amounts by combining multiple stages of the synthesized catalyst, where the reactant is exposed to different phases of hydrogenation in a continuous packed-bed.

### 1.3. Reactors

By comparing the results from the continuous packed-bed reactor (PBR) with those from the high-pressure slurry reactor (SSR), we can clearly determine the role of the reactor.

Monitoring the formation of tetrahydrofurfuryl alcohol, furfuryl alcohol, and pentanediols enabled us to determine how the reactor played a role in encouraging

## General Conclusions and future Work

the reaction to take certain routes over others. Under the same thermal conditions, reaction time and over the same catalyst, furfural reacted differently. In PBR, the dominant product was furfuryl alcohol, while in SSR it was tetrahydrofurfuryl alcohol.

The PBR reactor may make furfural suppressed as furfuryl alcohol and allow just a small amount of it to be converted into other products of furan ring hydrogenation and/or opening-ring rearrangement. However, in SSR the hydrogenation process persisted towards the double bonds in the furan ring and produced tetrahydrofurfuryl alcohol, which may be followed by the ring-opening and produce pentanediols.

These results could therefore be attributed to the short contact time between furfural and the catalyst surface, which enables furfural to remain adsorbed for a short time and impede the attack of hydrogen. Products of only one hydrogenation process were therefore formed in higher amounts in the PBR. Moreover, the small amount of pentanediols formed in the PBR explained the high energy needed to open the furan ring, which was not available in the reaction occurred PBR.

## 2. Future Work

Furfural hydrogenation products have demonstrated their importance in numerous sectors of the chemical industry. Working to optimize their selectivity will therefore be one of our future aims. This work could be conducted in the following ways.

**First**, by investigating the role catalyst support can play and replacing the support of alumina in our catalysts to other dispersed metals such as titania [1], other metal oxides, like  $\text{SiO}_2$ ,  $\text{La}_2\text{O}_3$ ,  $\text{CeO}_2$ ,  $\text{MnO}_2$ , and  $\text{ZrO}_2$ [2] or with active carbon [2].

## General Conclusions and future Work

**Second**, by altering the catalyst reduction conditions that take place before the reaction, e.g. by selecting a different temperature, thermal ramp, and/or reduction time, to obtain larger amounts of catalytically active phases such as the metallic phase  $M^0$  rather than the oxides  $MO_x$ .

**Third**, by conducting our reaction in different solvent mediums and studying their influence. Suggested solvents include 2-propanol [3], toluene [4], octane [5], and 2-butanol [6].

**Fourth**, by adding different promoter agents to the structure of our catalysts. Catalytical promotion is one of the keys to increasing the selectivity of unsaturated alcohols in the hydrogenation of unsaturated aldehydes [7]. This process can be done by metallic doping on our catalysts using basic promoters for instant calcium (Ca), strontium (Sr), barium (Ba), potassium (K), etc. [8].

**Fifth**, by preparing new catalysts based on other non-noble metals such as tin (Sn) [9], zinc (Zn) [10], iron (Fe) [11], and molybdenum (Mo) [12, 13], etc.

## 3. References

- [1] M.T, Nguyen Dinh.; C, Lancelot.; P, Blanchard.; C, Lamonier.; M, Bonne.; S, Royer.; P, Marécot.; F, Dumeignil.; E, Payen. Mesoporous TiO<sub>2</sub>-SBA15 composites used as supports for molybdenum-based hydrotreating catalysts, 175,2010,587-591,ISSN 0167-2991,ISBN 9780444536013.
- [2] Planeix, J. M.; Coustel, N.; Coq, B.; Brotons, V.; Kumbhar, P. S.; Dutartre, R.; Geneste, P.; Bernier, P.; Ajayan, P. M. Application of carbon nanotubes as supports in heterogeneous catalysis. *Journal American Chemical Society*. 1994;116(17):7935–7936.
- [3] Mizugaki, T.; Yamakawa, T.; Nagatsu, Y.; Maeno, Z.; Mitsudome, T.; Jitsukawa, K.; Kaneda, K. Direct transformation of furfural to 1,2-pentanediol using a hydrotalcite-supported platinum nanoparticle. doi.org/10.1021/sc500325g | *ACS Sustainable Chem. Eng.* 2014, 2, 2243-2247
- [4] Aldosari, O. F.; Iqbal, S.; Miedziak, P. J.; Brett, G. L.; Jones, D. R.; Liu, X.; Edwards, J. K.; Morgan, D. J.; Knight, D. K.; Hutchings, G. J. Pd–Ru/TiO<sub>2</sub> Catalyst – an Active and Selective Catalyst for Furfural Hydrogenation. *Catal. Sci. Technol.* 2016, 6, 234–242.
- [5] Zhao, Y. Facile Synthesis of Pd Nanoparticles on SiO<sub>2</sub> for Hydrogenation of Biomass-Derived Furfural. *Environ. Chem. Lett.* 2014, 12, 185–190.
- [6] Li, J.; Liu, J.; Zhou, H.; Fu, Y. Catalytic Transfer Hydrogenation of Furfural to Furfuryl Alcohol over Nitrogen-Doped Carbon-Supported Iron Catalysts. *ChemSusChem* 2016, 9, 1339–1347.
- [7] V, Ponec. On the role of promoters in hydrogenations on metals;  $\alpha$   $\beta$  -unsaturated aldehydes and ketones. *Applied Catalysis A: General* 149, 1997, 27-48.
- [8] Juntao, Ying.; Xueqing, Han.; Lei, Ma.; Chunshan, Lu.; Feng, Feng.; Qunfeng, Zhang.; Xiaonian, Li. Effects of Basic Promoters on the Catalytic Performance of Cu/SiO<sub>2</sub> in the Hydrogenation of Dimethyl Maleate. *Catalysts* 2019, 9, 704.
- [9] Rudiansono, R.; Syahrul, K.; Takayoshi, H.; Nobuyuki, I.; Shogo, S. Highly Efficient and Selective Hydrogenation of Unsaturated Carbonyl compounds Using Ni–Sn Alloy Catalysts. *Catal. Sci. Technol.* 2012, 2, 2139–2149.
- [10] Wang, Y.; Zhou, M.; Wang, T.; Xiao, G. Conversion of Furfural to Cyclopentanol on Cu/Zn/Al Catalysts Derived from Hydrotalcite-Like Materials. *Catal. Lett.* 2015, 145, 1557-1565.
- [11] Sitthisa, S.; An, W.; Resasco, D. E. Selective Conversion of Furfural to Methylfuran over Silica-Supported NiFe Bimetallic Catalysts. *J. Catal.* 2011, 284, 90–101.
- [12] Kristina, W, Golub.; Taylor, P, Sulmonetti.; Lalit, A, Darunte.; Michael, S, Shealy.; Christopher, W, Jones. Metal–Organic–Framework–Derived Co/Cu–Carbon Nanoparticle Catalysts for Furfural Hydrogenation. *ACS Applied Nano Materials* 2019, 2 (9), 6040-6056.

## General Conclusions and future Work

- [13] De Thomas, W. R.; Hort, E. V. Catalyst Comprising Raney Nickel with Adsorbed Molybdenum Compound. US4153578A, May 08, 1979.

## General Conclusions and future Work

## General Conclusions and future Work

# Indexes

## Index of Figures:

### Chapter 1

**Figure 1.1** The global consumption energy by 2019.

**Figure 1.2.** Process to produce fuel, hydrogen and high-value chemicals from biomass.

**Figure 1.3.** The three main components of lignocellulose; cellulose, hemicellulose and lignin.

**Figure 1.4.** Sites of proton attack during the hemicellulose hydrolysis.

**Figure 1.5.** The different stereo-chemical structure of Xylose.

**Figure 1.6.** The three suggested mechanism of furfural production from xylose.

**Figure 1.7.** The reactive sites of furfural.

**Figure 1.8.** Important reactions of furfural.

**Figure 1.9.** Furfural market value.

**Figure 1.10.** Furfural decarbonylation into furan.

**Figure 1.11.** Potential energy diagram of the furfural hydrogenation over heterogeneous catalysts.

**Figure 1.12.** The position of transition and noble metals in the periodic table of elements.

**Figure 1.13.** The adsorption of furfural at catalyst surface by  $\eta^1$ -(O)-Aldehyde.

**Figure 1.14.** The three adsorption positions of furfural  $\eta^1$ -(O)-Aldehyde configuration.

**Figure 1.15.** The adsorption of furfural at catalyst surface by  $\eta^2$ -(C,O)-Aldehyde configuration.

**Figure 1.16.** The adsorption of furfural at catalyst surface by  $\eta^1$ -(C)-acyl configuration.

**Figure 1.17.** Pathways hydrogenlysis/deoxygenation of tetrahydrofurfuryl alcohol over Rh catalyst.

**Figure 1.18.** The structure of HT,  $\text{Mg}_6\text{Al}_2(\text{OH})_{16}\text{CO}_3 \cdot 4\text{H}_2\text{O}$ .

**Figure 1.19.** Schematic overview of partial cation exchange in the LDH structure.

## Annexes

**Figure 1.20.** The anion exchange inside the Brucite-like layers.

**Figure 1.21.** The memory effect via thermal and rehydration exposure.

## Chapter 2

**Figure 2.1.** The synthesis of LDH materials by co-precipitation method.

**Figure 2.2.** The packed bed reactor used for the hydrogenation reaction of furfural.

**Figure 2.3.** The scheme of the packed bed reactor which utilized for the hydrogenation reaction of furfural.

**Figure 2.4.** The slurry batch reactor which was used in the hydrogenation reaction of furfural (100 mL Mini Reactor, Autoclave Engineers).

**Figure 2.5.** A cross section of the slurry batch reactor from the top.

## Chapter 3

**Figure 3.1.** N<sub>2</sub> physisorption isotherms of the LDHs precursors calcined at 673 K for 4h.

**Figure 3.2.** Pore volume (left) and surface (right) distributions of the LDHs calcined at 673 K for 4h, determined with the DFT model.

**Figure 3.3.** SEM imaging of the calcined materials (20 000 x magnification): Ni<sub>1.5</sub>Cu<sub>0.5</sub>Al<sub>1</sub> (top), Ni<sub>1</sub>Cu<sub>1</sub>Al<sub>1</sub> (center) and Ni<sub>0.5</sub>Cu<sub>1.5</sub>Al<sub>1</sub> (bottom)

**Figure 3.4.** Surface composition of the LDHs precursors calcined at 673 K for 4h measured by EFSEM-EDX.

**Figure 3.5.** XPS spectra of Ni 2p, Cu 2p, and O 1s of the LDHs precursors calcined at 673 K for 4h.

**Figure 3.6.** XRD patterns: (a) LDHs precursors calcined at 673 K for 4h; (b) reduced catalysts.

**Figure 3.7.** H<sub>2</sub>-TPR of the LDHs precursors calcined at 673 K for 4h.

**Figure 3.8.** Furfural conversion and product selectivity of the three catalysts in the atmospheric PBR and the SSR at 5.0 MPa H<sub>2</sub>. All experiments at 463 K.

**Figure 3.9.** Furfural conversion in the atmospheric PBR at 463 K and a WHSV of 2.85 g<sub>FF</sub> g<sub>cat</sub><sup>-1</sup> h<sup>-1</sup>.

## Annexes

### Chapter 4

**Figure 4.1.** FESEM-EDX imaging of the LDH precursors calcined at 400 °C for 4h.

**Figure 4.2.** SEM imaging of the LDH precursors calcined at 400 °C for 4h (35 000 × magnification).

**Figure 4.3.** N<sub>2</sub> physisorption isotherms of the LDHs precursors calcined at 400 °C for 4h (Black line: adsorption branch; red line: desorption branch).

**Figure 4.4.** Pore volume (left) and surface (right) distributions of LDHs calcined at 400 °C for 4h, determined with the BJH model.

**Figure 4.5.** XRD patterns of the LDH precursors calcined at 400 °C for 4 h (left) and the catalysts reduced at 500 °C for 1 h (right) (a: Ni<sub>2</sub>Al; b: Ni<sub>1.5</sub>Co<sub>0.5</sub>Al; c: Ni<sub>1</sub>Co<sub>1</sub>Al; d: Ni<sub>0.5</sub>Co<sub>1.5</sub>Al).

**Figure 4.6.** H<sub>2</sub>-TPR of LDH precursors calcined at 400 °C for 4h.

**Figure 4.7.** Ammonia concentration normalized to the mass of catalyst vs. the desorption temperature (a: Ni<sub>2</sub>Al-R; b: Ni<sub>1.5</sub>Co<sub>0.5</sub>Al-R; c: Ni<sub>1</sub>Co<sub>1</sub>Al-R; d: Ni<sub>0.5</sub>Co<sub>1.5</sub>Al-R) by TPD-NH<sub>3</sub>.

**Figure 4.8.** Temperature programmed desorption of ammonia (TPD-NH<sub>3</sub>): deconvolution of the ammonia concentration normalized to the mass of catalyst vs. the desorption temperature.

**Figure 4.9.** Product selectivity of furfural hydrogenolysis on the Ni<sub>1</sub>Co<sub>1</sub>Al-R catalyst at 190 °C, 5.0 MPa H<sub>2</sub>. Furfural conversion was >99.5% after 1 h.

**Figure 4.10.** Conversion and product selectivity of furfural (FF), furfuryl alcohol (FA) and tetrahydrofurfuryl alcohol (TFA) hydrogenolysis on the Ni<sub>1</sub>Co<sub>1</sub>Al-R catalyst at 190 °C, 5.0 MPa H<sub>2</sub> and 6 h.

**Figure 4.11.** Product selectivity during furfural hydrogenolysis on the four catalysts at 190 °C, 5.0 MPa H<sub>2</sub> and 4 h. Furfural conversion was always higher than 99.5%.

### Chapter 5

**Figure 5.1.** The LDH structure.

**Figure 5.2.** FESEM-EDX imaging of the LDH precursors calcined at 400 °C for 4h. Green color for Magnesium, blue color for Aluminum and red color for Nickel.

**Figure 5.3.** SEM imaging of the LDH precursors calcined at 400 °C for 4 h (10000 × magnification).

## Annexes

**Figure 5.4.** N<sub>2</sub> physisorption isotherms of the LDH precursors calcined at 400 °C for 4 h. The red symbols are the adsorption branch, and the black symbols represent the desorption branch of the isotherm.

**Figure 5.5.** Pore volume (left) and surface (right) distributions of the LDH precursors calcined at 400 °C for 4 h, determined with the DFT model.

**Figure 5.6.** XRD patterns of the LDH precursors calcined at 400 °C for 4 h (left), and the catalysts after reduction at 500 °C for 1h (right).

**Figure 5.7.** H<sub>2</sub>-TPR of the LDH precursors calcined at 400 °C for 4 h.

**Figure 5.8.** Ammonia concentration normalized to the mass of catalyst vs. the desorption temperature (a: Ni<sub>2</sub>Al-R; b: Ni<sub>2</sub>Mg<sub>1</sub>Al-R; c: Ni<sub>1</sub>Mg<sub>1</sub>Al-R) by TPD-NH<sub>3</sub>.

**Figure 5.9.** Temperature programmed desorption of ammonia (TPD-NH<sub>3</sub>): deconvolution of the ammonia concentration normalized to the mass of catalyst vs. the desorption temperature.

**Figure 5.10.** Furfural conversion and product selectivity over Ni<sub>2</sub>Mg<sub>1</sub>Al-R: effect of hydrogen pressure at 4 h and 190 °C using 5 wt% FF in ethanol (the dashed lines only indicate trends).

**Figure 5.11.** Furfural conversion and product selectivity over Ni<sub>2</sub>Mg<sub>1</sub>Al-R: effect of reaction time at 50 bar of H<sub>2</sub> and 190 °C using 5 wt% FF in ethanol (the dashed lines only indicate trends).

**Figure 5.12.** Furfural conversion and product selectivity over Ni<sub>2</sub>Mg<sub>1</sub>Al-R: effect of temperature at 2 h of reaction and 50 bar of H<sub>2</sub> using 5 wt% FF in ethanol (the dashed lines only indicate trends).

**Figure 5.13.** Furfural conversion and product selectivity using 5 wt% FF in ethanol at 190 °C: influence of the catalyst composition and the reactor type. Left: batch reactor at 50 bar of H<sub>2</sub> for 4 h. Right: tubular reactor at atmospheric pressure using a WHSV of 2.85 g<sub>FF</sub> g<sub>cat</sub><sup>-1</sup> h<sup>1</sup> and a hydrogen-to-furfural molar ratio of 12.7:1.0.

## Index of Schemes:

**Scheme 3.1.** Reaction pathways involved in the hydrogenolysis of furfural on the NiCuAl catalysts (both HO-R<sub>1</sub> and HO-R<sub>2</sub> may be either ethanol or FA).

**Scheme 4.1.** Reaction pathways involved in the hydrogenolysis of furfural on Ni-Co/Al catalysts.

## Annexes

**Scheme 5.1.** Reaction pathways involved in the hydrogenation of furfural on Ni-Mg/Al catalysts.

# Index of Equations:

Equation (1): the conversion of furfural ( $X_{FF}$ ).

Equation (2): the molar selectivity of the furfural hydrogenation products ( $S_j$ ).

# Index of Tables:

## Chapter 1

**Table 1.1.** Physical properties of furfural Properties.

**Table 1.2.** Applications of Furfuryl Alcohol (FA), Tetrahydrofurfuryl Alcohol (TFA), 1,2-Pentanediol (12PD) and 1,5-Pentanediol (15PD) in the chemical industry.

**Table 1.3.** Summary of relevant works on the conversion of furfural over different catalysts of Cu.

**Table 1.4.** Summary of relevant works on the conversion of furfural over different catalysts of Ni.

**Table 1.5.** Summary of relevant works on the conversion of furfural over different catalysts of Co.

**Table 1.6.** Summary of relevant works on the conversion of furfural over different catalysts of Fe and Mo.

**Table 1.7.** Summary of relevant works on the conversion of furfural over different catalysts of Pd.

**Table 1.8.** Summary of relevant works on the conversion of furfural over different catalysts of Ru.

**Table 1.9.** Summary of relevant works on the conversion of furfural over different catalysts of Pt

## Annexes

**Table 1.10.** Summary of relevant works on the conversion of furfural over different catalysts of Rh, Ir and Au.

## Chapter 2

**Table 2.1.** The microwave digester conditions of the catalyst (model: Ethos Easy)

## Chapter 3

**Table 3.1.** Composition and textural properties of the calcined catalyst precursors.

**Table 3.2.** Metal atomic ratios in the materials calcined at 673 K for 4h, measured by FAA, FESEM-EDX, and XPS.

**Table 3.3.** XPS analysis of the LDHs calcined at 673 K for 4h: binding energies of the metal oxides.

**Table 3.4.** Specific hydrogen consumptions during TPR of the calcined LDHs samples.

**Table 3.5.** Selectivity and conversion during furfural hydrogenation in the pressurized SSR and atmospheric PBR reactors.

## Chapter 4

**Table 4.1.** Summary of relevant works on the conversion of FF to PDs.

**Table 4.2.** Metal ratios in the calcined samples determined by FESEM-EDX and ICP-OES

**Table 4.3.** Textural properties of the calcined samples determined from N<sub>2</sub> physisorption

**Table 4.4.** Phase composition and average crystallite sizes of the calcined LDHs precursors and the reduced catalysts.

**Table 4.5.** TPR of the LDH precursors calcined at 400 °C for 4h. Peaks detected and specific hydrogen consumption.

**Table 4.6.** total concentration of acidic sites and estimation of weak, intermediate, and strong acidic sites based on signal deconvolution by TPD-NH<sub>3</sub>.

## Chapter 5

**Table 5.1.** Atomic ratios of the LDH precursors calcined at 400 °C for 4 h, measured by ICP-EOS and FESEM-EDX.

## Annexes

**Table 5.2.** Textural properties of the LDH precursors calcined at 400 °C for 4 h.

**Table 5.3.** Crystalline phases detected and average crystallite sizes calculated from the XRD diffraction patterns of the calcined and reduced samples.

**Table 5.4.** Specific hydrogen consumption during the TPR of the LDH precursors calcined at 400 °C for 4 h.

**Table 5.5.** Temperature programmed desorption of ammonia (TPD-NH<sub>3</sub>): total concentration of acidic sites and estimation of the weak, intermediate, and strong acidic sites based on signal deconvolution.

# Index of Catalysts:

## Copper catalysts (Chapter 3)

Ni<sub>0.5</sub>Cu<sub>1.5</sub>Al<sub>1</sub>: A calcined catalyst with an atomic ratio of Ni-to-Cu of 0.5:1.5

Ni<sub>1</sub>Cu<sub>1</sub>Al<sub>1</sub>: A calcined catalyst with an atomic ratio of Ni-to-Cu of 1.0:1.0

Ni<sub>1.5</sub>Cu<sub>0.5</sub>Al<sub>1</sub>: A calcined catalyst with an atomic ratio of Ni-to-Cu of 1.5:0.5

Ni<sub>0.5</sub>Cu<sub>1.5</sub>Al<sub>1</sub>-R: A reduced and calcined catalyst with an atomic ratio of Ni-to-Cu of 0.5:1.5

Ni<sub>1</sub>Cu<sub>1</sub>Al<sub>1</sub>-R: A reduced and calcined catalyst with an atomic ratio of Ni-to-Cu of 1.0:1.0

Ni<sub>1.5</sub>Cu<sub>0.5</sub>Al<sub>1</sub>-R: A reduced and calcined catalyst with an atomic ratio of Ni-to-Cu of 1.5:0.5

## Cobalt catalysts (Chapter 4)

Ni<sub>0.5</sub>Co<sub>1.5</sub>Al: A calcined catalyst with an atomic ratio of Ni-to-Co of 0.5:1.5

Ni<sub>1</sub>Co<sub>1</sub>Al: A calcined catalyst with an atomic ratio of Ni-to-Co of 1.0:1.0

Ni<sub>1.5</sub>Co<sub>0.5</sub>Al: A calcined catalyst with an atomic ratio of Ni-to-Co of 1.5:0.5

Ni<sub>0.5</sub>Co<sub>1.5</sub>Al-R: A reduced and calcined catalyst with an atomic ratio of Ni-to-Co of 0.5:1.5

Ni<sub>1</sub>Co<sub>1</sub>Al-R: A reduced and calcined catalyst with an atomic ratio of Ni-to-Co of 1.0:1.0

Ni<sub>1.5</sub>Co<sub>0.5</sub>Al-R: A reduced and calcined catalyst with an atomic ratio of Ni-to-Co of 1.5:0.5

## Magnesium catalysts (Chapter 5)

Ni<sub>1</sub>Mg<sub>1</sub>Al: A calcined catalyst with an atomic ratio of Ni-to-Mg of 1.0:1.0

## Annexes

Ni<sub>2</sub>Mg<sub>1</sub>Al: A calcined catalyst with an atomic ratio of Ni-to-Mg of 2.0:1.0

Ni<sub>1</sub>Mg<sub>1</sub>Al-R: A reduced and calcined catalyst with an atomic ratio of Ni-to-Mg of 1.0:1.0

Ni<sub>2</sub>Mg<sub>1</sub>Al-R: A reduced and calcined catalyst with an atomic ratio of Ni-to-Mg of 2.0:1.0

### **Nickel catalysts (Chapter 3, 4 & 5)**

Ni<sub>2</sub>Al: A calcined catalyst of only one active metal of nickel, supported on aluminum.

Ni<sub>2</sub>Al-R: A reduced and calcined catalyst of only one active metal of nickel, supported on aluminum

## **Index of abbreviation:**

### **1. Compounds**

FF: Furfural.

FA: Furfuryl alcohol.

TFA: Tetrahydrofurfuryl alcohol.

12PD: 1,2-Pentanediol.

15PD: 1,5-Pentanediol.

mTHF: 2-Methyltetrahydrofuran.

THF: Tetrahydrofuran.

FUR: Furan.

mFUR: 2-Methylfuran.

11DE: 1,1-Diethoxyethane.

FDA: 2-Furaldehyde diethyl acetal.

EFM: Ethoxy(furan-2-yl) methanol.

TFEE: Ethyl tetrahydrofurfuryl ether.

FEFA: 2-Furaldehyde ethyl furfuryl acetal.

DfE: Difurfuryl ether.

## Annexes

1BU: 1-Butanol.

CP: Cyclopentanone.

CPO: Cyclopentanol.

LA: Levulinic acid.

## 2. Reactors

PBR: Continuous Packed-Bed Reactor.

SSR: High-Batch Slurry Reactor.

## 3. Techniques and Analysis Methods

GC: Gas Chromatography.

FID: Flame Ionization Detector.

MS: Mass Spectrometry.

TPR: Temperature Programmed Reduction.

TCD: Thermal Conductivity Detector.

BET: Brunauer-Emmett-Teller.

DFT: Density Functional Theory.

BJH: Barrett-Joyner-Halenda.

FAA: Flame Atomic Absorption.

ICP: Inductively Coupled Plasma.

XRD: X-ray Diffraction.

XPS: X-ray Photoelectron Spectroscopy.

FESEM: Field Emission Scanning Electron Microscopy.

EDX: Energy Dispersive X-Ray Spectroscopy.

TPD: Temperature Programed Desorption of Ammonia (TPD- NH<sub>3</sub>)

# List of events attended and contributions

## Conferences:

The 71st Canadian Chemical Engineering Conference. 24-27/1/2021.

**Year:** 2021

**Place:** Polytechnique Montreal & McGill University, Montreal, Canada

**Organizer:** The Chemical Institute of Canada

**Contribution:** Poster presentation

**Title:** Hydrogenolysis of Furfural Over Bimetallic Ni/Cu Catalysts Prepared from Layered Double Hydroxides.

The 13<sup>th</sup> European Congress of Chemical Engineering and 6th European Congress of Applied Biotechnology. Frankfurt am Main, Germany, 20-23/09/2021.

**Year:** 2021

**Place:** Online event.

**Organizer:** European Federation of Chemical Engineering and European Society of Biochemical Engineering Sciences.

**Contribution:** Poster presentation.

**Title:** Hydrogenolysis of Furfural to Pentanediols Over Bimetallic Ni/Co Catalysts Prepared from Layered Double Hydroxides.

The 2020 EFCATS Summer School of the European Federation of Catalysis Societies (EFCATS),  
15-19/09/2020.

**Year:** 2020

**Place:** Portorož-Portorose, Slovenia,

**Organizer:** Catalysis section of the Slovenian Chemical Society and the Austrian Catalysis Society.

**Contribution:** Poster presentation.

**Title:** M/Al (M = Ni, Cu, Co) Catalysts Based on Layered Double Hydroxides (LDHs) Precursors for Furfural Hydrogenolysis.

## Annexes

### Doctoral days

The 17<sup>th</sup> doctoral day - URV Doctoral program in Nanoscience, Materials and Chemical Engineering

**Year:** 2022

**Place:** etsEQ building, URV (Tarragona, Spain)

**Organizer:** Universitat Rovira i Virgili (URV)

**Contribution:** Poster presentation

**Title:** Ni-Cu/Al<sub>2</sub>O<sub>3</sub> from Layered Double Hydroxides Hydrogenates Furfural to Alcohols

The 17<sup>th</sup> doctoral day - URV Doctoral program in Nanoscience, Materials and Chemical Engineering

**Year:** 2022

**Place:** etsEQ building, URV (Tarragona, Spain)

**Organizer:** Universitat Rovira i Virgili (URV)

**Contribution:** Oral presentation

**Title:** Catalytic hydrogenation/hydrogenolysis of biomass-derived platform chemicals

## List of thesis outcomes

**Title:** Ni-Cu/Al<sub>2</sub>O<sub>3</sub> from Layered Double Hydroxides Hydrogenates Furfural to Alcohols.

**Type:** Article

**Status:** Published DOI:10.3390/catal12040390

**Authors:** Abdulaziz Aldureid, Francisco Medina, Gregory S. Patience, Daniel Montané

**Journal:** catalysts

**Issue:** Catalysts for Biofuel and Bioenergy Production

**Area:** Physical and Theoretical Chemistry. Chemical Engineering: Catalysis

**Year:** 2022

## Annexes

**Title:** Furfural to diols over Ni-Co/Al catalysts.

**Type:** Article

**Status:** Sent

**Authors:** Abdulaziz Aldureid, Francesc Medina, Francesc Gispert Guirado, Daniel Montané

**Journal:** Catalysis Letters

**Area:** Catalysis, heterogeneous catalysis, homogeneous catalysis, bio catalysis

**Year:** 2022

**Title:** Ni-Mg/Al prepared from double layered hydroxides (LDHs) as catalysts for the selective conversion of furfural to tetrahydrofurfuryl alcohol.

**Type:** Article

**Status:** Sent

**Authors:** Abdulaziz Aldureid, Daniel Montané, Jordi Llorca, Francisco Medina

**Journal:** Chemistry

**Issue:** Heterogeneous Catalysis

**Area:** supramolecular and nanoscale chemistry, computational and modeling chemistry, crystallography and physical methods, molecular chemistry, medicinal and bioinorganic chemistry, catalysis and organometallic chemistry.

**Year:** 2022

## Annexes



**UNIVERSITAT  
ROVIRA i VIRGILI**